Óscar Juste Lorente

Guidelines for improving motorcycle helmet testing standards / Directrices para mejorar las normas de ensayo de los cascos de motocicleta

Director/es

López Valdés, Francisco José
Maza Frechín, Marío Vicente

Universidad Zaragoza
1542

Tesis Doctoral

GUIDELINES FOR IMPROVING MOTORCYCLE HELMET TESTING STANDARDS / DIRECTRICES PARA MEJORAR LAS NORMAS DE ENSAYO DE LOS CASCOS DE MOTOCICLETA

Autor

Óscar Juste Lorente

Director/es

López Valdés, Francisco José
Maza Frechín, Marío Vicente

UNIVERSIDAD DE ZARAGOZA
Escuela de Doctorado

Programa de Doctorado en Ingeniería Mecánica

2023

PhD Thesis

Guidelines for Improving Motorcycle Helmet Testing Standards

Author

Óscar Juste Lorente

Supervisors

Francisco J. López-Valdés

Mario Maza Frechín

Programa de Doctorado en Ingeniería Mecánica

Universidad de Zaragoza

February 2023

Acknowledgments

I would like to express my deepest gratitude to my supervisors, Dr Francisco J. López-Valdés and Dr Mario Maza Frechín for their invaluable guidance, expertise and support throughout this thesis. Their feedback, insights, and willingness to engage in thoughtful discussions have been critical to the success of this research. In particular, I am deeply indebted to Dr Francisco J. López-Valdés for introducing me to the field of impact biomechanics and encouraging me to pursue a thesis in this area. Additionally, this endeavour would not have been possible without the collaboration between the International Motorcycling Federation and the Impact Laboratory. The opportunity provided by this collaboration have been instrumental in the success of my academic journey, and I am deeply grateful for the support of both institutions.

Special thanks to Ramón Miralbes and Manuel Valdano for their assistance with the Hybrid III simulations. I would like to extend my sincere thanks to Mazdak Ghajari, who generously lent me the finite element model of the AGV-T2 motorcycle helmet. I am also grateful to all my colleagues at the Impact Laboratory who have supported me during the course of my doctoral studies, especially Javier Teller, Lorenzo Mulero, and Víctor Lasmarías, for their collaboration in the helmet testing.

I would like to acknowledge Cristina Lambán for helping me to navigate the emotional challenges during the final stages of this journey.

Lastly, I would be remiss in not mentioning my partner Ana for her unwavering support and patient throughout the process of writing this thesis, and of course, my family and my friends for their unending encouragement and understanding. Your support means the world to me.

Table of Contents

List of Figures

List of Tables

Resumen (Abstract in Spanish)

Directrices para Mejorar las Normas de Ensayo de los Cascos de Motocicleta

Investigaciones sobre accidentes reales de motocicletas han demostrado que lesiones graves en la cabeza, como las fracturas en la base del cráneo y las lesiones intracraneales, son todavía comunes entre los motociclistas a pesar de todos los avances en el diseño y fabricación de cascos. Curiosamente, este tipo de lesiones parecen estar correlacionadas con las deficiencias y discrepancias existentes entre las actuales normas de ensayo de cascos de motocicleta. Por lo tanto, el objetivo principal de esta tesis es investigar cómo se pueden mejorar las actuales normas de ensayo de cascos de motocicleta para reducir las fracturas en la base del cráneo y las lesiones intracraneales entre los motociclistas.

Aunque es bien conocido que las lesiones intracraneales son causadas principalmente por un movimiento rotacional de la cabeza, las actuales normas de ensayo de cascos se centran más en el movimiento traslacional que en el movimiento rotacional de la cabeza. Las cabezas de ensayo utilizadas actualmente en las normativas de ensayo de cascos no fueron inicialmente diseñadas para la evaluación del movimiento rotacional. Se compararon las propiedades de masa e inercia de las cabezas de ensayo EN960 con una base de datos de propiedades físicas de la cabeza humana creada a partir de una revisión de una selección de estudios realizados con cadáveres humanos. La mayoría de los valores de las cabezas de ensayo estaban dentro del intervalo de predicción del 95% para la mayoría de las propiedades físicas de la cabeza humana, pero se observaron algunas diferencias con respecto a los modelos de regresión calculados. Por lo tanto, un nuevo conjunto de cabezas de ensayo con propiedades de masa e inercia más similares a las calculadas con los modelos de regresión sería beneficioso para mejorar las actuales normas de ensayo de cascos.

Todas las normas de ensayo de cascos de motocicleta incluyen pruebas de impacto normal, en las que el vector de velocidad de impacto es normal a la superficie de impacto, para evaluar la protección proporcionada por el casco. Sin embargo, los métodos de impacto normal no miden o no permiten la rotación de la cabeza de ensayo. Se expusieron veinte modelos de cascos integrales y la cabeza de ensayo sin casco a pruebas de impacto normal para estudiar la idoneidad de las pruebas de impacto normal para evaluar el riesgo de lesiones intracraneales. Se demostró que el movimiento angular de la cabeza de ensayo equipada con casco disminuye a medida que la aceleración lineal disminuye durante las pruebas de impacto normal, pero el movimiento angular en este tipo de impactos también depende del diseño geométrico del casco. Este resultado sugiere que el movimiento angular de la cabeza de ensayo debe evaluarse en pruebas de impacto normal en combinación con la evaluación en impactos oblicuos, para evaluar el diseño geométrico del casco en una amplia gama de posibles escenarios de impacto en los que se podrían generar lesiones intracraneales.

A pesar de que algunas normas de ensayo de cascos incluyen pruebas de impacto oblicuo para evaluar el movimiento de rotación de la cabeza, requieren diferentes coeficientes de fricción entre el interior del casco y la cabeza de ensayo, lo que se ha

demostrado que es un factor crítico para la respuesta angular de la cabeza de ensayo en impactos oblicuos. Dieciocho muestras del mismo modelo de casco fueron probadas con la misma magnitud de la componente normal de la velocidad de impacto, pero con tres magnitudes diferentes de la componente tangencial de la velocidad de impacto y usando dos coeficientes de fricción diferentes entre el interior del casco y la cabeza de ensayo. Se concluyó que el coeficiente de fricción entre la cabeza de ensayo y la superficie interior del casco debe ser lo suficientemente alto como para garantizar el movimiento conjunto de la cabeza de ensayo y el casco, especialmente si la velocidad tangencial incluida en las normas de ensayo de cascos es menor que las encontradas en situaciones reales.

La carga axial en la zona superior del cuello fue propuesta como criterio de lesión para las fracturas de la base del cráneo y los accidentes reales de motocicleta han demostrado que las fracturas de la base del cráneo están altamente relacionadas con los impactos en la zona de la mentonera. Sin embargo, los métodos actuales de ensayo de la mentonera incluidos en las normas de prueba de cascos, no incluyen el cuello para medir la fuerza axial del cuello. Se utilizó una metodología combinada que utiliza la cinemática medida con una cabeza de ensayo aislada durante un ensayo físico como entrada para un modelo de elementos finitos de cuerpo completo para estudiar si es posible predecir la carga de tracción del cuello que el modelo del Hibrido III de cuerpo completo experimentaría en un impacto similar al de la prueba de la mentonera de la norma ECE 22.06 utilizando solo métricas basadas en la cinemática del ensayo de la mentonera descrito en la norma. Los resultados mostraron que una simple prueba de impacto en la mentonera utilizando las cabezas de ensayo EN960, como la que se incluye en algunas normas de ensayo de cascos, podría considerar el riesgo de fractura de la base del cráneo mediante una combinación del pico de aceleración lineal en el eje Z y la velocidad lineal resultante al final del impacto.

El ensayo de penetración es uno de los ensayos más controvertidos entre las normas de ensayo de cascos y actualmente no es requerido por algunos programas de ensayo, mientras que otros continúan exigiendo esta prueba. Basado en los resultados del ensayo de penetración de veinte modelos de casco, cuatro cascos fueron clasificados como cascos de calota dura, mientras que seis de ellos fueron clasificados como cascos de calota blanda. Solo estos diez modelos de cascos fueron sometidos a pruebas de impacto a dos velocidades diferentes para estudiar el efecto de incluir el ensayo de penetración en el comportamiento global de los cascos frente a impactos. Se concluyó que la prueba de penetración podría influir positivamente en el diseño del casco al proporcionar protección contra lesiones en la cabeza inducidas principalmente por la cinemática lineal, mientras que podría influir negativamente en el diseño del casco al proporcionar protección contra lesiones en la cabeza inducidas principalmente por la cinemática de rotación.

Abstract

Guidelines for Improving Motorcycle Helmet Testing Standards

Real-world investigations of motorcyclists crashes have shown that serious head injuries such as fractures at the base of the skull and intracranial injuries, despite all the advances made in helmet design and manufacturing, are still common among helmeted motorcyclists. Interestingly, these type of injuries seem to be correlated with the existing deficiencies and discrepancies among current motorcycle helmet testing standards. Therefore, the main objective of this thesis is to investigate how current motorcycle helmet testing standards can be improved for reducing basilar skull fracture and intracranial injuries among helmeted motorcyclists.

Although it is well-known that intracranial injuries are mainly caused by rotational motion of the head, current helmet testing standards are more focussed on translational motion than rotational motion. Headforms currently used in helmet testing standards were not initially designed for rotational motion assessment. Mass and inertia properties of EN960 headforms were compared with a database of human head physical properties which was created using a review of a selection of human cadaveric studies. Most headform values lied inside the 95% prediction interval for most human head physical properties but some differences were observed with respect to the calculated regression models. Therefore, a new set of headforms with more similar mass and inertia properties to the one calculated with the regression models would be beneficial for improving helmet testing standards.

All motorcycle helmet testing standards include normal impact tests, in which the impact velocity vector is normal to the impact surface, to assess the impact protection provided by the helmet. However, normal impact methods do not measure or do not allow the rotation of the headform. Twenty full-face motorcycle helmet models and the unhelmeted headform were exposed to free fall normal impact tests in order to study the suitability of the normal impact tests for evaluating intracranial injury risk. It was shown that the angular motion of the helmeted headform during free fall normal impact tests decreases as the linear acceleration decreases but it also depends on the helmet geometrical design. This result suggests that the angular motion of the headform should be assessed in free fall normal impact tests in combination with the assessment in oblique impacts in order to evaluate the helmet geometrical design for preventing intracranial injuries in a wide range of possible impact scenarios.

Despite the fact that some helmet testing standards include oblique impact tests to assess the rotational motion of the headform, they require different friction at the interface between the helmet and the headform, which has been shown to be a critical concern on the angular response of the helmeted headform in oblique impacts. Eighteen samples of the same helmet model were tested at the same magnitude of the normal component of the impact velocity but at three different magnitudes of the tangential component of the impact velocity using two different frictions at the headform/helmet interface. It was concluded that the coefficient of friction between the headform and the interior surface of the helmet

must be high enough to guarantee the joint motion of the helmeted headform specially if the tangential velocity included in helmet testing standards is lower than those found in real world situations.

Upper neck axial load was proposed as injury criterion of basilar skull fractures and real-world motorcycle crashes have shown that they are highly related to chin bar impacts. However, current chin bar test methods included in helmet testing standards do not include the neck to measure the upper neck axial force. A combined methodology using the output kinematics measured with an isolated headform during a physical test as input to a full-body finite element model was used to study if it was possible to predict the neck tensile load that the full-body Hybrid III model would experience in a similar impact to that of the ECE 22.06 chin bar test using only kinematic based metrics from the ECE 22.06 physical test. The results showed that simple chin bar impact test using isolated EN960 headforms which are included in some helmet testing standards could consider the risk of basilar skull fracture by a combination of the peak of the linear acceleration in the Z-axis and the resultant linear velocity at the end of the impact.

The penetration test is one of the most controversial tests among helmet testing standards and currently it is not required by some testing programs, while others continue demanding this test. Based on the penetration test results of twenty helmet models, four helmets were classified as hard shell helmets while six of them were classified as soft shell helmets. Only these ten helmet models were drop tested at two different velocities to study the effect of including a penetration test in the overall impact performance of helmets. It was concluded that penetration test would positively influence helmet design on providing protection against head injuries induced primarily by linear kinematics while it could negatively influence helmet design on providing protection against head injuries primarily induced by rotational kinematics.

List of Abbreviations

AIS	Abbreviated Injury Scale
ANOVA	ANalysis Of VAriance
BrIC	Brain Injury Criterion
BSF	Basilar Skull Fracture
CEN	European Committee for Standardization
CG	Centre of Gravity
CG_X	Centre of Gravity location in the X-axis
CG_Y	Centre of Gravity location in the X-axis
CG_Z	Centre of Gravity location in the Z-axis
COF	Coefficient Of Fiction
DAI	Diffuse Axonal Injury
DOT	United States Department of Transportation
ECE	United Nations Economic Commission for Europe
ECE 22.05	ECE Regulation 22 (05 series of amendments)
ECE 22.06	ECE Regulation 22 (06 series of amendments)
EN960	European Standard EN 960
EPS	Expanded polystyrene
FE	Finite Element
FIM	International Motorcycling Federation
FRHPhe-01	FIM Racing Homologation Programme for helmets
FRP	Fibre-Reinforced Plastic
HIC	Head Injury Criterion
JIS	Japanese Industrial Standard
LOOCV	Leave-One-Out Cross-Validation
MAIS	Maximum Abbreviated Injury Scale
MEP	Modular Elastomer Programmer
PAA	Peak of the resultant Angular Acceleration
PAV	Peak of the resultant Angular Velocity

PLA   Peak of the resultant Linear Acceleration

PLA@2ms   Peak of the resultant Linear Acceleration for a duration of 2 ms

PLA@4ms   Peak of the resultant Linear Acceleration for a duration of 4 ms

PLA@6ms   Peak of the resultant Linear Acceleration for a duration of 6 ms

SAH   Subarachnoid haemorrhage

SD   Standard Deviation

SDH   Subdural hematoma

SFC   Skull Fracture Criterion

Snell   Snell Foundation

V_T Tangential component of the impact velocity

V_N Normal component of the impact velocity

WHO   World Health Oganization

WSTC   Wayne State Tolerance Curve

<div align="right">

Chapter 1

Introduction

</div>

1.1.   Vulnerability of motorcyclists

Road traffic injuries are a leading cause of death and injury around the world and create enormous social costs, resulting in a major public health problem and a heavy burden on health services and economies (World Health Organization [WHO], 2006). Each year nearly 1.35 million people die and millions more are injured or disabled as a result of road crashes on the world (WHO, 2018). Vulnerable road users account for more than half of all road fatalities. For pedestrians, cyclists and motorcyclists, the lack of physical protection and specific infrastructure features that can ensure a safe journey makes them particularly vulnerable to being injured if they are involved in a collision. In addition, motorcycle and bicycle riders are at an increased risk of being involved in a crash because they often share the traffic space with fast-moving and heavy cars, buses and trucks, and also because they are less visible. However, motorcycle riders are at a higher risk to die in a crash than pedestrians or cyclists because they move at higher speeds.
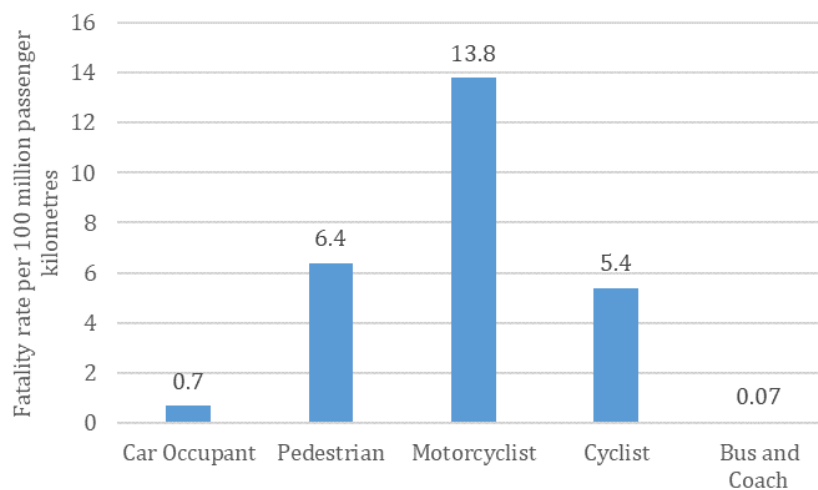
Figure 1.1: Fatalities in reported road crashes per 100 million passenger kilometres by road user type in European Union countries for the period 2001-2002. Source: (Peden et al., 2004).

Motorcyclist fatality rates vary across regions and countries mainly due to the differences in the types of road users. In low-income and middle-income countries, the use of motorcycles and bicycles is generally much higher than in high-income countries.

Globally, motorcyclists represent 28% of all deaths (WHO, 2018). In the European Union, about four thousand people died in 2019 as a direct result of moped and motorcycle crashes, accounting for 18% of the total motor vehicle fatalities (European Commission, 2021). However, when exposure is taken into account, the risks for motorcyclists are extremely high compared to other types of road user. In European Union countries, motorcyclists are 20 more times likely to die on the road than car drivers (see Figure 1.1). In the United States, the risk of death of motorcyclists is approximately 34 times higher than that of someone riding in a passenger car (National Highway Traffic Safety Administration [NHTSA], 2007).
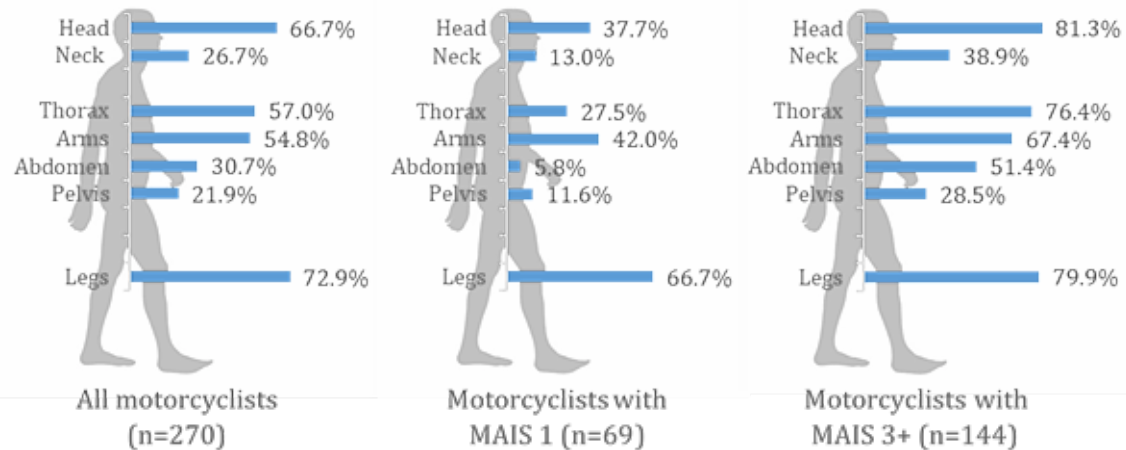
Figure 1.2: Frequency of injured body regions of all motorcyclists, motorcyclists with MAIS 1 and motorcyclists with MAIS 3+. Source: (Chinn et al., 2001).

The description of the injuries sustained by motorcyclists involved in traffic crashes is essential for reducing fatalities. Chinn et al. (2001) provided a detailed categorization by body part of injuries sustained by motorcyclists involved in traffic crashes. The individual injury severity was classified using the Abbreviated Injury Scale (AIS) which is a threat to life scale that classifies individual injury by body region on a 6-point ordinal severity scale ranging from slight injury at AIS 1 to almost certainly fatal injury at AIS 6. The overall injury severity for a patient was indicated using the Maximum AIS (MAIS) which is the highest single AIS code for a patient with multiple injuries. The most frequently injured parts of the body are the legs (72.9%), the head (66.7%) and the thorax (57%). However, when the injuries were classified, as the MAIS increased, the proportion of head injuries increased from 38% for MAIS 1 to 81% for MAIS 3 and greater (see Figure 1.2). Although the correct use of a motorcycle helmet can reduce the risk of death by almost 40% and the risk of serious injury by more than 70% (Liu et al., 2004), head injuries are the leading cause of death and long-term disability after a motorcycle crash (Lin & Kraus, 2009). Real-world motorcycle crash investigations showed that serious head injuries such as fractures at the base of the skull and intracranial injuries are still common lesions among helmeted motorcyclists (Chinn et al., 2001; Whyte et al., 2016). The success of motorcycle helmets in reducing head injuries is partly a result of the performance of the helmets. Requiring helmets to meet the requirements of an official helmet testing standard is important to guarantee that helmets can effectively reduce the effects of the impact to the head in the event of a crash (Ackaah et al., 2013). However, it depends on the quality of the standard and therefore, improving the requirements prescribed in helmet standards leads to better helmet design and consequently reduces the risk of head injury and fatalities of motorcyclists.

1.2.   Helmet protection as driven by helmet testing standards

Ideally, helmets would be designed to protect the head in all potential impact events but the wide range of impact situations makes it impracticable. In reality, most helmets are designed according to the requirements prescribed in the relevant helmet testing standards. There are numerous motorcycle helmet safety standards around the world: Regulation No. 22 from the United Nations Economic Commission for Europe (ECE) in Europe (ECE, 2021), Federal Motor Vehicle Safety Standards (FMVSS) No. 218 from the United States Department of Transportation (DOT) and M2020 from the Snell Foundation (Snell) in the United States (DOT, 2011; Snell, 2020), and Japanese Industrial Standard (JIS) T 8133 in Japan (JIS, 2015) are some of the most well-known among them. The target of a motorcycle helmet testing standard is to guarantee a minimum level of head protection under specified test conditions. All helmet testing standards assess, at a minimum, how the helmet performs in an impact (it shall be able to absorb impact energy) and if it remains in place during the impact. However, the methods for evaluating these common aspects and other additional requirements vary from one standard to another. These variations may play a part in determining the actual level of protection of the helmets (Mcintosh & Grzebieta, 2013). In particular, the impact protection assessment, which has the highest importance among almost every helmet standard, differs in the impact condition, in the head test surrogate and in the assessment criteria between different standards, influencing the performance against impact of motorcyclist helmets (Ghajari et al., 2010). A helmet that meets the impact requirements for one standard may fail the impact test for another. The considerable discrepancies concerning the assessment of helmet impact performance by testing standards is one of the main motivations of this thesis.

1.3.   Discrepancies in impact tests of current helmet testing standards

The crash event is simulated by current helmet testing standards under simplified loading conditions. For this purpose, helmet testing standards describe impact tests such as oblique impact tests, normal impact tests, chin bar impact tests and penetration tests. However, there are considerable discrepancies among the current motorcyclist helmet testing standards concerning the inclusion and testing methods of the mentioned impact tests.

The oblique impact test

The oblique impact test consists of dropping an instrumented headform, fitted with the test helmet, onto an inclined anvil in order to create an impact velocity vector of the helmeted headform composed of a normal component and a significant tangential component. Oblique impacts between the helmet and the ground are the most frequent collision scenarios in real world (Bourdet et al., 2016; Chinn et al., 2001) and they can induce rotational motion to the head of the motorcyclist if the friction is high enough. It is well-known that rotational motion of the head is capable of causing intracranial injuries (Holbourn, 1943; Kleiven, 2013). However, some helmet testing standards such as DOT, Snell and JIS, do not include an oblique impact in their testing methods (DOT, 2011; JIS, 2015; Snell, 2020). The 05 series of amendments of the ECE Regulation 22 (ECE 22.05) already included an oblique impact test in their test method A for projections and surface friction, which is also included in the current 06 series of amendments of the ECE Regulation 22 (ECE 22.06), but the headform is not instrumented and just the peak longitudinal force

measured on the anvil and its integral is assessed (ECE, 2002; ECE, 2021). Furthermore, the normal component of the impact velocity is relatively low (2.2 m/s) whereas some researchers have shown that the normal component of the impact velocity needs to be of a certain magnitude to be typical of serious helmet impacts (Meng et al., 2018; Mills et al., 2009). The FIM Racing Homologation Programme for helmets (FRHPhe-01) was the first to include an oblique impact test using an instrumented headform to assess the angular motion of the helmeted headform with an impact velocity component normal to the anvil exceeding 5 m/s (International Motorcycling Federation [FIM], 2017). Recently, the current version of the ECE regulation has included an oblique impact test similar to that of the FRHPhe-01 (ECE, 2021). Both standards call for the EN960 magnesium alloy full headforms to carry out the oblique impact test. Any impact test method designed for assessing the angular kinematics of the helmeted headform requires a headform with a defined inertia tensor. Although the requirements of the EN960 standard only specifies dimensional details and masses for some headform sizes (European Committee for Standardization [CEN], 2006), the moments of inertia of the headforms are defined in the mentioned helmet testing standards. However, it is not known to what extent mass and inertia tensor defined for the EN960 headforms match the human head properties. Even though both standards use the same set of headforms, they require different friction at the interface between the helmet and the headform and it has been shown to be a critical concern on the angular response of the helmeted headform in oblique impacts (Ebrahimi et al., 2015).

The normal impact tests

The normal impact test consists of dropping an instrumented headform, fitted with the test helmet, onto a flat or rounded anvil. In this type of impacts, there is no or little tangential component of the impact velocity vector. All motorcycle helmet testing standards include normal impact tests against a flat anvil and assess the protection offered by the helmet through the peak of the resultant linear acceleration (PLA) (DOT, 2011; ECE, 2021; FIM, 2017; JIS, 2015; Snell, 2020). However, this metric ignores the duration of the impact and some standards take into account the impact duration by limiting the duration of the impact (DOT, 2011; JIS, 2015) or through the head injury criterion (HIC) (ECE, 2021; FIM, 2017). Though the HIC is the most commonly used criterion for evaluating the risk of head injury, its validity for helmet evaluation has been intensively debated because it does not take into account angular head kinematics nor impact direction (Fernandes & Sousa, 2013).

Despite of the fact that in some test methods of motorcycle helmet standards, the helmeted headform is constrained to a monorail by means of a rigid arm attached to the headform (DOT, 2011; Snell, 2020), some others test methods allow the helmeted headform to rotate freely during the impact (ECE, 2021; FIM, 2017). The angular motion induced in normal impact tests carried out with unrestrained headforms dissipates energy into rotation decreasing linear acceleration (Thom et al., 1998) but increases the angular velocity and acceleration which lead to high intracranial injury risk. Despite some helmet testing standards measure the angular motion experienced by the helmeted headform during the impact against the oblique anvil and assess the protection offered by the helmet through the brain injury criterion (BrIC) and the peak of the resultant angular acceleration (PAA), they do not require to measure the angular motion experienced by the headform in normal impact tests (ECE, 2021; FIM, 2017).

The chin bar impact test

Many real-world motorcycle crashes studies have shown that fracture at the base of skull is one of the most common and severe injuries sustained by motorcyclists and that this type of injury is frequently caused by impacts to the chin (Chee and Ali 1991; Whyte et al. 2016). Not all helmet testing standards prescribe experimental tests for assessing the chin bar impact performance of full-face helmets. Although there are mainly two different chin bar impact test methods described in current helmet testing standards (ECE, 2021; Snell, 2020), none of these test methods assess the protection against basilar skull fracture.

The penetration test

The penetration test measures the resistance of the helmet shell to impact against sharp objects. In these tests, the helmet is positioned on a headform or a spherical device support. Then, a conical striker is dropped to hit the outer surface of the static helmet shell. The required performance criterion consists of ensuring that there is no contact between the striker tip and the headform or spherical support. The penetration test has been controversial over the last decades because the frequency of real-world motorcycle crashes involving sharp pointed objects is extremely small and some researchers stated that the penetration test causes helmets to be designed with a stiffer shell that could result in an increased risk of head injury in impacts against rigid flat surfaces (Ghajari et al., 2010). These concerns resulted in the elimination of the penetration tests from some standards (ECE, 2021), while others continue demanding this requirement as part of the helmet assessment program (DOT, 2011; FIM, 2017; JIS, 2015; Snell, 2020).

1.4.   Objective and Research Questions

The foregoing has shown that despite the effectiveness of motorcycle helmets in preventing some types of head injuries such as cranial vault fractures, other serious head injuries such as basilar skull fracture and intracranial injuries are still common lesions among helmeted motorcyclists. Interestingly, these types of injuries seem to be correlated with the existing discrepancies among current motorcycle helmet testing standards.

Therefore, the objective of this thesis is to investigate how current motorcycle helmet testing standards, with special focus on the FRHPhe-01, can be improved for reducing basilar skull fracture and intracranial injuries among helmeted motorcyclists. To this end, this thesis will investigate specifically the following research questions:

1.   How similar are EN960 headforms to human heads?

2.   Should angular measurements be included to assess helmet performance in normal impact tests?

3.   How relevant is the effect of friction at the headform/helmet interface in oblique impact tests?

4.   Is it possible to draw information to prevent basilar skull fractures from existing chin bar impact tests?

5.   Is including a penetration test beneficial for helmet performance assessment?

1.5.   Thesis Outline

In this thesis, some of the discrepancies found between relevant motorcycle helmet testing standards are analysed using mainly experimental testing methods. The thesis starts with a review of the biomechanical behaviour of the human head and a summary of real-world motorcycle crashes studies are presented together with a brief explanation of how a motorcycle helmet works.

In chapter 3, the external geometry, mass, location of the centre of gravity and tensor of inertia of EN960 headforms are compared with published human head physical properties and the biofidelity of EN960 headforms is discussed based on literature review.

Several normal impact tests were carried out in Chapter 4. Normal impact means that the component of the impact velocity tangential to the anvil surface is zero. This chapter studied if the angular motion of the helmeted headform must be considered in normal impacts and is discussed if the duration of the linear acceleration must be used as head injury assessment criterion.

Chapter 5 investigated the effect of the friction coefficient between the interior surface of the helmet and the headform in oblique impacts at different tangential velocities. The experimental data included in this chapter are particularly relevant to design helmet oblique testing protocols capable of including real-world characteristics that influence the kinematics of the helmet/head unit and therefore its injury prediction. The data gathered here highlights the importance of the friction coefficient between the head and the helmet in the resulting kinematics of the head.

Given the high probability of skull base fracture from chin bar impacts of helmeted motorcyclists, the relationship between chin bar impact tests from helmet testing standards and the risk of basilar skull fracture is studied in Chapter 6. This chapter uses an original methodology that combines physical testing and computational simulations to predict the neck axial force that a full-body would experience in a chin bar impact test using a combination of some kinematic metrics from the simple chin bar impact test using an isolated headform included in helmet testing standards.

In Chapter 7, the effect of the penetration test requirements in helmet impact performance is analysed given the controversial topic of including or not a penetration test in helmet testing standards.

Finally, the last chapter summarises the findings of this thesis, proposes new research lines and the discusses implications of this research in the field.

Chapter 2

Background

2.1.   Impact biomechanics of the human head

Crash helmets are still the most common personal protective equipment protecting the head in real-world motorcycle crashes. An effective motorcycle helmet design should be based on a thorough understanding of the impact biomechanics of the human head and on an exhaustive investigation of real-world motorcycle crashes (Otte et al., 1984).

Biomechanics is defined as the study of the mechanical behaviour of biological systems. More specifically, the role of impact biomechanics of the human head is to determine the mechanisms of injury and the human head tissue tolerance to impacts.

2.1.1.   Anatomy of the human head

The human head is composed of the scalp, the soft-tissues of the face, the skull, the meninges and the brain.

The scalp (Claessens, 1994; Ellis & Mahadevan, 2014)

The scalp is composed of five soft tissue layers that cover the cranium: the skin, connective tissue, aponeurosis, loose connective tissue, and the periosteum. The scalp serves as a physical barrier to protect the cranial vault from physical trauma.

The soft-tissues of the face (Burrows & Cohn, 2009)

The soft-tissue of the face are structures attached to the bones of the face, including epidermis, dermis, subcutaneous fascia, and mimetic musculature.

The skull (Claessens, 1994; Scanlon, 2007)

The human skull is made up of the cranium, the face and the mandible. It consists of 22 individual bones in one structural unit. The cranium is formed from 8 bones joined together by suture lines. These bones include the frontal, two parietals, two temporal, sphenoid, occipital and ethmoid (see Figure 2.1). Cranial bones are flat bones with a sandwich structure that consist of two thin layers of compact bones surrounding spongy bone. The face is formed from 14 bones including the mandible, two maxillae, two zygomatic bones, two nasals, two palatines, two lacrimal, two nasal conchae and vomer (see Figure 2.1). The purpose of the skull is to protect the brain from injury and to support the soft tissues of the face.
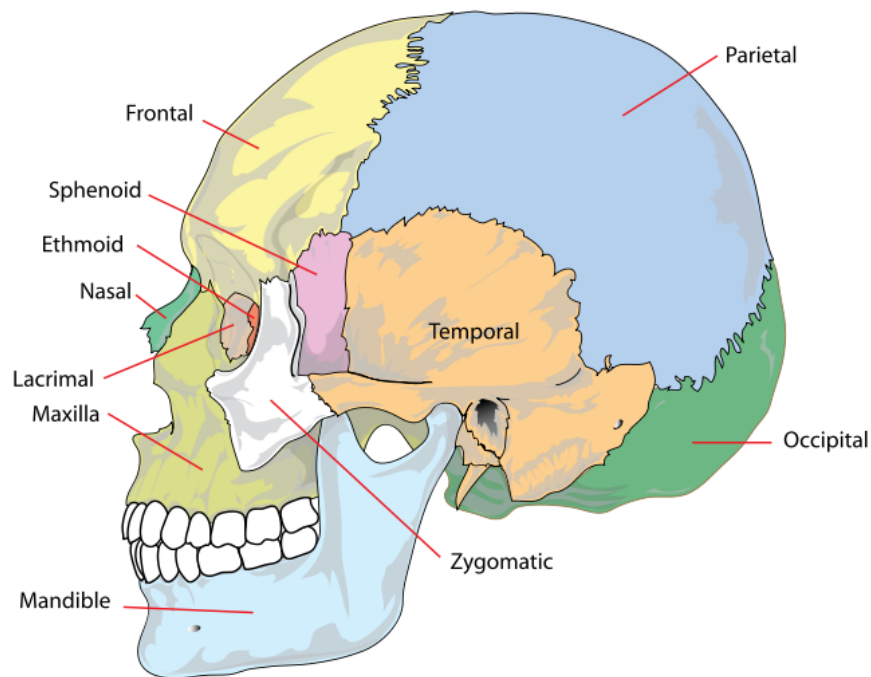
Figure 2.1: Bones of the human skull (by Ruiz M. from Wikimedia Commons, licensed under Public domain).

The meninges (Claessens, 1994; Clarke, 1944)

The meninges are three layers of tissue that envelop and protect the brain and the spinal cord. From the outside to the inside they are: the dura mater, arachnoid mater, and pia mater (see Figure 2.2).
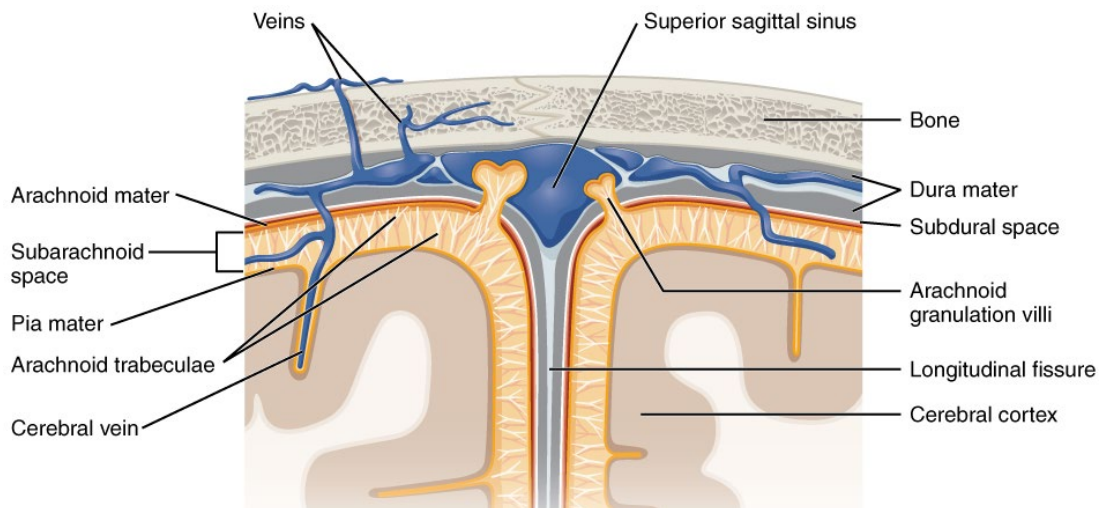
Figure 2.2: Meningeal layers (by OpenStax from Wikimedia Commons, licensed under CC BY 4.0).

- The dura mater is a strong and thick membrane. Cranial dura mater has two layers, the periosteal and the meningeal, which run together throughout most of the cranium and separate only to form venous sinuses. The dura creates little folds or compartments. There are two main folds: the falx cerebri, and the tentorium. The right and left hemispheres of the cerebrum are separated by the falx cerebri, while the tentorium separates the cerebrum and the cerebellum.
- The arachnoid mater is a thin and delicate membrane adjoined but not attached to

the inside of the dura. The potential space between the dura and arachnoid membranes is called the subdural space.

- The pia mater is a thin membrane firmly attached to the surface of the brain and loosely connected to the arachnoid layer. It lines the brain down into its folds and grooves and it has many blood vessels that reach deep into the brain. The arachnoid and pia membranes are separated by the subarachnoid space. This space is crossed by large veins called bridging veins and it is here where the cerebrospinal fluid bathes and cushions the brain. The cerebrospinal fluid is produced in the ventricular system which is a set of four interconnected cavities known as cerebral ventricles in the brain.

The brain (Claessens, 1994; Scanlon, 2007)

The brain is a complex organ that, together with the spinal cord, makes up the central nervous system. It consists of many parts that are interconnected and work as an integrated whole. The main parts of the brain are the cerebrum, the diencephalon, the cerebellum and the brainstem (see Figure 2.3).
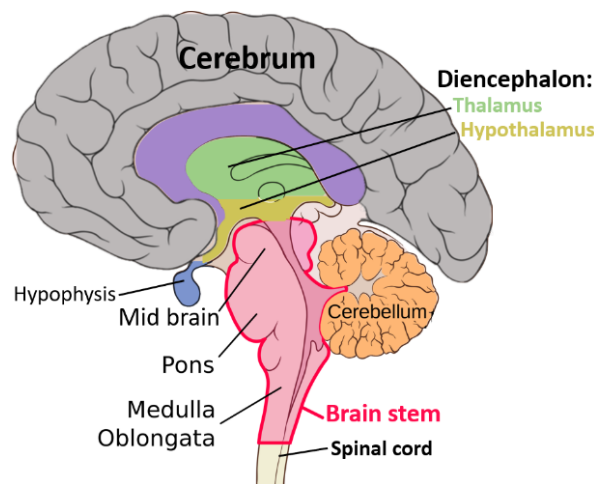
Figure 2.3: Basic structures of the brain (by Belfaqih co. from Wikimedia Commons, licensed under CC BY-SA 4.0).

- The cerebrum is the largest part of the brain and is made up of right and left hemispheres. They are connected by a band of fibres called the corpus callosum that communicate with one another. Each cerebral hemisphere is comprised of a grey matter, which has a large surface area due to its folds and it is called cortex, covering a core of white matter. Grey matter is primarily composed of the round central cell bodies (neuron somas), and white matter is mostly made of the long stems that connects neurons together (axons) wrapped in a protective coating (myelin). Each hemisphere is divided into four main functional sections, called lobes: frontal, temporal, parietal, and occipital. Once again, each lobe may be divided into areas that serve very specific functions. Some specific functions of the cerebrum include initiation and coordination of the movement, regulation of the temperature, speaking, judgment, thinking, reasoning, problem-solving, emotions, learning, vision, hearing, touch and other senses.
- The diencephalon consists of two major structures: the thalamus and the hypothalamus. It has many diverse functions such as those concerned with sensation, helps to regulate body rhythms and influences secretion of different hormones.

- The cerebellum is located under the cerebrum at the back of the head. In front of it there are the fourth ventricle, pons and medulla. Like the cerebrum, it has two hemispheres. It helps to coordinate voluntary muscle movements, maintain posture, and balance.
- The brainstem is the posterior subcortical part of the brain that connects the cerebrum and the cerebellum with the spinal cord. It is composed of the midbrain, the pons and the medulla. It performs many automatic and critical functions such as heart rate, breathing, body temperature, wake and sleep cycles, digestion, coughing, vomiting, sneezing, and swallowing.

2.1.2.   Traumatic head injuries

Traumatic head injury happens when a sudden external physical assault damages the scalp, the soft-tissues of the face, the skull, the meninges or the brain. Traumatic head injuries can be divided into primary and secondary injuries (Miller, 1993). Primary injuries are those that occur at the time of trauma as a direct result of the traumatic force such as scalp laceration, skull fracture, cerebral contusions or lacerations, intracranial haemorrhage or diffuse axonal injury whereas secondary injuries occur as a consequence of primary lesions such as ischemia, hypoxia, cerebral swelling or infection. Since the role of helmet safety standards is to prevent or minimize the risk of acute injuries sustained at the time of impact, head injuries and injury mechanisms described in this chapter refers only to the primary injuries. In general, primary head injuries can be broadly divided into three distinct varieties: skull fracture, focal intracranial injuries and diffuse brain injuries.

Skull fracture (Arregui et al., 2007; Mahapatra et al., 2012)

A skull fracture is a break in the skull bone and it can occur with or without damage to the brain. There are three major types of skull fractures: linear skull fracture, depressed skull fracture and basilar skull fracture.
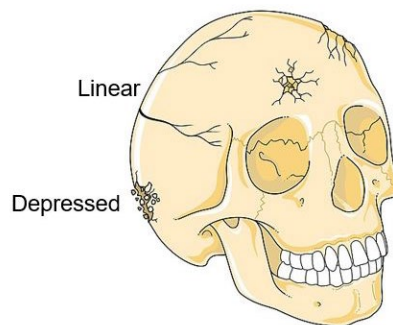
Figure 2.4: Skull fractures (adapted from Servier Medical art by Servier, licensed under CC BY 3.0).

- Linear skull fracture, there is a break in the bone that transverse the full thickness of the skull but it does not move the bone.
- Depressed skull fracture, there is a break in a cranial bone with depression of the bone in toward the brain.
- Basilar skull fracture (BSF), this is the most serious type of skull fracture, and involves a break in the bone at the base of the skull.

Focal intracranial injuries (Arregui et al., 2007; Inder et al., 2018; Mahapatra et al., 2012)

- Focal intracranial injuries result from a localized damage in or around the brain and includes contusions, lacerations and haemorrhages or hematomas.

- Contusions are bruises in the brain tissue and they result from local skull deformation or movements of the skull against blunt skull surfaces. Contusions formed at the site of impact are coup contusions while those formed at remote sites from the impact are contrecoup contusions.
- Lacerations are tears in the brain tissue and they are caused by penetrating objects, the sharp edges of fractured skull bones or movements of the skull against sharped skull surfaces.
- Haemorrhage is a bleeding in or around the brain while hematoma is a collection of blood in or around the brain. The bleeding or collection of blood can occur anywhere between the dura mater, arachnoid, pia mater and inside the brain tissue.
  - Epidural hematoma occurs when blood dissects into the potential space between the dura and inner table of the skull. This usually occurs after a skull fracture.
  - Subdural hematoma (SDH) occurs when the blood enters in the space between dura mater and arachnoid mater. The clotting can lead to pressure building up inside the skull which can cause loss of consciousness or result in permanent brain damage.
  - Subarachnoid haemorrhage (SAH) is a bleeding between the arachnoid membrane and the pia membrane. Head trauma is the most common cause of SAH however the injury mechanism of traumatic SAH is still unknown.
  - Intracerebral haemorrhage (ICH) is an acute loss of blood from a damaged blood vessel into the brain. The signs and symptoms will correlate with the location of the damage.

Diffuse brain injuries (Mahapatra et al., 2012; Mesfin et al., 2022; Mullally, 2017)

Diffuse brain injuries are associated with widespread damage in the brain and includes cerebral concussion and diffuse axonal injury.

- Cerebral concussion, also known as mild traumatic brain injury (mTBI), occurs when the impact on the head is severe enough to affects the brain function creating a series of neurochemical changes. Effects can include loss of consciousness, headaches and problems with concentration, memory, balance and coordination. The effects are usually temporal, however, repeated concussions may lead to develop a progressive neurodegenerative disorder.
- Diffuse axonal injury (DAI): DAI is associated with mechanical disconnection or malfunction of neurons interconnection. It commonly affects white matter involved in the corpus callosum, brainstem and axons at the junction of the grey and white matter. Clinically, patients with DAI can present a spectrum of neurological dysfunction, however, most patients are identified to be severe.

2.1.3. Mechanisms of head injury

Knowledge of the mechanism of injury in head trauma is important for the correct development of effective helmets against head injuries. The mechanism of injury describes the particular circumstances that caused a specific injury. From the tissue-level deformation point of view, strains are the principal causes of injury. Strain is the amount of deformation that the tissue undergoes as a result of a mechanical loading. Traumatic injuries are often caused by one of the three types of strains: compression, tension, and shear. The specific

injury that results from a particular circumstance is determined by the type and location of the induced strains and by ability of the affected tissue to endure the effects of those particular strains (Gennarelli, 1985).

Despite the fact that it is possible to measure the human brain motion under potentially injurious loading (Alshareef et al., 2020), the measurement of brain strain in physical anthropomorphic test devices is currently impossible. Therefore, measurable variables from head kinematic are used as alternative parameters to characterize the mechanisms of head injuries. One of the well-known debates in the field of head injury biomechanics has been how linear or rotational kinematics contribute to intracranial injuries. Since Holbourn (1943) hypothesized that rotational motion of the brain could explain some head injuries unlikely to be caused by translational motion, a substantial amount of research has supported the relationship between head rotation and intracranial injuries (Alshareef et al., 2020; Gennarelli et al., 1971; Zhang et al., 2006). The principal mechanism of linear kinematic appears to be pressure gradient which creates shear stresses that result in local deformation of brain tissue (Gurdjian et al., 1968) while rotational kinematic creates shear stains and produces rotation of the skull relative to the brain (Gabler et al., 2018; Unterharnscheidt, 1972). However, pure translation or pure rotation of the head are very rare in real-world motorcycle crashes and a combination of both types of motion can often cause severe brain injuries. This has led to theories assuming that despite head rotation is the key factor in producing brain damage, a combination of translational and rotational motion is considered as a more plausible source of injury (Bandak & Eppinger, 1994). Although brain injury mechanisms are still principally at the hypothesis level, the dominant hypothesis of the mechanisms of head injuries are included in Figure 2.5.
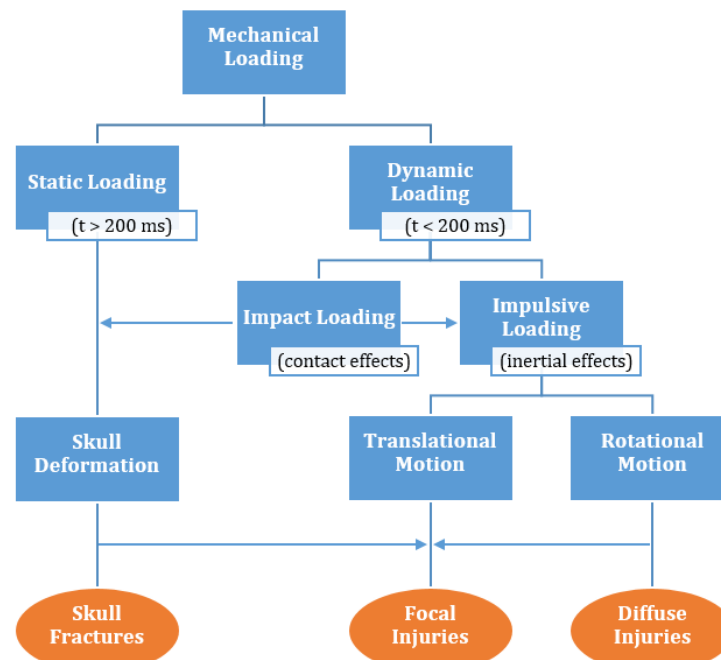
Figure 2.5: Diagram of the mechanisms of traumatic head injuries.

Two types of mechanical loading can be considered depending on the time over the forces are applied. Static loading includes forces applied gradually over 200 ms or longer whereas dynamic loading involves forces applied in less than 200 ms and in most cases in less than 50 ms (Gennarelli, 1985). Dynamic loading is the most common cause of head

injury in real-world motorcycle crashes and it can be initiated either by direct blows to the head (impact loading) or by sudden movement of the head (impulse loading) produced by impacts elsewhere. In general, injuries from skull deformation such as skull fractures are caused by contact forces that occur during impact. Since most impacts also set the head into motion, skull deformation injuries have often overlapped with injuries from head motion (inertial effects). Head motion injuries are the result of a sudden movement of the head, regardless of whether the head moves due to a direct impact or not. The type of head injury that occurs depends on the type of motion (translational motion or rotational motion), the amount of motion, the direction and duration of head movement (Gennarelli, 1985). Considering these two types of head motion, translational motion produces only focal intracranial injuries such as contusions, lacerations and hematomas or haemorrhages while rotational motion is considered to produce both focal and diffuse brain injuries such as cerebral concussion and DAI (Kleiven, 2013).

2.1.4. Biomechanical tolerance of the human head

The biomechanical tolerance of the human head is the ability of the human head tissues and bony structures to endure the effects of a mechanical impact loading without sustaining any type of injury. Bone, vascular and brain tissues have the common property of being more able to resist compression strains than shear strains, with a tolerance for tensile strain somewhere in between. In the case of bone, the difference between the three strain tolerances is proportionally smaller, while in the case of brain there is a considerable difference in its ability to resist compression and shear (Gennarelli, 1985).
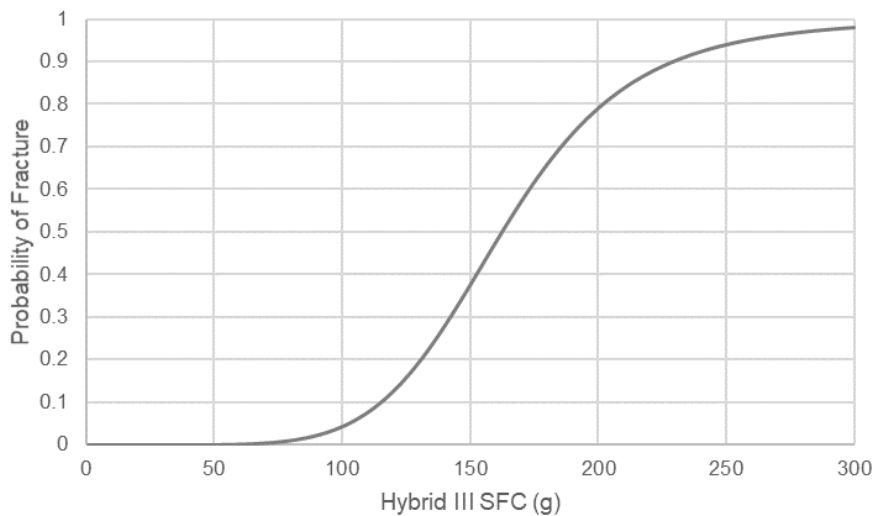
Figure 2.6: Plot of the probability of linear skull fracture vs. skull fracture criterion (SFC) for the Hybrid III. Source: (Chan et al., 2007).

The tolerance of biological tissues and bony structures is assessed by a parameter called injury criterion. An injury criterion is a physical parameter which correlates well with the injury severity under consideration. The biomechanical tolerance limit is the maximum value of the injury criterion for which a specific injury occurs in an individual. The variation of the biomechanical tolerance limit among different individuals lead researchers to define injury risk curves. Injury risk curves predict the chance of sustaining an injury at a specific value of the injury criterion (see Figure 2.6). Some biological tissues may exhibit anisotropy, their tolerance to strain changes in different directions (Takhounts et al., 2013), and as biological tissues are viscoelastic, their tolerance to strain changes with the rate at which

the mechanical load is applied (Wood, 1971). In order to consider these properties of the biological tissues, some researchers have defined some injury criteria as a function of several physical parameters.

Each type of head injury involves a specific head tissue and it is governed by a certain injury mechanism (Kleiven, 2013). Therefore, the biomechanical tolerance of the human head must be addressed with a multi-tolerance approach in which there is a tolerance limit for each specific head injury. Since the purpose of a motorcycle helmet is head protection against skull fractures and intracranial injures and clinical studies have demonstrated that SDH and DAI are the two worst types of intracranial injuries that result in permanent disability or even death (Gennarelli, 1983), the human head tolerance to skull fracture, SDH and DAI are presented in this section.

Skull fracture

The skull fracture tolerance and type of fracture are dependent on hardness and geometry of impacting structure. Impacts against flat targets, in which the force is transferred over a wide area of the skull, are the common cause of linear skull fractures while impacts against concentrated surfaces, in which the force is distributed over a small area of the skull, are the common cause of depressed skull fractures. In general, fractures occur at lower impact speeds against harder surfaces than softer ones (Hodgson & Thomas, 1973) and the force required to fracture the skull in impacts against hemispherical surfaces decreases as the radius of the surface decreases (Hodgson & Thomas, 1971). In addition, skull fracture tolerance is also dependent on the different anatomic regions of the human skull (Yoganandan & Pintar, 2004). Linear skull fractures are the most common type of skull fractures. The skull fracture criterion (SFC) is the average linear acceleration over the head injury criterion (HIC) time interval (Vander Vorst et al., 2003). It assumes that forces are applied over a wide impact area and the fractures that occur are linear skull fractures. Its biomechanical basis was demonstrated by its good correlation with the skull strain for different anatomic regions of the human skull and for various flat target compliances. The SFC of 124 g corresponds to 15% mean probability of fracture (Chan et al., 2007).

Basilar skull fractures require neck compressive or tensile loading to occur. However, a direct temporomandibular loading in conjunction with tensile neck loading seems to be the most probable loading condition that can produce BSF. An upper neck tensile load of 4300 ± 350 N is considered as a biomechanical tolerance limit for BSF (McElhaney et al., 1995).

Subdural hematoma (SDH)

Subdural haematoma is caused by motion of the brain relative to the skull which can break bridging veins. This injury is sensitive to the rate at which the head is accelerated and to the impact direction. It is produced by short duration and high amplitude of angular accelerations (Gennarelli & Thibault, 1982) and it is more likely to be produced in the sagittal plane (Kleiven, 2003). Depreitere et al. (2006) carried out a cadaveric study of SDH resulting from bridging vein rupture and they reported a biomechanical tolerance limit of approximately 10 krad/s^2 for pulse durations shorter than 10 ms.

Diffuse axonal injury (DAI)

Brain strains are dependent in a very complex manner to the mechanical properties of the multi-component, anisotropic inhomogeneous brain as well as the location of bony protrusions, dural partitions, vascular anatomy, and other sources of tissue interfaces with

different densities (Ommaya & Gennarelli, 1974). Gennarelli et al. (1987) demonstrated that the brain has directional sensitivity to the brain damage and recently, a human brain biomechanics study showed that head rotation in the axial plane caused the largest brain displacements while sagittal and coronal directions had similar displacement magnitudes (Alshareef et al., 2020). Alshareef et al. (2020) also showed that brain motion depends on the angular velocity and duration of the rotation pulse, increasing angular velocity and decreasing pulse duration resulted in larger brain displacements across all loading directions.

Margulies & Thibault (1992) presented a DAI criterion specific to lateral rotations of the head. It was developed by experiments on primates in combination with physical gel models and analytical scaling procedures. This criterion is represented by curves delimiting equal strain levels in the analytical model as a function of angular acceleration and maximum angular velocity change. Rotational accelerations exceeding 10 krad/s^2 combined with a rotational velocity of 100 rad/s or higher suppose a risk of DAI (Margulies & Thibault, 1992). Gennarelli et al. (2003) reviewed tolerances suggested for concussion and DAI to describe tolerances for different severities of DAI and concussion, proposing the angular acceleration values given in the second column of the Table 2.1. Later, Zhang et al. (2008) established angular velocity tolerances (given in the third column of the Table 2.1) based on the angular acceleration tolerances proposed by Gennarelli et al. (2003) for a spectrum of diffuse brain injury. Recently, Gennarelli, (2019) re-analysed three old groups of experiments (Gennarelli et al., 1971, 1982; Gennarelli & Thibault, 1982) leading him to propose the revised angular acceleration tolerances included in the fourth column of the Table 2.1.

Table 2.1: Biomechanical tolerance limit for different severities of DAI and concussion.

Injury severity	Angular acceleration (rad/s^2)	Angular velocity (rad/s)	Revised Angular acceleration (rad/s^2)
Mild cerebral concussion	3000	25	6000
Classical cerebral concussion	4500	50	9000
Severe cerebral concussion	8000	75	16000
Mild DAI	12000	100	24000
Moderate DAI	14500	125	29000
Severe DAI	16500	150	33000

However, the contribution of contact phenomena, such as skull deformation, to diffuse brain damage has not yet been adequately determined. Ommaya & Hirsch (1971) discovered that about twice of head rotation was required to produce cerebral concussions in rhesus monkeys by indirect impact (whiplash) than when the head received direct occipital impacts.

2.2. Investigation of real-world motorcycle crashes

Real-world motorcycle crash investigations have the potential to improve the head protection for helmeted motorcyclists. These investigation studies can highlight both the basic conditions of a helmeted head impact, such as the impact velocity vector of the head, the helmet damage and the impact object or surface, which can be very useful for the definition of the impact tests for motorcycle helmet testing standards. In addition, knowing the head injuries occurring in real-world crashes is essential to select appropriate head injury criteria.

Impact velocity vector of the head

The impact velocity vector of the head describes both the speed and direction at which the head is moving at the moment of impact. The impact velocity vector of the head can be decomposed into two components: a normal component perpendicular to the impact surface and a tangential component parallel to the impact surface. In a rider ejection from the motorbike, the normal component is related mainly to the height of the rider's fall on the ground while the tangential component is associated to the motorcyclist's travelling speed (Lloyd, 2016). In real-world crashes, the determination of the head impact velocity vector is very difficult because of the complexity of the impact kinematics. Therefore, some real-world motorcycle investigations do not report the impact velocity vector of the head but based on the helmet damage patterns, they classify the impact type as normal or tangential impacts, which gives an indication of the direction the impact velocity of the head. Liner crush beneath the impact site and shell cracks reveal the presence of a normal component of the impact velocity (normal impacts) while scratches reveal the presence of a tangential component of the impact velocity. Dowdell et al. (1988) presented data obtained from the examination of 200 motorcycle crashes, 72 fatal and 128 non-fatal cases, collected from April, 1985 to September, 1986 in a study focussed on the improvement of the design of Australian Motorcycle Helmet Standard (AS1698) approved helmets. They concluded that there were twice as many tangential impacts as there were normal however the 73% of the severe impacts were classified as normal. Whyte et al. (2015) assessed the type of helmet damage in 69 non-fatal real-world crashes and reported that tangentially directed force damage was more common (62.5%) than normally directed force damage (44.9%) and 24.6% of cases had areas of both types of damage.

Chinn et al. (2001) during the COST 327 project development process, analysed 253 motorcycle crashes that were collected within a three year period from July 1995 until June 1998 in Finland, Germany and the United Kingdom. They reported the cumulative frequency of estimated head impact speed for all 181 cases where the speed was known, showing that the 50% cumulative frequency occurs at approximately 44 km/h (12.2 m/s). They also reported the angle of body impact and the head impact angle to conclude that 68% of the cases occurred at an angle of 30 degree or less to a line vertically through the body whereas 19% were at an angle greater than 60 degrees. Bourdet et al. (2016) used multibody systems to reconstruct the kinematics of 19 motorcyclists during a real-world collision in order to extract the head impact conditions in terms of head impact point and crash velocity vector. The results of this study were added to pervious crash reconstructions for a total of 56 real-world motorcycle crashes. They observed that the mean impact angle was 44 ± 22 degrees with an impact velocity of 11.2 ± 6.2 m/s, which showed the importance of tangential velocity during real-world motorcycle crashes.

The reviewed real-world motorcycle crash investigations highlight the importance of the direction of the head impact velocity. While a tangential component of the head impact velocity is present in most of the real-world crashes, the normal component is strongly related to the severity of the impact.

Helmet damage

Otte et al. (1984) reported the results of a study of the Federal Highway Department Cologne which documented, reconstructed and analysed 272 motorcyclist involved in crashes, with and without helmets. They found damage to the helmet in 70.2% of the cases and pointed out the high frequency of impact points in the forehead and chin region on the

right side as well as on the left side. The 200 helmets examined by Dowdell et al. (1988) received an average of two impacts each with a total of 401 impacts (137 fatal, 264 non-fatal). They reported that almost 50% of severe impacts were frontal, only 10% of all impacts were to the top and 35% of all impacts were outside of the AS1698 test area with 40% of these impacts to the chin bar region.

Otte (1991) compared the defined test conditions of the United Nations Economic Commission for Europe (ECE) regulation with 598 integral helmet-protected motorcyclists involved in real-world crashes in the area of Hannover from 1973 to 1989. He observed that 63.5 % of the helmets had an impact point on the exterior of the helmet shell, 14.9% had two impact points, 0.2% impacted more than twice and 21.5% of the helmets were not impacted. An impact to the chin region was established with 23.1% of the integral helmets and 18.3% of impact points on the crashed helmets were located in the forehead just above the visor. Chinn et al. (2001) reported that scratch was the most frequent type of damage followed by deformation and cracks with the location of damage distributed fairly evenly, except for the crown, with 26.9% lateral right, 26.3% lateral left, 23.6% frontal, 21.0% to the rear and 2.2% to the crown . They highlighted that the chin guard was a frequently damaged region (15,4%), together with the right and left temporal fossa region (9.6% and 8.8% respectively). Whyte et al. (2015) observed damage to the helmet in 76 cases and reported that scratches were most common type of damage (observed in 72 cases), followed by cracks to the shell (16) and liner damage (10). The damage on 65 inspected helmets was mainly located on the face (despite 11 open face helmets and 5 without visor) and the remainder of the damage was concentrated in a band around the sides and the rear of the mid-level of the helmet with relatively infrequent damage to the crown (Whyte et al., 2015).

Most of the reviewed real-world motorcycle crash investigations pointed out that the front of the helmet, including the chin region, was the most frequently damaged region while the crown was the least frequently damaged region.

Impact object or surface

Otte et al. (1984) reported that the most frequent impact object for the head was the road (35.7% of non-helmeted motorcyclists and 59.8% of helmeted motorcyclists) and that the shape of the impact object that caused injuries was predominately flat (65.7%) and in 24.1% edged respectively arched. Dowdell et al. (1988) found that impacts against sharp pointed objects were almost non-existent but there were severe local loading that resulted in penetration of the helmet shells. In a different study, Otte (1991) registered that 69.4% of the impacts were caused by the road and 22.3% by a vehicle. He reported that the shape of impact objects was flat in 72% of all impacts and edged in 28%. Chinn et al. (2001) found that a round object was impacted in 79% of cases, an edge object in 4% but it was the most likely to cause a severe injury and a flat object was struck in 9% of cases but was the least likely to cause an injury. Piantini et al. (2016) analysed a sample of 40 serious urban road crashes involving powered two-wheelers and other vehicles, in order to provide more recent data on serious motorcycle collisions in terms of crash configurations and injury causes. They reported that for primary impacts, the windscreen was the major injury source with 53.3%, followed by pillars (15.6%) and door (11.1%) and the ground was the most harmful cause for secondary impacts.

The reviewed real-world motorcycle crash investigations showed that the shape of impact objects was predominately flat or slightly rounded while impacts against edged or considerably rounded objects or surfaces were less frequent but were associated with an

increased risk of injury.

Head injury type and severity

Otte et al., (1984) observed that although helmet-protected motorcyclists outnumbered unprotected motorcyclists in their study, about 73% of all injuries were recorded in the latter. They found that approximately 33% of all injuries to helmet-protected and unprotected heads of motorcyclists were minor soft-tissue injuries and more serious soft-tissue injuries such as lacerations and contusions accounted for a further 22% of helmet-protected heads and 26% of unprotected heads. Concussion occurred in 29% of those wearing helmets and 17% of those not wearing helmets while serious injuries, such as fractures and contusions, accounted for only 16% of injuries in helmet-protected heads and 24% in unprotected heads.

Dowdell et al. (1988) found that all injuries recorded in non-fatal cases were, with one exception, of AIS 3 severity or lower and these injuries were usually related to loss of consciousness. They also reported that 67% of the AIS 3 head injuries were to the brain and the remainder were base of skull and vault fractures, 45% of the AIS 4 head injuries were subdural haematomas, another 42% were to the brain and the remainder were cranium fractures. All AIS 5 head injuries and 45% of AIS 6 head injuries involved the brain stem. Otte (1991) revealed that of all impact types the chin impact causes the injuries with the most severe consequences. He also found that about 72% of all head injured motorcyclists sustained soft-tissue injuries, 26% suffered fractures of which 47% experienced skull base fractures, and 63% suffered brain injuries of which 69% sustained concussion.

Within the COST 327 database, Chinn et al. (2001) observed that of the motorcyclists who sustained a head injury, 28.9% sustained only a minor injury (AIS 1), 16.7% sustained a moderate injury (AIS 2), 11.1% sustained AIS 3 and the same proportion sustained AIS 4 head injuries, 16.7% of riders sustained an AIS 5 head injury and almost the same proportion (15.6%) sustained a fatal head injury (AIS 6). In a special COST 327 study, 81 cases were selected with 409 head injuries AIS 2 and greater sufficiently comprehensive for detailed analysis. Within this reduced database, they reported that 18.5% of the injuries were soft tissue injuries, 23.6% were skull injuries and 57.1% were brain injuries of which 27.8% were subarachnoid bleeding and 21% subdural haematoma (Chinn et al., 2001).

Whyte et al. (2016) provided a description of the specific impact type and the resulting injury out-come. They reported that at the point of impact, facial fracture occurred in 21% of the 47 fatal cases and cranial vault fracture in 26%. They also found that remote contact basilar skull fracture occurred in 66% of the cases and inertial injuries to the brain occurred in 49% of the cases. Underlying local contact brain contusions/lacerations were observed in 92% of the cases with cranial vault fractures while contusion/laceration of the brain or brainstem were associated to 71% of the cases with a remote fracture. Finally, Piantini et al. (2016) found that 22 out of 40 motorcyclists reported 82 head injuries of which 65% were intracranial and 32% to skull. They reported that cranium suffered injuries mostly to the base (69%) and vault (26.9%) and that cerebrum was the intracranial organ most subject to injuries (96%). The most frequent intracranial injury type was contusion (28%) followed by intraventricular haemorrhage (19%) and subdural hematoma (17%).

The reviewed real-world motorcycle crash investigations showed that despite the success of the motorcycle helmet in preventing local cranial vault fractures, serious head injuries such as BSF and intracranial injuries are still common lesions among helmeted motorcyclists and therefore, the head still needs a more adequate level of protection.

2.3.   How motorcycle helmets work

After the introduction of the motorcycle in the early 1900s, the need for a crash helmet arose. Despite the fact that the concept of hard shell helmets dates back to the medieval times, first motorcycle helmets used in racing events were no more than leather bonnets usually worn with googles (Newman, 2005). Their main purpose was to keep the head comfortable and they offered almost no protection to the head. Since then, the crash helmet evolved based on a broad understanding of what a helmet should do. The basic principles have always been to provide a hard outer shell to protect against external agents and padding to help cushion the blow. The first hard shell motorcyclist helmet was made of several layers of cardboard glued in the early 1930s. Later, linen or other fine cloth impregnated with varnish resins was used. In 1953, Roth and Lombard altered crash helmet design in ways that have basically not changed since then filling the gap between the head and the hard shell with crushable material such as polyurethane foam (Newman, 2005). Since the publication of the first crash helmet standard by the British Standard Institute (BS 1869) in 1952, what actually constituted a helmet was no longer at the helmet manufacturer's discretion. Therefore, the evolution of crash helmets is not side by side with the evolution of the understanding of head impact biomechanics, but follows the evolution of standards, which means that even if a standard is outdated from a biomechanical perspective, helmets would continue being manufactured according to the standard in place (Fernandes & Sousa, 2013).

A current motorcycle helmet generally consists of four main parts: the outer shell, the protective padding liner, the comfort padding liner and the retention system as shown in Figure 2.7.

- The outer shell, which directly experiences the impact, has three main functions to protect the head. It distributes the impact load on a wider area of the underlying liner, prevents from penetration of sharp objects and protects the protective padding against abrasion. In addition, it can also contribute to the impact energy absorption. Helmet shells are commonly made of thermoplastic materials such as polycarbonate (PC) or acrylonitrile-butadiene-styrene (ABS) and composite materials such as fibre reinforced plastic (FRP). The main advantage of using composite materials lies in their ability to absorb more energy by rupture compared to thermoplastic materials, especially at high impact velocities. However, stiffness of FRP shells is higher than the stiffness of thermoplastic shells and it has an important influence in the overall dynamic performance of the helmet (Beusenberg & Happee, 1993). Helmets shells are already very smooth to reduce friction between the impacted object and the helmet in order to address the absorption of rotational energies during head impacts.

- The protective padding liner provides the main contribution to the impact energy absorption during the impact. The impact load dispersed by the outer shell is attenuated by the protective padding liner increasing the distance and period of time over which the head stops. It is often made of crushable foams such as expanded polystyrene (EPS) and sometimes in combination with other materials such as expanded polypropylene foam (EPP). The EPS density is an important property because the yielding stress at which the foam crushes is directly related to it (Fernandes & Sousa, 2013). EPS with higher densities are able to absorb larger amounts of energy than EPS with lower densities, but transfer higher forces localized at the impact point (Di Landro et al., 2002).

- The comfort padding liner increases the wearing comfort of the helmet and provides a good fit on the head. It is generally made of soft and flexible open cell foams such as polyurethane (PU) or polyvinyl chloride (PVC) faced with a cloth layer. As a result of the low stiffness, the comfort padding liner crushes completely without absorbing any relevant amount of energy during an impact.
- The retention system, or chin strap, should retain the helmet attached to the head during an impact. It generally consists of a strap bolted to each side of the outer shell and it is usually made of polyethylene terephthalate (PET) or nylon.
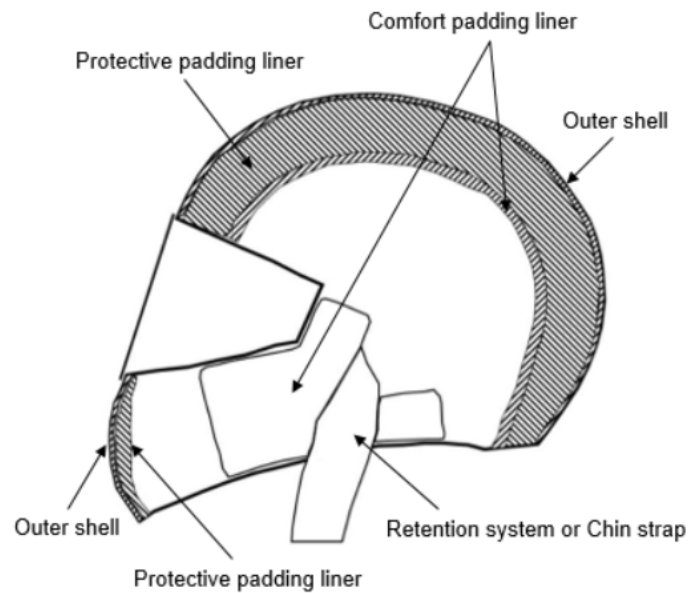
Figure 2.7. Main parts of a motorcycle helmet.

Chapter 3

Mass and Inertia Properties of EN960 Headforms and Human Heads

3.1. Introduction

Physical models that simulate human heads (anthropomorphic test devices/headforms) are required to assess helmet protection in helmet testing standards. Most helmet test methods involve simplified impacts in the laboratory where only the peak of the resultant translational acceleration is measured at the centre of gravity of a headform. In these simplified test methods, most helmet testing standards currently use rigid headforms with a defined mass and a very simplified representation of a human head shape. These headforms have been used successfully for many years as a human head surrogate in helmet testing and have undoubtedly contributed to improvements in helmet design (Liu et al., 2008; MacLeod et al., 2010).

However, studies have shown that rotation of the head during an impact is the leading cause of most intracranial injuries (Holbourn, 1943; Kleiven, 2013) and that intracranial injuries can occur ever if helmets were effectively reducing the peak of the linear acceleration of the head (Whyte et al., 2016). Since oblique impacts between the helmet and the ground are the most frequent collision scenarios in real-world crashes (Bourdet et al., 2016; Chinn et al., 2001) and can produce substantial rotation of the head, some researchers have proposed different laboratory testing protocols to represent the human head in oblique impacts (Aare & Halldin, 2003; Aldman et al., 1976; Halldin et al., 2001; Pang et al., 2011).

Consequently, two helmet testing standards have included an oblique impact test method using an instrumented headform to assess the angular motion of the helmeted headform (United Nations Economic Commission for Europe [ECE], 2021; International Motorcycling Federation [FIM], 2017). Both helmet testing standards use detached full headforms based on the EN 960 standard (European Committee for Standardization [CEN], 2006) for the oblique impact test. The EN 960 standard only specifies the external geometry, mass and location of the centre of gravity, but no inertial properties are required. However, an oblique impact test method requires a headform with a well-defined and biofidelic inertia tensor. Despite EN960 headforms were not initially designed for measurements of rotational kinematics, they were selected as human head surrogates in oblique test methods probably due to their widespread use in helmet testing standards and their availability in

different sizes. To address the rotational design limitation of the EN960 headforms, their moments of inertia were specified in the corresponding helmet testing standards (ECE, 2021; FIM, 2017). However, the biofidelity of the EN960 headforms in terms of inertia used in helmet testing standards has not been validated. Bonin et al. (2017) compared the dynamic response between cadaver heads and standard headforms, but rotational kinematics was not studied. Connor et al. (2019) compared the mass and inertia properties of two EN960 headform sizes with a human head cadaver dataset however, the moments of inertia of the EN960 headforms used in that study do not correspond with the moments of inertia defined in the helmet testing standards for the EN960 headforms.

In this chapter, a dataset of human head physical properties was created based on a review of a selection of human cadaveric studies. This dataset includes a larger dataset than the one used in Connor et al. (2019). The aim of this chapter is to compare the physical properties of EN960 headforms defined for helmet testing standards with those of a set of human heads and discuss their influence in the impact test methods defined in helmet testing standards.

3.2. Materials and Methods

This chapter reviews published cadaver studies to define the anthropometry and mass properties of human heads and compare them with those of a EN960 headform family compliant with the 06 series of amendments of the ECE Regulation 22 (ECE 22.06) and the FIM Racing Homologation Programme for helmets (FRHPhe-01) (ECE, 2021; FIM, 2017).

3.2.1. Human head data

Several published cadaver studies were reviewed to define the external geometry (length, breadth and circumference), mass, centre of gravity location and inertia tensor of human heads. However, published cadaver studies had different objectives and did not necessarily present all the above mentioned physical properties for each subject studied. Therefore, different sets of published data had to be used for each physical property. To ensure comparability, studies were chosen where the head was removed from the neck in a similar dissection plane.

Hodgson & Thomas (1971, 1973) studied the impact tolerance of the human skull against different impact surface hardness and geometries using eighty embalmed cadavers. Isolated head data from some cadavers were published. The head dissection plane was not reported in this study. However, Hodgson et al. (1972) used 13 head data from the previous study (those whose circumference fell into the 56-58 cm range) to develop a human head model and the head dissection plane was then reported. The heads were decapitated on a plane running from the base of the occiput to the base of the mandible (Hodgson et al., 1972).

Walker et al. (1973) determined the mass, volume, centre of mass, and mass moment of inertia of the head and the head and neck for 20 embalmed male cadavers. The head was separated from the neck along a plane that originates just below the external occipital protuberance, and continues anteriorly and inferiorly through the atlanto-occipital joint to a point anterior to the prevertebral muscle mass. At this point, it intersects with a plane that originates at a point immediately inferior to the hyoid bone and extends superiorly and posteriorly to the intersection described above.

Chandler et al. (1975) measured the mass, centre of mass location and principal

moments of inertia of six embalmed cadavers. Beier et al. (1979) determined the centre of gravity and moments of inertia of 21 unpreserved human heads. Albery & Whitestone (2003) published human head mass properties from 15 unpreserved cadavers and later, Ching (2007) reported additional anthropometry data for the same specimens. Head segmentation of the last three mentioned data sets was performed using a technique similar to the one used in Walker et al. (1973).

Length, breadth and circumference of human heads

Since standard headforms use a circumference-based sizing system, in this chapter the relationship between the circumference and length or breadth of the human head is analysed. To calculate the length-circumference and breadth-circumference relationships, 63 data from Hodgson & Thomas (1971, 1973), 6 data from Chandler et al. (1975) and 14 data from Ching (2007) were used. The data are represented in Table A1 in the Appendix. Simple linear regression using ordinary least squares was used to obtain an equation to calculate head length or breadth for a given circumference with the corresponding 95% prediction intervals. Correlations between head length or breadth and circumference were based on the coefficient of determination (R^2). Testing if the regression line is a good fit was evaluated with a significance level of 0.05.

Mass of human heads

Due to the sizing system of the headforms, mass of the head was given for a particular head circumference size. To calculate the mass-circumference relationship, 67 data from Hodgson & Thomas (1971, 1973), 6 data from Chandler et al. (1975) and 14 data from Ching (2007) were used. The data are represented in Table A2 in the Appendix. Simple linear regression using ordinary least squares was used to obtain an equation to calculate head mass for a given circumference with the corresponding 95% prediction intervals. Correlation between head mass and circumference were based on the coefficient of determination (R^2). Testing if the regression line is a good fit was evaluated with a significance level of 0.05.

Centre of gravity location of human heads

Since mass-circumference relationship have already been defined and centre of gravity (CG) and inertia tensor properties are more frequently reported together with the head mass instead of the head circumference, these head properties were given for a particular head mass instead of a particular head circumference size in this chapter.
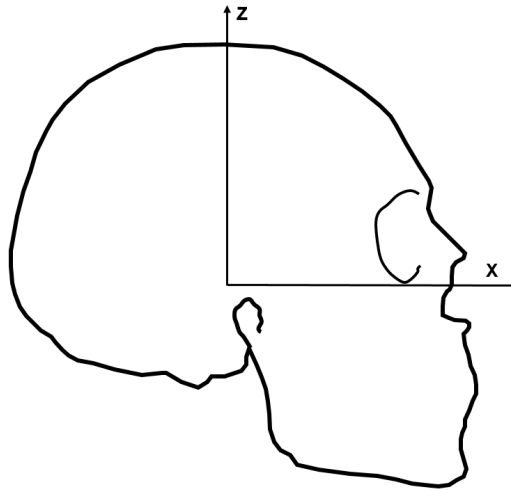
Figure 3.1: Head anatomical coordinate system.

First of all, it is necessary to describe a head anatomical coordinate system for the centre of gravity location and the inertia tensor. The chosen head anatomical coordinate system is based on the Frankfort plane of the head (Figure 3.1). The coordinate system has its origin at the midpoint of a line between the external auditory meatuses. The X-axis is positive anteriorly and passes through a plane horizontal to the most inferior point of the right inferior orbital margin. The Z-axis lies in the mid-sagittal plane, 90° from the X-axis, and is positive superiorly. The Y-axis is a line between the midpoint of each external auditory meatus, is positive toward the left meatus and is perpendicular to the mid-sagittal plane.

The CG location is the average location of all the weight of an object. Due to the symmetry of the human heads, it was assumed that the CG was located in the mid-sagittal plane of the head. Beier et al. (1979) concluded that the centre of gravity is located almost exactly in the mid-sagittal plane of the head. Therefore, the centre of gravity location in the X-axis (CG_X) and the centre of gravity location in the Z-axis (CG_Z) were given for a head mass with respect to the origin of the coordinate system. To calculate the CG_X-mass and CG_Z-mass relationships, 17 data from Walker et al. (1973), 6 data from Chandler et al. (1975), 21 data from Beier et al. (1979) and 14 data from Albery & Whitestone, (2003) were used. Walker et al. (1973) determined the CG location by photographs and radio-graphically. The location of the CG performed radio-graphically was used in this study because it was referenced using the anatomical coordinate system. The CG_X and CG_Z were calculated from the given distance and angle. The data are represented in Table A3 in the Appendix. Simple linear regression using ordinary least squares was used to obtain an equation to calculate CG_X or CG_Z for a given mass with the corresponding 95% prediction intervals. Correlations between CG_X or CG_Z and mass were based on the coefficient of determination (R^2). Testing if the regression line is a good fit was evaluated with a significance level of 0.05. Moreover, a scatter plot was used to show the CG location in the mid-sagittal plane including a 95% probability ellipse for the CG_X versus CG_Z data.

Inertia tensor of human heads

The rotational inertia of a body is a quantity that determines the torque needed for a desired angular acceleration about a rotational axis. The inertia tensor is a symmetric 3 x 3 matrix for a set of perpendicular axes which describes the rotational inertia for bodies free to rotate in three dimensions. The diagonal elements in the inertia tensor are called moments of inertia while the rest of the elements are called products of inertia. Every fixed

point in a body has a specific inertia tensor and the inertia tensor at a specific point depends on the orientation of the coordinate system. Every object has a set of mutually perpendicular principal axes for which the inertia tensor is diagonal and torques around the axes act independently of each other.

The inertia tensor of human heads in this study was given with respect to the centre of mass and the anatomical coordinate system above described. Since the human heads can be considered symmetric with respect to the mid-sagittal plane there is only one non-zero product of inertia. Therefore, moment of inertia around X-axis (I_{XX}), moment of inertia around Y-axis (I_{YY}), moment of inertia around Z-axis (I_{ZZ}) and the non-zero product of inertia (I_{XZ}) were given for a head mass with respect to the centre of gravity and according to the anatomical coordinate system. Since some published cadaver studies did not present all the elements of the inertia tensor for each head studied, different sets of published data were used for each moment or product of inertia. To calculate the I_{XX}-mass relationship, 7 data from Hodgson & Thomas (1971), 6 data from Chandler et al. (1975), 20 data from Beier et al. (1979) and 14 data from Albery & Whitestone (2003) were used. To calculate the I_{YY}-mass relationship, 31 data from Hodgson & Thomas (1971), 17 data from Walker et al. (1973), 6 data from Chandler et al. (1975), 20 data from Beier et al. (1979) and 14 data from Albery & Whitestone (2003) were used. To calculate the I_{ZZ}-mass relationship, 6 data from Chandler et al. (1975), 20 data from Beier et al. (1979) and 14 data from Albery & Whitestone (2003) were used. To calculate the I_{XZ}-mass relationship, 6 data from Chandler et al. (1975) and 20 data from Beier et al. (1979) were used. Chandler et al. (1975) and Beier et al. (1979) reported principal moments of inertia and the orientation of the principal axis with respect to the anatomical coordinate system, therefore the inertia tensor with respect to the anatomical coordinate system was calculated in this study. The data are represented in Table A4 in the Appendix. Simple linear regression using ordinary least squares was used to obtain an equation to calculate I_{XX}, I_{YY}, I_{ZZ}, or I_{XZ} for a given mass with the corresponding 95% prediction intervals. Correlations between CG_X or CG_Z and mass were based on the coefficient of determination (R^2). Testing if the regression line is a good fit was evaluated with a significance level of 0.05.

3.2.2.   Headform data

A commercially available EN960 headform family manufactured according to EN 960 standard and FRHPhe-01 was used for the comparison with the human head cadaver data (CEN, 2006; FIM, 2017). The EN960 headform family included the A (495), C (515), E (535), J (575), M (605) and O (625) magnesium alloy full headform sizes (Model: 100_04_FMH, Cadex Inc., Saint-Jean-sur-Richelieu, QC, Canada). Mass, centre of gravity location and inertia tensor of headforms including a compatible wireless instrumentation system (Model: iCONO, +D, Pozuelo de Alarcón, Spain) were checked to ensure that they fell within the tolerances of the standards. The mass was verified using a calibrated balance (Model: FCB 30K1, KERN & SOHN GmbH, Balingen-Frommern, Germany). The CG location was checked with the use of the balance and a moment table assembly. The moment table is supported by two steel knife-edge blades with their edges parallel to each other and separated by a known distance. One of the two steel knife-edge blades is placed on the balance (see Figure 3.2).
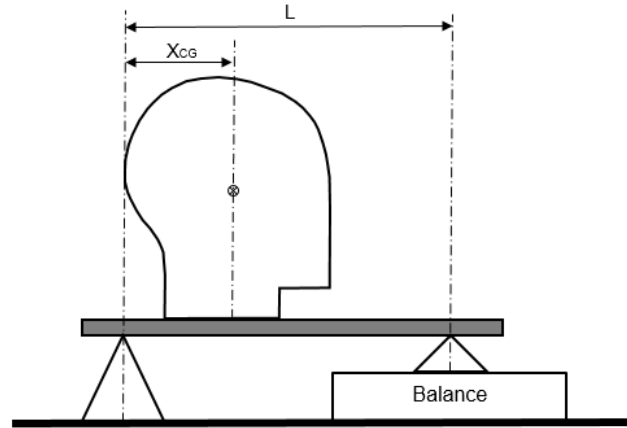
Figure 3.2: Assembly for checking the centre of gravity location of the EN960 headforms.

First, the reaction force in the steel knife-edge blade supported by the balance (in mass units) produced by the moment table alone is determined directly from the balance reading (M_{b1}). With the mass of the table (M_t) and the separation distance (L) the centre of gravity location of the moment table (X_t) is calculated using summation of moments about the steel knife-edge blade not supported by the balance.

$$X_t = \frac{M_{b1}L}{M_t} \tag{3.1}$$

To determine the location of the CG of the headform (X_{CG}), the entire procedure was repeated for the headform and the moment table together. The reaction force in the steel knife-edge blade supported by the balance (in mass units) produced by the headform and the moment table together is determined directly from the balance reading (M_{b2}). Since moments are additive, knowing the mass of the headform (M_h), the CG of the headform alone was determined by subtracting the moment table contribution.

$$X_{CG} = \frac{M_{b2}L - M_tX_t}{M_h} \tag{3.2}$$

The moments of inertia around X-axis (I_{XX}), Y-axis (I_{YY}) and Z-axis (I_{ZZ}) with respect to the centre of gravity and the anatomical coordinate system were verified using a classic air-bearing pendulum that measures a simple moment of inertia at a time (Model: Resonic 8T, Resonic GmbH, Berlin, Germany). Despite the fact that FRHPhe-01 and ECE 22.06 only report the moments of inertia around X-axis (I_{XX}), Y-axis (I_{YY}) and Z-axis (I_{ZZ}) with respect to the centre of gravity and the anatomical coordinate system, in this study the non-zero product of inertia (I_{XZ}) was also calculated for each headform. To calculate the non-zero product of inertia (I_{XZ}), the moment of inertia around X'-axis ($I_{X'X'}$) of a new coordinate system was measured. The new coordinate system was obtained by rotating the anatomical coordinate system around the Y-axis by θ. The inertia matrix of the headform with respect to the anatomical coordinate system, I, can be transformed to the new coordinate system as:

$$I' = RIR^T, \quad \text{with } R = \begin{pmatrix} cos\theta & 0 & -sin\theta \\ 0 & 1 & 0 \\ sin\theta & 0 & cos\theta \end{pmatrix} \tag{3.3}$$

Upon performing the above calculations, the inertia matrix with respect to the new coordinate system is:

$$I' = \begin{pmatrix} I_{XX}c^2 - 2I_{XZ}cs + I_{ZZ}s^2 & 0 & (I_{XX} - I_{ZZ})cs + I_{XZ}(c^2 - s^2) \\ 0 & I_{YY} & 0 \\ (I_{XX} - I_{ZZ})cs + I_{XZ}(c^2 - s^2) & 0 & I_{XX}s^2 + 2I_{XZ}cs + I_{ZZ}c^2 \end{pmatrix} \qquad (3.4)$$

Where $c = cos\theta$ and $s = \sin\theta$. Therefore, the non-zero product of inertia (I_{XZ}) was obtained from the first element of the above matrix.

3.3. Results

The following sections show scatter plots and linear regressions for the human head cadaver data and the comparison with the EN960 headform family.

3.3.1. Length, breadth and circumference of EN960 headforms and human heads

Figure 3.3 and Figure 3.4 show the correlation and the linear regression between length or breadth and circumference for a data set of cadaver human heads with the corresponding 95% prediction intervals and EN960 headforms data. The relationship between length and circumference showed a moderate-low linear correlation while the relationship between length and circumference showed a moderate-high linear correlation.
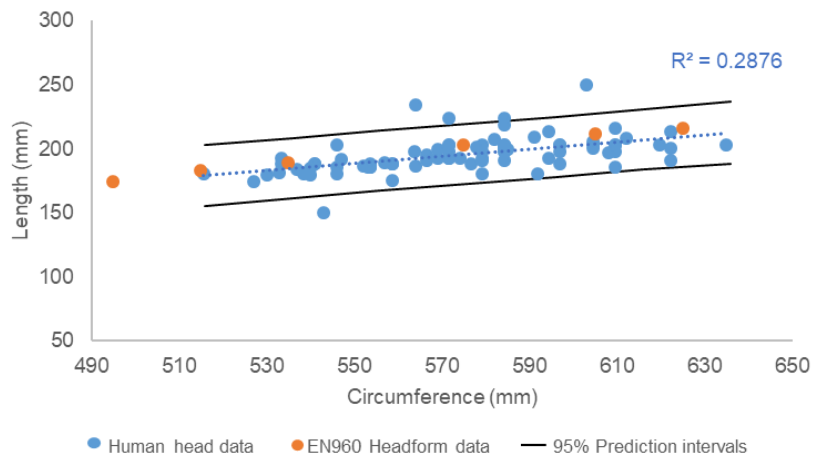
Figure 3.3: Scatter plot showing correlation between length and circumference for a set of human cadaver heads and EN960 headforms.
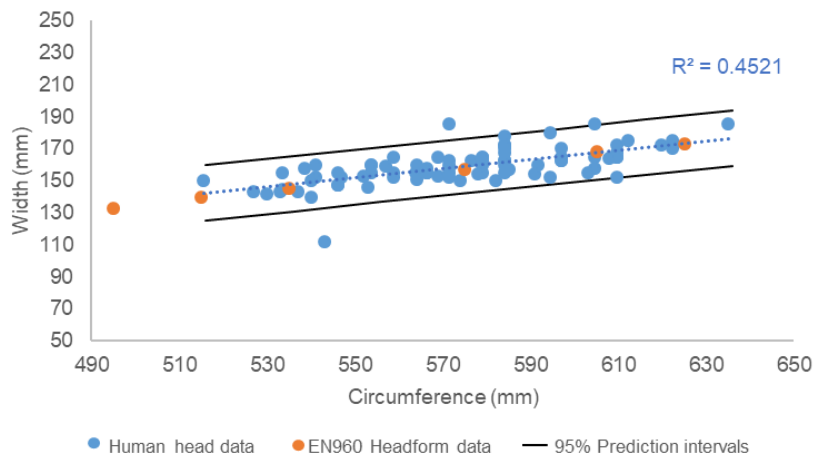
Figure 3.4: Scatter plot showing correlation between breadth and circumference for a set of human cadaver heads and EN960 headforms.

Both regression lines resulted in a good fit for the human cadaver data. Details from the linear regression analysis are provided in Table A5 in the Appendix. Intercept and slope coefficients were statistically significant unless otherwise indicated.

3.3.2. Mass of EN960 headforms and human heads

Figure 3.5 shows the correlation and the linear regression between head mass and circumference for a data set of cadaver human heads with the corresponding 95% prediction intervals and EN960 headforms data. The relationship between head mass and circumference showed a moderate-high linear correlation.

The regression line resulted in a good fit for the human cadaver data. Details from the linear regression analysis are provided in Table A5 in the Appendix. Intercept and slope coefficients were statistically significant unless otherwise indicated.
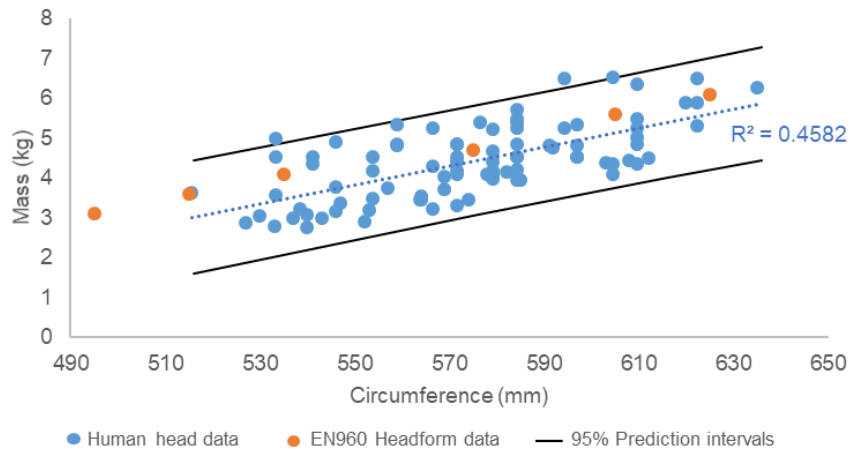
Figure 3.5: Scatter plot showing correlation between mass and circumference for a set of human cadaver heads and EN960 headforms.

3.3.3. Centre of mass location of EN960 headforms and human heads

Figure 3.6 and Figure 3.7 show the correlation and the linear regression between CG_X or CG_Z and head mass for a data set of cadaver human heads with the corresponding 95% prediction intervals and EN960 headforms data. The relationship between CG_X and head mass showed a moderate-low linear correlation while the relationship between CG_Z and head mass showed a very low linear correlation.
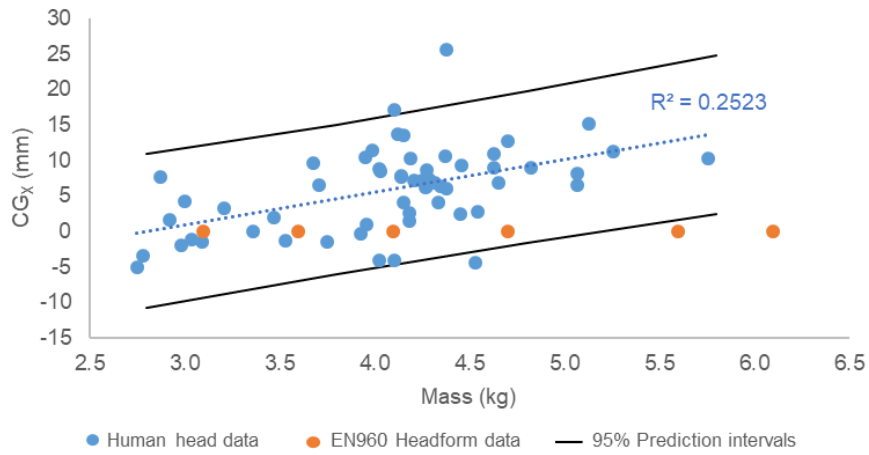
Figure 3.6: Scatter plot showing correlation between CG_X and head mass for a set of human cadaver heads and EN960 headforms.
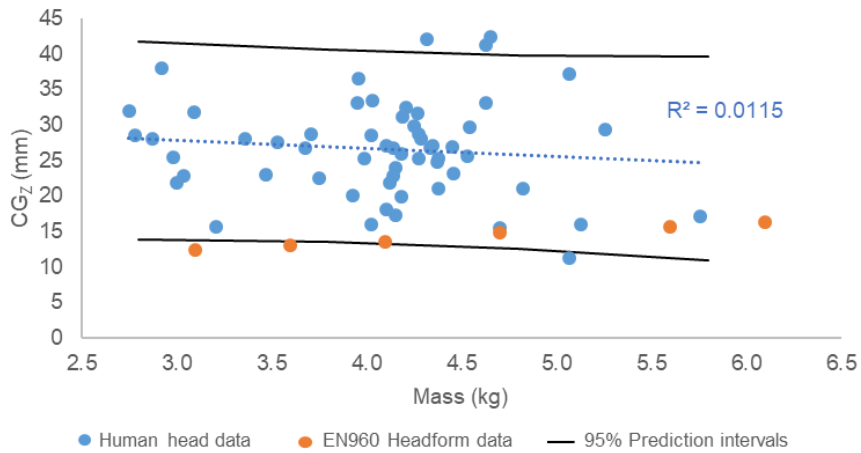
Figure 3.7. Scatter plot showing correlation between CG_Z and head mass for a set of human cadaver heads and EN960 headforms.

The CG_X regression line resulted in a good fit for the human cadaver data whereas the CG_Z regression line did not result in a good fit. Details from the linear regression analysis are provided in Table A5 in the Appendix. Intercept and slope coefficients were statistically significant unless otherwise indicated.

Figure 3.8 showed that EN960 headform data are inside of the 95% probability ellipse defined for a set of human cadaver heads.
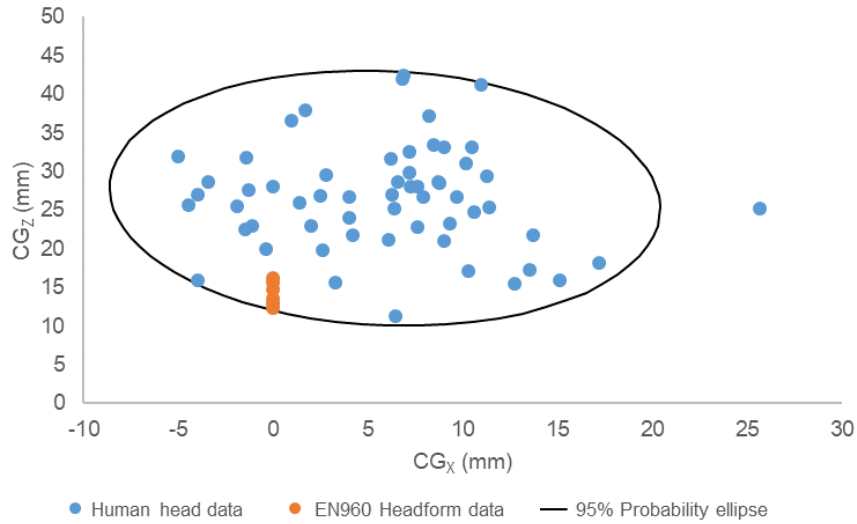
Figure 3.8: Scatter plot showing the CG location in the mid-sagittal plane including a 95% probability ellipse for a set of human cadaver heads and EN960 headform data.

3.3.4. Inertia tensor of EN960 headforms and human heads

Figure 3.9, Figure 3.10, Figure 3.11 and Figure 3.12 show the correlation and the linear regression between I_{XX}, I_{YY}, I_{ZZ} or I_{XZ} and head mass for a data set of cadaver human heads with the corresponding 95% prediction intervals and EN960 headform data. The relationship between I_{YY} and head mass showed a very high linear correlation and the relationships between I_{XX} or I_{ZZ} and head mass showed a high linear correlation while the relationship between I_{XZ} and head mass showed a moderate linear correlation.

All the regression lines resulted in a good fit for the human cadaver data. Details from the linear regression analysis are provided in Table A5 in the Appendix. Intercept and slope coefficients were statistically significant unless otherwise indicated.
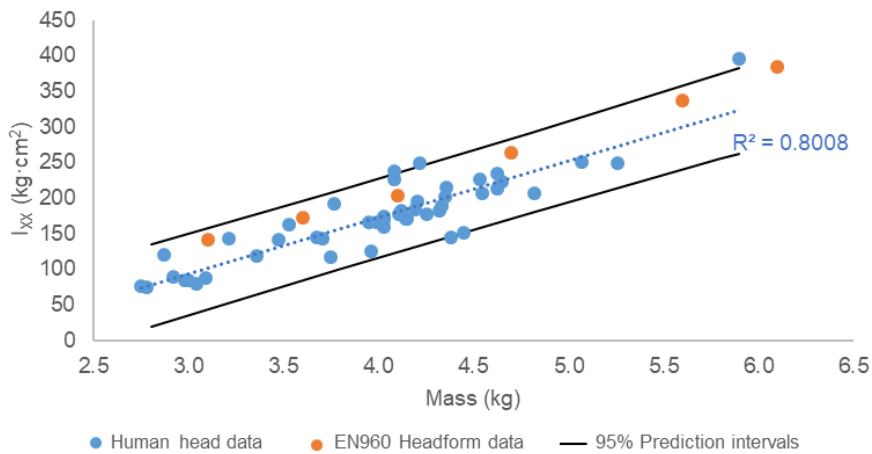
Figure 3.9: Scatter plot showing correlation between I_{XX} and head mass for a set of human cadaver heads and EN960 headforms.
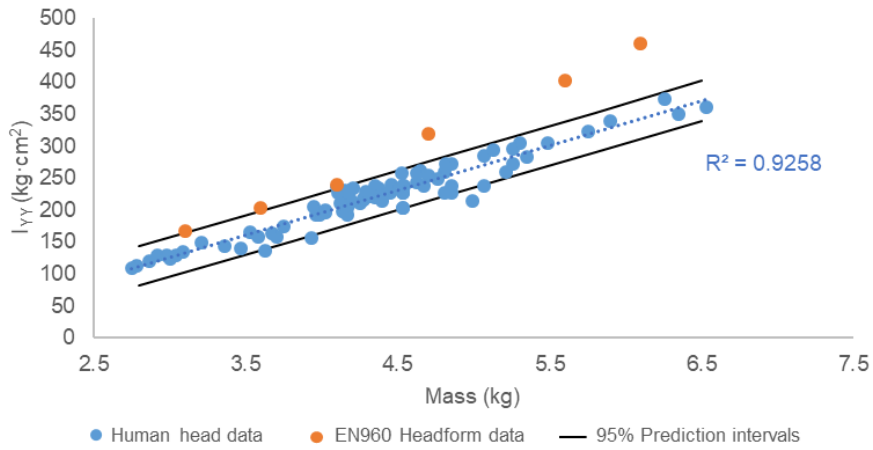
Figure 3.10: Scatter plot showing correlation between I_{YY} and head mass for a set of human cadaver heads and EN960 headforms.
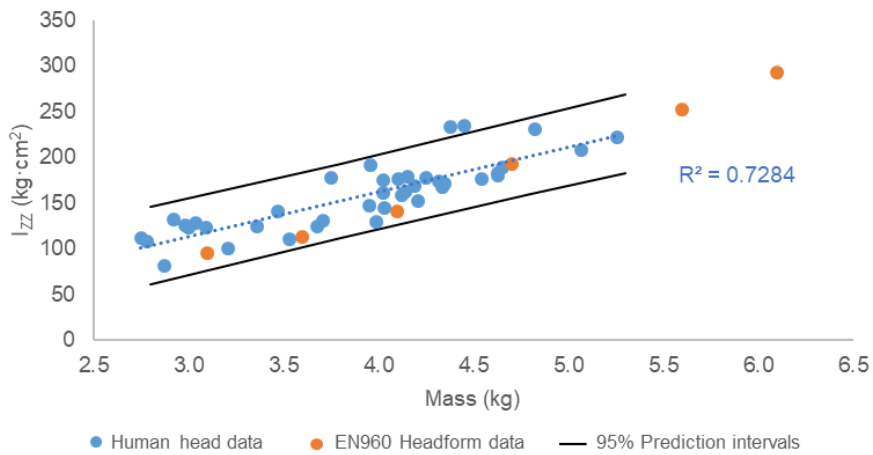
Figure 3.11: Scatter plot showing correlation between I_{ZZ} and head mass for a set of human cadaver heads and EN960 headforms.
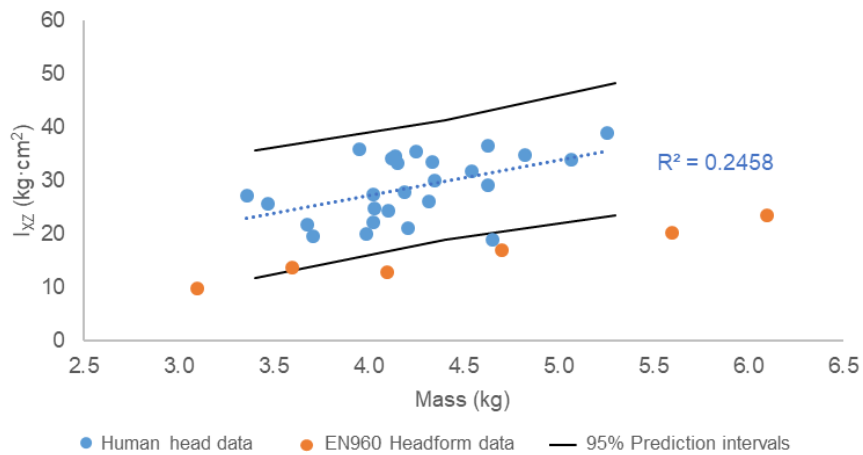
Figure 3.12: Scatter plot showing correlation between I_{XZ} and head mass for a set of human cadaver heads and EN960 headforms.

3.3.5. Human physical properties for EN960 headform sizes based on head cadaver data

Table 3.1 includes the physical properties for the EN960 headform sizes used in most helmet testing standards calculated from the linear regressions obtained with the human head dataset. Since CG_Z regression line did not result in a good fit for the human cadaver

data, the mean value of all CG_Z was used for all headform sizes.

Table 3.1: Physical properties for the EN960 headform sizes used in most helmet testing standards calculated from the linear regressions obtained for the human head dataset.

Circumference	Length	Breadth	Mass	CGₓ	CG𝓏	Iₓₓ	Iyy	I𝓏𝓏	Iₓ𝓏
495	174	136	2.5	1	27	56	94	90	17
515	179	142	3.0	4	27	94	127	113	21
535	185	148	3.5	6	27	131	160	137	24
575	196	159	4.4	9	27	206	226	183	30
605	204	168	5.1	13	27	262	275	218	35
625	210	174	5.6	15	27	300	308	241	38

Measurement units: Circumference, length, breadth, CG_X and CG_Z in mm. Mass in kg. I_{XX}, I_{YY}, I_{ZZ} and I_{XZ} in kg·cm². CG_Y = 0 mm due to the symmetry of the human head.

Figure 3.13 shows the differences between EN960 headforms properties and those predicted by the analysis based on published cadaver studies. In general, EN960 headforms have slightly higher head length (0-4%) and slightly lower head breadth (0-2%) than the predicted by the regression models. Regarding the head mass, the three smaller EN960 headforms sizes have an 18-22% higher mass while the three largest sizes only have a 6-9% higher mass than the predicted by the regression model. Since the CG_X for all the EN960 headforms is located at the origin of the head anatomical coordinate system, it is 1 to 15 mm further back than the predicted by the regression model. CG_Z location for the EN960 headforms is from 39% further down for the largest headform size to 53% for the smaller than the mean value from the human cadaver data. With respect to the inertia tensor, I_{XX}, I_{YY} and I_{ZZ} showed higher values (28-154%, 41-78% and 0-22% respectively) for EN960 headforms, while I_{XZ} showed lower values (33-46%) than the predicted by the regression models.
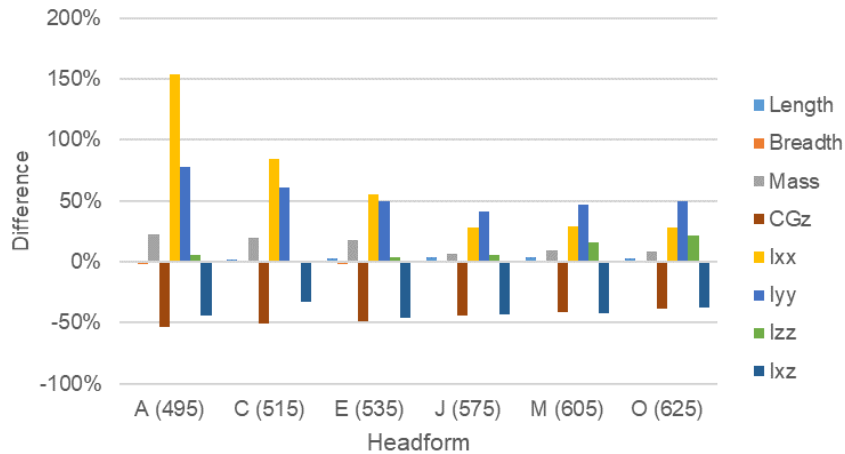
Figure 3.13: Differences in percentage between EN960 headforms and the predicted human physical properties.

3.4. Discussion

The objective of this study was to compare the physical properties of the EN960 headforms and human heads and discuss their potential influence in the results of the normal and oblique impact tests included in helmet testing standards. Normal impact tests refer to impacts in which the impact velocity vector is perpendicular to the impacting surface while oblique impacts refer to impacts in which the impact velocity vector can be apportioned as a perpendicular (normal) and a parallel (tangential) components to the impacting surface.

The determination of human head properties from cadavers requires the preparation of the cadaver, the isolation of the head, the definition of the coordinate system and the quantification of the human head properties. Differences in specimen preparation such as embalmed or unpreserved conditions and head isolation techniques might influence the measurements of physical properties (Yoganandan et al., 2009). Regarding isolation, all the selected studies for the human head dataset used in this study have defined head as the anatomy superior to the skull base traversing along the anterior-inferior direction to the hyoid bone. To ensure that the samples of cadaver could represent the living population, head mass and moments of inertia for each circumference size used in helmet testing standards were compared with linear equations associated with a database of human head physical properties based on a living adult population (Connor et al., 2020). Cadaver dataset presented in this chapter showed in general good agreement with the living adult population dataset, however there were some relevant differences. As for the living population dataset, it was found that the head masses were 11.7%, 6.1%, 2.1%, -3.5%, -6.3% and -7.8% different than the cadaveric heads, for the 495, 515, 535, 575, 605, and 625 head circumference sizes, respectively. Regarding the inertia, the living population I_{XX}, were 24.0%, 14.6%, 10.6%, 7.0%, 5.6% and 5.0% larger than the cadaver dataset (again for the 495, 515, 535, 575, 605, and 625 head sizes). The differences in I_{YY} between living heads (495, 515, 535, 575, 605, and 625 head sizes) and cadaveric heads were -16.1%, -7.5%, -2.4%, -3.4%, -5.8% and -7.1%, respectively. However, the largest differences between the living heads and the cadaveric heads were obtained for the I_{ZZ}, showing differences up to -44.7%, -33.6%, -26.2%, -17.1%, -12.9% and -10.7% (for the 495, 515, 535, 575, 605, and 625 head sizes).

Since some cadaver studies reported principal moments of inertia, the inertia tensor with respect to the anatomical coordinate system was calculated in this study. While the Y-axis of the anatomical coordinate system is a principal direction due to the symmetry of the human head with respect to its midsagittal plane, X and Z axes are not necessarily principal directions. The indirect measurement of I_{XX} and I_{ZZ} might explain the lower correlations with head mass and the larger differences obtained for I_{XX} and I_{ZZ} than for I_{YY}.

The fit between the head and the helmet depends on the external dimensions of the head (Thai et al., 2015). The external geometry of the heads has simply been assessed by means of head length, breadth and circumference. Despite varying specimen demographics, it was observed that the head shape of the EN960 headforms represented quite well the human head dataset used in this study (differences lower than 5%). A computational study concluded that the fit conditions between the headform shape and the helmet dramatically affects the protective performance of helmets because of the contact area between the headform and the protective padding liner (Chang et al., 2001). Dynamic responses of helmeted cadaver heads and standard headforms were compared during normal impacts and the authors observed that the local fit of a headform to the helmet around the impact point may affect the peak linear acceleration (PLA) and the head injury criterion (HIC) (Bonin et al., 2017). A higher contact area causes the head to bear more linear acceleration but less compression of the protective padding. Since a study identified a difference in head shape proportion between Chinese and Caucasian populations (Ball et al., 2010), it may be necessary to evaluate helmet protection with different shaped headforms depending on the population they are intended for.

Although EN960 headforms showed greater masses than the predicted by the regression model for a particular head circumference, the headform masses are still within

the 95% prediction interval. Halldin & Fahlstedt (2018) carried out oblique impacts in a computational study in which the mass of the Hybrid III was altered ±20% and showed that the variation for the PLA and the peak value of the angular velocity (PAV) was around 10% while the peak of the angular acceleration (PAA) hardly changed. According to the analytical model of normal impact test presented by Ghajari (Ghajari, 2011), a more heavy headform increases the liner crushing distance of the helmet during an impact. Therefore, depending on the helmet design the PLA might increase sharply in case of complete bottoming out of the protective padding or decrease if there is enough thickness and the liner is not compressed in excess. Connor et al. found that the mass distribution about the impact location is the primary factor influencing PLA for oblique impacts (Connor et al., 2019).

As for the position of the center of gravity, the CG of the human heads is not coincident with the origin of the defined anatomical head coordinate system (Figure 3.1). In general, according to the cadaver dataset, the CG of the human head is a few centimetres forward and above the defined origin and the same trend was observed in other studies (Bonin et al., 2017; Connor et al., 2020). If we observe the human head, it is not difficult to see that the majority of its mass is located above of the transverse plane due to the cranium and forward of the coronal plane due to the face and mandible. It was observed that while CG_Z varies for each EN960 headform size and CG_X is constant with respect to the origin of the anatomical head coordinate system, the human head dataset suggests keeping CG_Z fixed and varying CG_X for each headform size. In normal and oblique impact tests prescribed in helmet standards, the angular motion that the headform experiences is related to the distance between the CG location and the impact point location and therefore the variation in angular motion will depends on the impact point. This was observed in the computational study performed by Halldin & Fahlstedt (2018) in which the CG location was varied ± 1 cm in the X and Z-axis for two oblique impact locations, the PLA hardy changed while the variations of PAV and PAA were different for each impact location.

Regarding the moments of inertia, Halldin & Fahlstedt (2018) altered a 20% the moments of inertia in two impact directions, they found around 10% of difference in the PAA and around 5% in the PAV while the PLA hardly changed with respect to the baseline. Connor et al. (2019) found a close relationship between headform inertia and impact response for helmeted oblique impacts but it was not as obvious for un-helmeted impacts. However, differences observed for un-helmeted impacts were more in line with the differences observed in Halldin & Fahlstedt (2018).In addition, Connor et al. (2019) concluded that the different friction between each headform and the inside of the helmet did not appear to affect PAA, but Ebrahimi et al. (2015) concluded that it plays an important role.

Considering a planar analysis for a rigidly coupled and perfectly spherical helmeted headform in an oblique impact, the sum of the torques acting on the helmeted headform about a fixed axis equals the moment of inertia times the angular acceleration (Newton's second law). According to the analytical model of helmet rolling and sliding from Meng et al. (2020) the tangential force is directly proportional to the moment of inertia if the helmet is in rolling regime while it does not depend on the moment of inertia if the helmet is sliding regime. Consequently, the angular motion of the headform does not depend on the inertia of the helmeted headform if the helmet is rolling but it does depend on the inertia of the helmeted headform if the helmet is sliding. In normal impact tests, the torque is generated by the normal force and the offset between the normal force and the CG of the headform and therefore the angular motion of the headform does depend on the inertia of the helmeted

headform. Thus, the influence of the moment of inertia of the headform on the angular motion in normal or oblique impacts depends on the impact point, on the type of impact (normal or oblique) and on the rotational regime (rolling or sliding).

In the field of crash tests, biofidelity is the degree to which anthropomorphic test devices are able to represent the real behaviour of human beings in crash situations. Therefore, a simple anthropomorphic test device such as an isolated headform, may be appropriate for a specific impact condition if it is able to represent the real behaviour of human beings in the given impact condition. For instance, Ghajari (2011) suggested increasing the mass of an isolated headform in order to take into account the influence of the body on the head linear acceleration and liner crushing distance measured in linear impact tests. Although the headform meets all the anthropometry and mass properties requirements, it does not mean that it represents the human head behaviour sufficiently well in all impact conditions. Dummies used in crash test of vehicles are designed according to their use in different types of crash tests in order to improve their biofidelity (Jaśkiewicz et al., 2013) however, in helmet testing the same type of headform is used in different types of impact conditions. Thus, headforms designed to model the anthropometry and mass properties of human heads might be only a biofidelic head surrogate if the neck and the rest of the body play a small role in the helmeted head impact responses. Despite the fact that most helmet testing standards assume a negligible effect of the neck and the rest of the body, its influence is dependent on the impact condition and the assessment criteria (Whyte et al., 2019). In addition, Halldin & Fahlstedt (2018) concluded that all parameters studied (headform compliance, location of CG, headform mass, headform moments of inertia, initial position of the helmeted headform, coefficient of friction at helmet/anvil interface and at helmet/headform interface) seemed to have about the same influence in oblique helmet impacts. Therefore, to improve the biofidelity of EN960 headforms, the influence of other parameters such as headform compliance (Bosch, 2006), external surface friction (Ebrahimi et al., 2015), scalp tissue (Trotta et al., 2018b) and boundary conditions (Hering & Derler, 2000) must be analysed for each impact condition.

Limitations

All the limitations related to the determination of human head properties that applied for the reviewed cadaver studies apply to this study as well.

For some physical properties, the range of values for the human cadaver datasets was shorter than the range of values for the EN960 headforms. Therefore, the predictions for these extreme values that lie outside the regression range of values must be carefully treated. Since the published cadaver studies had different objectives and did not present the same physical properties for each studied subject, different sets of published data were used for each physical property. Therefore, not all physical properties correspond to the same set of subjects.

Only the head length, breadth and circumference have been used to assess the head shape in this study. However, a more detailed 3D geometry comparison between EN960 headforms and human heads could reveal additional differences (Plaga et al., 2005). Especially at the chin region for which EN960 headforms are very simple.

Chapter 4

Discrepancies and Deficiencies in Assessment Criteria of Normal Impact Tests

4.1.   Introduction

All motorcycle helmet testing standards include normal impact tests to assess the impact protection provided by the helmet. The normal impact test consists of dropping an instrumented headform, fitted within the test helmet, onto a flat or shaped anvil. In this type of impact, the impact velocity vector is normal to the impact surface because there is no tangential component of the impact velocity vector. All testing standards agree to use the maximum linear acceleration as assessment criterion in normal impact tests, while not all of them agree to use the duration of the linear acceleration, despite the fact that the time dependence of the linear acceleration in the production of linear skull fractures has been demonstrated in the literature (Gurdjian et al., 1966; Lissner et al., 1960; Mertz et al., 1996). Some standards disregard completely the duration of the impact (Snell Foundation [Snell], 2020) while others consider duration (United States Department of Transport [DOT], 2011; United Nations Economic Commission for Europe [ECE], 2021; International Motorcycling Federation [FIM], 2017; Japanese Industrial Standard [JIS], 2015).

Currently, different normal impact test methods are defined by the existing helmet testing standards. Standards in the United States employ the guided fall method in which the motion of the headform is constrained and only translational motion in the vertical direction is permitted (DOT, 2011; Snell, 2020). Standards in Europe use the free fall method in which the headform is unrestrained and it can move in three-dimensional space during the impact (ECE, 2021; FIM, 2017). In Japan, both normal impact test methods are allowed (JIS, 2015).

More than two decades ago, guided and free fall methods were compared using the same headform and impact velocity and it was found a significant reduction of peak linear acceleration in the free fall method (Thom et al., 1998). Attending to the impact energy management, Becker (2012) argued that guided fall method aligns the headform centre of gravity (CG) with the impact point assuring that almost all the impact energy must be managed by the helmet, but in the free fall method as much as 20% of the impact energy might be lost to rotation due to the eccentric impact which has a normal force offset to the

CG of the headform. However, these studies only focused on the linear acceleration results while some studies have shown that rotation of the head during an impact is the leading cause of most intracranial injuries (Holbourn, 1943; Kleiven, 2013). Unlike normal impacts according to guided fall method, in normal impacts using free fall method, significant rotational motion of the helmeted headform occurs (Mills et al., 2009; Zellmer, 1993) and it was demonstrated that the level of this angular head motion can cause traumatic brain injuries by deformation of brain tissue (Meng et al., 2019). Since current normal impact methods do not measure or do not allow the rotation of the headform, some researchers have asserted that these methods have limited applicability for evaluating brain injury risk (Bourdet et al., 2018; Meng et al., 2019).

One important aspect of a standard test method is that it must be able to distinguish between protective and non-protective helmets. Mellor et al. (2007) did a theoretical analysis concerning the significance of helmet geometry in normal impact tests and concluded that sculptured rear geometry of modern helmets could induce excessive angular acceleration. In a simulation study that investigated the influence of the body on head kinematics in oblique impacts, Fahlstedt et al. (2016) concluded that helmet geometry affects the lever arm between the impact point and the centre of gravity of the head, which in turn influences the rotation of the head. However, a series of mini-sled experiments was conducted to determine changes in head accelerations when a football helmet was added to a Hybrid III head and neck complex and it was clearly demonstrated that the linear acceleration measured at the CG of the dummy head underwent a significant reduction when the helmet was used but reduction of angular acceleration due to the addition of a helmet was not as obvious as that observed for linear acceleration (Zhang et al., 2003). Meng et al. (2019) published the rotational velocity and acceleration of one helmet model for front, side, top and rear normal impacts and found that the level of angular velocity and angular acceleration varied depending on the impact directions in free fall tests. Zellmer (1993) published the rotational acceleration of eight different helmets tested for a front impact and a maximum difference around 2 krad/s^2 was observed among the helmet models however it is still not known how much rotation was due to the inherent geometry of the headform or to the helmet geometrical design.

Ebrahimi et al. (2015) studied two factors that influence the results of oblique impact tests concluding that the friction between the interior of the helmet and the headform had a high influence in the rotational motion. However, it is still not known the influence of this factor in the rotational motion during free fall normal impact test.

The general objective of this chapter is to provide insight into the discrepancies and deficiencies of normal impact tests currently included in helmet testing standards. One specific aim is to study the suitability of the free fall normal impact tests for evaluating intracranial injury risk. For that, the influence of the helmet geometrical design in rotational motion during free fall normal test is assessed and, in the light of the high influence of the friction between the headform and the interior of the helmet during oblique impacts, the implication of this factor in the rotational motion during free fall normal tests is also studied. The second specific goal of this chapter is to discuss if the duration of linear acceleration must be taken in consideration in helmet impact testing.

4.2.   Materials and Methods

In order to study the suitability of the free fall normal impact tests for evaluating

intracranial injury risk, one helmet model was used for the analysis of the influence of the friction and 20 full-face motorcycle helmet models and just the headform were exposed to free fall normal impact tests for the analysis helmet geometrical design. The discussion about the consideration of the linear acceleration duration as assessment criteria is mainly based on literature review. In addition, a comparison of metrics which involve the duration of linear acceleration from the 20 full-face motorcycle helmet tests was use as additional support.

All the helmets were composed of composite shell and the protective padding was made of expanded polystyrene (EPS). The retention system of the helmets was based on the double D-ring buckle. All the helmets complied with the European or Japanese regulations (ECE, 2002; JIS, 2015).

4.2.1. Free fall normal impact test method

The tests were performed at the Impact Laboratory of the University of Zaragoza. A free fall guided impact machine (Model: Quebrantahuesos 6.0, +D, Pozuelo de Alarcón, Spain) was used for the free fall normal impact tests. In the free fall normal impact tests, the helmeted headform is placed on a carriage and restrained by pre-cut paper tape to prevent headform motion during the fall. After releasing the carriage assembly from a specific height, the helmeted headform impacts the top surface of an anvil and the carriage assembly continues to fall onto a cushioned bed plate without interfering with the helmeted headform kinematics.

When a helmet was tested, the headform was positioned inside the helmet according to the requirements of Annex 5 of the ECE Regulation 22 (ECE, 2021). The retention system was adjusted under the chin of the headform and tightened to a tension of 75 N. Before each impact, the helmet was re-positioned and the retention system re-tensioned.

A wireless system (Model: iCONO, +D, Pozuelo de Alarcón, Spain) was used to measure linear acceleration and angular velocity at the CG of the headform. The wireless system incorporates three linear accelerometers (Model: 64C-2000, MEAS, Nanshan District Shenzhen, China), three angular rate sensors (Model: ARS PRO-8k, DTS, Seal Beach, CA, USA) and an acquisition system (Model: SLICE NANO, DTS, Seal Beach, CA, USA). Data were recorded at 10 kHz. Head linear acceleration signals were filtered using a low-pass filter CFC-1000 and angular velocities signals were filtered using a CFC-180. High-speed video was captured at 1000 Hz (Model: Eosens mini, Mikrotron, Unterschleissheim, Germany). The end of the impact was estimated when the measured acceleration was lower than 5 g, which correlated well with the instant in which the helmeted headform separated from the anvil. Data post-processing was performed using an in-house developed and validated script of Matlab (Matlab R2021b, MathWorks, Natick, MA, USA).

Figure 4.1: Impact points for the analysis of the friction and helmet geometrical design factors.

4.2.2.   Impacts for the analysis of the friction factor

The influence of the friction between the headform and the interior of the helmet in the rotational motion during normal impact test was studied before analyzing the influence of the helmet geometrical design in the rotational motion. For this purpose, six identical helmets were tested according to the free fall normal impact test method described above at 8.2 m/s on the points B, X (right), P and R as described in the European regulation (ECE, 2021) and illustrated in Figure 4.1. The helmets were tested against a 130 mm diameter flat steel anvil with a 575-size magnesium alloy full headform (Model: 100_04_FMH, Cadex Inc., Saint-Jean-sur-Richelieu, QC, Canada). Three helmets were tested with the original metal surface of the headform (bare headform) and the other three helmets were tested with the headform covered with a thin uniform layer of high-performance silicone rubber (Model: Dragon Skin 10, Smooth-On, Inc., Macungie, PA, USA). A total of 40 g of silicone rubber was uniformly spread to meet the thickness requirement of the FIM Racing Homologation Programme for helmets (FRHPhe-01) (FIM, 2017). A spring balance method was used to provide an indication of the friction associated with the coating treatment. The average coefficient of friction (COF) measured between a cotton fabric and the bare headform and the coated headform was 0.20 and 0.78, respectively. Two independent samples t-test were carried out in order to analyze the influence of the coating on the brain injury criterion (BrIC) (Takhounts et al., 2013) and on the peak of the resultant angular acceleration (PAA) for each impact point. Significance level used for statistical tests was $\alpha = 0.05$. The mean difference between the tests with the bare and covered headform was used as effect size to complement statistical hypothesis testing. Statistical analyses were performed using the Real Statistics Resource Pack add-in in Excel (Excel 2016, Microsoft, Redmond, WA, USA).

4.2.3.   Impacts for helmet geometrical design analysis and impact duration discussion

Twenty full-face motorcycle helmet models were tested according to the free fall normal impact test method described above at 5 m/s and 8.2 m/s. Each helmet was tested on the points B, X, P and R as described in the European regulation (ECE, 2021) and illustrated in Figure 4.1. A new helmet was used for each impact speed, resulting in a total of 40 helmets and 160 impacts. All the helmets were tested with a 575-size magnesium alloy full headform (Model: 100_04_FMH, Cadex Inc., Saint-Jean-sur-Richelieu, QC, Canada) with the original metal surface of the headform. They were impacted onto a 130 mm diameter flat steel anvil. The peak of the resultant linear acceleration (PLA), the peak of the resultant linear acceleration for a duration of 2 ms, 4 ms and 6 ms (PLA@2ms, PLA@4ms and PLA@6ms respectively), the head injury criterion (HIC) (Versace, 1971), the skull fracture criterion (SFC) (Chan et al., 2007), the BrIC and PAA were calculated for each impact.

In order to study how much rotation was due to the inherent geometry of the headform or to the helmet geometrical design, the unhelmeted headform was tested on the points B, X and R points against a modular elastomer programmer (MEP) from 15, 40, 65 and 90 cm height. The MEP is a 130 mm diameter cylindrical pad, and 25 mm thick consisting of a polyurethane rubber of 60A Shore hardness. The MEP provides a uniform impact surface with highly consistent impact properties and it is used for checking drops in helmet testing standards (DOT, 2011). Due to the fact that there was no offset between the centre of gravity of the headform and the P impact point, the motion of the headform after impact was vertical. Since the rebound of the headform was not limited by any mechanism, this impact point was not tested with the unhelmeted headform in order to avoid any damage to the testing equipment. Three replicas were carried out per each impact point and

height, resulting in a total of 36 unhelmeted headform drop tests. The average of the three replicas for each impact point and height and their standard deviation (SD) was calculated for PLA, BrIC and PAA variables.

4.3. Results

The results of this study are presented into three subsections. First, the results of the influence of the headform coating are shown. Second, the results of the influence of the helmet geometrical design in the rotational motion of normal impact tests are presented. Finally, the comparison of metrics which involve the duration of the linear acceleration is reported.

4.3.1. Effect of the headform coating

The average and the standard deviation (SD) of the BrIC and PAA for the normal impact tests for friction factor analysis are given in Figure 4.2. Data were sorted by impact point and the headform coating. No trend was observed for BrIC or PAA due to the coating factor.
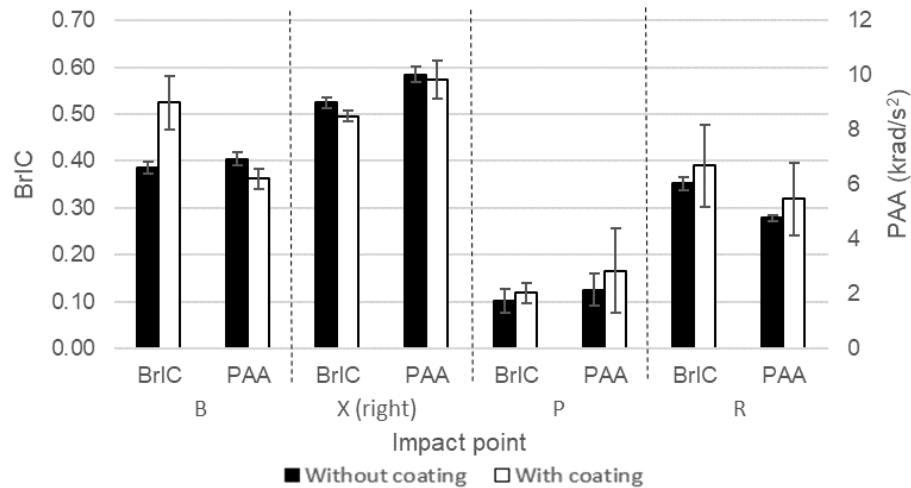
Figure 4.2: Brain Injury Criterion (BrIC) and Peak resultant Angular Acceleration (PAA) average ± standard deviation for the normal impact tests with and without headform coating.

Table 4.1: Average and standard deviation of the Brain Injury Criterion (BrIC) and Peak resultant Angular Acceleration (PAA) for each headform surface condition with the t-tests results (p-value) and effect size for each impact point. Significant values are shown in bold font.

Variable	Point	Bare Headform	Covered Headform	*p*-value	Effect size
BrIC	B	0.386 ± 0.012	0.524 ± 0.057	**0.0472**	0.138
	X (right)	0.524 ± 0.011	0.495 ± 0.011	**0.0315**	0.029
	P	0.102 ± 0.025	0.119 ± 0.022	0.4261	0.017
	R	0.353 ± 0.014	0.390 ± 0.087	0.0537	0.037
PAA **(rad/s²)**	B	6928 ± 245	6221 ± 372	0.0515	707
	X (right)	10027 ± 273	9826 ± 679	0.6721	201
	P	2160 ± 583	2851 ± 1550	0.5304	691
	R	4773 ± 93	5473 ± 1337	0.4604	700

The results of the statistical analyses were showed in Table 4.1. Only BrIC resulted in significant differences for B and X impact points. While BrIC was significantly higher for the covered headform when testing B impact point, it was significantly lower for the covered headform when testing X impact point.

4.3.2.   Influence of the helmet geometrical design in the rotational motion

In order to show the variability of the rotational motion due to the helmet geometrical design, Figure 4.3 and Figure 4.4 show descriptive statistics of BrIC and PAA outcomes for each impact point and each impact speed from the twenty full-face helmet models tested. The boxplot is a standardized way of displaying the distribution of data based on a five number summary ("minimum", first quartile, median, third quartile, and "maximum"). The whiskers extend no more than 1.5 times the interquartile range (IQR), which is the distance between the first and third quartile, and outliers are plotted as separate dots. For both variables the standard deviation was higher when the testing speed was higher. For BrIC, the impact point R showed the higher dispersion followed by the impact point X.
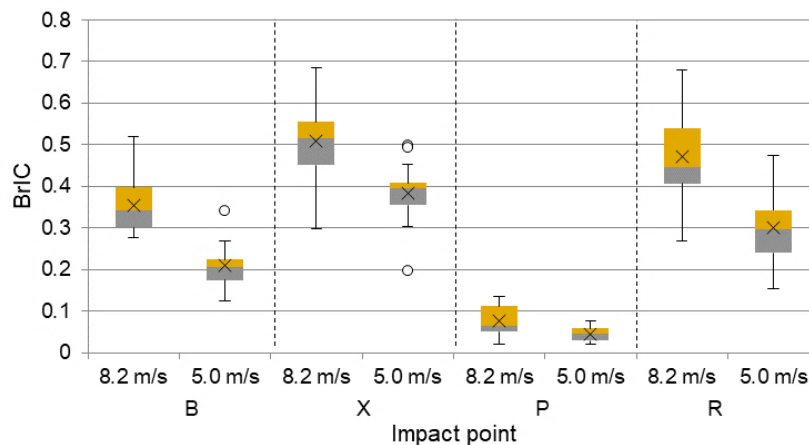
Figure 4.3: Descriptive statistics of Brain Injury Criterion (BrIC) for each impact point and each impact speed from the twenty full-face helmet models tested.

In the case of PAA, the impact point X showed the highest standard deviation, followed by the impact point R.
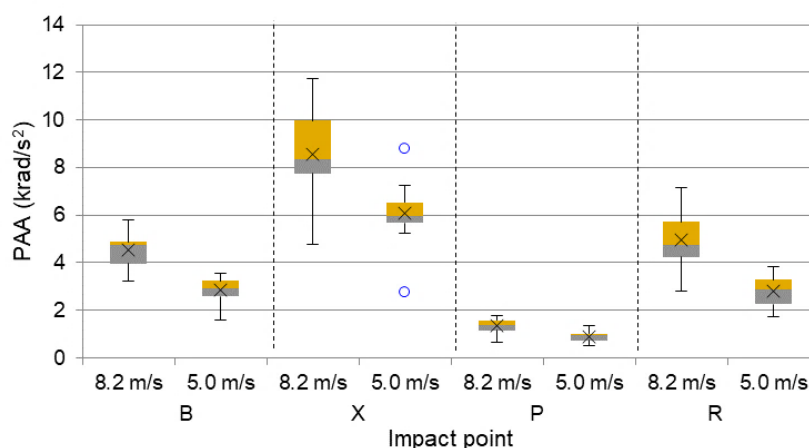
Figure 4.4: Descriptive statistics of Peak of the resultant Angular Acceleration (PAA) for each impact point and each impact speed from the twenty full-face helmet models tested.

Scatter plots were used to display values for the PLA and the BrIC or PAA using the results from the twenty full-face helmet models tested and the headform tests. In general, for a given value of PLA, the BrIC was higher in helmeted tests than in non-helmeted tests (see Figure 4.5). The biggest differences between BrIC values for a similar value of PLA from helmeted and non-helmeted tests were observed for the R impact point. Just two points for the impact point X, which belong to the same helmet model tested at 8.2 m/s and 5 m/s,

resulted in lower BrIC for a similar magnitude of PLA in helmeted tests than in non-helmeted tests.

In normal impacts the rotational motion is due to the offset between the normal force and the CG of the headform and the PLA is related to the impact reaction force through the second's Newton law. Since all the tests were carried out with the same headform, the variation in BrIC or PAA for a given PLA magnitude is due to the offset between the normal force and the CG of the headform. Therefore, the results from the non-helmeted tests are showing how much rotation was due to the inherent geometry of the headform for each impact point while the results from the helmeted tests are showing how much rotation was due to both the inherent geometry of the headform and the helmet geometrical design.
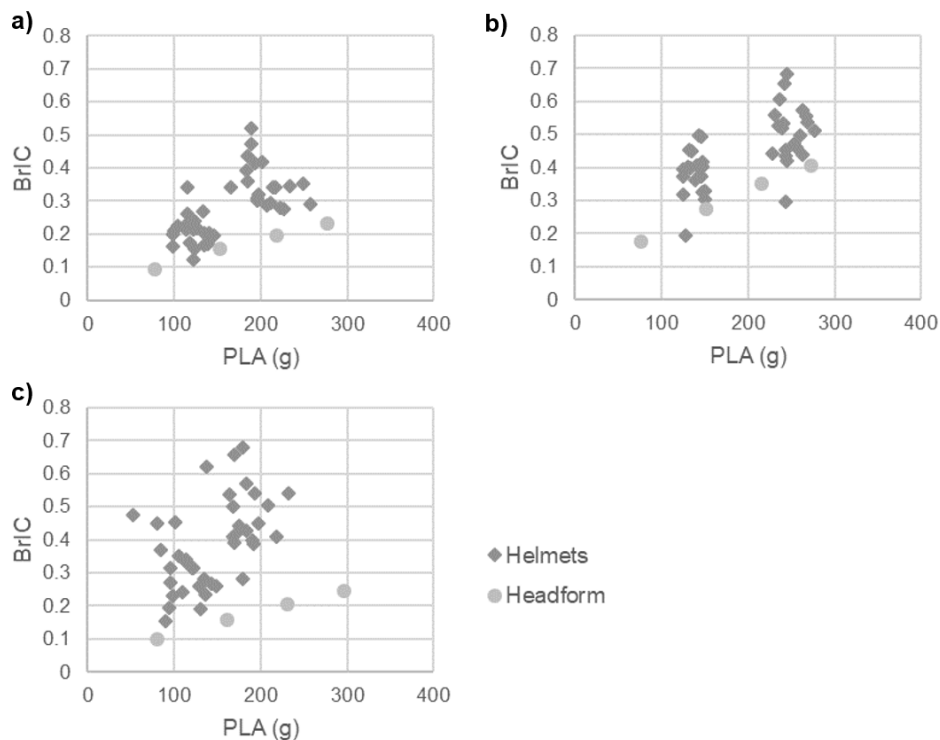
Figure 4.5: Scatter plots showing the relationship between the Brain Injury Criterion (BrIC) and the Peak of the resultant Linear Acceleration (PLA) in normal impact tests for the helmeted and non-helmeted headform: a) B impact point, b) X impact point, c) R impact point.

Different from BrIC results, the PAA values from helmeted tests were higher and lower than from the non-helmeted tests for the three impact points (see Figure 4.6). While most of the helmeted tests showed higher PAA values than non-helmeted tests in B and R impact points, most of the helmeted tests showed lower PAA values than non-helmeted tests in X impact points.
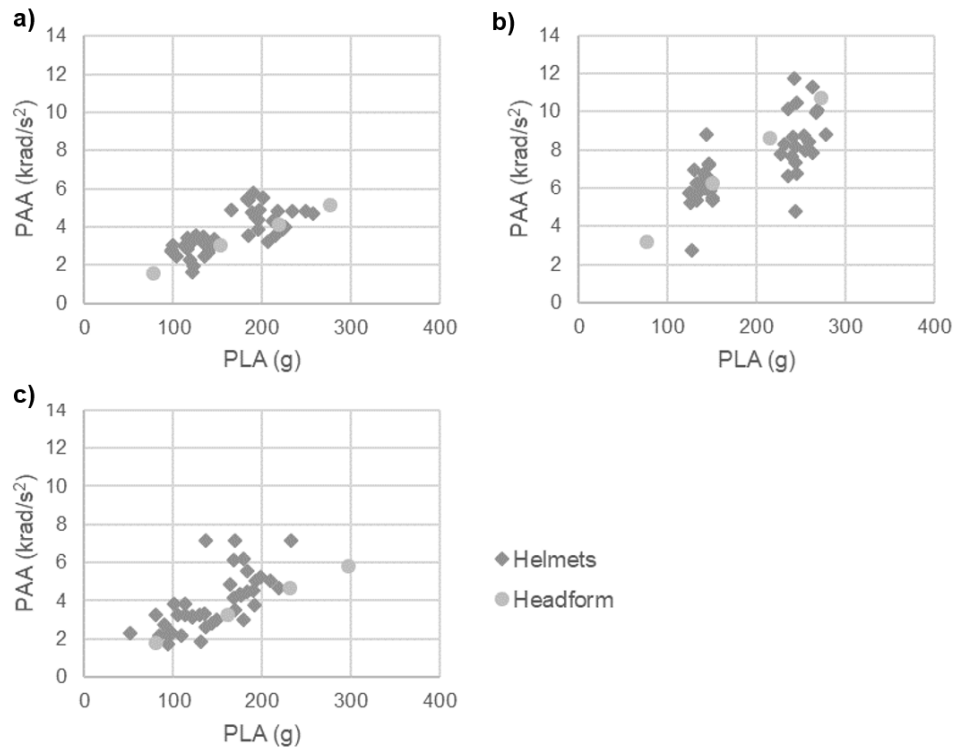
Figure 4.6: Scatter plots showing the relationship between the Peak of the resultant Angular Acceleration (PAA) and the Peak of the resultant Linear Acceleration (PLA) in normal impact tests for the helmeted and non-helmeted headform: a) B impact point, b) X impact point, c) R impact point.

4.3.3.   Comparison of metrics which involve the duration of linear acceleration

The PLA@2ms, PLA@4ms, PLA@6ms, HIC and SFC were calculated using the data from the twenty full-face motorcycle tested helmet models at two impact velocities (8.2 m/s and 5 m/s). Each one of these metrics was plotted in a scatter plot with the PLA, which is the common metric used in all helmet testing standards, in order to compare them. Figure 4.7 showed a very high linear correlation for PLA@2ms, HIC and SFC. The correlation for PLA@2ms, PLA@4 ms and PLA@6ms decreases as the duration increases.
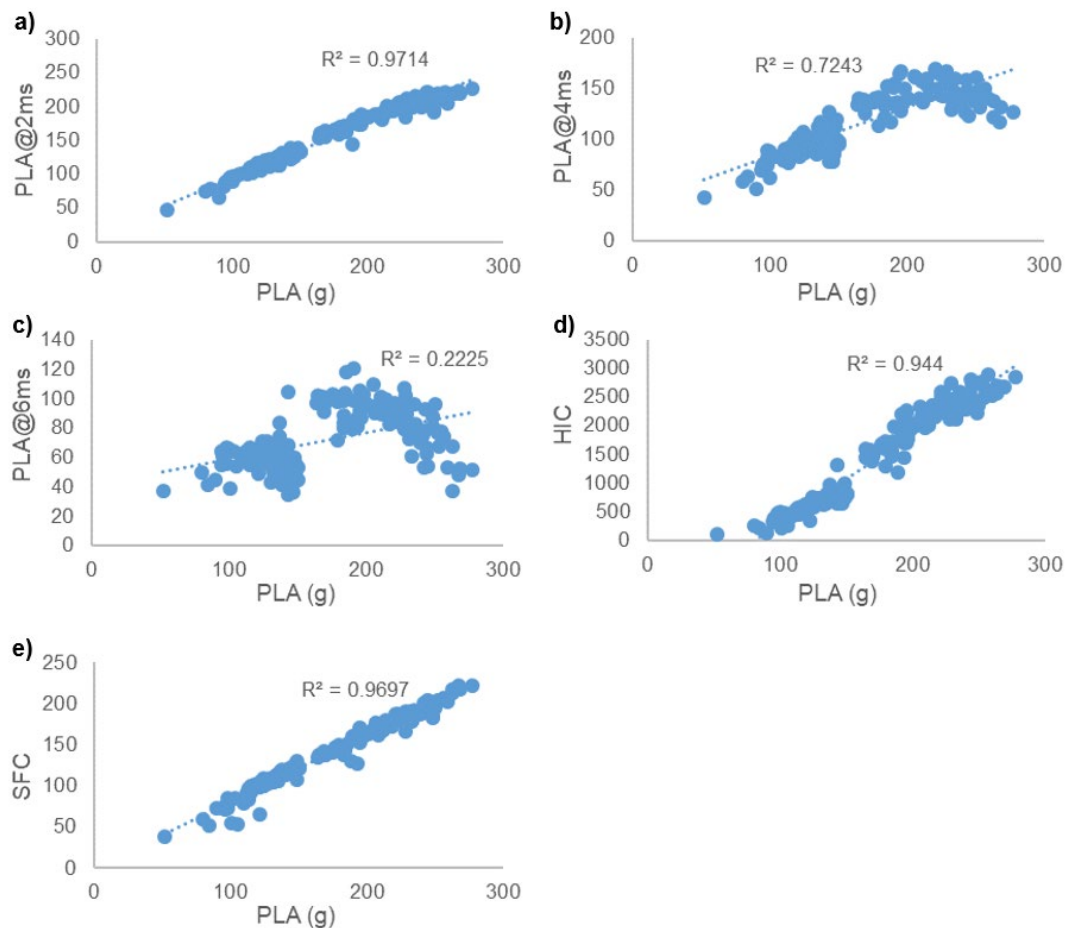
Figure 4.7: Scatter plots showing correlations between the Peak of the resultant Linear Acceleration (PLA) and metrics which involve the duration of linear acceleration: a) Peak of the resultant Linear Acceleration for a duration of 2 ms (PLA@2ms), b) Peak of the resultant Linear Acceleration for a duration of 4 ms (PLA@4ms), c) Peak of the resultant Linear Acceleration for a duration of 6 ms (PLA@6ms), d) Head Injury Criterion (HIC), e) Skull Fracture Criterion (SFC).

4.4.   Discussion

The objectives of this study were to provide insight into the discrepancies of helmet testing standards for normal impact tests such as the use of the duration of linear acceleration as assessment criteria and to study the suitability of the normal impact tests for evaluating brain injury risk.

4.4.1.   Influence of the headform friction

Regarding the analysis of the influence of the friction between the headform and the interior of the helmet in rotational motion during free fall normal test, the test results showed significant differences in BrIC for B and X impact points but with an opposite trend. In order to clarify these results, high-speed videos were carefully reviewed and it was found that the higher BrIC magnitudes observed for the covered headform while testing B point were more due to imprecisions in the helmet positioning than friction.

In contrast to oblique impacts in which the tangential impulse is transmitted from the helmet to the headform mainly by friction effects, in normal impacts there is not tangential impulse and the rotational motion is due to the offset between the normal force and the CG of the headform. Therefore, if the friction between the interior of the helmet is high enough the headform and the helmet will rotate together but if not, the headform will rotate inside

the helmet. This is what occurred when testing X impact point where the slightly higher magnitude of the BrIC and PAA for the bare headform was due to the inertia effect of the helmet when the helmet and the headform rotated together during the covered headform tests. The small effect size for the BrIC when testing X impact point suggest that the significant difference found for this metric was not relevant. Therefore, it can be considered that given the absence of tangential impulse in normal impacts, the friction between the headform surface and the interior of the helmet does not have a relevant effect in rotational motion during free fall normal impacts.

4.4.2.   Influence of the helmet geometrical design

The descriptive statistics of BrIC and PAA outcomes from the twenty full-face helmet models tested showed that X and R impact points resulted in higher dispersion than B and P impact points. This is due to the more irregular side and rear geometries of motorcycle helmets in contrast to the more regular and rounded front and top geometries. This confirms that the helmet geometrical design can influence the rotational response in normal impacts.

As Meng et al. (2019) concluded for one helmet model, the mean values of this study confirmed that the level of angular velocity and acceleration also varied depending on the impact directions for different helmet models. Since the rotational motion in normal impact tests is caused by the normal force offset to the CG of the headform, for each impact point the rotational motion decreased as the impact velocity decreased because the peak linear acceleration, which is proportional to the reaction impact force, also decreased (see Figure 4.8).
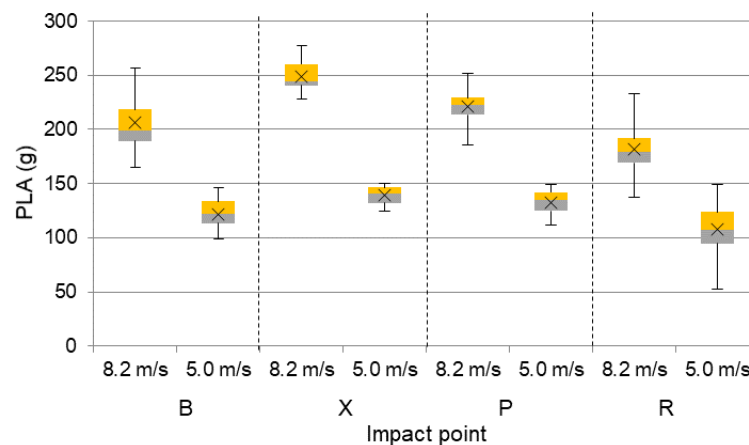
Figure 4.8: Descriptive statistics of Peak of the resultant Linear Acceleration (PLA) for each impact point and each impact speed from the twenty full-face helmet models tested.

The headform tests were used to show how much rotation in normal impact tests was due to the inherent geometry of the headform or to the helmet geometrical design. It has been showed that the inherent geometry of the headform causes angular motion when the headform was tested without helmet and it also increases as the PLA increases (see Figure 4.5 and Figure 4.6). For the same magnitude of PLA, higher BrIC and PAA magnitudes were obtained for the X impact point than for the B and R impact points. This is mainly related to the offset between the impact point and the CG of the headform because there is only a 20% of difference between the headform moment of inertia in the X-axis (I_{xx} = 264 kg·m³) and in the Y-axis (I_{yy} = 318 kg·m³) while the BrIC and PAA magnitude differences were almost double. Since helmet testing procedures define that the impact point must be tangential to

the impacting surface, the external helmet shape can modify the offset between the impact point and the CG of the headform. While this was clearly confirmed for the PAA results, where there were higher and lower PAA magnitudes from the twenty full-face helmet models tested than those obtained in the headform tests without helmet, the BrIC results from the twenty full-face helmet models tested hardly were lower than the headform tests. Different from PAA which is directly proportional to the reaction impact force and its offset to the CG of the headform, BrIC also implicates the duration of the angular acceleration.

The duration of the angular acceleration pulse during an impact is related to the hardness of the impacting surface or the stiffness of the helmet. To study the influence of the hardness of the impact some additional headform tests were performed against an expanded polystyrene foam (EPE) with a density of 33 kg/m³. The headform was dropped without helmet on the point X from 95, 120 and 145 cm heights which do not bottomed out the EPE pad. Figure 4.9 shows higher BrIC magnitudes for the softer impact surface (EPE) while it shows lower PAA magnitudes for the same impact surface. The compliance of the helmet or the impacting surface may reduce the PAA magnitudes because of the contact area increases but it may increase the BrIC magnitudes because the duration of the angular acceleration increases and therefore the angular velocity increases. Although for the same impact force the BrIC magnitude increases with softer impact surfaces, softer impact surfaces reduce PLA, BrIC and PAA magnitudes for the same impact velocity.
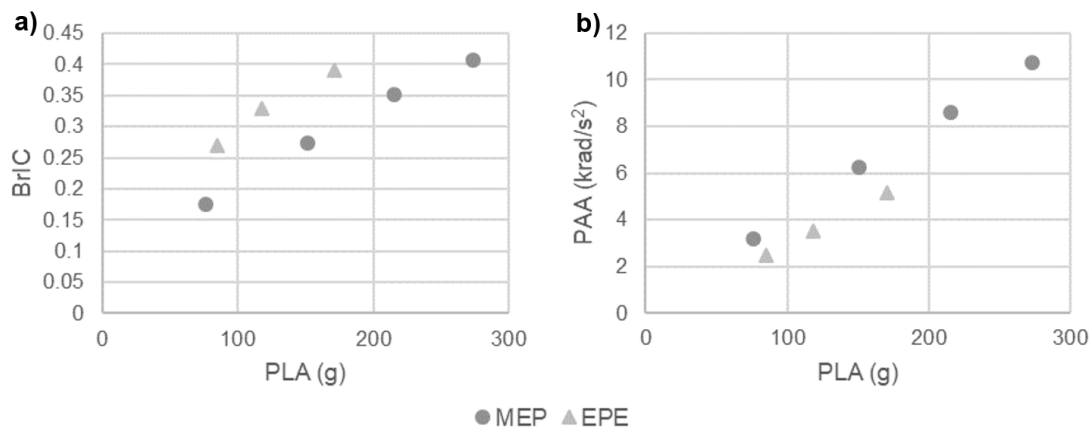
Figure 4.9: Scatter plots showing the influence of the compliance of the impact surface on the Brain Injury Criterion (BrIC) and on the Peak of the resultant Angular Acceleration (PAA) against the Peak of the resultant Linear Acceleration (PLA) in normal impact tests using a non-helmeted headform.

4.4.3.   Duration of linear acceleration

For a fixed impact speed of a moving head, the occurrence of skull fracture depends on geometry and hardness of the impact surface and on the effective mass of the head. If any of these parameters are changed, the magnitude of the impact force will change but also the impact duration. The breaking stress and breaking strain of the human skull are rate sensitive, and breaking stress increases as strain rate increases (Wood, 1971). Short duration impact forces will lead to greater strain rates than long duration impact forces. Therefore, skull fracture will occur at higher magnitude impact forces for short duration impacts than for long duration impacts. This was empirically observed by Lissner et al. (1960) testing four heads falling freely and two heads falling with the body attached against the same impact surface. This work constituted the first part of the Wayne State Tolerance Curve (WSTC) (Gurdjian et al., 1966). The curve shows that human head can tolerate higher accelerations if the duration of the acceleration exposure is short. The WSTC was supported

by experiments conducted by Ono et al. (1980) in primates and scaled to humans, which led to the Japan Head Tolerance Curve (JHTC) that is very similar to the WSTC.

Currently, PLA is the common metric used in all helmet testing standards and it was found that it can be used as an appropriate assessment criterion for skull fracture in guided and free fall methods (Rigby et al., 2011; Rigby & Chan, 2009). However, this metric ignores impact duration, that is, it ignores the viscoelasticity of the human skull. Some helmet testing standards take into account the impact duration through the cumulative duration for a particular magnitude of the resultant linear acceleration (dwell times) and the HIC. Despite the fact that the dwell times seem to reflect the concept of the WSTC, it is not the case at all because the ordinate of the WSTC is effective acceleration which is the area under the curve divided by its time duration (Versace, 1971) and not the cumulative time at which the acceleration versus time exceeds a specific acceleration value. Rigby & Chan (2009) concluded that dwell times do not correlate well with skull strain and this study has showed that the correlation between PLA and dwell times decreases as the duration increases. Therefore, the compatibility of dwell time with PLA for helmet impacts is very limited to short cumulative times ($\leq$ 2ms). On the contrary, the HIC, which is a formulation of the WSTC, showed a very good correlation with the PLA for impact duration consideration (HIC time interval) of 6.0 ± 1.3 ms (mean ± SD) for the dataset used in this study. However the HIC is not a consistent predictor for skull fracture because the HIC tolerance to fracture depends on the target hardness (Hodgson & Thomas, 1973; Vander Vorst et al., 2003).

The SFC is the average acceleration over the HIC time interval and it correlated slightly better with PLA than HIC probably due to its independence from the target hardness. Since SFC only uses the most representative part of the curve duration (HIC duration), it captures well the effects of target compliance and contact area and correlates well with skull fracture data (Chan et al., 2007; Vander Vorst et al., 2003; Vander Vorst et al., 2004). However, the SFC assumes that forces are applied over a wide impact area and the correlation between SFC and skull strain could be significantly off if there are areas of local high pressure on the skull (Chan et al., 2007; Rigby et al., 2011).

One of the main functions of the helmet shell is to distribute the impact load over a greater area of the underlying liner and therefore, areas of local high pressure only occurs when the protective padding has been bottomed out. Due to the rigid design of head surrogates used in helmet testing standards, when the protective padding bottoms out a high acceleration peak of very short duration is observed. Therefore, a combination of PLA and SFC assessment criteria may be appropriate for skull fracture prevention in helmet testing standards because PLA will restrict high magnitude acceleration curves of short duration while SFC will restrict long duration acceleration curves.

4.4.4. Limitations

Although normal impacts are less likely to occur in real-world crashes than oblique impacts, in oblique impacts there is only a significant tangential reaction force if the friction between the helmet and the impacting surface is high enough. An oblique impact with a very low tangential reaction force is similar to a normal impact at equivalent impact velocities. Some helmet testing standards have recently included oblique impact test methods in their certification tests (ECE, 2021; FIM, 2017) in order to assess the rotational motion of the head in a more realistic impact in which the head has a relative speed parallel to the impacting surface. The impacting surface in these oblique test methods is covered with abrasive paper which has showed higher friction than 'typical' roadway surfaces (Bonugli

et al., 2017). However, since friction between the helmet and the impacting surface varies in real-world crashes and it has been shown that low friction can increase rotational motion in some impact scenarios (Finan et al., 2008), the combination of the assessment of the rotational motion in oblique impacts and in normal impacts covers the evaluation of the helmet in a wide range of impact scenarios in which the head of the motorcyclist is liable to suffer intracranial injuries.

Another limitation of this study is the influence of the neck and body on the kinematics of the head. It has been shown that the effects of the neck and body are less significant for oblique impacts than for normal impacts onto the flat anvil (Hering & Derler, 2000). However, the conclusion of this study is based on using the Hybrid III dummy as a surrogate for the human body and the biofidelity of the neck surrogate also plays an important role in the influence on the kinematics of the head (Whyte et al., 2019). It has been shown that the neck of the Hybrid III dummy is too stiff in the axial direction compared to the human neck and it overestimates the effect of the body on the linear kinematics of the head (Ghajari, et al., 2011). Moreover, other studies have suggested that the neck and body play only a small role during helmeted head impacts (Fahlstedt et al., 2016; Willinger et al., 2014).

Chapter 5

Coefficient of Friction at the Headform/Helmet Interface in Oblique Impact Tests

5.1. Introduction

In most real-world motorcycle crashes, the helmeted head of the rider impacts with a certain angle. Therefore, if the friction between the helmet and the impacting surface is high enough, the reaction force that the helmeted head experiences can be decomposed into two components: a normal component perpendicular to the impact surface and a tangential component parallel to the impact surface. In a typical fall to the ground, the magnitude of the reaction force normal component is related mainly to the height of the rider's fall on the ground while the reaction force tangential component is associated to the motorcyclist's travelling speed (Lloyd, 2016). The magnitude of this tangential component is also related to the friction between the helmet and the impact surface and determines the rotation experienced by the head of the rider. Since Holbourn (1943) hypothesized that rotational motion of the incompressible brain could explain some head injuries unlikely to be caused by translational motion, a substantial amount of experimental research has supported the relationship between head rotation and brain injuries (Gennarelli et al., 1982; Gennarelli & Thibault, 1982; Ommaya & Gennarelli, 1974).

Previous research shows that oblique impacts between the helmet and the ground, in which a relevant tangential force is transmitted to the helmeted head, are the most frequent collision scenarios in real world (Bourdet et al., 2016; Chinn et al., 2001). Consequently, researchers have designed different laboratory testing methods to measure the helmet energy absorption capabilities in oblique impacts and the resulting kinematics of a headform that represents the human head (Aare & Halldin, 2003; Aldman et al., 1976; Halldin et al., 2001; Pang et al., 2011). A simple and robust oblique impact test that consists of dropping an instrumented headform, fitted with the test helmet, onto an inclined anvil was included in the FIM Racing Homologation Programme for helmets (FRHPhe-01) (International Motorcycling Federation [FIM], 2017). Recently, the 06 series of amendments of the ECE Regulation 22 (ECE 22.06) has included a similar oblique impact test similar to that of the FRHPhe-01 (United Nations Economic Commission for Europe [ECE], 2021). Even though both standards use the same set of headforms, they require

different friction at the interface between the helmet and the headform, which has been shown to be a critical concern on the angular response of the helmeted headform in oblique impacts (Ebrahimi et al., 2015).

A recent computational research studied the dynamics of rolling and sliding motions of the helmeted head on the road surface in oblique impacts at different tangential velocities. This study revealed that, from lower to higher tangential impact velocities, the motion of the helmet transitions from rolling to sliding, which affected head kinematics and its injury outcome (Meng et al., 2020). However, the tangential component of the contact force causes not only the rolling/sliding motion of the helmet on the ground but, due to similar underlying mechanics, it can also cause a relative motion between the head and the interior surface of the helmet, depending again on the existing friction between these two surfaces (Ebrahimi et al., 2015). Since the influence of the friction between the helmet and the road has been effectively analysed in Meng et al. (2020), the objective of this chapter is to quantify the influence of the coefficient of friction (COF) between the interior surface of the helmet and the headform in the resulting kinematics of the headform at different magnitudes of the tangential impact velocity.

5.2.   Materials and Methods

5.2.1.   Test matrix and helmet model

The test matrix consisted of 54 drop tests performed on a full-face motorcycle helmet (model: FF104 RAPIDE, MT, Cartagena, Spain). Three different impact speeds were used in combination with three different angles of oblique anvils so that the same normal component of the impact velocity was kept but resulted in a variation of the tangential component of the impact velocity (see Figure 5.1). There was not variation in the COF between the helmet surface and the impact surface of the anvils. Two friction coefficients (low COF: bare headform; high COF: coated headform) were used at the interface between the headform and the interior of the helmet. For each anvil angle, three different relative orientations between the helmet and the anvil and three repetitions per each orientation were done to ensure the repeatability of the results.
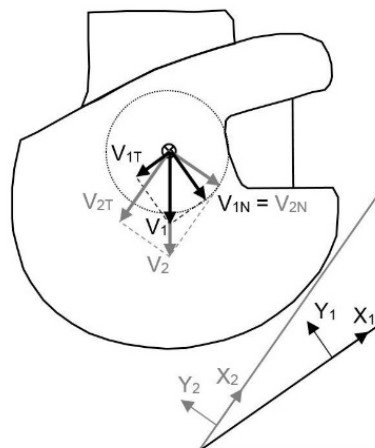
Figure 5.1: Impact velocities diagram. Modifying the angle of the anvil and the impact speed, the tangential component of the impact velocity can be modified keeping constant the magnitude of the normal component.

In total, 18 full face helmets of the M (57-58) size were used in this study (each impact location on each helmet was tested just one time). The outer shell of the tested helmet was

made of Fibre-reinforce plastic (FRP). The liner of the helmet was made of expanded polystyrene (EPS). The retention system of the helmet was based on a double D-ring buckle. The helmet complied with the ECE regulation and the United States Department of Transportation (DOT) standard. Table 5.1 summarizes the test conditions and the associated test numbers.

Table 5.1: Test matrix. For N from 1 to 3, indicating repeated tests for a particular condition.

Impact velocity	Anvil	Headform	Impact point	Test ID
6.5 m/s	60°	Bare headform	Front (Y-rot)	DT0322-0N-01
			Left side (X-rot)	DT0322-0N-02
			Right side (Z-rot)	DT0322-0N-04
		Covered headform	Front (Y-rot)	DT0321-0N-01
			Left side (X-rot)	DT0321-0N-02
			Right side (Z-rot)	DT0321-0N-04
8.0 m/s	45°	Bare headform	Front (Y-rot)	DT0320-0N-01
			Left side (X-rot)	DT0320-0N-02
			Right side (Z-rot)	DT0320-0N-04
		Covered headform	Front (Y-rot)	DT0319-0N-01
			Left side (X-rot)	DT0319-0N-02
			Right side (Z-rot)	DT0319-0N-04
9.9 m/s	35°	Bare headform	Front (Y-rot)	DT0318-0N-01
			Left side (X-rot)	DT0318-0N-02
			Right side (Z-rot)	DT0318-0N-04
		Covered headform	Front (Y-rot)	DT0317-0N-01
			Left side (X-rot)	DT0317-0N-02
			Right side (Z-rot)	DT0317-0N-04

5.2.2.   Testing procedure

The tests were performed at the Impact Laboratory of the University of Zaragoza. A free fall guided impact machine (Model: Quebrantahuesos 6.0, +D, Pozuelo de Alarcón, Spain) was used for the drop tests. The helmeted headform is placed on a carriage and restrained by pre-cut paper tape to prevent helmet motion during the fall. After releasing the carriage assembly from a specific height, the helmeted headform impacts the top surface of an anvil and the carriage assembly continues to fall onto a cushioned bed plate without interfering with the helmeted headform kinematics. Six helmets were drop tested at an impact velocity of 8.0 m/s onto a 45° oblique anvil, which originated two impact velocity components (normal and tangential) with the same magnitude of 5.66 m/s. The tangential velocity component (V_T) of this test set-up (subsequently referred to as the base case) was altered approximately ±40% while keeping constant the normal velocity component (V_N). Therefore, six helmets were drop tested at 6.5 m/s onto a 60° oblique anvil, obtaining a V_N of 5.66 m/s and a V_T of 3.27 m/s. Finally, six more helmets were drop tested at 9.9 m/s onto a 35° oblique anvil to obtain the same V_N and a V_T of 8.08 m/s. These two test conditions are referred as -40% V_T and +40% V_T respectively. Figure 5.1 illustrates how the combination of different impact velocities and different anvil angles resulted in constant normal component velocities with varying tangential component velocities.

The oblique anvils were made from a solid steel cylinder with the diameter of 130 mm cut with an angle of 60°, 45° and 35° defined from the vertical plane. The impact surface of the anvil was covered with a sheet of grade 80 close-coat aluminium oxide abrasive paper. The abrasive paper was replaced after significant damage or up to three impacts, whatever occurred first. All the helmets were tested with a 575-size magnesium alloy full headform (Model: 100_04_FMH, Cadex Inc., Saint-Jean-sur-Richelieu, QC, Canada).

To vary the value of the COF between the interior of the helmet and the surface of the headform, half of the helmets per test condition were tested with the original metallic surface of the headform (bare headform) and half of them were tested with the headform covered with a uniform thin layer of high-performance silicone rubber (Model: Dragon Skin 10, Smooth-On, Inc., Macungie, PA, USA). A total of 40 g of silicone rubber was uniformly spread to meet the thickness requirement of FRHPhe-01 (FIM, 2017). A spring balance method was used to provide an indication of the friction associated with the coating treatment. The average coefficient of friction (COF) measured between a cotton fabric and the bare headform and the coated headform was 0.20 and 0.78, respectively.

The headform was positioned inside the helmets using a helmet positioning index (HPI) of 40 mm. The retention system was adjusted under the chin of the headform and tightened to a tension of 75 N (FIM, 2017). Before each impact, the helmet was re-positioned and the retention system re-tensioned.

Three new helmet samples were used per each tangential velocity and headform surface condition. Each helmet was tested on front (Y-rot), left side (X-rot) and right side (Z-rot) (see Figure 5.2 for the position and orientation of the helmet coordinate system). The first impact was a frontal impact, leading to rotation in the sagittal plane around the Y-axis. The second impact was a parietal impact on the left side, leading to rotation in the frontal plane around the X-axis. In these two impacts, the central vertical axis (Z-axis) of the headform was aligned to the vertical. The third impact was a temporal impact on the right side, leading to rotation in the transverse plane around the Z-axis. For this oblique impact, the sagittal plane of the headform was positioned parallel to the impact surface of the anvil and the transverse plane of the headform was coincident with the vertical plane of symmetry of the anvil.

| Front (Y-rot) | Left side (X-rot) | Right side (Z-rot) |

Figure 5.2: Oblique impact point configurations.

A wireless system (Model: iCONO, +D, Pozuelo de Alarcón, Spain) was used to measure linear acceleration and angular velocity at the centre of gravity of the headform. The wireless system incorporates three linear accelerometers (Model: 64C-2000, MEAS, Nanshan District Shenzhen, China), three angular rate sensors (Model: ARS PRO-8k, DTS, Seal Beach USA) and an acquisition system (Model: SLICE NANO, DTS, Seal Beach, USA). Data were recorded at 10 kHz. Head linear acceleration signals were filtered using a low-pass filter CFC-1000 and angular velocities signals were filtered using a CFC-180. High-speed video was captured at 1000 Hz with a high-speed video camera (Model: Eosens mini, Mikrotron, Unterschleissheim, Germany). The view included a close-up of the left side of the oblique anvil to capture the helmeted headform motion in the main plane of rotation. The end of the impact was estimated when the measured acceleration was lower than 5 g. High-speed video captures showed good correlation with the instant in which the helmeted headform separated from the anvil. Data post-processing was performed using an in-house

developed and validated script of Matlab (Matlab R2021b, MathWorks, Natick, MA, USA).

5.2.3. Data analysis

Data were sorted by impact direction (front, left side & right side), tangential velocity (-40% V_T, base case & +40% V_T) and headform COF (bare headform & covered headform). Four kinematically-based head injury predictors were used to assess the protective performance of the helmet: the peak of the resultant linear acceleration (PLA), the head injury criterion (HIC) (Versace, 1971), the brain injury criterion (BrIC) (Takhounts et al., 2013) and the peak of the resultant angular acceleration (PAA). These head injury predictors were chosen for this study because they are used in the two standards that require different friction at the interface between the helmet and the headform (ECE, 2021; FIM, 2017). For each impact direction, a two-way analysis of variance (ANOVA) was used to estimate how each injury predictor changed according to the levels of tangential velocity and headform COF. The two-way ANOVA also checks for interactions between the two factors – for example, if the effect of the covered headform depends on the levels of the tangential velocities. When there were not significant differences in the interaction, the one-way ANOVA and the Tuckey's HSD post-hoc test were performed to study each factor individually. In case of a significant interaction, the two-way ANOVA is transformed into a one-way ANOVA and the Tuckey's HSD post-hoc test was performed to study each possible combination between the two factors. Significance level used for all statistical tests was $\alpha = 0.05$. To increase the statistical power of the post-hoc tests that resulted in significant differences, only those comparisons with the largest effect sizes (as measured by Cohen's d) were considered in this study. Statistical analysis was performed using the Real Statistics Resource Pack add-in in Excel (Excel 2016, Microsoft, Redmond, WA, USA).

5.3. Results

5.3.1. Front impact kinematics

At this impact location, differences were observed between the motion of the bare and covered headform inside the helmet. Figure 5.3 shows high-speed video captures at t=14 ms (about the end of the impact). The figure shows the change in the angle between a reference line on the helmet shell (initially oriented parallel to the horizontal direction) and a reference line on the neck of the headform, illustrating the relative motion between the helmet and the headform for each V_T observed in the case of the bare headform. However, in the case of the high COF of the coated headform, the angle remained constant at 96 degrees regardless of the V_T value.
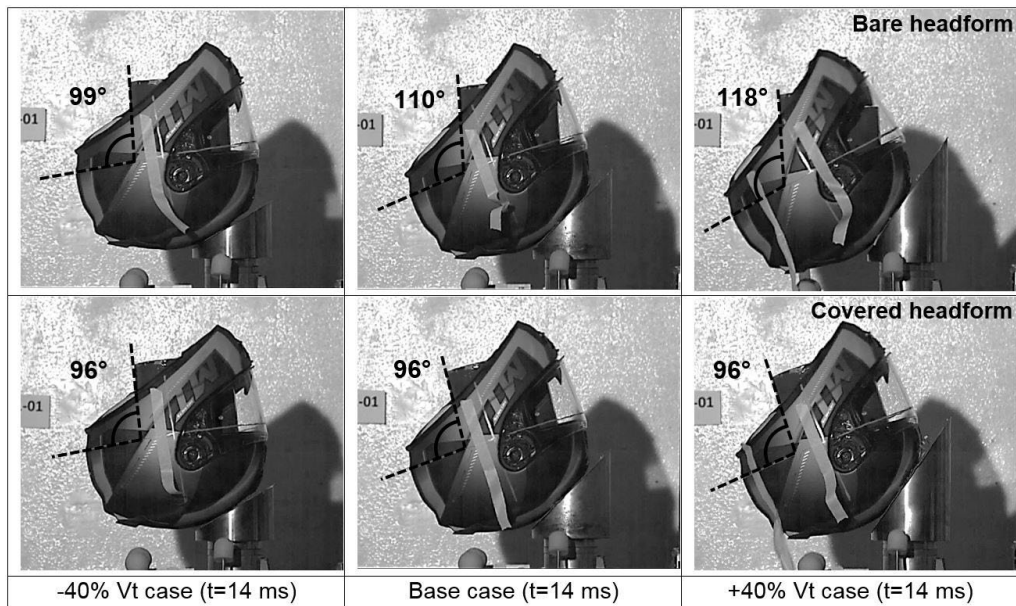
Figure 5.3: Relative motion of the headform inside the helmet about the end of the impact duration in the front impact configuration.

The comparison of the time history plots of the resultant linear acceleration is shown in Figure 5.4. The plot shows that the -40% V_T case (light grey traces) resulted in higher peak resultant linear acceleration and slightly shorter impact durations than the other two tangential velocities.
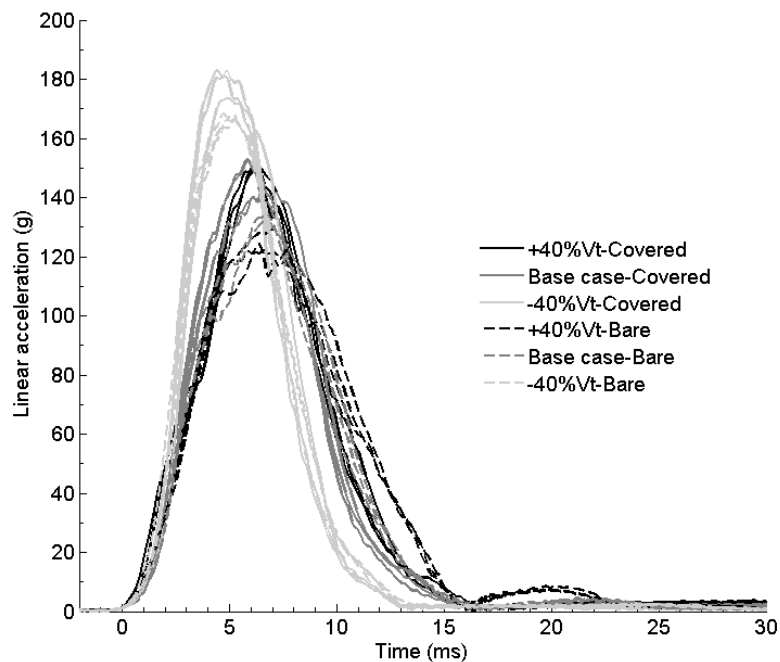
Figure 5.4: Resultant linear acceleration for the front impacts. Solid lines correspond to covered headform and dashed lines correspond to bare headform test.

The observed results might be influenced by the different location of the impact point between the helmet and the anvil, which was dependant on the tangential velocity component (as shown in Figure 5.5), reducing the magnitude of V_T shifted the impact point in the negative X direction. Within each value of V_T, the peak resultant acceleration of the high COF cases was consistently higher than the one in the bare headform cases.

| Front (Y-rot) | Left side (X-rot) | Right side (Z-rot) |
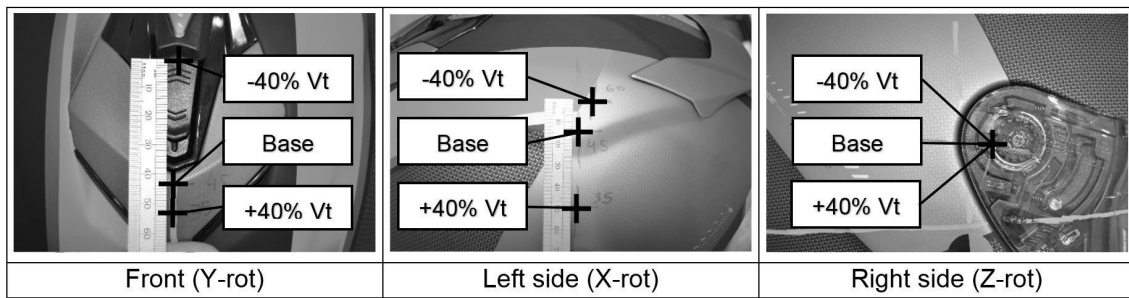
Figure 5.5: Impact point locations for each impact configuration and tangential velocity.

Figure 5.6 and Figure 5.7 show the time history plot of the resultant angular velocity and the resultant angular acceleration. As expected, the influence of the magnitude of V_T in the angular velocity can be clearly identified in Figure 5.6. The largest peak of the angular velocity was obtained for one of the tests with the +40% V_T, while the other two repeats of the same condition resulted in two different responses and were comparable in peak magnitude to the base case results with the covered headform (Figure 5.6). This lack of repeatability was attributed to the detachment of the helmet front vent in these two latter tests of the high COF tests. Regardless of the COF, the higher the magnitude of V_T, the higher the peak value of the angular velocity. Within each value of V_T, the coated headform (higher COF) resulted in higher magnitudes of angular velocity and a distinct maximum of the data trace, while the tests with the bare headform resulted in a monotonously growing curve.
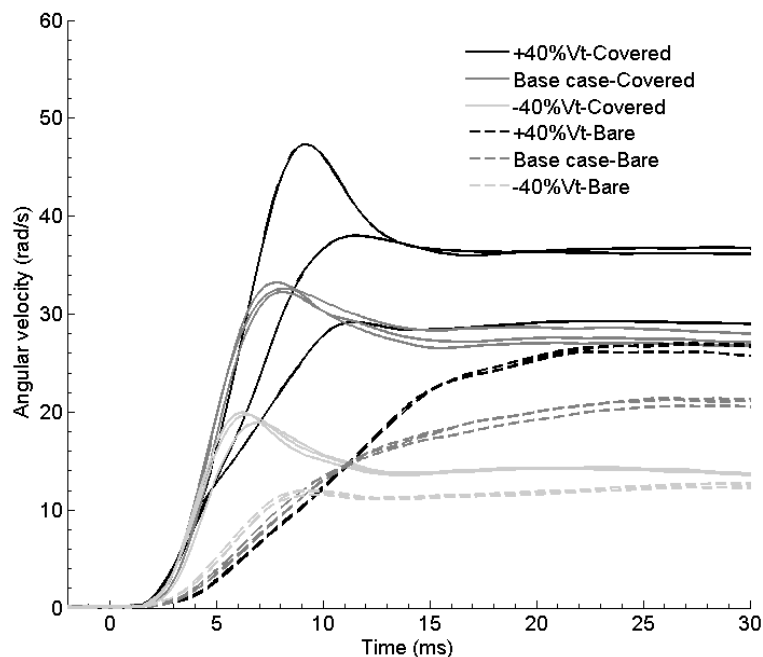
Figure 5.6: Resultant angular velocity for the front impacts. Solid lines correspond to covered headform and dashed lines correspond to bare headform test.

Again, the largest peak angular acceleration was obtained for one of the tests with the +40% V_T, while the other two repeats of the same condition resulted in two different responses due to the detachment of the helmet front vent. In the comparison between the baseline and the -40% V_T case with the coated headform, where the repeatability of the tests was clear and the vent did not detach from the helmet, the decrease in V_T is associated to a decrease in peak acceleration and shorter duration of the acceleration pulse. However, the peak angular acceleration did not show important differences between the different magnitudes of V_T while the duration of the acceleration pulse increased as the V_T increased

in the low COF tests. Regardless the value of V_T, coating the headform with the silicone resulted in higher angular acceleration levels and shorter durations of the pulse, indicating a better coupling between the headform and the helmet.
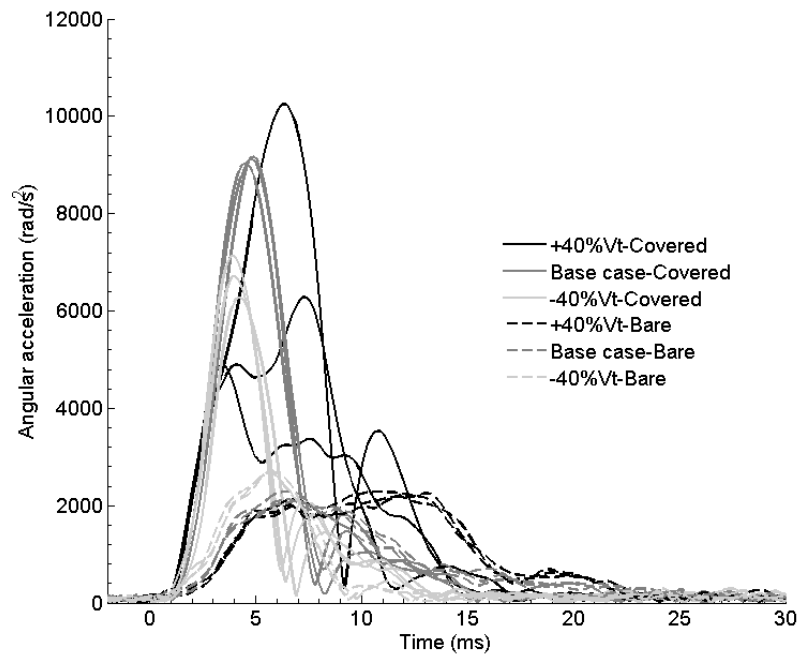
Figure 5.7: Resultant angular acceleration for the front impacts. Solid lines correspond to covered headform and dashed lines correspond to bare headform test.

5.3.2.   Left side impact kinematics

Figure 5.8 shows the high-speed video frames of the left-side impacts about the end of the impact (t=14 ms). Similarly to the previous configuration, the angle between a reference line on the helmet and the vertical central axis of the headform illustrated the relative motion between the helmet and the headform for each tangential velocity. The relative motion of the bare headform with respect to the helmet increased as the tangential velocity increased. In the +40% V_T case, when there was no additional room for the headform to move within the helmet, the shell of the helmet even deformed elastically. In the covered headform tests, the relative motion of the headform was reduced substantially.
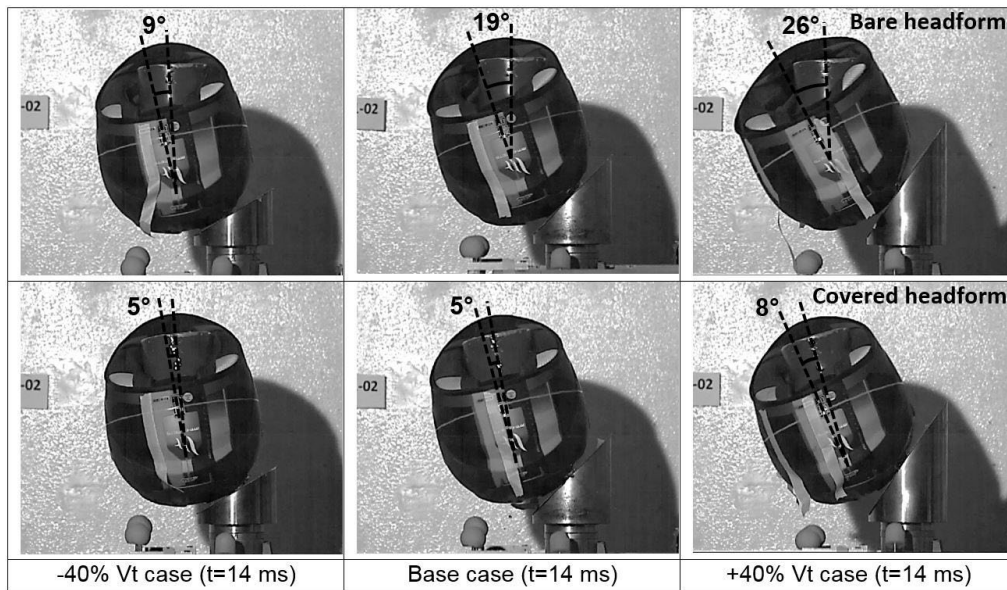
Figure 5.8: Relative motion of the headform inside the helmet about the end of the impact duration in the left-side impact configuration.

No important differences were observed in the time history plots of the resultant linear acceleration (Figure 5.9) in left-side impacts: slightly lower peaks were observed in the lower COF tests, but the differences were not relevant.
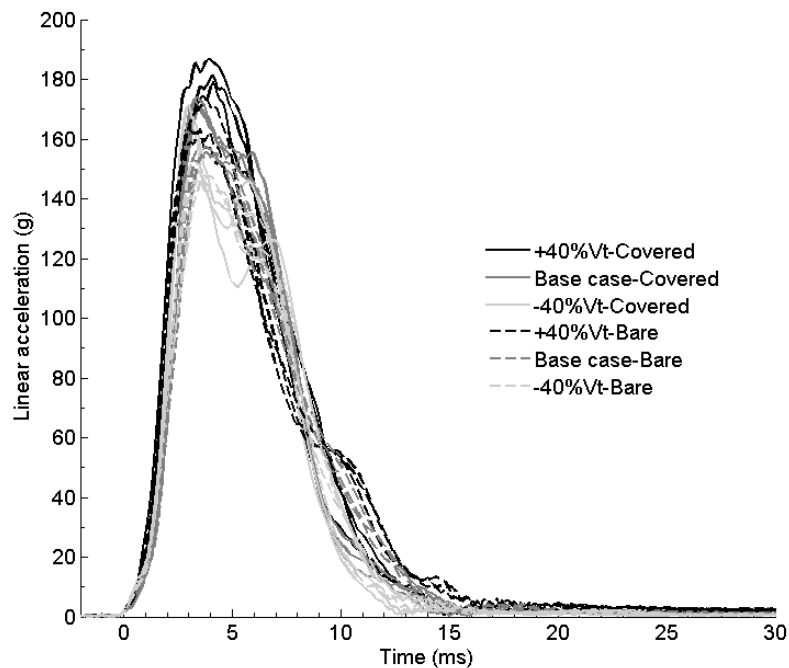
Figure 5.9: Resultant linear acceleration for the left side impacts. Solid lines correspond to covered headform and dashed lines correspond to bare headform test.

It is in the rotational behaviour of the headform where the differences begin to arise. Figure 5.10 shows that the slopes of the traces corresponding to high COF are more similar than the slopes of the curves for the low COF at different magnitudes of V_T. As there was no relative motion between the headform and the helmet in the covered headform tests, the unique factor that influenced these slopes was the different magnitudes of V_T. On the contrary, in the bare headform tests, in which the relative motion increased as the V_T increased, there was a higher increase of the slopes of the curves as the magnitude of the

tangential velocity increased resulting in that the +40% V_T slope was similar to the slopes of the high COF tests. This similitude at the highest V_T can be explained as the relative motion between the headform and the helmet is limited by the interaction of the geometry of the two solids. Higher values of V_T made this interaction to occur, and the headform and the helmet moved without relative motion increasing suddenly the slope and the magnitude of the angular velocity.
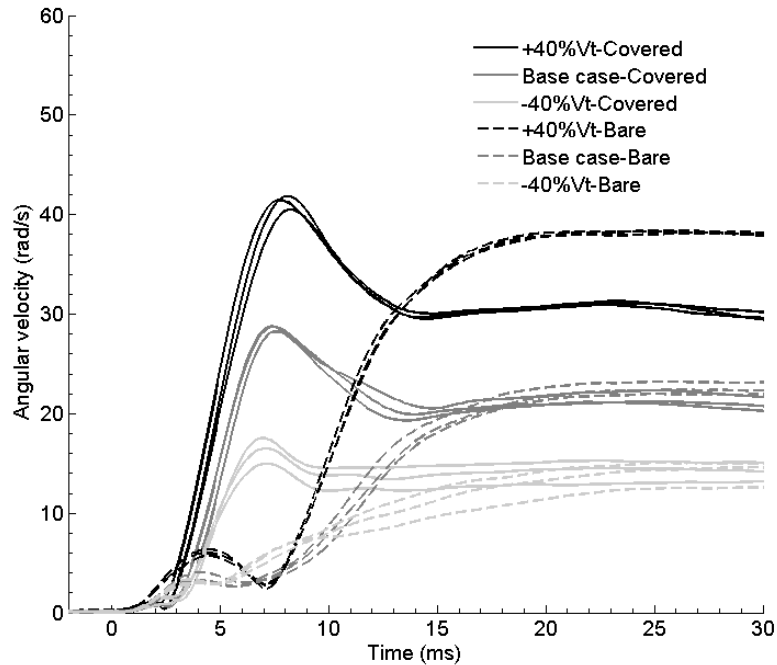
Figure 5.10: Resultant angular velocity for the left side impacts. Solid lines correspond to covered headform and dashed lines correspond to bare headform test.

Figure 5.11 shows completely different kinematics depending on the value of the COF between the helmet and the headform: while the higher COF tests showed an initial global maximum and then a second local maximum, in the case of the lower COF tests, the first maximum was local with the global maximum occurring about 8-10 ms later. The duration of the acceleration curve was longer also in the case of the lower COF tests. As for the influence of the magnitude of V_T, and independently of the value of the COF, higher values of V_T resulted in higher angular acceleration peaks.
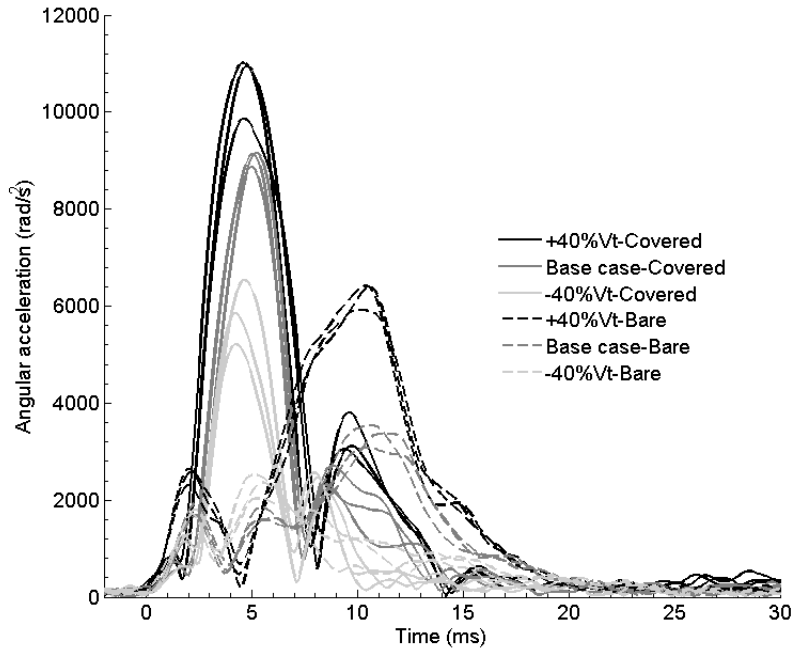
Figure 5.11: Resultant angular acceleration for the left side impacts. Solid lines correspond to covered headform and dashed lines correspond to bare headform test.

5.3.3. Right side impact kinematics

Attending to the images from the high-speed video (Figure 5.12), it can be seen two different relative motions (indicated by the two dotted white lines in the Figure 5.12). The first one is a relative rotation around the Z-axis because of the tangential input applied to the helmet, which was only observed with the bare headform and it increased as the V_T increased (illustrated by the angular misalignment of the two dotted white lines). The second one is a relative rotation around the X-axis because of the torque created by the distance from the impact point and the centre of gravity of the helmeted headform. It is observed with both COF (clearly shown by the parallel misalignment between the two dotted white lines for the -40% V_T case) and remained almost constant for the different magnitudes of the V_T (more clearly illustrated for the covered headform than the bare headform due to the absence of the angular misalignment of the two dotted white lines).
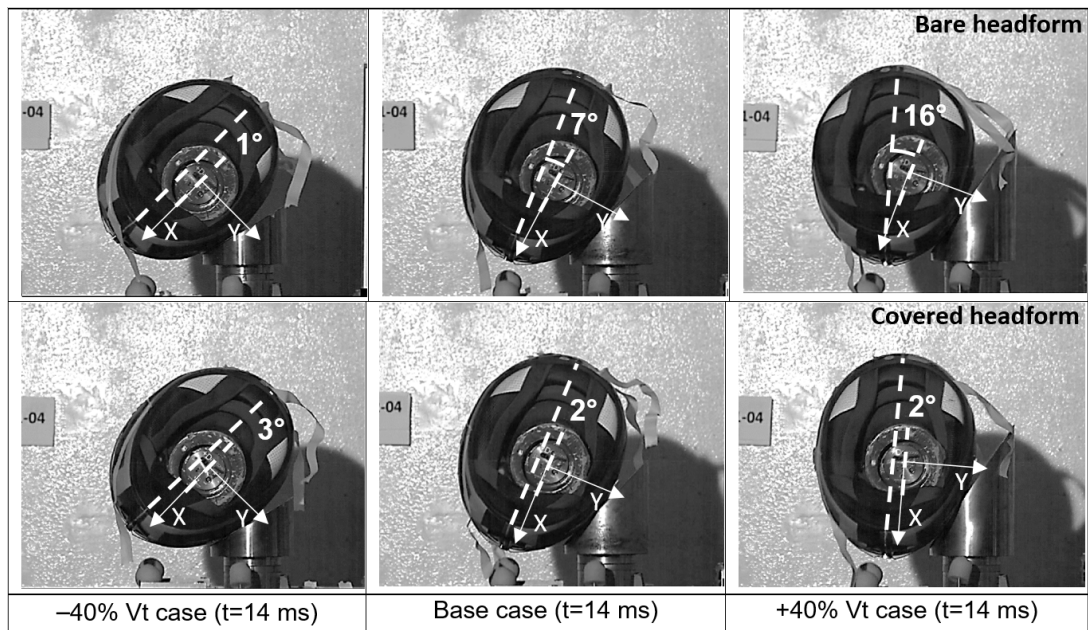
Figure 5.12: Relative motion of the headform inside the helmet about the end of the impact duration in the right-side impact configuration. Dashed lines indicate the headform position with respect to the helmet.

Similarly to the left-side impacts, the time history plot of the resultant linear acceleration did not show differences associated to either the magnitude of V_T or the value of the COF (Figure 5.13).
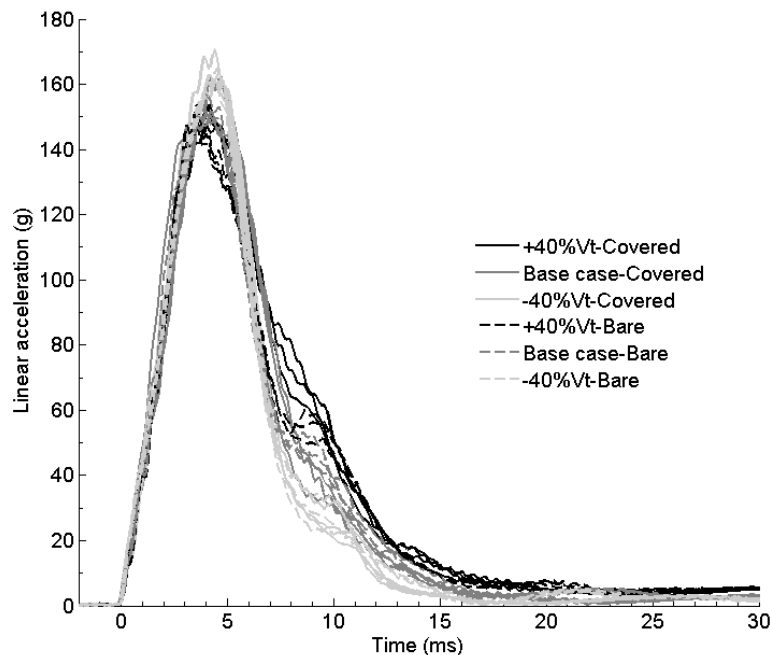
Figure 5.13: Resultant linear acceleration for the right side impacts. Solid lines correspond to covered headform and dashed lines correspond to bare headform test.

Again, it is the rotational magnitudes the ones that were influenced by the change in these two parameters. The peak of the angular velocity was higher for higher values of V_T, independently of the COF magnitude (Figure 5.14). Increasing the COF between the helmet and headform resulted in a more identifiable angular velocity maximum, while the response of the bare headform produced slower increasing curve of the angular velocity, especially in the larger V_T cases.
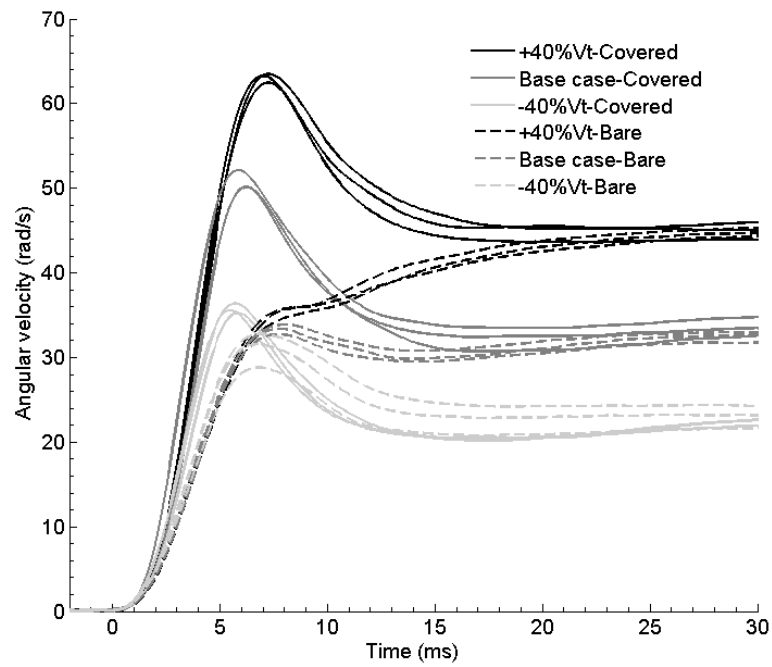
Figure 5.14: Resultant angular velocity for the right side impacts. Solid lines correspond to covered headform and dashed lines correspond to bare headform test.

In the case of the angular acceleration, Figure 5.15 shows that higher values of V_T resulted in higher peaks of angular acceleration only when the headform was coated (high COF values). When the COF was low (bare headform), no important differences were identified between the different values of V_T.
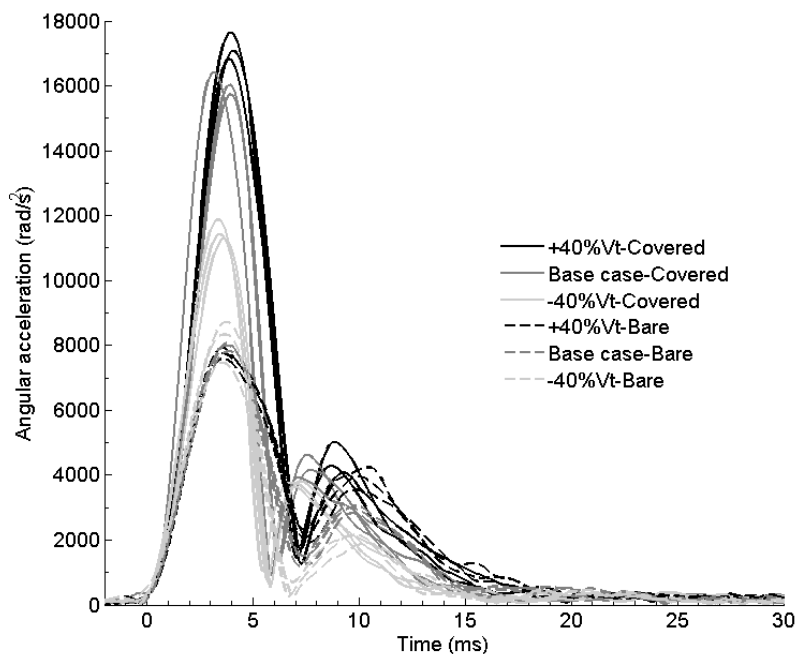
Figure 5.15: Resultant angular acceleration for the right side impacts. Solid lines correspond to covered headform and dashed lines correspond to bare headform test.

5.3.4.   Data statistical analysis

Statistical results of the two-way ANOVA are presented for each injury predictor and each impact direction. Two factors were studied: the influence of the change of V_T and the effect of changing the COF in each of the proposed injury predictors. Also, the effect of the

interaction of the two factors on each injury predictor was studied.

In addition, in the post-hoc tests after the ANOVA, the effect of the headform surface treatment (bare vs. coated) was analysed for each level of the tangential velocity (-40% V_T, base case and +40% V_T) and the effect of the tangential velocity was studied with respect to the base case level.

Regarding the PLA, there were significant differences in the coating factor for the front and left side impacts. The tangential velocity factor was significantly different for the three impact directions and the interaction term was statistically different only for the front impact. Statistical results of the two-way ANOVA are included in Table 5.2.

Table 5.2: Two-way ANOVA results (p-values) for the PLA. Significant values are shown in bold font.

	Front (Y-rot)	Left side (X-rot)	Right side (Z-rot)
Coating	**4.7×10^{-7}**	**0.00016**	0.11161
Tangential velocity	**2.3×10^{-9}**	**0.00095**	**0.00031**
Interaction	**0.03058**	0.99408	0.73341

Descriptive statistics of the test results and statistical results from the post-hoc tests for the PLA are presented in Table 5.3. Nine of the twenty-one PLA post-hoc comparisons resulted in significant differences. However, attending to the effect size only three comparisons were considered relevant. These relevant differences were identified only in frontal impacts as follows: the increased PLA between the -40% V_T and baseline for the bare headform (167 ± 1 g vs. 135 ± 3 g), the increased PLA between the -40% V_T and baseline for the covered headform (180 ± 5 g vs. 149 ± 6 g), and the decreased PLA between the bare and covered headform (125 ± 4 g vs. 150 ± 0 g) for the +40% V_T.

Table 5.3: Averages, standard deviation (SD), coefficient of variation (CV) and post-hoc results for PLA. Significant values are shown in bold font.

	PLA (g)	Front (Y-Rot)			Left Side (X-Rot)			Right Side (Z-Rot)		
		−40% V_T	Base Case	+40% V_T	−40% V_T	Base Case	+40% V_T	−40% V_T	Base Case	+40% V_T
Bare	Average	167	135	125	149	156	167	163	153	149
	SD	1	3	4	3	1	6	2	3	4
	CV(%)	0.64%	2.59%	2.90%	2.19%	0.73%	3.50%	1.28%	1.89%	2.40%
V_T	Cohen's d	8.10		2.53	1.77		2.79	2.53		1.01
effect	*p*-value	**2.7×10^{-6}**		0.07149	0.12211		**0.03969**	**0.01523**		0.38922
Covered	Average	180	149	150	164	172	182	165	158	151
	SD	5	6	0	13	2	4	5	6	3
	CV(%)	2.98%	3.70%	0.25%	7.78%	1.23%	2.16%	3.09%	3.67%	2.09%
V_T	Cohen's d	7.85		0.25	2.03		2.53	1.77		1.77
effect	*p*-value	**5.0×10^{-6}**		0.99961	>0.05		>0.05	0.27546		0.27695
Coating	Cohen's d	3.29	3.54	6.33	3.80	4.05	3.80	0.51	1.27	0.51
effect	*p*-value	**0.01439**	**0.0054**	**3.7×10^{-5}**	0.11458	**0.00032**	**0.01765**	>0.05	>0.05	>0.05

Concerning the HIC, there were significant differences for the coating factor, the tangential velocity factor and the interaction for the three impact directions (Table 5.4).

Table 5.4: Two-way ANOVA results (p-values) for the HIC. Significant values are shown in bold font.

	Front (Y-rot)	Left side (X-rot)	Right side (Z-rot)
Coating	**5.7×10^{-8}**	**7.4×10^{-6}**	**2.5×10^{-6}**
Tangential velocity	**1.3×10^{-11}**	**0.00012**	**0.00692**
Interaction	**0.01841**	**0.00319**	**0.04017**

Eleven of the twenty-one HIC post-hoc comparisons resulted in significant differences but attending to the effect size (Cohen's d), only five were considered relevant (Table 5.5).

Table 5.5: Averages, standard deviation (SD), coefficient of variation (CV) and post-hoc results for HIC. Significant values are shown in bold font.

	HIC	Front (Y-Rot)			Left Side (X-Rot)			Right Side (Z-Rot)		
		$-40\%\ V_T$	Base Case	$+40\%\ V_T$	$-40\%\ V_T$	Base Case	$+40\%\ V_T$	$-40\%\ V_T$	Base Case	$+40\%\ V_T$
Bare	Average	1213	870	857	1049	1056	1145	893	825	781
	SD	30	11	15	58	20	68	32	15	16
	CV(%)	2.51%	1.31%	1.73%	5.53%	1.86%	5.98%	3.64%	1.81%	2.10%
V_T	Cohen's d	9.07		0.34	0.19		2.35	1.80		1.16
effect	*p*-value	**2.6 x 10⁻⁸**		0.98957	0.99999		0.68434	0.10190		0.46244
Covered	Average	1382	1058	947	1099	1378	1552	953	949	936
	SD	25	12	47	116	11	102	39	30	32
	CV(%)	1.82%	1.13%	4.96%	10.56%	0.83%	6.59%	4.04%	3.11%	3.47%
V_T	Cohen's d	8.57		2.94	7.38		4.60	0.11		0.34
effect	*p*-value	**5.0 x 10⁻⁸**		**0.00279**	**0.00576**		0.10668	0.99995		0.99216
Coating	Cohen's d	4.47	4.97	2.38	1.32	8.52	10.76	1.59	3.28	4.10
effect	*p*-value	**6.0 x 10⁻⁵**	**2.0 x 10⁻⁵**	**0.01364**	0.95603	**0.00184**	**0.00022**	0.18190	**0.00204**	**0.00028**

The identified relevant differences were the following: the increased HIC between the -40% V_T and base case for the bare headform (1213 ± 30 vs. 870 ± 11) and covered headform (1382 ± 25 vs. 1058 ± 12) in the front impact; the decreased HIC between the -40% V_T and base case for the covered headform (1099 ± 116 vs. 1378 ± 11) in the left side impact; and the decreased HIC between the bare and covered headform for the base case (1056 ± 20 vs. 1378 ± 11) and for the +40% V_T case (1145 ± 68 vs. 1552 ± 102) in the left side impact.

Regarding BrIC, the two-way ANOVA resulted in significant differences for the two factors in the three impact configurations and the interaction in the left and right-side impacts (Table 5.6).

Table 5.6: Two-way ANOVA results (p-values) for the BrIC. Significant values are shown in bold font.

	Front (Y-rot)	Left side (X-rot)	Right side (Z-rot)
Coating	**7.5 x 10⁻⁶**	**2.9 x 10⁻¹⁰**	**1.7 x 10⁻¹²**
Tangential velocity	**5.2 x 10⁻⁵**	**1.6 x 10⁻¹⁴**	**6.4 x 10⁻¹⁴**
Interaction	0.15082	**0.00131**	**9.1 x 10⁻⁷**

Only two of the twenty-one BrIC post-hoc comparisons were statistically non-significant, but the results are probably influenced by the low repeatability obtained for the angular velocity in the +40% V_T case with the covered headform (Table 5.7). The effect size revealed significant differences for all comparisons; however, it is worth highlighting the differences between the baseline case and the +40 V_T case for the bare headform in the left side impact (0.280 ± 0.008 vs. 0.540 ± 0.002) and in the right-side impact (0.750 ± 0.007 vs. 1.060 ± 0.015).

Table 5.7: Averages, standard deviation (SD), coefficient of variation (CV) and post-hoc results for BrIC. Significant values are shown in bold font.

BrIC		Front (Y-Rot)			Left Side (X-Rot)			Right Side (Z-Rot)		
		$-40\%\ V_T$	Base Case	$+40\%\ V_T$	$-40\%\ V_T$	Base Case	$+40\%\ V_T$	$-40\%\ V_T$	Base Case	$+40\%\ V_T$
Bare	Average	0.210	0.310	0.400	0.170	0.280	0.540	0.620	0.750	1.060
	SD	0.004	0.007	0.001	0.020	0.008	0.002	0.040	0.007	0.015
	CV(%)	1.88%	2.35%	0.27%	11.88%	2.78%	0.43%	6.54%	0.98%	1.44%
	V_T effect Cohen's d	8.81		7.93	9.69		22.90	11.45		27.30
	V_T effect *p*-value	**5.3×10^{-7}**		**1.2×10^{-6}**	**2.5×10^{-6}**		**2.9×10^{-10}**	**9.2×10^{-5}**		**1.0×10^{-8}**
Covered	Average	0.350	0.580	0.680	0.260	0.440	0.630	0.770	1.140	1.430
	SD	0.011	0.008	0.158	0.022	0.002	0.010	0.013	0.029	0.004
	CV(%)	3.03%	1.33%	23.25%	8.47%	0.49%	1.63%	1.73%	2.51%	0.30%
	V_T effect Cohen's d	20.25		8.81	15.85		16.73	32.58		25.54
	V_T effect *p*-value	**6.5×10^{-6}**		0.39176	**1.3×10^{-8}**		**6.8×10^{-9}**	**1.2×10^{-9}**		**2.0×10^{-8}**
Coating effect	Cohen's d	12.33	23.78	24.66	7.93	14.09	7.93	13.21	34.34	32.58
	p-value	**3.0×10^{-5}**	**1.6×10^{-6}**	0.09232	**2.0×10^{-5}**	**5.1×10^{-8}**	**1.2×10^{-5}**	**3.2×10^{-5}**	**7.6×10^{-10}**	**1.2×10^{-9}**

Finally, significant differences of the two-way ANOVA for the PAA were found for the coating factor in all three impact configurations and for the magnitude of the tangential velocity and the interaction in the left and right-side impacts (Table 5.8).

Table 5.8: Two-way ANOVA results (p-values) for the PAA. Significant values are shown in bold font.

	Front (Y-rot)	Left side (X-rot)	Right side (Z-rot)
Coating	**4.7×10^{-7}**	**3.0×10^{-11}**	**4.6×10^{-14}**
Tangential velocity	0.29474	**2.4×10^{-9}**	**9.1×10^{-8}**
Interaction	0.11984	**0.00280**	**2.0×10^{-8}**

In this case, thirteen of fifteen post-hoc comparisons for the covered headform resulted in significant differences and the effect size revealed strong differences in all cases. The two non-significant comparisons were also related with the $+40\%\ V_T$ case in the frontal impact, where the front vent of the helmet influenced the angular measurements increasing the variability. However, only two of six comparisons for the tangential velocity with the bare headform resulted in significant differences and just one was considered relevant due to the effect size (Table 5.9). This comparison was between the base case and the $+40\%\ V_T$ case in the left side impact (3330 ± 233 rad/s^2 vs. 6241 ± 277 rad/s^2).

Table 5.9: Averages, standard deviation (SD), coefficient of variation (CV) and post-hoc results for PAA. Significant values are shown in bold font.

BrIC		Front (Y-Rot)			Left Side (X-Rot)			Right Side (Z-Rot)		
		$-40\%\ V_T$	Base Case	$+40\%\ V_T$	$-40\%\ V_T$	Base Case	$+40\%\ V_T$	$-40\%\ V_T$	Base Case	$+40\%\ V_T$
Bare	Average	2681	2168	2241	2305	3330	6241	8171	7955	7753
	SD	14	101	51	248	233	277	641	127	166
	CV(%)	0.51%	4.66%	2.26%	10.76%	7.01%	4.43%	7.84%	1.60%	2.15%
	V_T Cohen's d	1.89		0.27	3.77		10.70	0.79		0.74
	V_T effect *p*-value	**0.00018**		0.41116	0.09604		**2.6×10^{-5}**	0.97741		0.98343
Covered	Average	6702	9106	7141	5864	9050	10607	11524	16055	17173
	SD	433	70	2778	663	161	646	308	339	421
	CV(%)	6.46%	0.77%	38.90%	11.30%	1.78%	6.09%	2.67%	2.11%	2.45%
	V_T Cohen's d	8.83		7.22	11.71		5.72	16.65		4.11
	V_T effect *p*-value	**0.00068**		0.34510	**1.0×10^{-5}**		**0.00729**	**5.4×10^{-8}**		**0.03035**
Coating effect	Cohen's d	14.78	25.49	18.01	13.08	21.02	16.04	12.32	29.76	34.61
	p-value	**0.00381**	**6.5×10^{-8}**	0.09246	**3.1×10^{-6}**	**1.5×10^{-8}**	**3.3×10^{-7}**	**1.6×10^{-6}**	**7.0×10^{-11}**	**7.6×10^{-12}**

5.4. Discussion

The objective of this chapter was to quantify the influence of the COF between the interior surface of the helmet and the headform in the resulting kinematics of the headform at different magnitudes of the tangential impact velocity. The discussion is divided into four parts: first, the variability of the friction between the human skin and the helmet is reviewed. Second, the influence of the COF between the interior surface of the helmet and the headform in the resulting linear kinematics is debated. Third, the influence of the COF between the interior surface of the helmet and the headform in the resulting angular kinematics is discussed. Finally, the limitations of this study are exposed.

5.4.1. The variability of the friction between the human skin and the helmet inner liner

Human skin has been shown to exhibit a complex and highly variable friction behaviour. Ebrahimi et al. (2015) obtained an average friction coefficient between the interior of the helmet (nylon fabric) and the human skin of 0.683. However, other experiments using human cadaver heads estimated substantially lower values for the coefficient of friction between the interior of the helmet (polyester fabric, a common material used in the interior liner of helmets) and the scalp (0.29 ± 0.07) (Trotta et al., 2018a). In a tactile perception study unrelated to helmets, Ramalho et al. (2013) reported a COF about 0.7 between polyester fabric and the volar forearm of in vivo volunteers. This value could be even higher in the case of the head as other experimental studies have revealed that friction coefficients at volar forearm were lower (COF = 0.26) than those measured on the forehead (COF = 0.34) (Cua et al., 1990). The variation of friction coefficients measured for the human skin has been suggested to depend on skin hydration (Derler et al., 2015), with moisture increasing the value of the COF between the skin and the fabric (Gerhardt et al., 2008). As sweating is very common among helmeted riders specially in warmer weathers, this study is essential to understand how the performance of helmets can be affected by changes in the COF.

Although the influence of the COF had already been addressed by Ebrahimi et al. (2015), this is the first time that an experimental study combines the effect of varying the tangential component of the impact velocity and the COF at the same time. The results of this chapter show that the combination of different magnitudes of V_T and COF influences differently the helmet performance.

5.4.2. Linear acceleration-based injury predictors

The experimental results included here regarding the V_T variation are consistent with two computational studies which concluded that the influence of increasing tangential velocity on the linear acceleration is insignificant (Meng et al., 2020; Mills et al., 2009). In the right-side impacts, where the impact point was exactly the same for the three tangential velocities, the PLA and HIC magnitudes decreased slightly as the tangential velocity increased (Figure 5.13). This slight decrease can be explained by an increased helmet rotation caused by higher values of V_T, which could bring new areas of uncrushed liner into the impact area, contributing to the decrease of PLA and HIC magnitudes (Mills & Gilchrist, 2008).

It is true that in the front and left side impact directions the statistical analyses resulted in significant differences for the PLA and HIC magnitudes. However, for these impact directions, the central vertical axis (Z-axis) of the headform was aligned to the vertical and, consequently, the impact point location changed with the angle of the anvil (see

Figure 5.5). PLA and HIC magnitudes decreased as the V_T increased in the front impacts while they increased as the tangential velocity increased in the left side impact direction. This opposite trend suggests that these differences are due to the variation of the impact point location and not due to the change in V_T.

Most helmet standards call for helmets to be tested in normal impacts (without tangential component) at the highest levels of severity ignoring the helmet response to lower severity impacts. Recently, some helmet standards such as FRHPhe-01 (FIM, 2017) and ECE 22.06 (ECE, 2021) included a low severity linear impact test at 5 m/s and 6 m/s respectively in their test methods in order to avoid that helmets transmit unacceptably high levels of linear acceleration in low severity impact events. Beside of these low severity impact tests, these standards also include an oblique impact test at 8.0 m/s against a 45-degree anvil, which originate two impact velocity components (normal and tangential) with the same magnitude of 5.66 m/s. Since the influence of the V_T on the linear acceleration is insignificant and the magnitude of the normal component of the impact velocity of the oblique test (5.66 m/s) is already within the range of the low-speed tests recently included in the aforementioned standards, this study supports that the oblique impact test also included in these helmet standards could be sufficient to characterize the linear acceleration in low severity impacts without the need of a specific low severity test.

Regarding the coating effect, the PLA and HIC magnitudes obtained were always higher for the tests with the high COF. The relative motion of the headform in the helmet, which depends on the tangential velocity for the bare headform, modify the crushing liner area depending on the geometry of the headform close to the impact point. Therefore, depending on the liner density around the impact point and the crushing liner area variation, the PLA and HIC could decrease, maintain or even increase. This is supported by Ebrahimi et al. (2015) that found that the average linear acceleration of the headform with the highest COF for the 15° anvil decreased by 26% while it increased by 10% for the 30° anvil.

5.4.3. Angular motion-based injury predictors

The coefficient of friction between the interior of the helmet and the headform plays an important role in the angular motion-based injury predictors during an oblique impact. The interaction of the two-way ANOVA for the two angular injury predictors showed that the effect of the COF depends on the magnitude of the tangential velocity (except for the front direction probably influenced by the low repeatability in the +40% V_T case). This dependence of the COF's effects with the V_T is mainly due to the combination of the rolling and sliding phenomena at the helmet/anvil interface, which was observed in the high COF tests and it was studied in detail by Meng et al. (2020) and to the relative motion between the headform and the helmet, which was observed in the low COF tests.

In the case of the coated headform, BrIC and PAA increased as the tangential velocity increased for the three impact directions (except in the two repeats of the frontal impacts in the +40% V_T case in which the front vent was detached from the helmet). Interestingly, our experiments showed that the relative increase of the angular injury predictors was higher from the -40% V_T case to the base case than from the base case to the +40% V_T case. As demonstrated in Meng et al. (2020) the effect of increasing V_T in the rotation of the helmet is negligible once the helmet is sliding. This suggest that from -40% V_T case to the base case the helmets were in rolling phase while from base case to the +40% V_T case the helmets were in the transition phase from rolling to sliding.

In the bare headform tests, BrIC also increased as the V_T increased but PAA did not in the front and right-side directions, in which PAA were almost constant. In this case, the lower COF between the headform and the helmet caused the bare headform to slide inside the helmet. This sliding motion limited the maximum angular acceleration (slope of the angular velocities curves) but not the maximum angular velocity, which also depends on the duration of the angular acceleration, which was higher for the higher V_T values (see Figure 5.7 and Figure 5.15). In the left side impacts, the relative motion of the headform inside the helmet was prevented by the interaction of the geometry of the headform and the geometry of the helmet, as the V_T increased. In the +40% V_T case, the relative motion came to an end and helmet and headform moved jointly increasing the headform rotational motion significantly.

The existing interaction of the COF between the helmet and the headform and V_T needs to be recognized when a testing program is being planned. Existing helmet testing methods have been shown to use speeds which are lower than those found in real world situations (Meng et al., 2020), mainly due to limitation of the height of the helmet drop facilities of the testing laboratories. This implies lower magnitude for the tangential component of the velocity than those found in real world situations. Therefore, even if the normal component of the impact velocity and the friction between the anvil and the helmet are high enough so that the helmet is rolling on the anvil, the tests in these laboratories will underestimate the angular motion that the motorcyclist's head could undergo in a real crash. Our experiments show that there may be an additional underestimation of the rotational motion of the head if the COF between the headform and the helmet is low and, consequently, the headform slides inside the helmet during the impact phase. As discussed above, there is evidence showing that the friction coefficient between the human head and the liner of the helmet can be around 0.7. This friction it is expected to increase if there is sweating, which can be common especially in warm weathers (Gerhardt et al., 2008). Thus, as several existing testing programs are starting to look into different injury metrics related to the rotation of the headform and these programs should be looking into testing the helmets so that they are effective in a worst-case (but possible) scenario, this study suggests that the COF at the interface helmet/headform in oblique helmet programs should be high enough to guarantee the joint motion of the unit without sliding of the headform.

5.4.4. Limitations

As aforementioned, the high-speed video analysis revealed that the front vent of the helmet was detached during the impact in two of the three replicas of the +40% V_T case with the headform covered. This fact was the cause of the low repeatability obtained for the angular velocity and angular acceleration in the mentioned condition. This may have been a limitation for the statistical analysis however, this finding suggest that the appendices of the helmet shells may be designed to be detached easily in order to reduce the angular motion of the head of the motorcyclist in case of oblique impact.

The rigid magnesium EN960 headforms do not have an outer layer to simulate the scalp tissue because they are not designed to respond like a human head to impact. Therefore, slippage between the scalp and skull and the tensioning effect of the skin were not covered in this work (Trotta et al., 2018a). Even if a study identified that scalp tissue affects head biomechanics in a significant way (Trotta et al. 2018b), it also concluded that the friction coefficient of the outer layer of the headform and the interaction with the helmet reduced the relative effect of the scalp.

Another limitation of this chapter is that only one full-face helmet model and three impact directions were tested. Therefore, the results of this study may vary for other helmet types and other impact directions.

Note: This chapter is a slightly modified version of the paper titled: The Influence of Headform/Helmet Friction on Head Impact Biomechanics in Oblique Impacts at Different Tangential Velocities published in Applied Sciences under an open access Creative Common CC BY license (Juste-Lorente et al., 2021).

Chapter 6

Chin Bar Impact Test and Basilar Skull Fracture Prevention

6.1.   Introduction

Several real-world motorcycle crashes studies have shown that basilar skull fracture (BSF) is one of the most common and severe injuries sustained by motorcyclists (Chee & Ali, 1991; Cooter & David, 1990; Piantini et al., 2016; Whyte et al., 2016). In a study of 100 patients with BSF, Chee & Ali (1991) reported that half of the injured patients were motorcyclists. An injury analysis of 40 motorcyclist urban crashes found that almost 69% of cranium injuries took place at the base of skull (Piantini et al., 2016). A study based in 47 fatal motorcycle crashes confirmed the prevalence of BSF and intracranial lesions despite helmet protection (Whyte et al., 2016). Dowdell et al. (1988) studied 200 crashes involving helmeted motorcyclists and found that almost all BSF injuries were caused by frontal impacts to the chin alone, the brow alone or both. The crash analysis of 598 riders wearing full-face helmets revealed that the chin impact causes the injuries with the most severe consequences in which basilar skull fracture was a frequent outcome (Otte, 1991). Many other in-depth motorcycle crash investigation studies have observed that the chin bar is a frequently impacted region of full-face motorcycle helmets (Chinn et al., 2001; Whyte et al., 2015).

Basilar skull fractures have been attributed to a variety of causal mechanisms such as skull bending, cervical axial loading or facial impact, however, hyperextension from frontal head impact is likely to lead to BSF with or without a helmet (Thom & Hurt, 1993). In an experimental study on cadavers specifically focused on mandibular impact and neck loading as potential mechanisms, McElhaney et al. (1995) showed that a direct temporomandibular loading in conjunction with tensile neck loading was the most probable loading condition that can produce BSF while direct chin impact in absence of neck loading produced mandibular fractures but no basilar skull fractures. They proposed an upper neck tensile load of 4300 ± 350 N as a biomechanical tolerance limit for BSF. The mentioned study is in agreement with the observations from Cooter & David (1990) who observed that hospitalized motorcyclists who had worn open-face helmets, or full-face helmets with flexible chin bars, had sustained facial fracturing. In contrast, motorcyclists killed from anterior craniofacial impacts while wearing full-face helmets with rigid chin bars had sustained BSF in the absence of significant facial trauma. They postulated that impacts to

rigid chin bar of full face helmets might create a temporomandibular loading via the chin strap and such loading would be sufficient to produce basilar skull fracture.

Some helmet testing standards prescribe simple tests for assessing the chin bar of full-face helmets (United Nations Economic Commission for Europe [ECE], 2021; International Motorcycling Federation [FIM], 2017; Snell Foundation [Snell], 2020). The Snell chin bar test limits the deflection of the chin bar towards the face. The helmet is affixed to a rigid base with the chin bar facing upward. A 5 kg weight is dropped through a guided fall to strike the central portion of the chin bar (see Figure 6.1). The chin bar test of the 06 series of amendments of the ECE Regulation 22 (ECE 22.06) and the chin bar test of the FIM Racing Homologation Programme for helmets (FRHPhe-01) limits the peak of the resultant linear acceleration (PLA) and the head injury criterion (HIC) measured at the centre of gravity of the headform. The helmeted headform is dropped in a free fall onto a rigid flat anvil (see Figure 6.2). The Snell test method provides a less realistic and accurate assessment of the ability of the chin bar to protect against head injuries than the ECE 22.06 or FRHPhe-01 chin bar test because it does not use any head surrogate (headform) for the chin bar assessment (Chang et al., 1999). Despite ECE 22.06 and FRHPhe-01 chin bar test uses a headform for the chin bar assessment, it is an isolated head surrogate, without the rest of the body, and therefore, none of these test procedures consider the neck tensile load to assess the risk of basilar skull fracture.
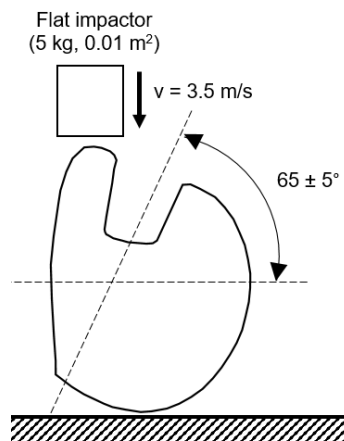
Figure 6.1: Snell chin bar impact test configuration

A combined methodology using the output kinematics measured with a dummy headform during a physical test as input to a Finite Element (FE) model has become common practice in brain injury assessment (Bourdet et al., 2016; Fahlstedt et al., 2020; Gabler et al., 2016). This is the first study that used a combination of physical tests with an isolated headform and computational methods with a full-body FE model in BSF assessment. The main objective of this chapter is to study if the neck axial load that a full-body experiences in a chin bar impact could be predicted from the head kinematics measured by an isolated headform in similar impact conditions. The final goal of this study is to predict the neck axial load for BSF assessment from ECE 22.06 and FRHPhe-01 chin bar test methods.

6.2. Material and Methods

The experimental method was designed to study if it is possible to predict the neck tensile load that the Hybrid III would experience in a similar impact to that of the ECE 22.06

chin bar test using only some kinematic based metrics from the ECE 22.06 physical test. Since the neck tensile load at the upper neck was proposed as BSF injury metric but ECE 22.06 physical tests use an isolated headform, the method to predict the upper neck axial force from chin bar physical tests was developed in a two-step procedure. First, a FE model of the Hybrid III and a FE helmet model were used to establish a relationship between the maximum upper neck axial load from full-body chin bar impacts and the head kinematics from isolated head chin bar impacts (Figure 6.2). Second, using the previously mentioned relationship, the upper neck axial force was calculated for several chin bar physical tests through full-body Hybrid III simulations. Then, a relationship was established between kinematic metrics calculated from the chin bar physical tests and the predicted neck force.

6.2.1.   Hybrid III FE model

In this study, a detailed model of the Hybrid III 50th percentile male dummy (LSTC.NCAC_H3_50TH_130528_BETA) was used to represent the human body behaviour. This FE model has been developed by Livermore Software Technology Corporation (LSTC) and it has been validated at the component and system levels (Guha, 2014; Mohan et al., 2010). This FE model has been previously used in computational studies for assessing motorcycle chin bar impacts (Khosroshahi et al., 2017; Khosroshahi et al., 2015). Although the neck of the Hybrid III dummy shows a stiffer response than the human neck under axial loading in direct impacts to the head (Ghajari et al., 2011), it is widely used by researchers in direct impacts due to the availability of its physical models.

6.2.2.   Upper neck axial force prediction from Hybrid III simulations

In order to establish a relationship between the neck axial force measured in full-body chin bar impacts and the kinematics from isolated headform chin bar impacts, chin bar impact tests were simulated using the detached head of the Hybrid III and the full-body of the Hybrid III equipped with a helmet model. The chin bar test configuration was performed according to the ECE 22.06 chin bar test (ECE, 2021) illustrated in Figure 6.2. Since just one helmet model was available to establish this relationship, three impact speeds (5 m/s, 6 m/s and 7 m/s) for the 65° headform positioning and two headform positioning angles (63° and 68°) for the 6 m/s impact speed were simulated in order to increase the number of observations.
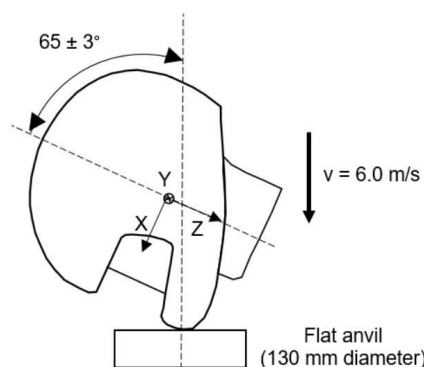
Figure 6.2: ECE 22.06 chin bar impact test configuration and headform coordinate system.

The FE model of the AGV-T2 helmet was used in these simulations. This helmet model has been previously validated (Ghajari et al., 2013; Ghajari et al., 2011) and used in computational studies for assessing motorcycle chin bar impacts (Khosroshahi et al., 2017; Khosroshahi et al., 2015).

Since previous studies have shown that the head motion in normal impact tests (impact velocity vector perpendicular to the impacting surface) with a neck coupling is more complex than with an isolated headform (Beusenberg et al., 2013; Hering & Derler, 2000), the head kinematics from full-body and detached headform chin bar impact simulations was compared before using it as input of the full-body FE model (see Figure 6.3). Based on this comparison, only the three components of the linear acceleration from the detached head of the Hybrid III simulations were prescribed to the rigid skull at the head centre of gravity of the unrestrained full-body Hybrid III FE model without helmet to obtain the neck axial force.
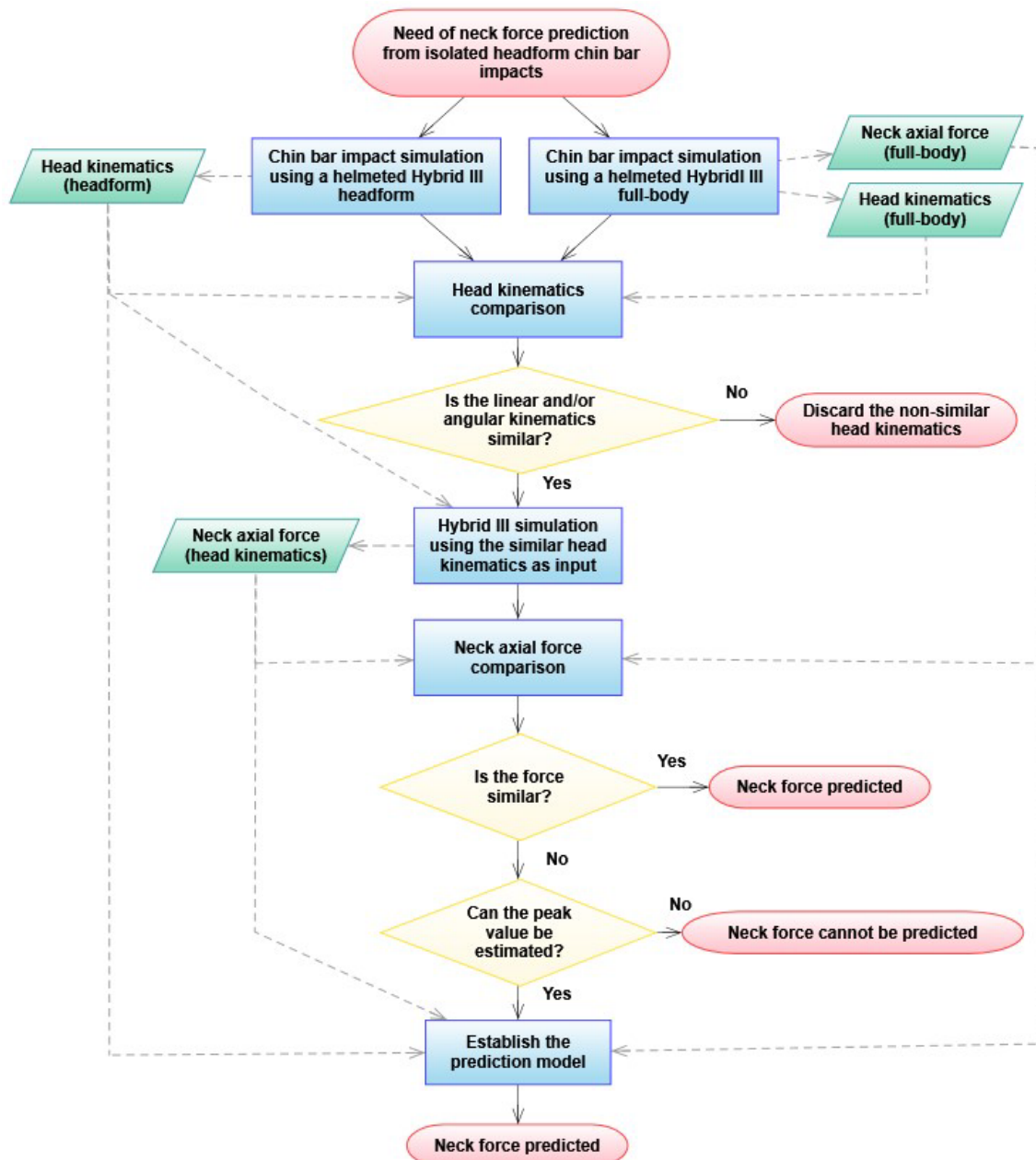
Figure 6.3: Flow chart used to establish the relationship between the maximum upper neck axial force obtained from full-body chin bar impacts and the head kinematics from isolated head chin bar impacts.

Since the maximum peak of the neck axial force obtained from linear kinematics and that one obtained from full-body chin bar impacts resulted different, it was analysed if the peak of the neck axial force obtained from full-body chin bar impacts could be estimated

using the neck axial force obtained from linear kinematics. A first attempt was made to estimate the peak of the neck axial force from full-body chin bar impacts by selecting the neck force magnitude from linear kinematics at the instant in which the resultant linear acceleration decreases below a given magnitude after its maximum peak. Later, it was observed a good correlation between the slope of the neck axial force obtained from linear kinematics and the peak of the neck axial force obtained from full-body chin bar impacts. Therefore, a simple linear regression was used for modelling the relationship between the maximum upper neck axial load from the full-body Hybrid III chin impact test simulations (dependent variable) and the slope (force rate) of the upper neck axial load from the Hybrid III with linear kinematic input simulations (independent variable). The force rate was calculated as the slope of a linear function that was fitted using ordinary lest squares method to the part of the curve between the 25% and the 75% of the maximum value of the curve. Since there is a limited number of observations, a leave-one-out cross-validation (LOOCV) was done in order to assess the ability of the regression model to predict the maximum upper neck axial load from the force rate.

All simulations started immediately prior to impact and ended after 20 ms. The kinematics were filtered before being applied to the Hybrid III FE model, signals were filtered using a low-pass filter CFC-1000. Simulation data post-processing was performed using an in-house developed and validated script of Matlab (Matlab R2021b, MathWorks, Natick, MA, USA) and regression analysis was performed using the Real Statistics Resource Pack add-in in Excel (Excel 2016, Microsoft, Redmond, WA, USA).

6.2.3.   Chin bar physical test

In total, 18 full-face motorcycle helmet models were exposed to the ECE 22.06 chin bar test. All the helmets were composed of composite shell and the protective padding was made of expanded polystyrene (EPS). The retention system of the helmets was based on the double D-ring buckle.

A free fall guided impact machine (Model: Quebrantahuesos 6.0, +D, Pozuelo de Alarcón, Spain) was used for the chin bar tests. All the helmets were tested with a 575-size magnesium alloy full headform (Model: 100_04_FMH, Cadex Inc., Saint-Jean-sur-Richelieu, QC, Canada). In the chin bar tests, the helmeted headform is placed on a carriage and restrained by pre-cut paper tape to prevent helmet motion during the fall. After releasing the carriage assembly from a specific height to achieve an impact velocity of 6.0 m/s, the helmeted headform impacts the top surface of a flat anvil and the carriage assembly continues to fall onto a cushioned bed plate without interfering with the helmeted headform kinematics. The helmeted headform was placed on the carriage so that the central vertical axis of the headform was inclined 65 ± 3° to the vertical with the vertical longitudinal plane of symmetry of the helmeted headform in the vertical position (see Figure 6.2). The headform was positioned inside the helmets according to the requirements of Annex 5 of ECE 22.06 (ECE, 2021), and the retention system was adjusted under the chin of the headforms and tightened to a tension of 75N (FIM, 2017).

A wireless system (Model: iCONO, +D, Pozuelo de Alarcón, Spain) was used to measure linear acceleration and angular velocity at the centre of gravity of the headform in accordance with the three components of the headform coordinate system (see Figure 6.2). The wireless system incorporates three linear accelerometers (Model: 64C-2000, MEAS, Nanshan District Shenzhen, China), three angular rate sensors (Model: ARS PRO-8k, DTS, Seal Beach, CA, USA) and an acquisition system (Model: SLICE NANO, DTS, Seal Beach, CA,

USA). Data were recorded at 10 kHz. Head linear acceleration signals were filtered using a low-pass filter CFC-1000 and angular velocities signals were filtered using a CFC-180. High-speed video was captured at 1000 Hz (Model: Eosens mini, Mikrotron, Unterschleissheim, Germany).

6.2.4.   Upper neck axial force prediction from chin bar physical tests

The established relationship between the neck axial force measured in full-body chin bar impacts and the kinematics from isolated headform chin bar impacts allows to predict maximum upper neck axial force from an isolated headform chin bar impact test but it requires to perform a simulation with the Hybrid III FE model. FE simulations requires specific computational skills and it is time consuming. In order to address these drawbacks, it was analysed if the peak of the neck axial force could be predicted using only some kinematic based metrics from the ECE 22.06 physical test.

 For that, first the three components of the linear acceleration from the 18 chin bar physical tests were prescribed to the rigid skull at the head centre of gravity of the full-body Hybrid III FE model to predict the maximum upper neck axial load (Fz) through the force rate.

Then, the data from the chin bar physical tests were post-processed to calculate the peak of the resultant linear acceleration (PLA), the peak of the resultant angular velocity (PAV), the peak of the resultant angular acceleration (PAA), the peak of the linear acceleration in the X-axis (PAx), the peak of the linear acceleration in the Z-axis (PAz), the peak of the angular velocity in the sagittal plane around the Y-axis (PWy) and the resultant linear velocity at the end of the impact (RLV). Data post-processing was performed using an in-house developed and validated script of Matlab (Matlab R2021b, MathWorks, Natick, MA, USA). For data post-processing, the end of the impact was estimated when the measured resultant linear acceleration was lower than 5 g, which correlated well with the instant in which the helmeted headform separated from the anvil.

Finally, a stepwise regression procedure was carried out to find the fewest number of independent variables (PLA, PAV, PAA, PAx, PAz, PWy, RLV) that are needed to adequately predict the dependent variable (Fz). A significance level of 0.15 was established for the stepwise regression. Testing significance of the regression model and coefficients was evaluated with a significance level of 0.05. Since there is a limited number of observations, a LOOCV was performed in order to assess the ability of the multiple regression model to predict the maximum upper neck axial load from the selected variables.

6.3.   Results

The results section in this chapter is divided into two subsections. First, Hybrid III simulation results and the neck force prediction model from Hybrid III simulations are presented. Second, the neck force prediction model from chin bar physical tests is presented.

6.3.1.   Hybrid III simulations results

Similarities were observed at least during the first instants of the impact between the linear kinematics of the chin bar impacts that were simulated using the detached head of the Hybrid III and the full-body of the Hybrid III equipped with a helmet model. Figure 6.4 shows the time history plots of the resultant linear acceleration for the chin bar impacts simulations at 7 m/s, 6 m/s and 5 m/s and headform positioning angle of 65° using the

detached helmeted head and the helmeted full-body of the Hybrid III. Resultant linear accelerations from chin bar impact simulations at 6 m/s impact speed and headform positioning angles of 63°, 65° and 68° are showed in Figure 6.5.
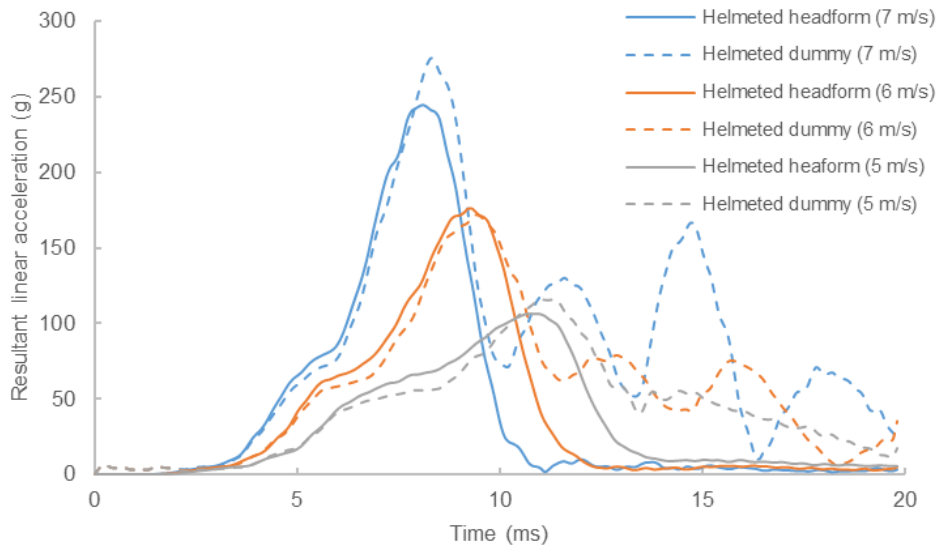
Figure 6.4: Resultant linear accelerations from the chin bar impact simulations at three impact speeds using the detached helmeted head and the helmeted full-body of the Hybrid III model.
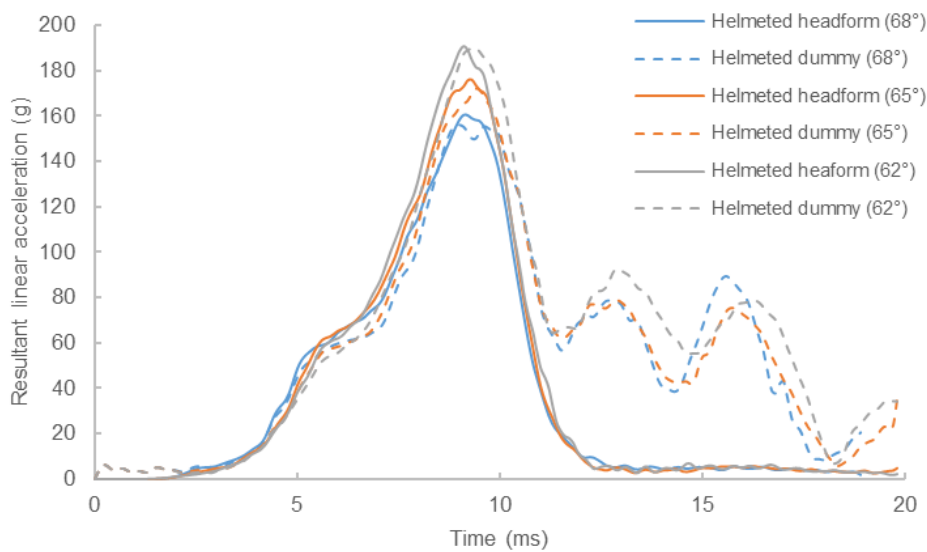
Figure 6.5: Resultant linear accelerations from the chin bar impact simulations at 6 m/s and three headform positioning angles using the detached helmeted head and the helmeted full-body of the Hybrid III model.

However, differences were observed between the angular kinematics of the chin bar impacts that were simulated using the detached head of the Hybrid III and the full-body of the Hybrid III. Since in chin bar impacts the head mainly rotates around the Y-axis, Y-axis angular velocities and accelerations instead of the resultant angular velocities or accelerations are given in Figure 6.6, Figure 6.7, Figure 6.8 and Figure 6.9 to show the direction of the motion.
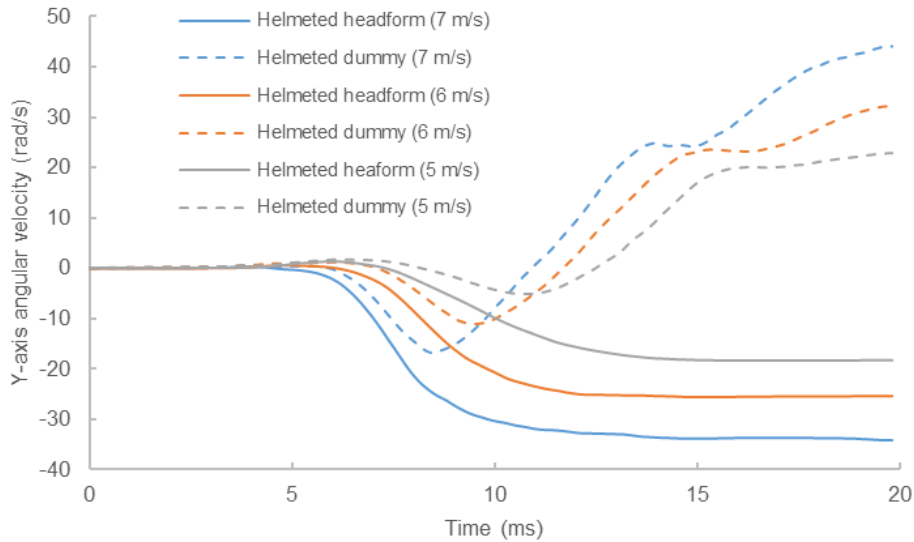
Figure 6.6: Y-axis angular velocities from the chin bar impact simulations at three impact speeds using the detached helmeted head and the helmeted full-body of the Hybrid III mode
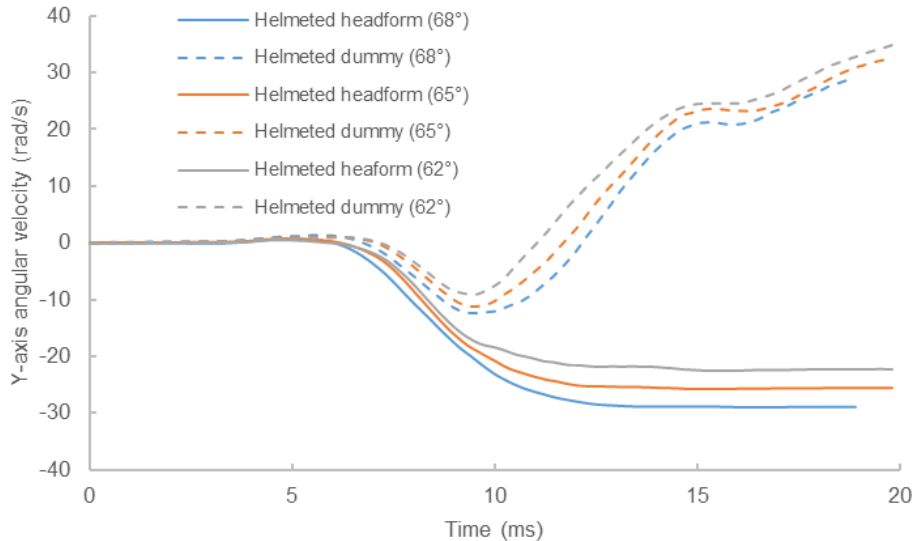
Figure 6.7: Y-axis angular velocities from the chin bar impact simulations at 6 m/s and three headform positioning angles using the detached helmeted head and the helmeted full-body of the Hybrid III model.

Figure 6.6 and Figure 6.8 show the time history plots of the Y-axis angular velocity and acceleration for the chin bar impacts simulations at 7 m/s, 6 m/s and 5 m/s impact speeds and headform positioning angle of 65° using the detached helmeted head and the helmeted full-body of the Hybrid III. Results from chin bar impact simulations at 6 m/s impact speed and headform positioning angles of 63°, 65° and 68° were shown in Figure 6.7 and in Figure 6.9. All the graphs show how the head started to rotate in the same direction during the first milliseconds (flexion motion) but then the direction of the motion changed for the full-body impact simulations (extension motion) reaching the maximum value during this second phase of the motion.
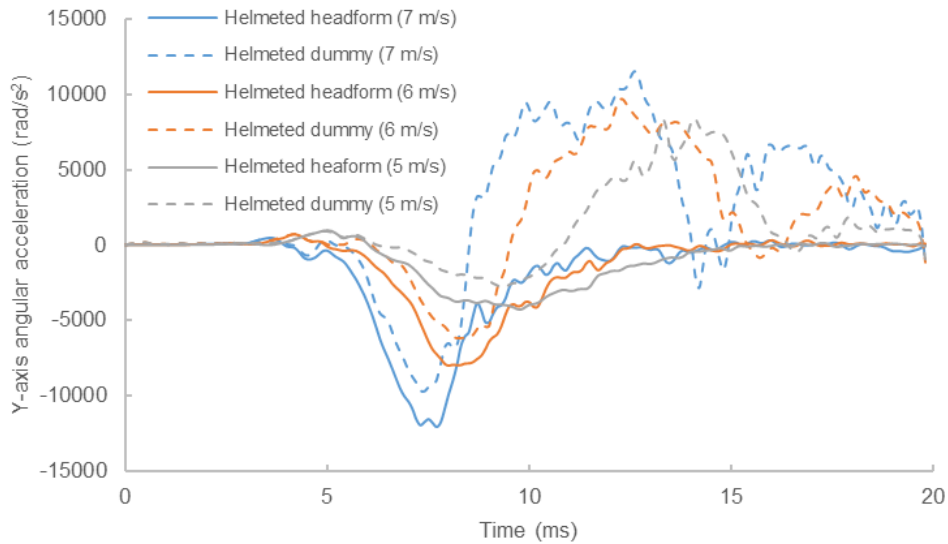
Figure 6.8: Y-axis angular accelerations from the chin bar impact simulations at three impact speeds using the detached helmeted head and the helmeted full-body of the Hybrid III model.
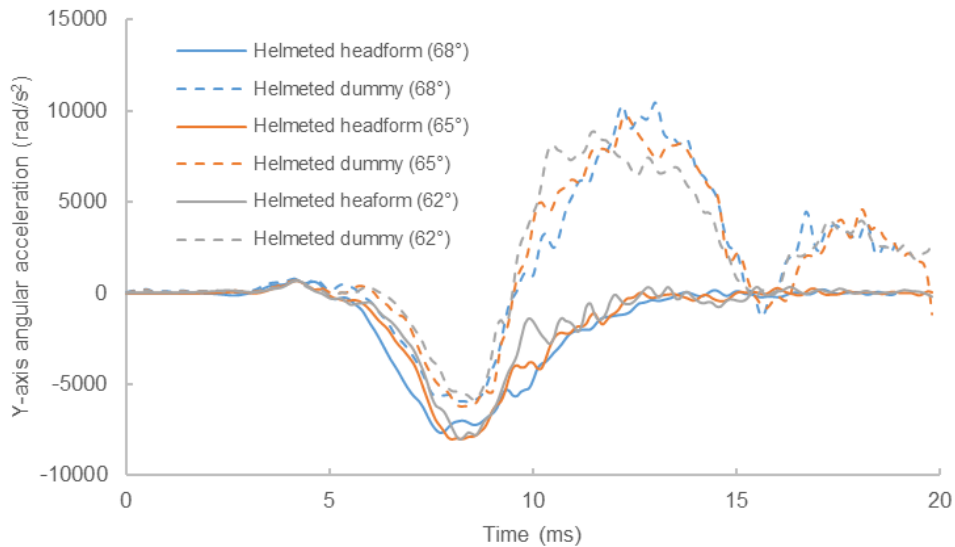
Figure 6.9: Y-axis angular accelerations from the chin bar impact simulations at 6 m/s and three headform positioning angles using the detached helmeted head and the helmeted full-body of the Hybrid III model.

Figure 6.10 shows the upper neck axial force from the helmeted full-body chin bar impact simulations together with the upper neck axial force obtained from the full-body simulations in which the linear accelerations from the detached helmeted head impact simulations have been prescribed to the rigid skull of the Hybrid III.
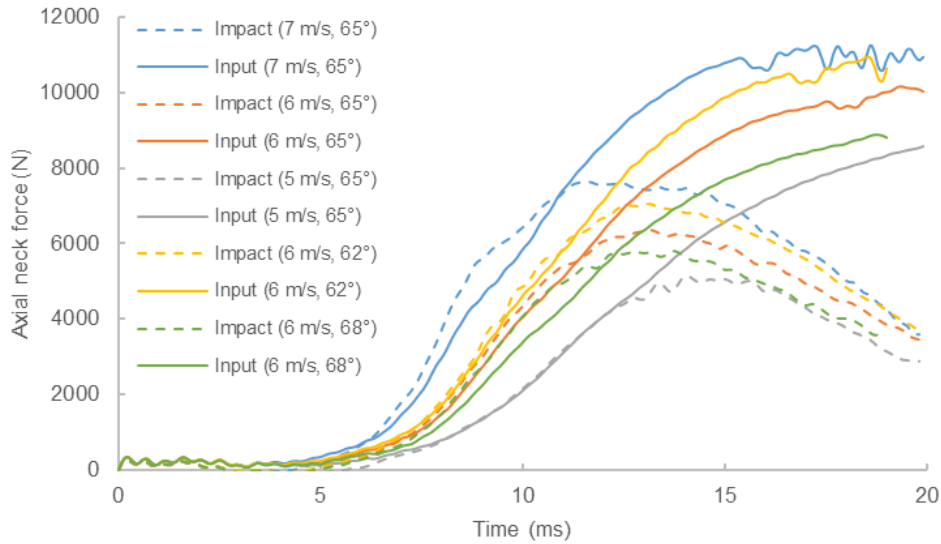
Figure 6.10: Upper neck axial force from the chin bar impact simulations using the helmeted full-body Hybrid III and from the full-body Hybrid III simulations using as input the linear accelerations obtained in the chin bar impact simulations with the detached helmeted head of the Hybrid III for all the impact simulation conditions.

The graph shows how the maximum value of the upper neck axial force from the helmeted full-body chin bar impact simulations is reached between 10 and 15 ms while the neck axial force from the full-body Hybrid III simulations in which the linear accelerations were prescribed continued to increase beyond 15 ms. Figure 6.4 and Figure 6.10 show that the maximum value of the upper neck axial force from the helmeted full-body chin bar impact simulations is reached at the same time than the end of the resultant acceleration pulse occurred from the chin bar impact simulations using the detached headform. Figure 6.10 also shows that there was a close relationship between the maximum value of the upper neck axial force from the helmeted full-body chin bar impact simulations and the slope (force rate) of the upper neck axial force obtained from the full-body Hybrid III simulations with the linear acceleration input. After discarding the estimation of the maximum neck axial force using the upper neck axial force obtained from the kinematic input simulations and the duration of the resultant acceleration pulses, simple linear regression was used to study the relationship between the maximum neck axial force from the helmeted full-body chin bar impact simulations and the slope (force rate) of the upper neck axial force obtained from the full-body Hybrid III simulations with the linear acceleration input. The fitted regression model was:

$$Maximum\ upper\ neck\ axial\ force\ (N) = 729.9007 + 4.8797 \cdot Force\ rate\ (\frac{N}{ms}) \qquad (6.1)$$

The overall regression was statistically significant (R^2 = 0.993, *p*-value < 0.000). The predictive R^2 given by the cross validation was 0.985.

All the linear functions that were fitted using ordinary lest squares method to calculate the force rate on the part of the curve between the 25% and the 75% of the maximum value of the curve were statistically significant (R^2 > 0.99, *p*-value < 0.000).

6.3.2.   Upper neck axial force prediction from chin bar physical tests

In order to develop a model capable of predicting the maximum upper neck axial force without the need to carry out FE simulations, the linear accelerations from the 18 chin bar physical tests were prescribed to the rigid skull of the Hybrid III model to predict the

maximum upper neck axial force through the regression model presented in previous section (Equation 6.1). Therefore, the resultant linear accelerations from chin bar physical tests and the estimated upper neck forces were compared with the linear accelerations and upper neck forces used to develop the predictive model presented in previous section (Equation 6.1). Figure 6.11 shows that the range of linear accelerations obtained in the chin bar physical tests with different helmet models was fairly good covered by the impact simulations used for the simple linear regression model. Figure 6.12 shows that the range of upper neck axial loads obtained from the Hybrid III simulations with chin bar physical test linear accelerations was fairly good covered by the impact simulations used for the simple linear regression model.
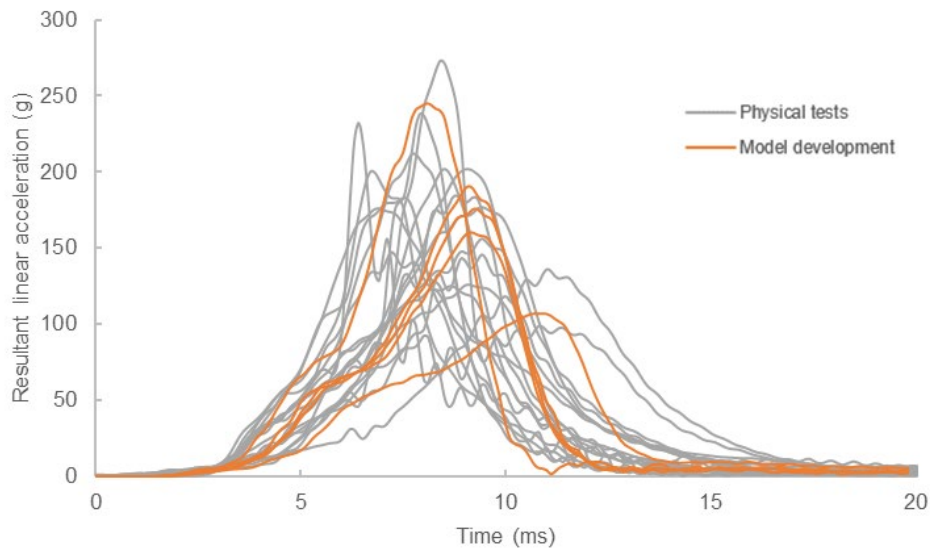
Figure 6.11: Comparison between resultant linear accelerations from physical chin bar test and linear accelerations used to develop the predictive model.
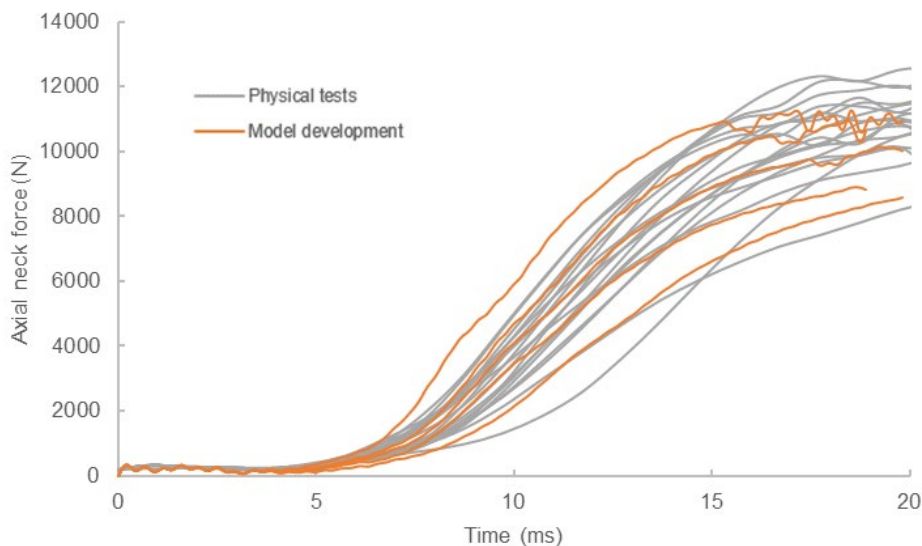
Figure 6.12: Comparison between the upper axial neck force from Hybrid III simulations with physical chin bar test linear accelerations and upper neck axial forces used to develop the predictive model.

The stepwise regression process first built simple linear regression models containing each one of the selected independent variables (see Table 6.1). It was found that PLA, PAA and PAx did not significantly predict the maximum upper neck axial force while PAV, PAz, PWy and RLV significantly predicted the maximum upper neck axial force.

Table 6.1: Coefficients for the simple linear regression analysis between the maximum upper neck axial force (Fz) and each one of the selected variables (the peak of the resultant linear acceleration (PLA), the peak of the resultant angular velocity (PAV), the peak of the resultant angular acceleration (PAA), the peak of the linear acceleration in the X-axis (PAx), the peak of the linear acceleration in the Z-axis (PAz), the peak of the angular velocity in the sagittal plane around the Y-axis (PWy) and the resultant linear velocity at the end of the impact (RLV)).

Dependent variable	Independent variables	Intercept (Std. Error)	Slope (Std. Error)	R²	*p-value*
Fz (N)	**PLA (g)**	5540.39 (935.700)	6.61019 (5.08956)*	0.095	0.2124
	PAV (rad/s)	**9951.68 (1079.75)**	**-130.017 (42.7992)**	**0.366**	**0.0078**
	PAA (rad/s²)	7371.88 (592.395)	-0.09287 (0.07821)*	0.081	0.2524
	PAx (g)	6139.45 (933.806)	3.67377 (5.71785)*	0.025	0.5296
	PAz (g)	**4193.82 (568.726)**	**30.1361 (6.53163)**	**0.571**	**0.0003**
	PWy (rad/s)	**9881.58 (1056.32)**	**-127.749 (42.0241)**	**0.366**	**0.0078**
	RLV (m/s)	**5517.85 (445.289)**	**936.053 (314.230)**	**0.357**	**0.0089**

Regression lines that are a good fit for the data are shown in bold font.

* Indicates non-significant result (p-value > 0.05).

Starting with seven independent variables, the stepwise regression process reduced them to two, concluding that PAz and RLV are good predictors of the maximum upper neck axial force. The fitted regression model was:

$$Maximum\ upper\ neck\ axial\ force\ (N) = 3149.879 + 29.0709 \cdot PAz\ (g) + 881.836 \cdot RLV\ (m/s) \tag{6.2}$$

The overall regression was statistically significant (R^2 = 0.871, *p*-value < 0.000). The predictive R^2 given by the cross validation was 0.821.

6.4. Discussion

Currently, chin bar test methods do not include the neck to measure the upper neck axial force and it is not expected to be included in the short future. Given the lack of test methods that address chin bar design for BSF mitigation, this chapter investigated if it is possible to reduce the risk of BSF with the current tests. For that, the relationship between the kinematics measured by an isolated headform during chin bar impact tests and the neck tensile load predicted by the Hybrid III FE model under similar impact conditions was studied. A combined approach including physical ECE 22.06 chin bar impact tests and a FE model of the Hybrid III was used to study this relationship.
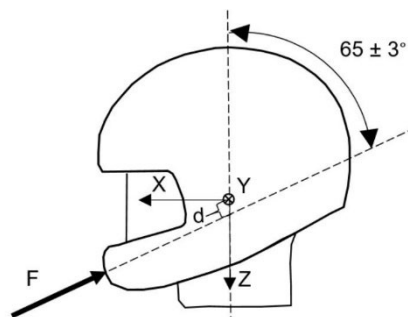
Figure 6.13: Loading experienced by a helmeted headform subjected to a chin bar impact test.

A similar methodology has become a common practice in brain injury assessment (Bourdet et al., 2016; Fahlstedt et al., 2020; Gabler et al., 2016). Some studies used the output kinematics measured with an isolated headform as input of brain FE models assuming that the neck has a limited effect on the helmet response at the time of impact

(Bourdet et al., 2021). However, other studies have shown that the head motion in normal impact tests (impact velocity vector perpendicular to the impacting surface) with a full-body dummy is more complex than with an isolated headform (Hering & Derler, 2000). Therefore, the head kinematics between a helmeted isolated head and a helmeted full-body dummy during a chin bar impact had to be compared before using the output kinematics measured with an isolated headform as input of the full-body dummy. Similarities were found for the linear kinematics up to a certain point while differences were found for the angular kinematics.
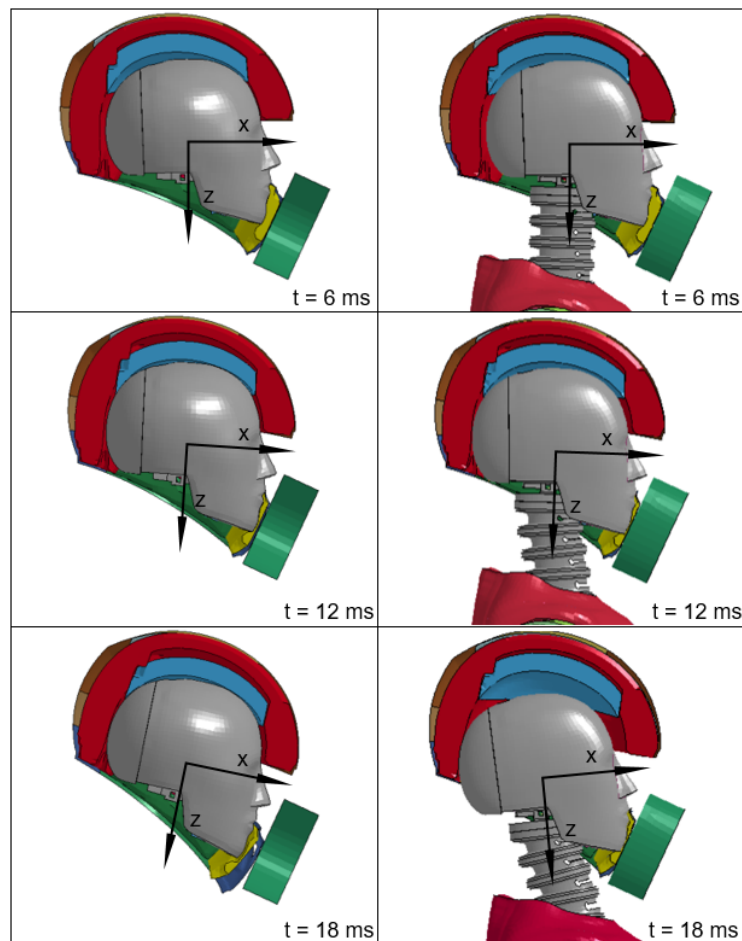
Figure 6.14: Sequence of video frames showing the different head rotation during chin bar impacts with an isolated headform or a full-body dummy.

In the chin bar impacts, the direction of the impact force passes at a distance d from the centre of gravity towards the neck leading to rotation of the isolated head in the negative direction of the Y-axis around the centre of gravity (see Figure 6.13 and Figure 6.14). However, in full-body impacts the rotation in the negative Y-axis direction is limited by the neck coupling. Therefore, after a negative Y-axis rotation the head started to rotate in the positive Y-axis direction (see Figure 6.6 and Figure 6.14). Similar findings were observed by Beusenberg et al. (2013), who performed a mathematical modelling study to investigate neck coupling in helmeted head impacts and found that neck coupling, while having a limited effect on the linear accelerations, can reverse the direction of angular motion. Therefore, rotational kinematics measured in chin bar impacts using an isolated headform are unrealistic. However, it seems that they are not important to predict upper neck axial force because the upper neck axial force was adequately predicted using only the linear kinematics from isolated headform impacts.

Although the head only rotated in the positive Y-axis direction when linear kinematics from isolated headform impacts were used as input of the full-body simulations, the upper neck axial load was similar to the chin bar impact simulation with the full-body Hybrid III (see Figure 6.10) at least for the duration of the resultant linear acceleration pulse of the isolated headform impact (see Figure 6.4). However, after the end of the resultant linear acceleration pulse, the upper neck axial load continued increasing in the linear kinematic input simulations because the effective mass of the head increased due to the effect of the body.

A first attempt to estimate the axial neck force was done by selecting the neck force magnitude at the instant in which the resultant linear acceleration decreases below 5g after the maximum peak but the high magnitude of the axial neck force slope at this moment made the estimation not very accurate when it was applied for different impacts. Therefore, this methodology to predict the maximum axial neck force was dropped out and a new methodology was established using the slope (force rate) of the axial neck force curves. The maximum upper neck axial load was very accurately predicted by the force rate which suggests a non-linearity in the impact behaviour of the Hybrid III neck model. Using the results from the Hybrid III simulations with linear acceleration prescription to estimate the axial neck force makes the relationship between full-body and isolated head independent of the headform type. Therefore, it can be used for physical chin bar tests that use an EN960 headform. Although, this relationship is used as an intermediate prediction model in this study, it seems well suited to the task given its high predictive capability.

The goal of helmet testing standards is to create the simplest set of tests that capture the greatest number of injury related risk factors. Therefore, this study analyzed if any of the kinematic metrics measured in a chin bar impact using an isolated headform are able to predict the maximum upper neck axial force that a full-body dummy would experience in similar impact conditions. It was found that a combination of PAz and RLV was able to fairly good predict the maximum upper neck axial force. Unlike PLA and PAx showed a weak and a very weak positive correlation with Fz, PAz showed a strong positive correlation. Probably because it is aligned with the axial direction of the neck. These results suggest that PLA which is a common metric used to assess the chin bar impact performance in some helmet testing standards (ECE, 2021; FIM, 2017) has nothing to do with BSF prevention. RLV, which is related to the impact energy that is not absorbed by the helmet during the impact, showed a moderate-strong positive correlation.

Since in chin bar impacts the head rotates mainly around the Y-axis, PAV and PWy showed a very similar moderate-strong negative correlation while PAA showed a weak negative correlation. Despite the fact that a positive correlation was observed between PWy and Fz when the impact speed was increased (see Figure 6.6 and Figure 6.10), a negative correlation was also observed when the impact speed was the same but the angle was modified for the detached headform (see Figure 6.7 and Figure 6.10). In isolated headform chin bar tests, the angular velocity increases as the direction of the impact reaction force is closer to the neck (see Figure 6.13) but the contrary seems to occur with neck coupling (see Figure 6.7). These results suggest that the relationship between Fz and the unrealistic PWy measured in isolated headform chin bar impacts was differently influenced by impact speed or impact geometry.

Limitations

The main limitation of this study is that a Hybrid III FE model was used as the human

body surrogate and therefore the relationships found in this study might be affected by the human body surrogate chosen. Since this dummy has a very stiff neck compared to the human neck when it is subjected to axial loading (Herbst et al., 1998), the biomechanical tolerance limit proposed by McElhaney et al. (1995) could not be applied for the results of this study. Therefore, the risk of BSF of current helmets for the chin bar test requirements is still unknown.

Another limitation of this study is that the neck force relationships found in this study were developed using only a rigid flat anvil and therefore they could not be valid for other geometries or compliances of the impacting surface. Finally, the regression model to predict the neck axial force from PAz and RLV has been developed using results from a 575-size EN960 headform and therefore it could not be valid for other headform types.

<div align="right">

Chapter 7

</div>

Effects of Including a Penetration Test in Helmet Testing Standards

7.1.   Introduction

Most helmets are manufactured in order to fulfil the requirements prescribed in helmet testing standards. There are numerous motorcycle helmet safety standards around the world: Regulation No. 22 from the United Nations Economic Commission for Europe (ECE) in Europe (ECE, 2021), Federal Motor Vehicle Safety Standards (FMVSS) No. 218 from the United States Department of Transportation (DOT) and M2020 from the Snell Foundation (Snell) in the United States (DOT, 2011; Snell, 2020), and Japanese Industrial Standard (JIS) T 8133 in Japan (JIS, 2015) are among some of them. The objective of a motorcycle helmet standard is to ensure a minimum level of head protection under some specific test conditions. However, methods and requirements vary from one standard to another and, therefore, the performance against impact of motorcyclist helmets is influenced by the requirements included in each standard (Bourdet et al., 2018; Mcintosh & Grzebieta, 2013).

One of these requirements, which has been controversial over the last decades, is the need of a penetration test. The penetration test measures the resistance of the helmet shell to impacts against sharp objects. In these tests, the helmet is positioned on a headform or a spherical device support. Then, a conical striker is dropped to hit the outer surface of the static helmet shell. The required performance criterion consists of ensuring that there is no contact between the striker tip and the headform or spherical support.

During years, some research has pointed out that the penetration test was either not necessary or that it could influence negatively helmet performance in more common real-life crash scenarios. In a statistical study, Otte et al. (1997) found that the frequency of motorcycle crashes involving penetrating objects was extremely small. Shuaeib et al. (2002) stated that the penetration test is the main parameter that would determine the thickness of the helmet shell, leading to a thicker shell that would account for about 50% of the weight of the helmet. Furthermore, some researchers stated that the penetration test causes helmets to be designed with a stiffer shell that could result in an increased risk of head injury in impacts against rigid flat surfaces (Fernandes & Sousa, 2013; Ghajari et al., 2010). These concerns resulted in the elimination of the penetration tests from some standards, while others continue demanding this requirement. In Europe, a penetration test is not

required in the 06 series of amendments of the ECE Regulation 22 (ECE 22.06) (ECE, 2021), while several other standards and regulations do require this procedure as part of the helmet assessment program (DOT, 2011; International Motorcycling Federation [FIM], 2017; JIS, 2015; Snell, 2020). To provide further insight into this discussion, this chapter aims to assess the effect of including a penetration test in the overall impact performance of helmets.

7.2.   Material and Methods

The experimental method was designed to study if the shell stiffness assessed by the penetration test influences the impact absorption capabilities and rotational behaviour of motorcycle helmets. First, twenty full-face motorcycle helmet models were exposed to a penetration test. Then, based on the observed results from the penetration tests, four helmet models were classified as hard shell helmets while six of them were classified as soft shell helmets. Only these ten helmet models were selected to be drop tested at two different velocities. A new helmet sample was used for each velocity, and therefore twenty helmets were drop tested. Thus, a total of forty helmet samples were used in this study.

All the helmets were composed of composite shell and the protective padding was made of expanded polystyrene (EPS). The retention system of the helmets was based on the double D-ring buckle. All the helmets complied with the European regulation (ECE, 2002).

7.2.1.   Penetration test

A conventional penetration test was done on one sample of each helmet model. The striker mass was 3 kg with a 60° conical head and it was dropped from a height of 2 m above the surface of the helmet shell (FIM, 2017). Between 2 and 4 points were randomly tested on each sample. Typical impacted areas were the front, top, lateral and rear of the helmet shell on or above the test line as defined by Snell (Snell, 2020). Impacts on vent openings were not performed. The locations for the impact points as well as the order in which they were tested were randomly selected for each helmet. The intrusion of the conical tip of the striker into the helmet was measured after each impact. Then, the average and the standard deviation values of the intrusion measurements were calculated for each helmet. Only helmets with an average intrusion higher than 15 mm (soft shell helmets) and lower than 10 mm (hard shell helmets) were selected for the impact performance comparison and were exposed to the drop test. The rest of the helmets that resulted in intermediate values of intrusion were not further considered in the study.

7.2.2.   Normal impact tests

The test matrix consisted of 60 impacts onto a flat anvil. After the selection process based on the penetration test results, a new sample of each selected helmet model was drop tested at low-speed (5 m/s) and another sample at high-speed (8.2 m/s). In normal impact tests, the direction of the impact velocity vector is perpendicular to the impacting surface. Each helmet was tested on front, lateral and top areas (three impacts per helmet sample at each impact speed). The selected impact areas corresponded with the points B, X (right), and P as described in the European regulation (ECE, 2021) and shown in Figure 7.1.
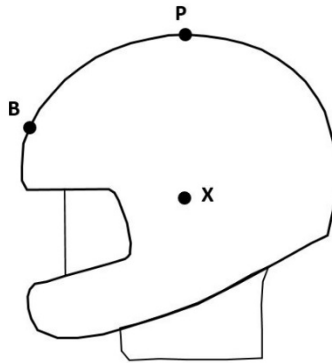
Figure 7.1: Impact points for the normal impact tests.

A free fall guided impact machine (Model: Quebrantahuesos 6.0, +D, Pozuelo de Alarcón, Spain) was used for the normal impact tests. As the helmets tested were not of the same size, three metallic headform sizes were used (Model: 100_04_FMH, Cadex Inc., Saint-Jean-sur-Richelieu, QC, Canada) to ensure an appropriate fitting of the headform for each helmet size. Four helmet models were tested with the 535 mm headform circumference, three with the 575 mm and three with the 605 mm headform (European Committee for Standardization [CEN], 2006). The corresponding headform masses were 4.1 kg, 4.7 kg and 5.6 kg respectively. The headforms were positioned inside the helmets according to the requirements of Annex 5 of ECE 22.06 (ECE, 2021) and the retention system was adjusted under the chin of the headforms and tightened to a tension of 75 N (FIM, 2017) . Before each impact, the headform was re-positioned and the retention system re-tensioned.

A wireless system (Model: iCONO, +D, Pozuelo de Alarcón, Spain) was used to measure linear acceleration and angular velocity at the centre of gravity of the headform. The wireless system incorporates three orthogonal uniaxial accelerometers (Model: 64C-2000, MEAS, Nanshan District Shenzhen, China), three orthogonal uniaxial angular rate sensors (Model: ARS PRO-8k, DTS, Seal Beach, CA, USA) and an acquisition system (Model: SLICE NANO, DTS, Seal Beach, CA, USA). Data were recorded at 10 kHz. Head linear acceleration signals were filtered using a low-pass filter CFC-1000 and angular velocities signals were filtered using a CFC-180. Data were post processed using a validated and developed in-house script of Matlab (Matlab R2021b, MathWorks, Natick, MA, USA).

7.2.3. Statistical hypothesis testing

The objective of the main statistical hypothesis testing was to assess the influence of the shell stiffness on the impact absorption capabilities of the helmets and their rotational behaviour. For that reason, the helmet models were classified into two groups (soft and hard shell group) depending on the result of the penetration test. As aforementioned, ten out of the twenty penetration tested helmets were selected for the impact performance comparison. Within the selected group, four helmet models were grouped into the hard shell group while the remaining six helmet models were included in the soft shell group. Both groups had helmets of three different sizes. The hard shell group was composed of two helmets that were tested with the 535 headform, one with the 575 and one with the 605. The soft shell group was composed of two helmets tested with the 535 headform, two with the 575 and two with the 605.

The peak resultant linear acceleration (PLA) and the head injury criterion (HIC) were the selected metrics to determine the impact absorption capabilities of the helmets because they are the usual parameters included in helmet standards to assess head protection (ECE,

2021). In addition, the brain injury criterion (BrIC) (Takhounts et al., 2013) and the peak of the resultant angular acceleration (PAA) were also calculated in order to assess the influence of the shell stiffness on the rotational behaviour of the helmets.

Since three different headform sizes were used in this study, a preliminary statistical hypothesis testing was carried out to study any possible influence of the headform size on the selected variables. A non-parametric Kruskal-Wallis H test with a significance level of 0.05 was performed to analyze whether the size of the headform (three different sizes) was significantly related to the values of the PLA, HIC, BrIC or PAA. The Kruskal-Wallis test is an extension of the two sample hypothesis testing to more than two independent samples and it replaces the ANOVA test when sample sizes are small.

The main statistical analysis for the comparison between the two shell groups was only carried out for the cases in which the independence of the PLA, HIC, BrIC or PAA variables from the headform size was demonstrated. A non-parametric test, the Mann-Whitney U test for independent samples with a significance level of 0.05, was used for this analysis due to the limited sample size. Statistical analyses were performed using the Real Statistics Resource Pack add-in in Excel (Excel 2016, Microsoft, Redmond, WA, USA).

7.3.   Results

The results are presented into three subsections. First, the penetration test results of all tested helmets are reported. Second, the results of the normal impact tests at two impact speeds are presented. Finally, the statistical analysis results of the influence of the shell stiffness on the impact absorption capabilities and rotational behaviour of the helmets are shown.

7.3.1.   Penetration test results

Out of a total of twenty penetration tested helmets, ten helmets were selected and classified into the hard or soft shell group. The hard shell helmet group consisted of the four helmets in which the measured average intrusion in the penetration tests was under 10 mm. The six helmets that were included in the soft shell helmet group resulted in average intrusion higher than 15 mm. The helmets that exhibited results in between these two magnitudes were no longer considered in the study. Figure 7.2 includes the average and the standard deviation (SD) of the intrusion measured in the penetration test for each helmet. The mean average value of intrusion and SD for the hard shell group was 7 ± 3 mm while the mean averages of intrusion and SD for the soft shell group was 21 ± 6 mm.
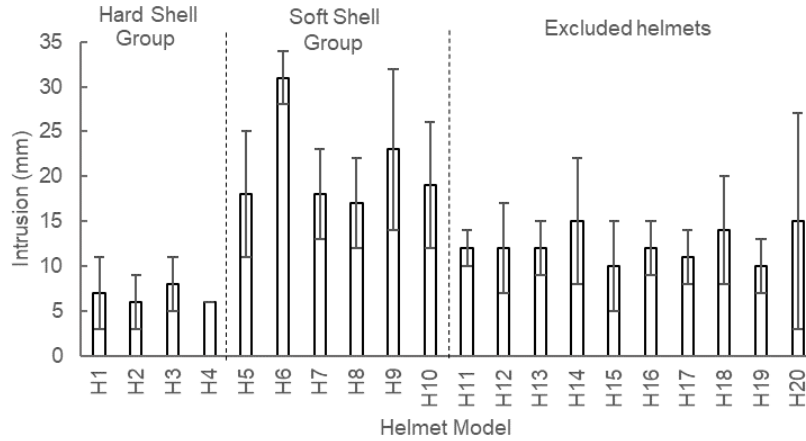
Figure 7.2: Mean and Standard Deviation (SD) of the intrusion measured in the penetration tests for each helmet model. The standard deviation of H4 was zero (3 sites were tested in this case).

7.3.2.   Normal impact test results

At low-speed (5.0 m/s), PLA and HIC values were similar regardless of impact point and shell type (Figure 7.3). The similarity between PLA and HIC values was even more noticeable when considering the standard deviations, due to their similar range of values. While PLA values were between 120 g and 140 g, regardless of the impact point and the shell stiffness, the HIC value was slightly higher for both shell groups when the helmet was dropped on the P point.
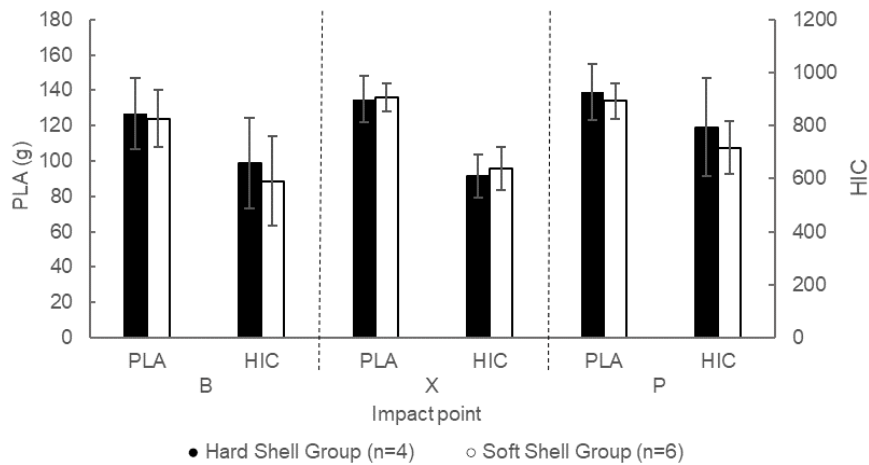
Figure 7.3: Mean and Standard Deviation (SD) of the Peak resultant Linear Acceleration (PLA) and Head Injury Criterion (HIC) for each shell group and each impact point at low-speed normal impact tests.

BrIC and PAA values were very different depending on the impact point (Figure 7.4). While BrIC and PAA were similar regardless of shell type for B and P point, there was a considerable difference when testing the X impact point.
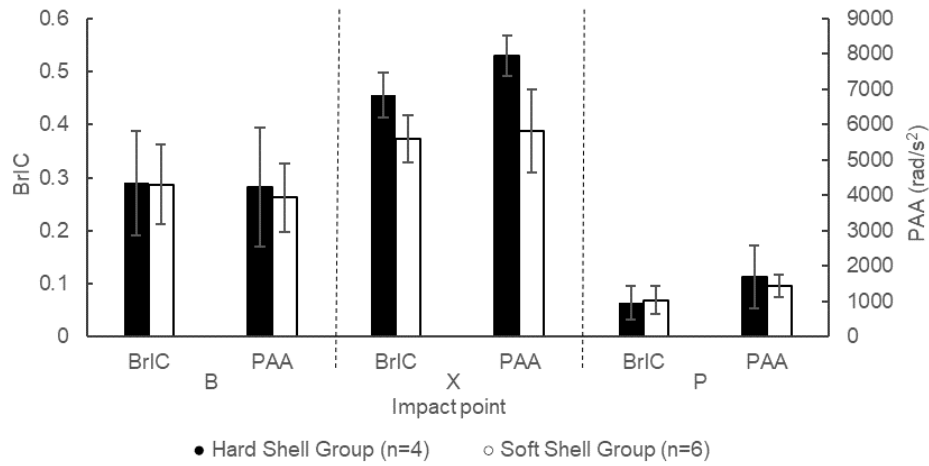
Figure 7.4: Mean and Standard Deviation (SD) of the Brain Injury Criterion (BrIC) and the Peak of the resultant Angular Acceleration (PAA) for each shell group and each impact point at low-speed normal impact tests.

Figure 7.5 includes the mean and the SD of the PLA and HIC for each impact point at high-speed (8.2 m/s). One of the helmets of the soft shell group had a higher acceleration peak when testing B point, causing the SD to be larger than in the other tests. Regardless of this helmet, the values measured for the hard shell helmets at high-speed resulted in more repeatable results and therefore reduced SD values. This effect was particularly true for HIC at the P location of the helmet.
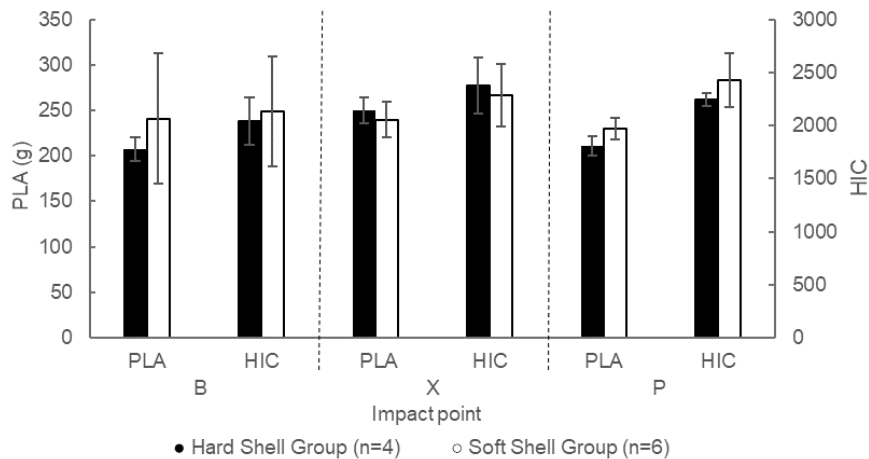
Figure 7.5: Mean and Standard Deviation (SD) of the Peak resultant Linear Acceleration (PLA) and Head Injury Criterion (HIC) for each shell group and each impact point at high-speed normal impact tests.

BrIC and PAA values showed similar trend for the same impact point but they were very different for each impact point. Similar to the low-speed impact test results, an important difference between shell type was observed for the X impact point (Figure 7.6). The larger SD observed in the linear metrics for the soft shell group when testing the B point was not observed in the rotational metrics. However, the B impact point resulted in a consistently larger SD than the other two impact points.
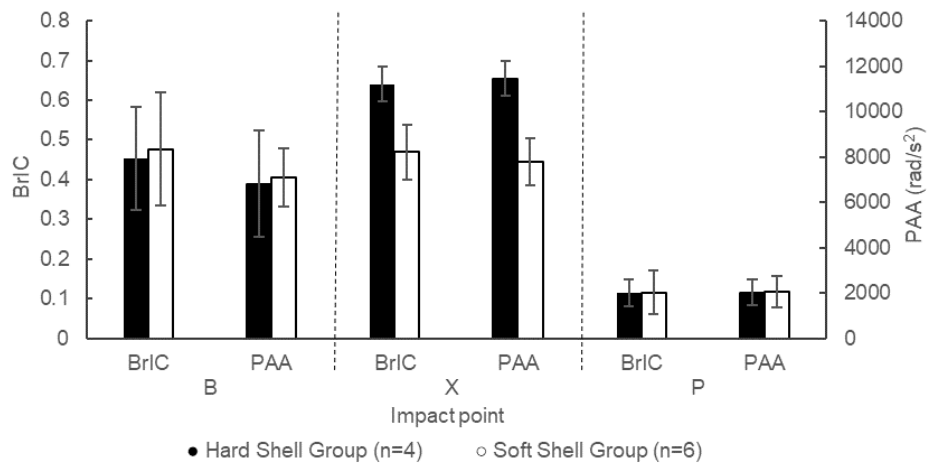
Figure 7.6: Mean and Standard Deviation (SD) of the Brain Injury Criterion (BrIC) and the Peak of the resultant Angular Acceleration (PAA) for each shell group and each impact point at high-speed normal impact tests.

7.3.3. Statistical hypothesis testing results

Since three headform sizes were used in the normal impact tests, the influence of the headform size on the PLA, HIC, BrIC and PAA variables was analyzed prior to carry out the main statistical analysis of this study. Table 7.1 and Table 7.2 include the PLA and HIC mean and the SD for each headform group together with the *p*-value for each impact point tested at low and high-speed respectively. Since all *p*-values resulted higher than the selected significance level (0.05), the statistical analysis could not prove any influence on the PLA or HIC due to the size of the headform for neither tested speeds.

Table 7.1: PLA and HIC mean and SD for each headform group with the Kruskal-Wallis H test results (p-value) for each impact point tested at low-speed.

Impact point	Variable	Headform (E)	Headform (J)	Headform (M)	*p*-value
B point	PLA (g)	125 ± 20	131 ± 8	120 ± 23	0.7967
	HIC	615 ± 174	691 ± 79	551 ± 235	0.7047
X point	PLA (g)	136 ± 14	135 ± 6	137 ± 9	0.9775
	HIC	610 ± 94	598 ± 68	679 ± 61	0.4372
P point	PLA (g)	136 ± 17	135 ± 11	135 ± 11	0.9426
	HIC	776 ± 168	707 ± 128	751 ± 141	0.7275

Table 7.2: PLA and HIC mean and SD for each headform group with the Kruskal-Wallis H test results (p-value) for each impact point tested at high-speed.

Impact point	Variable	Headform (E)	Headform (J)	Headform (M)	*p*-value
B point	PLA (g)	203 ± 16	213 ± 10	275 ± 96	0.2367
	HIC	1934 ± 287	2091 ± 251	2330 ± 657	0.6889
X point	PLA (g)	243 ± 16	238 ± 25	251 ± 16	0.5538
	HIC	2361 ± 274	2132 ± 330	2458 ± 165	0.3039
P point	PLA (g)	222 ± 12	221 ± 5	225 ± 26	0.7859
	HIC	2439 ± 212	2259 ± 127	2343 ± 314	0.3166

Table 7.3 and Table 7.4 include the BrIC and PAA mean and the SD for each headform group together with the *p*-value for each impact point tested at low and high-speed respectively. In contrast to PLA and HIC metrics, some *p*-values indicated an influence on the BrIC or PAA due to the size of the headform for both tested speeds. In particular, the X impact location was the only impact location in which the influence of the headform size on both angular metrics could not be proved for both impact speeds. In general, lower *p*-values were obtained for the BrIC and PAA than for the PLA and HIC variables and in most cases, the highest BrIC and PAA magnitudes were obtained for the smaller headform size.

Table 7.3: BrIC and PAA mean and SD for each headform group with the Kruskal-Wallis H test results (p-value) for each impact point tested at low-speed. Significant values are shown in bold font.

Impact point	Variable	Headform (E)	Headform (J)	Headform (M)	*p*-value
B point	BrIC	0.343 ± 0.095	0.242 ± 0.058	0.262 ±0.039	0.2152
	PAA (rad/s²)	5190 ± 1216	3465 ± 277	3127 ± 202	**0.0357**
X point	BrIC	0.426 ± 0.045	0.440 ± 0.053	0.346 ± 0.048	0.1155
	PAA (rad/s²)	7444 ± 1025	6924 ± 1138	5391 ± 1640	0.3166
P point	BrIC	0.095 ± 0.014	0.053 ± 0.016	0.043 ± 0.003	**0.0349**
	PAA (rad/s²)	1867 ± 744	1233 ± 294	1423 ± 484	0.1860

Table 7.4: BrIC and PAA mean and SD for each headform group with the Kruskal-Wallis H test results (p-value) for each impact point tested at high-speed. Significant values are shown in bold font.

Impact point	Variable	Headform (E)	Headform (J)	Headform (M)	*p*-value
B point	BrIC	0.523 ± 0.161	0.427 ± 0.159	0.434 ± 0.049	0.5538
	PAA (rad/s²)	7894 ± 2156	6061 ± 492	6673 ± 1507	0.3166
X point	BrIC	0.561 ± 0.118	0.574 ± 0.070	0.470 ± 0.122	0.4372
	PAA (rad/s²)	9872 ± 2412	9780 ± 1617	7911 ± 2116	0.3329
P point	BrIC	0.161 ± 0.036	0.093 ± 0.005	0.078 ± 0.008	**0.0181**
	PAA (rad/s²)	2560 ± 443	1873 ± 393	1495 ± 408	**0.0461**

Table 7.5 includes the results of the main statistical hypothesis testing (*p*-values) for each impact point tested at low-speed together with the mean and SD of the PLA and HIC for each shell stiffness group. Since all *p*-values are much higher than the significance level (0.05), the statistical analysis could not find any significant difference in PLA or HIC variables between the two shell groups at low-speed. Therefore, shell stiffness did not influence the energy absorption capabilities of the helmets tested at low-speed.

Table 7.5: Mean and SD of the PLA and HIC for each shell group with the Mann-Whitney U test results (p-value) for each impact point tested at low-speed.

Impact point	Variable	Hard Shell Group (n=4)	Soft Shell Group (n=6)	*p*-value
B	PLA (g)	127 ± 20	124 ± 16	0.9143
	HIC	659 ±171	591 ± 170	0.6095
X	PLA (g)	135 ± 13	136 ± 8	0.6095
	HIC	609 ± 81	639 ± 82	0.4762
P	PLA (g)	139 ± 16	134 ± 10	0.9143
	HIC	794 ± 184	717 ± 100	0.6095

The same analysis was repeated for the data obtained in the high-speed drop tests. As above, Table 7.6 includes the mean and SD of the PLA and HIC for each shell group together with the *p*-value for each impact point tested. In this case, PLA was significantly higher for the soft shell group (*p*-value = 0.0381) but only when the testing point was the P location.

Table 7.6: Mean and SD of the PLA and HIC for each shell group with the Mann-Whitney U test results (p-value) for each impact point tested at high-speed. Significant values are shown in bold font.

Impact point	Variable	Hard Shell Group (n=4)	Soft Shell Group (n=6)	*p*-value
B	PLA (g)	207 ± 13	241 ± 72	0.1714
	HIC	2042 ± 220	2138 ± 517	0.9143
X	PLA (g)	250 ± 14	240 ± 20	0.6095
	HIC	2377 ± 264	2284 ± 296	0.9143
P	PLA (g)	211 ± 11	230 ± 12	**0.0381**
	HIC	2244 ± 62	2431 ± 255	0.3524

Table 7.7 and Table 7.8 include the mean and SD of the BrIC and PAA for each shell stiffness group and each impact point tested at low and high-speed respectively. The tables also include the results of the main statistical hypothesis testing (*p*-values) for the impact

points in which the influence of the headform size factor could not be demonstrated in the previous analyses. For both impact speeds, BrIC and PAA were significantly higher for the hard shell group when testing X impact point.

Table 7.7: Mean and SD of the BrIC and PAA for each shell group with the Mann-Whitney U test results (p-value) for the impact points tested at low-speed in which the influence of the headform size factor could not be confirmed. Significant values are shown in bold font.

Impact point	Variable	Hard Shell Group (n=4)	Soft Shell Group (n=6)	*p*-value
B	BrIC	0.290 ± 0.098	0.287 ± 0.075	0.9143
B	PAA (rad/s²)	4227 ± 1686	3938 ± 971	-
X	BrIC	0.456 ± 0.042	0.373 ± 0.045	**0.0381**
X	PAA (rad/s²)	7940 ± 580	5827 ± 1174	**0.0095**
P	BrIC	0.064 ± 0.032	0.069 ± 0.027	-
P	PAA (rad/s²)	1696 ± 890	1442 ± 322	0.9143

Table 7.8: Mean and SD of the BrIC and PAA for each shell group with the Mann-Whitney U test results (p-value) for the impact points tested at high-speed in which the influence of the headform size factor could not be confirmed. Significant values are shown in bold font.

Impact point	Variable	Hard Shell Group (n=4)	Soft Shell Group (n=6)	*p*-value
B	BrIC	0.453 ± 0.130	0.477 ± 0.143	0.9143
B	PAA (rad/s²)	6818 ± 2347	7085 ± 1299	0.4762
X	BrIC	0.640 ± 0.044	0.469 ± 0.070	**0.0095**
X	PAA (rad/s²)	11457 ± 751	7789 ± 1042	**0.0095**
P	BrIC	0.115 ± 0.034	0.116 ± 0.054	-
P	PAA (rad/s²)	2021 ± 563	2044 ± 683	-

7.4. Discussion

The objective of this chapter was to provide insight into the effects of including a penetration test, which is the main driver that determines helmet shell thickness and therefore of its stiffness, to improve the protective performance of helmets. To that end, the impact absorption capabilities and rotational behaviour of ten helmet types, that were sorted into either hard or soft shell groups, were compared at two impact speeds. PLA and HIC variables were selected to determine the impact absorption capability of the helmets while BrIC and PAA metrics were selected to analyze the rotational behaviour. This is the first time that an experimental study combines the results of the penetration test with the linear and angular kinematics from normal impact tests.

Since three headform sizes were used in the normal impact tests, the influence of the headform size on the PLA, HIC, BrIC and PAA variables was analyzed prior to carry out the main statistical analysis of this study. Table 7.1 and Table 7.2 include the PLA and HIC mean and the SD for each headform group together with the *p*-value for each impact point tested at low and high-speed respectively. The preliminary statistical hypothesis testing could not find any significant influence of the headform size on the PLA or HIC values at neither of the tested speeds. This result was expected because normally, the PLA and HIC requirements of the helmet standards are the same for all headform sizes and therefore helmet manufacturers adjust individually the performance of each helmet size. However, significant influence of the headform size on the BrIC and PAA values was found for some impact points at both tested speeds (see Table 7.3 and Table 7.4). In normal impact tests, the torque that cause the angular motion of the helmeted headform is generated by the reaction force at the impact point and the offset between the reaction force and the CG of

the headform. Therefore, the significant influence of the headform size in the rotational metrics was expected because of the lower magnitude of the moments of inertia for the smaller headform sizes.

Regarding the main statistical hypothesis testing, there was no significant difference between the hard shell group and the soft shell group on the PLA and HIC results of the normal impact tests at low-speed. Similar PLA and HIC results were observed in the high-speed tests, except for the impacts on the helmet P point which resulted in significantly higher PLA for the soft shell group (p-value = 0.038), even if the HIC value was not significantly different (p-value = 0.352). It should be noted that even if one helmet within the soft shell group exhibited an extremely high acceleration peak in the impact on the B point, probably due to the bottoming out of the protective padding, this result alone did not modify the lack of statistically significant differences between the stiff and the soft shell groups at high-speed.

These findings seem to be contradictory with the statement that including a penetration test in regulations causes helmets to be designed with a stiffer shell that behave very rigidly when striking flat surfaces (Fernandes & Sousa, 2013; Ghajari et al., 2010). While the above statement could be correct for helmets in which only the shell thickness is increased, it does not hold for actual helmets in which both the shell and the protective padding can be varied jointly. Indeed, the impact absorption capabilities of a motorcycle helmet depend both on the material and dimensions of the shell and on the characteristics of the protective padding or liner. In fact, the main function of the protective padding is to absorb the impact energy, while the main function of the shell is to distribute the impact load on a wider area and to ensure the helmet integrity during impacts.

The effective stiffness of the shell depends on the material, thickness and external geometry. During an impact, a stiffer shell distributes the impact load on a greater area of the helmet, reducing the crushed volume of the liner and, therefore, increasing the linear acceleration. However, this effect can be compensated using a lower density of protective padding as long as its thickness is enough to prevent a bottom out effect. This practice is very common in helmet design. For example, the higher shell stiffness due to the concavity form of the top part of full-face helmets is compensated with lower density or grooved shape liner at the top part. Therefore, a stiffer shell does not necessarily mean that the helmet will exhibit a global stiff mechanical behavior, but that the characteristics of the liner will be chosen to balance the effects of the stiffer shell.

The significant difference of the PLA for the point P at high-speed suggest that hard shell helmets would provide better protection at high-speed impacts against head injuries induced by linear kinematics such as skull fractures. This result is in line with a simulation study which stated that the impact speed is an important parameter in helmet design and concluded that for high impact speeds the helmet should be designed with stiffer shell and denser protective padding than for low-speeds (Chang et al., 1999). In addition, hard shell helmets would provide better protection when striking objects with a greater variety of shapes, especially during concentrated impacts on small or sharp objects (Williams, 1990). Another effect of the penetration test is the control of the size of the vent openings of the helmet, which could result in a decrease load distribution capacity on those areas if the size of the openings was large enough. On the negative side, hard shell helmets result in heavier helmets that may impact negatively rider's comfort. In this study, the hard shell helmets were around 200 g heaviest when comparing with soft-shell helmets of the same size.

In those cases in which the influence of the headform size factor could not be

demonstrated for the BrIC and PAA, the main statistical hypothesis testing was carried out. There was significant difference between the hard shell group and the soft shell group on the BrIC and PAA results at both impact speeds for the X impact point. Since rotational motion has been proposed as the main mechanim of intracranial injures (Kleiven, 2013), this result suggests that hard shell helmets would provide a worst protection against intracranial injuries than soft shell helmets. Even if a significant influence of the headform size was not found in these cases, the results concerning the rotational metrics should be carefully considered in this study because it was observed that in most cases the highest BrIC and PAA magnitudes were obtained for the smaller headform size (see Table 7.3 and Table 7.4). Moreover, as diferent helmet models were used in this study and the angular motion of the helmeted headform in normal impact tests is related to the distance between the impact point and the CG of the headform, the BrIC and PAA results could be also influenced by the helmet model design. In this regard, the project COST 327 carried out oblique tests at different impact speeds with two almost identical helmets that differed only in mass and shell stiffness, concluding that neither the helmet mass nor the shell stiffness seems to affect significantly the rotational accelerations and tangential forces in oblique impacts (Chinn et al., 2001).

Limitations

A clear limitation of this study was the use of different headform sizes to assess the influence of the shell stiffness in the rotational behavior of the helmets. Three headform sizes were used in this study because test results from other studies were used to carried out the study of this chapter. Despite this limitation, this study has highlighted a potential influence of the shell stiffness in the rotational behaviour of the helmets but it should be further investigated tacking into account the headform size and the helmet design factors.

A potential limitation of this study is the energy of the penetration test. The penetration tests used in this study were performed from 2 m (FIM, 2017; JIS, 2015) but other helmet testing standards prescrive striker drops from 3 m (DOT, 2011; Snell, 2020). Therefore, the conclusions of this study might be influenced by the penetration test energy and should not be extrapolated to higher penetration test energies. In this regard, high energy penetration tests could lead composite shells to do not delaminate for impacts into real-life crash scenarios (Gilchrist & Mills, 1994), and delamination is an additional energy absorbing mechanism of composite shells that improves helmet impact performance (Kostopoulos et al., 2002).

Note: This chapter is a slightly modified version of the paper titled: Effects of Including a Penetration Test in Motorcyclist Helmet Standards: Influence on Helmet Stiffness and Impact Performance published in Applied Sciences under an open access Creative Common CC BY license (Juste-Lorente et al., 2022).

<div align="right">

Chapter 8

Conclusions

</div>

8.1. Conclusions and future work

A brief review of the impact biomechanics of the human head has shown that there are different types of head injuries, each one involving specific head tissue/s and being governed by a certain injury mechanism. Despite the fact that tissue strains are the principal causes of injuries, head kinematics are conveniently used to characterize the mechanisms of head injuries. Although intracranial injury mechanisms are still at the hypothesis level, the dominant hypothesis considers that human head is more sensitive to rotational motion than to translational motion (Kleiven, 2013). However, a review of the most relevant helmet testing standards has shown that they are more focussed on translational motion than rotational motion. Even though some standards require oblique testing in order to asess the rotational performance of the helmets, there are differences in testing procedures such as the friction between the interior of the helmet and the headform which has an important influence on the rotational motion experieced by the headform during the tests (Ebrahimi et al., 2015). Other discrepancies among helmet testing standards include chin bar impacts which are potentially related to basilar skull fractures or the controvelsial topic of including or not a penetration test. Interestingly, a review of real-world motorcylce crashes has shown that despite the success of the motorcycle helmet in preventing local cranial vault fractures, serious head injuries such as intracranial injuries and basilar skull fractures are still common lesions among helmeted motorcyclists (Chinn et al., 2001; Whyte et al., 2016). Due to all the aforementioned discrepancies, the main objective of this thesis was to investigate how current motorcycle helmet testing standards can be improved to reduce basilar skull fractures and intracraneal injuries.

To this end, several specific research questions were planned and investigated in this thesis. The paragraphs below list these research questions and summerize the main results obtained in the investigation.

1. How similar are EN960 headforms to human heads?

A database of human head physical properties has been created based on a review of a selection of human cadaveric studies showing an acceptable agreement with a living adult population dataset. It was observed that EN960 headform properties such as length, width, mass, centre of gravity location and moments of inertia lied inside the 95% prediction intervals calculated from the human cadaver datasets for most of the EN960 headform sizes

but some differences were observed with respect to the calculated regression models. Therefore, a new set of headforms with more similar mass and inertia properties to the one calculated with the regression models would be beneficial for improving helmet testing standards. In addition, it may be necessary to evaluate helmet protection with different shaped headforms depending on the head anthropometry population they are intended for. However, even if the anthropometry and all mass properties matched perfectly the human head properties, it does not mean that it represents the human head behaviour sufficiently well in all impact conditions. Other factors such as headform compliance (Bosch, 2006), external surface friction (Ebrahimi et al., 2015), scalp tissue (Trotta et al., 2018b) and boundary conditions (Hering & Derler, 2000) can significantly influence the impact behaviour of the headform depending on the impact condition.

Therefore, the biofidelity of EN960 headforms should be further investigated taking into account all the headform parameters that might influence the assessment criteria for each impact condition. Each impact condition should be defined including location of impact point, shape, compliance and roughness of impact surface and magnitude and angle of the impact velocity. The headform parameters that might influence the assessment criteria for each impact condition are headform compliance, external surface friction, relative motion of scalp tissue, external geometry, mass properties and boundary conditions.

2. Should angular measurements be included to assess helmet performance in normal impact tests?

Twenty full-face motorcycle helmet models and the unhelmeted headform were exposed to free fall normal impact tests in order to study the suitability of the normal impact tests for evaluating intracranial injury risk. It has been shown that the angular motion of the helmeted headform during free fall normal impact tests decreases as the linear acceleration decreases but it also depends on the helmet geometrical design.

Therefore, the angular motion of the headform must be assessed in free fall normal impact tests in combination with the assessment in oblique impacts on order to evaluate the helmet geometrical design for preventing intracranial injuries in a wide range of possible impact scenarios.

Different from oblique tests in which the friction between the interior of the helmet and the headform plays an important role in the rotational motion of the headform (Ebrahimi et al., 2015), friction does not have a significant influence in the angular kinematics of the headform during free fall normal impact tests. However, previous studies have shown that the effects of the neck and body are less significant for oblique impacts than for normal impacts onto the flat anvil (Hering & Derler, 2000). Therefore, further investigations should study the influence of the neck and body on the angular kinematics of the head in normal impacts using a realistic neck.

3. How relevant is the effect of friction at the headform/helmet interface in oblique impact tests?

One helmet model was tested at the same magnitude of the normal component of the impact velocity but at three different magnitudes of the tangential component of the impact velocity using two different frictions at the headform/helmet interface.

The results of the experiments showed that the combination of low friction coefficients with low tangential component of the impact velocity may result into underprediction of the rotational headform variables that would not be representative of

real-world conditions, in which a higher tangential component of the impact velocity or the sweat of the head of the rider would increase the rotational motion experienced by the head of the rider.

Since the influence of the coefficient of friction between the headform and the interior surface of the helmet in oblique impacts depends on the magnitude of the tangential velocity, the magnitude of these two factors must be chosen jointly.

A literature review of the complex and highly variable friction behaviour of the human skin has suggested that it strongly depends on skin hydration and moisture, therefore, future researches should investigate the coefficient of friction between different materials used as comfort padding and the human scalp, taking into account the physiological skin condition and the effect of sweat.

4.   Is it possible to draw information to prevent basilar skull fractures from existing chin bar impact tests?

A combined methodology using the output kinematics measured with an isolated headform during a physical test as input to a full-body finite element (FE) model was used to study if it was possible to predict the neck tensile load that the full-body Hybrid III model would experience in a similar impact to that of the ECE 22.06 chin bar test using only kinematic based metrics from the ECE 22.06 physical test.

The results of this study have shown that simple chin bar impact test using isolated EN960 headforms which are included in some helmet testing standards could consider the risk of basilar skull fracture by a combination of the peak of the linear acceleration in the Z-axis (PAz) and the resultant linear velocity at the end of the impact (RLV). This multiple regression model was developed in a two-step procedure.

First, it was shown that the neck axial force measured by the full-body Hybrid III FE model during a helmeted chin bar impact can be accurately predicted through simulation prescribing the head linear kinematics measured in a similar impact with the detached headform. Consequently, a first relationship was established between the neck axial force from full-body chin bar impacts and the neck axial force from full-body simulations using head linear kinematics from isolated headform chin bar impacts. While this relationship is independent on the headform type used in the isolated headform chin bar impacts, it is dependent on the FE model used as human body surrogate. Therefore, further research should be carried out using a human body surrogate with a more biofidelic neck than the Hybrid III model.

Finally, using the previously mentioned relationship and a set of eighteen ECE 22.06 chin bar physical tests, a multiple regression model was established to predict the neck axial force from PAz and RLV measured the physical chin bar tests. Thus, it has been found that data that are currently collected in regular helmet testing could be used to predict the peak of neck tension and therefore to assess the risk of basilar skull fracture.

5.   Is including a penetration test beneficial for helmet performance assessment?

A set of twenty different full-face motorcycle helmets were exposed to a penetration test. Then, based on the observed results from the penetration tests, four helmets were classified as hard shell helmets while six of them were classified as soft shell helmets. Only these ten helmet models were selected to be drop tested at two different velocities to study the effect of including a penetration test in the overall impact performance of helmets.

The results of this study suggested that hard shell helmets, even if they can be strongly

influenced by the penetration test, would provide better protection against head injuries induced primarily by linear kinematics at high-speed impacts without harming the helmet performance at low-impact speeds. It is not completely clear whether hard shell helmets could provide a worst protection against head injuries primarily induced by rotational kinematics than soft shell helmets at low and high impact speeds. This question should be the focus of further research.

Additional findings

In addition, during the investigation of the previously mentioned specific research questions, this work also reached the following conclusions:

The duration of the linear acceleration must be considered in helmet impact testing. A combination of the peak of the resultant linear acceleration (PLA) and the skull fracture criterion (SFC) metrics are the most appropriate assessment criterion for skull fracture prevention in helmet testing standards because PLA will restrict high magnitude acceleration curves of short duration while SFC will restrict long duration acceleration curves.

It has been shown experimentally that the influence of increasing tangential velocity on the linear acceleration measured by the headform is negligible. Therefore, oblique testing programs including a normal component of the impact velocity that represents a low severity impact would assess if helmets transmit unacceptably high levels of linear acceleration even in low severity impact events.

Finally, this work has observed that linear kinematics from a full-body chin bar impact can be well estimated by a simple chin bar impact test using an isolated headform but unrealistic rotational kinematics are obtained due to the absence of neck coupling. Since rotational kinematics of the head has been proposed as the main mechanism of intracranial injuries (Kleiven, 2013), a similar methodology as the one used in Chapter 6 for neck axial force prediction should be carried out to study it is possible to predict the rotational kinematics that a full-body FE model would experience in a similar impact to that of the ECE 22.06 chin bar test using only kinematic based metrics from the ECE 22.06 physical test.

8.2. Implications of the research and publications

This dissertation emerges from the collaboration agreement between the Impact Laboratory of the University of Zaragoza and the International Motorcycling Federation (FIM) for the continuous improvement of rider protection during competitions.

Part of the work included in this dissertation was used for the development of the Homologation Manual – FRHPhe-01 (FIM, 2017), which was launched by the FIM in October 2017. The main innovation of the FRHPhe-01 was the assessment of the response of the helmet to oblique impacts. The testing protocol was presented in the International Motorcycle Conference of the Institute for Motorcycle Safety (ifz) in October 2018 (Manfredi et al., 2018). FIM Homologated helmets have been required in all Circuit Racing disciplines as of 2019. In addition, the new version of the ECE Regulation No. 22 was notably influenced by the FRHPhe-01 (ECE, 2021).

In November 2019, started the project entitled "DEVELOPMENT OF NEW HELMET HOMOLOGATION STANDARDS FRHPhe-OFF ROAD and FRHPhe-02" between the Impact Laboratory and the FIM with the aim to extend the helmet homologation program to all other disciplines and to carry out an improvement of the testing procedure making use of

the acquired knowledge during the previous two years of validity of the FRHPhe-01.

In November 2022, FIM launched the Homologation Manual – FRHPhe-02, which includes the main recommendations for the improvement of the helmet testing standards suggested in this dissertation (FIM, 2022). It includes the assessment of the angular motion in free fall normal impact tests, the use of the combination of PLA and SFC as assessment criterion for head injuries induced primarily by linear kinematics, the use of a high friction at the helmet/headform interface during oblique impacts, the non-consideration of the angular motion during chin bar impacts and the use of the oblique tests to assess the protection against head injuries induced primarily by linear kinematics in low severity impact events. FIM Homologated helmets of FRHPhe-02 will be strongly recommended as of 2025 and become mandatory as of 2026, in most FIM competitions.

Publications

The work presented in this dissertation resulted in the following publications which are respectively included in the annexes A and B:

Juste-Lorente, O.; Maza, M.; Piccand, M.; López-Valdés, F.J. (2021). The Influence of Headform/Helmet Friction on Head Impact Biomechanics in Oblique Impacts at Different Tangential Velocities. *Applied Sciences, 11*, 11318. https://doi.org/10.3390/app112311318

Juste-Lorente, O.; Maza, M.; Piqueras, A.; Lorente, A.I.; López-Valdés, F.J. (2022). Effects of Including a Penetration Test in Motorcyclist Helmet Standards: Influence on Helmet Stiffness and Impact Performance. *Applied Sciences*, *12*, 2455. https://doi.org/10.3390/app12052455

Conclusiones (Conclusions in Spanish)

Una breve revisión de la biomecánica del impacto de la cabeza humana ha mostrado que existen diferentes tipos de lesiones en la cabeza, cada una de ellas implica tejidos específicos de la cabeza y es producida por un mecanismo de lesión determinado. A pesar de que las deformaciones en los tejidos son las principales causas de lesiones, la cinemática de la cabeza se utiliza convenientemente para caracterizar los mecanismos de las lesiones en la cabeza. Aunque los mecanismos de lesión intracraneal aún se encuentran a nivel de hipótesis, la hipótesis dominante considera que la cabeza humana es más sensible al movimiento rotacional que al movimiento traslacional (Kleiven, 2013). Sin embargo, una revisión de las normas de ensayo de cascos más relevantes ha mostrado que están más enfocadas en el movimiento traslacional que en el movimiento rotacional. Aunque algunas normas requieren pruebas oblicuas para evaluar el rendimiento rotacional de los cascos, existen diferencias en los procedimientos de prueba, como la fricción entre el interior del casco y la cabeza de ensayo, que tiene una influencia importante en el movimiento rotacional experimentado por la cabeza de ensayo durante las pruebas (Ebrahimi et al., 2015). Otras discrepancias entre las normas de ensayo de cascos incluyen los impactos en la mentonera del casco, que están potencialmente relacionados con fracturas de la base del cráneo, o el controvertido tema de incluir o no un ensayo de penetración. Curiosamente, una revisión de los accidentes de motocicleta que se producen en el mundo real ha mostrado que, a pesar del éxito del casco de motocicleta en la prevención de fracturas locales en el cráneo, lesiones graves en la cabeza, como las lesiones intracraneales y las fracturas de la base del cráneo, siguen siendo lesiones comunes entre los motociclistas (Chinn et al., 2001; Whyte et al., 2016). Debido a todas las discrepancias mencionadas anteriormente, el objetivo principal de esta tesis fue investigar cómo se pueden mejorar las normas actuales de ensayo de cascos de motocicleta para reducir las fracturas de la base del cráneo y las lesiones intracraneales.

Para ello, en esta tesis se planificaron e investigaron varias preguntas de investigación específicas. Los párrafos a continuación enumeran estas preguntas de investigación y resumen los principales resultados obtenidos en la investigación.

1. *¿Cómo de similares son las cabezas de ensayo EN960 a las cabezas humanas?*

Se ha creado una base de datos de propiedades físicas de cabezas humanas en base a una revisión de una selección de estudios realizados con cadáveres humanos mostrando una aceptable concordancia con un conjunto de datos de una población adulta viva. Se observó que las propiedades de las cabezas de ensayo EN960, como la longitud, el ancho, la masa, la ubicación del centro de gravedad y los momentos de inercia, se encontraban dentro de los intervalos de predicción del 95% calculados a partir de los conjuntos de datos de cadáveres humanos para la mayoría de los tamaños de las cabezas de ensayo EN960, pero se observaron algunas diferencias con respecto a los modelos de regresión calculados. Por lo tanto, sería beneficioso contar con un nuevo conjunto de cabezas de ensayo con propiedades de masa e inercia más similares a las calculadas con los modelos de regresión para mejorar las actuales normas de ensayo de cascos. Además, podría ser necesario evaluar la protección del casco con cabezas de ensayo con diferentes geometrías según la

antropometría de la población para la que están destinados. Sin embargo, aunque la antropometría y todas las propiedades de masa coincidieran perfectamente con las propiedades de la cabeza humana, no significa que la cabeza de ensayo represente suficientemente bien el comportamiento de la cabeza humana en todas las condiciones de impacto. Otros factores como la rigidez de la cabeza de ensayo (Bosch, 2006), la fricción de la superficie externa (Ebrahimi et al., 2015), el tejido del cuero cabelludo (Trotta et al., 2018b) y las condiciones de contorno para la unión con el cuello y el resto del cuerpo (Hering & Derler, 2000) pueden influir significativamente en el comportamiento a impacto de la cabeza de ensayo dependiendo de la condición de impacto.

Por lo tanto, la biofidelidad de las cabezas de ensayo EN960 debe ser investigada aún más teniendo en cuenta todos los parámetros de la cabeza de ensayo que puedan influir en los criterios de evaluación para cada condición de impacto. Cada condición de impacto debe definirse, incluyendo la ubicación del punto de impacto, la forma, la rigidez y la rugosidad de la superficie de impacto, y la magnitud y el ángulo de la velocidad de impacto. Los parámetros de la cabeza de ensayo que podrían influir en los criterios de evaluación para cada condición de impacto son la rigidez de la cabeza de ensayo, la fricción de la superficie externa, el movimiento relativo del tejido del cuero cabelludo, la geometría externa, las propiedades de masa y las condiciones de contorno para la unión con el cuello y el resto del cuerpo.

2.   ¿Deberían incluirse las mediciones angulares para evaluar el comportamiento de los cascos en pruebas de impacto normal?

Veinte modelos de cascos integrales de motocicleta y la cabeza de ensayo sin casco fueron expuestos a pruebas de impacto normal para estudiar la idoneidad de estas pruebas para evaluar el riesgo de lesiones intracraneales. Se ha demostrado que el movimiento angular de la cabeza de ensayo con casco durante las pruebas de impacto normal disminuye a medida que la aceleración lineal disminuye, pero también depende del diseño geométrico del casco. Por lo tanto, se debe evaluar el movimiento angular de la cabeza de ensayo durante las pruebas de impacto normal en combinación con la evaluación durante impactos oblicuos para evaluar el diseño geométrico del casco frente a lesiones intracraneales en una amplia gama de posibles escenarios de impacto.

A diferencia de los ensayos oblicuos en los que la fricción entre el interior del casco y la cabeza de ensayo juega un papel importante en el movimiento rotacional de la cabeza (Ebrahimi et al., 2015), la fricción no tiene una influencia significativa en la cinemática angular de la cabeza de ensayo durante las pruebas de impacto normal. Sin embargo, estudios previos han demostrado que los efectos del cuello y el cuerpo son menos significativos para los impactos oblicuos que para los impactos normales sobre el yunque plano (Hering & Derler, 2000). Por lo tanto, investigaciones adicionales deberían estudiar la influencia del cuello y el cuerpo en la cinemática angular de la cabeza en impactos normales utilizando un cuello realista.

3.   ¿Cómo de relevante es el efecto de la fricción entre la cabeza de ensayo y el interior del casco en pruebas de impacto oblicuo?

Se probó un modelo de casco a la misma magnitud de la componente normal de la velocidad de impacto, pero a tres magnitudes diferentes de la componente tangencial de la velocidad de impacto y usando dos fricciones diferentes entre la cabeza de ensayo y el interior del casco.

Los resultados de los experimentos mostraron que la combinación de coeficientes de fricción bajos con una componente tangencial baja de la velocidad de impacto puede resultar en una subestimación de las variables rotacionales de la cabeza de ensayo que no serían representativas de las condiciones del mundo real, en las cuales una componente tangencial más alta de la velocidad de impacto o el sudor de la cabeza del motociclista aumentaría el movimiento rotacional experimentado por la cabeza del motociclista.

Dado que la influencia del coeficiente de fricción entre la cabeza de ensayo y la superficie interior del casco en impactos oblicuos depende de la magnitud de la velocidad tangencial, la magnitud de estos dos factores debe ser elegida conjuntamente.

Una revisión de la literatura sobre el comportamiento de la compleja y altamente variable fricción de la piel humana ha sugerido que la fricción depende fuertemente de la hidratación y la humedad de la piel, por lo tanto, las investigaciones futuras deberían investigar el coeficiente de fricción entre diferentes materiales utilizados como acolchado de confort y el cuero cabelludo humano, teniendo en cuenta la condición fisiológica de la piel y el efecto del sudor.

4. *¿Es posible obtener información para prevenir fracturas en la base del cráneo a partir de los ensayos de impacto en la mentonera existentes?*

Se utilizó una metodología combinada que empleaba la cinemática resultante medida en una cabeza de ensayo durante un ensayo físico como entrada en un modelo de elementos finitos de cuerpo completo, para estudiar si es posible predecir la carga de tracción en el cuello que experimentaría el modelo del Híbrido III de cuerpo completo en un impacto similar al ensayo de la mentonera incluido en la última versión del Reglamento No. 22 de las Naciones Unidas (ECE 22.06) utilizando solo métricas cinemáticas medidas en el ensayo físico.

Los resultados de este estudio han demostrado que un simple ensayo de impacto en la mentonera usando cabezas de ensayo EN960, como el que se incluye en algunas normas de ensayo de cascos, podrían considerar el riesgo de fractura de la base del cráneo mediante una combinación del pico de aceleración lineal en el eje Z (PAz, por sus siglas en inglés) y la velocidad lineal resultante al final del impacto (RLV, por sus siglas in inglés). Este modelo de regresión múltiple se desarrolló en un procedimiento de dos etapas.

En primer lugar, se demostró que la fuerza axial en el cuello medida por el modelo de elementos finitos del Híbrido III de cuerpo completo durante un impacto en la mentonera del casco se puede predecir con precisión a través de simulaciones prescribiendo la cinemática lineal de la cabeza medida en un impacto similar con la cabeza aislada del resto del cuerpo. En consecuencia, se estableció una primera relación entre la fuerza axial en el cuello medida durante los impactos en la mentonera con cuerpo completo y la fuerza axial en el cuello medida durante las simulaciones de cuerpo completo que utilizan la cinemática lineal de la cabeza medida durante los impactos en la mentonera con la cabeza aislada. Si bien esta relación es independiente del tipo de cabeza de ensayo utilizado en los impactos en la mentonera con cabezas de ensayo aisladas, depende del modelo de cuerpo completo utilizado como sustituto del cuerpo humano. Por lo tanto, investigaciones futuras deberían estudiar esta relación utilizando un sustituto del cuerpo humano con un cuello más realista que el del modelo del Híbrido III.

Finalmente, utilizando la relación mencionada anteriormente y un conjunto de dieciocho pruebas físicas realizadas en la mentonera de acuerdo a la ECE 22.06, se estableció un modelo de regresión múltiple para predecir la fuerza axial en el cuello a partir

de PAz y RLV medidos en las pruebas físicas de la mentonera. Así, se ha descubierto que los datos que actualmente se recopilan en las pruebas existentes de cascos podrían utilizarse para predecir el pico de fuerza axial en el cuello y, por lo tanto, evaluar el riesgo de fractura de la base del cráneo.

5. *¿Es beneficioso incluir un ensayo de penetración para la evaluación del comportamiento del casco?*

Se sometió a un conjunto de veinte cascos integrales para motocicleta a una prueba de penetración. Según los resultados observados en las pruebas de penetración, se clasificaron cuatro cascos como cascos con calota dura, mientras que seis de ellos se clasificaron como cascos con calota blanda. Solo estos diez modelos de cascos fueron seleccionados para ser sometidos a una prueba de caída a dos velocidades diferentes para estudiar el efecto de incluir un ensayo de penetración en el comportamiento general de los cascos frente a impacto.

Los resultados de este estudio sugieren que los cascos con calota dura, aunque pueden verse fuertemente influenciados por la prueba de penetración, proporcionarían una mejor protección contra lesiones en la cabeza inducidas principalmente por cinemática lineal en impactos a altas velocidades de impacto sin afectar el rendimiento del casco a bajas velocidades de impacto. No está completamente claro si los cascos con calota dura podrían proporcionar una peor protección contra lesiones en la cabeza inducidas principalmente por cinemática rotacional que los cascos con calota blanda a velocidades de impacto bajas y altas. Esta pregunta debería ser el foco de investigaciones futuras.

Hallazgos adicionales

Además, durante el estudio de las preguntas de investigación específicas previamente mencionadas, este trabajo también llegó a las siguientes conclusiones:

La duración de la aceleración lineal debe considerarse en las pruebas de impacto de cascos. Una combinación del pico de la aceleración lineal resultante (PLA, por sus siglas en inglés) y el criterio de fractura del cráneo (SFC, por sus siglas en inglés) son los criterios de evaluación más apropiados para la prevención de fracturas del cráneo en las normas de ensayo de cascos, porque PLA restringirá las curvas de aceleración de alta magnitud y de corta duración mientras que SFC restringirá las curvas de aceleración de larga duración.

Experimentalmente se ha demostrado que la influencia del aumento de la velocidad tangencial en la aceleración lineal medida por la cabeza de ensayo es insignificante. Por lo tanto, los ensayos oblicuos que incluyen una componente normal de la velocidad de impacto que representa un impacto de baja severidad, también evalúan si los cascos transmiten niveles de aceleración lineal inaceptablemente altos en impactos de baja severidad.

Finalmente, este trabajo ha observado que la cinemática lineal de un impacto en la mentonera con cuerpo completo puede ser bien estimada por una simple prueba de impacto en la mentonera utilizando una cabeza de ensayo aislada, pero se obtienen cinemáticas rotacionales irreales debido a la ausencia de acoplamiento del cuello. Dado que se ha propuesto que la cinemática rotacional de la cabeza es el principal mecanismo de lesiones intracraneales (Kleiven, 2013), se podría llevar a cabo una metodología similar a la utilizada en el Capítulo 6 para predecir la fuerza axial del cuello para estudiar si es posible predecir la cinemática rotacional que experimentaría un modelo de elementos finitos de cuerpo completo en un impacto similar al de la prueba de la mentonera de la ECE 22.06 utilizando solo métricas basadas en la cinemática de la prueba física de la ECE 22.06.

Bibliography

Aare, M., & Halldin, P. (2003). A new laboratory rig for evaluating helmets subject to oblique impacts. *Traffic Injury Prevention*, *4*(3), 240–248. https://doi.org/10.1080/15389580309879

Ackaah, W., Afukaar, F., Agyemang, W., Anh, T. T., Hejar, A. R., Abdul, G., Gururaj, G., Elisa, H. S., Martha, H., Hyder, A. A., Inclán-Valadez, C., Kulanthayan, S., Norton, R., Odero, W., Owoaje, E. T., Peden, M., Rajam, K., Razzak, J. A., Sangowawa, A. O., … Yu, J. (2013). The use of non-standard motorcycle helmets in low- and middle-income countries: A multicentre study. *Injury Prevention*, *19*(3), 158–163. https://doi.org/10.1136/injuryprev-2012-040348

Albery, C., & Whitestone, J. (2003, 23 October). Comparison of Cadaveric Human Head Mass Properties: Mechanical Measurement vs. Calculation from Medical Imaging. In *Proceedings of the 31st International Workshop on Human Subjects for Biomechanics Research, San Diego, California, United States*, 157–172.

Aldman, B., Lundell, B., & Thorngren, L. (1976, 7-8 Spetember). Non-perpendicular impacts - An experimental study on crash helmets. In *IRCOBI Conference Proceedings, Amsterdam, The Netherlands,* 322-331.

Alshareef, A., Giudice, J. S., Forman, J., Shedd, D. F., Reynier, K. A., Wu, T., Sochor, S., Sochor, M. R., Salzar, R. S., & Panzer, M. B. (2020). Biomechanics of the Human Brain during Dynamic Rotation of the Head. *Journal of Neurotrauma*, *37*(13), 1546–1555. https://doi.org/10.1089/neu.2019.6847

Arregui, C., Luzón, J., López-Valdés, F. J., del Pozo de Dios, E., & Seguí-Gómez, M. (2007). *Fundamentos de biomecánica en las lesiones por accidente de tráfico*. Etrasa Editorial Tráfico Vial.

Ball, R., Shu, C., Xi, P., Rioux, M., Luximon, Y., & Molenbroek, J. (2010). A comparison between Chinese and Caucasian head shapes. *Applied Ergonomics*, *41*(6), 832–839. https://doi.org/10.1016/j.apergo.2010.02.002

Bandak, F. A., & Eppinger, R. H. (1994). A Three-Dimensional Finite Element Analysis of the Human Brain Under Combined Rotational and Translational Accelerations. *SAE Technical Paper 942215.* https://doi.org/10.4271/942215

Becker, E. B. (2012, 2 October). Voluntary and mandatory motorcycle helmet standards. In *Proceedings of the 9th International Motorcycle Conference, Cologne, Germany*, 424-439.

Beier, G., Schuck, M., Schuller, E., & Spann, W. (1979). Determination of Physical Data of the Head I. Center of Gravity and Moments of Inertia of Human Heads*. Institute of Forensic Medicine, University of Munich*.

Beusenberg, M, & Happee, R. (1993, 8-10 September). An experimental evaluation of crash helmet design and effectiveness in standard impact tests. In *IRCOBI Conference Proceedings, Eindhoven, The Netherlands*, 307–323.

Beusenberg, Marc, Shewchenko, N., Newman, J. A., de Lange, R., & Cappon, H. (2013). Head, Neck, and Body Coupling in Reconstructions of Helmeted Head Impacts. *Journal of Chemical Information and Modeling*, *53*(9), 1689–1699.

Bonin, S. J., Luck, J. F., Bass, C. R., Gardiner, J. C., Onar-Thomas, A., Asfour, S. S., & Siegmund, G. P. (2017). Dynamic Response and Residual Helmet Liner Crush Using Cadaver Heads and Standard Headforms. *Annals of Biomedical Engineering*, *45*(3), 656–667. https://doi.org/10.1007/s10439-016-1712-5

Bonugli, E., Cormier, J., Reilly, M., & Reinhart, L. (2017). Replicating Real-World Friction of Motorcycle Helmet Impacts and Its Effects on Head Injury Metrics. *SAE Technical Paper 2017-01-1433*. https://doi.org/10.4271/2017-01-1433

Bosch, van den, H. L. A. (2006). *Crash helmet testing and design specifications.* [Phd Thesis 1 (Research TU/e/Graduation TU/e), Mechanical Engineering]. Technische Universiteit Eindhoven. https://doi.org/10.6100/IR613094

Bourdet, N., Deck, C., Mojumder, S., & Willinger, R. (2018, 12-14 September). Comparative Evaluation of DOT vs. ECE Motorcycle Helmet Test Method. In *IRCOBI Conference Proceedings, Athens, Greece*, 470–479.

Bourdet, N., Deck, C., Trog, A., Meyer, F., Noblet, V., & Willinger, R. (2021, 8-10 September). Deep Learning methods applied to the assessment of Brain Injury Risk. In *IRCOBI Conference Proceedings, held online (due to corona pandemic)*, 709–719.

Bourdet, N., Mojumder, S., Piantini, S., Deck, C., Pierini, M., & Willinger, R. (2016, 14-16 September). Proposal of a new motorcycle helmet test method for tangencial impact. In *IRCOBI Conference Proceedings, Malaga, Spain,* 479–489.

Burrows, A. M., & Cohn, J. F. (2009). Anatomy of Face. In *Encyclopedia of Biometrics* (pp. 16–23). Springer, Boston, MA. https://doi.org/10.1007/978-0-387-73003-5_190

Chan, P., Lu, Z., Rigby, P., Takhounts, E., Zhang, J., Yoganandan, N., & Pintar, F. (2007, 18-21 June). Development Of Generalized Linear Skull Fracture Criterion. In *Proceedings of the 20th International Technical Conference on the Enhanced Safety of Vehicles, Lyon, France*, 1–11.

Chandler, R. F., Clauser, C. E., McConville, J. T., Reynolds, H. M., & Young, J. W. (1975). Investigation of inertial properties of the human body. *Air Force Aerospace Medical Research Lab Wright-Patterson AFB OH,* 1–162.

Chang, L.-T., Chang, C.-H., & Chang, G.-L. (1999). Experimental Evaluation of Chin Bar on Head Injury in Facial Impact. *JSME International Journal*, *42, No.2*, 294–299.

Chang, L.-T., Chang, C.-H., & Chang, G.-L. (2001). Fit Effect of Motorcycle Helmet - A Finite Element Modeling. *JSME International Journal*, *44*(Series A, No. 1), 185–192.

Chang, L.-T., Chang, C.-H., Huang, J.-Z., & Chang, G.-L. (1999, 23-24 September). A dynamic analysis of motorcycle helmet by finite element methods. In *IRCOBI Conference Proceedings, Sitges, Spain*, 371–382.

Chee, C. P., & Ali, A. (1991). Basal skull fractures. A prospective study of 100 consecuttive admissions. *Aust. N.Z. J. Surg.*, *61*(8), 597–602. https://doi.org/10.1111/j.1445-2197.1991.tb00299.x

Ching, R. P. (2007). Relationship between Head Mass and Circumference in Human Adults. *University of Washington. Technical Brief.* 1–5.

Chinn, B., Canaple, B., Derler, S., Doyle, D., Otte, D., Schuller, E., & Willinger, R. (2001). Final report of the action COST 327: Motorcycle Safety Helmets. *European Commission, Directorate General for Energy and Transport, Brussels, Belgium.*

Claessens, M. H. A. (1994). A*natomical description of the human head.* (DCT rapporten; Vol. 1994.003). Technische Universiteit Eindhoven.

Clarke, A. G. (1944). The anatomy of the meninges. *Postgraduate Medical Journal*, *20*, 74–78. https://doi.org/10.1136/pgmj.20.220.74

Connor, T. A., Colgan, N., Stewart, M., Ní Annaidh, A., & Gilchrist, M. D. (2020). Inertial properties of a living population for the development of biofidelic headforms. *Proceedings of the Institution of Mechanical Engineers, Part P: Journal of Sports Engineering and Technology*. https://doi.org/10.1177/1754337120921646

Connor, T. A., Stewart, M., Burek, R., & Gilchrist, M. D. (2019). Influence of headform mass and inertia on the response to oblique impacts. *International Journal of Crashworthiness*, *24*(6), 677–698. https://doi.org/10.1080/13588265.2018.1525859

Cooter, R. D., & David, D. A. (1990, 31 October - 3 November). Motorcyclist craniofacial injury patterns. In *Proceedings of the International Motorcycle Safety Conference, Orlando, Florida, United States.*

Cua, A. B., Wilhelm, K. P., & Maibach, H. I. (1990). Elastic properties of human skin: relation to age, sex, and anatomical region. *Archives of Dermatological Research*, *282*(5), 283–288. https://doi.org/10.1007/BF00375720

Depreitere, B., Van Lierde, C., Vander Sloten, J., Van Audekercke, R., Van Der Perre, G., Plets, C., & Goffin, J. (2006). Mechanics of acute subdural hematomas resulting from bridging vein rupture. *Journal of Neurosurgery*, *104*(6), 950–956. https://doi.org/10.3171/JNS.2006.104.6.950

Derler, S., Rossi, R. M., & Rotaru, G. M. (2015). Understanding the variation of friction coefficients of human skin as a function of skin hydration and interfacial water films. *Proceedings of the Institution of Mechanical Engineers, Part J: Journal of Engineering Tribology*, *229*(3), 285–293. https://doi.org/10.1177/1350650114527922

Di Landro, L., Sala, G., & Olivieri, D. (2002). Deformation mechanisms and energy absorption of polystyrene foams for protective helmets. *Polymer Testing*, *21*(2), 217–228. https://doi.org/10.1016/S0142-9418(01)00073-3

Dowdell, B., Long, G. J., Ward, J., & Griffiths, M. (1988). A Study of helmet damage and rider head/neck injuries for crash involved motorcyclists. *Roads and Traffic Authority, Road Safety Bureau, New South Wales, Australia.*

Ebrahimi, I., Golnaraghi, F., & Wang, G. G. (2015). Factors Influencing the Oblique Impact Test of Motorcycle Helmets. *Traffic Injury Prevention*, *16*(4), 404–408. https://doi.org/10.1080/15389588.2014.937804

Ellis, H., & Mahadevan, V. (2014). The surgical anatomy of the scalp. *Surgery (Oxford)*, *32*(SUPPL. 1). https://doi.org/10.1016/j.mpsur.2013.04.024

European Commission. (2021). Road safety thematic report - Fatigue. European Road Safety Observatory. *Brussels, European Commission, Directorate General for Transport.*

European Committee for Standardization. (2006). *Headforms for use in the testing of protective helmets* (EN 960:2006).

Fahlstedt, M., Abayazid, F., Panzer, M. B., Trotta, A., Zhao, W., Ghajari, M., Gilchrist, M. D., Ji, S., Kleiven, S., Li, X., Annaidh, A. N., & Halldin, P. (2020). Ranking and Rating Bicycle Helmet Safety Performance in Oblique Impacts Using Eight Different Brain Injury Models. *Annals of Biomedical Engineering*. https://doi.org/10.1007/s10439-020-02703-w

Fahlstedt, M., Halldin, P., Alvarez, V. S., & Kleiven, S. (2016, 14-16 September). Influence of the Body and Neck on Head Kinematics and Brain Injury Risk in Bicycle Accident Situations. In *IRCOBI Conference Proceedings, Malaga, Spain,* 459–478.

Farajzadeh Khosroshahi, S., Galvanetto, U., & Ghajari, M. (2017). Optimization of the Chin Bar of a Composite-Shell Helmet to Mitigate the Upper Neck Force. *Applied Composite Materials*, *24*(4), 931–944. https://doi.org/10.1007/s10443-016-9566-4

Fernandes, F. A. O., & Sousa, R. J. A. De. (2013). Motorcycle helmets — A state of the art review. *Accident Analysis and Prevention*, *56*, 1–21. https://doi.org/10.1016/j.aap.2013.03.011

Finan, J. D., Nightingale, R. W., & Myers, B. S. (2008). The influence of reduced friction on head injury metrics in helmeted head impacts. *Traffic Injury Prevention*, *9*(5), 483–488. https://doi.org/10.1080/15389580802272427

Gabler, L. F., Crandall, J. R., & Panzer, M. B. (2016). Assessment of Kinematic Brain Injury Metrics for Predicting Strain Responses in Diverse Automotive Impact Conditions. *Annals of Biomedical Engineering*, *44*(12), 3705–3718. https://doi.org/10.1007/s10439-016-1697-0

Gabler, L. F., Crandall, J. R., & Panzer, M. B. (2018). Development of a Metric for Predicting Brain Strain Responses Using Head Kinematics. *Annals of Biomedical Engineering*, *46*(7), 972–985. https://doi.org/10.1007/s10439-018-2015-9

Gennarelli, T. A. (1983). Head Injury in Man and Experimental Animals: Clinical Aspects. In: *Adams, J.H. (eds) Trauma and Regeneration. Acta Neurochirurgica Supplementum, vol 32. Springer, Vienna.* https://doi.org/10.1007/978-3-7091-4147-2_1

Gennarelli, T. A. (1985). Biomechanics of Head Injury. *Neurosurgery*, *2*, 1531–1536.

Gennarelli, T. A., Ommaya, A. K., & Thibault, L. E. (1971, 17-19 November). Comparison of translational and rotational head motions in experimental cerebral concussion. In *Proceedings of the 15th Stapp Car Crash Conference, Coronado, California, United States*, 797–803.

Gennarelli, T. A., Thibault, L. E., Adams, J. H., Graham, D. I., Thompson, C. J., & Marcincin, R. P. (1982). Diffuse axonal injury and traumatic coma in the primate. *Annals of Neurology*, *12*(6), 564–574. https://doi.org/10.1002/ana.410120611

Gennarelli, T. A. (2019, 11–13 September). Back to the Basics: Revisiting the future, a retrospective of reminiscences. In *IRCOBI Conference Proceedings, Florence, Italy.*

Gennarelli, T. A., Pintar, F. A., & Yoganandan, N. (2003). Biomechanical Tolerances for Diffuse Brain Injury and a Hypothesis for Genotypic Variability in Response to Trauma. *Annual Proceedings/Association for the Advancement of Automotive Medicine*, *47*, 624-628.

Gennarelli, T. A., & Thibault, L. E. (1982). Biomechanics of Acute Subdural Hematoma. *The Journal of Trauma: Injury, Infection, and Critical Care*, *22*(8), 680–686. https://doi.org/10.1097/00005373-198208000-00005

Gennarelli, T. A., Thibault, L. E., Tomei, G., Wiser, R., Graham, D., & Adams, J. (1987). Directional dependence of axonal brain injury due to centroidal and non-centroidal acceleration. *SAE Technical Paper 872197*. https://doi.org/10.4271/872197

Gerhardt, L.-C., Strässle, V., Lenz, A., Spencer, N. ., & Derler, S. (2008). Influence of epidermal hydration on the friction of human skin against textiles. *Journal of The Royal Society Interface*, *5*(28), 1317–1328. https://doi.org/10.1098/rsif.2008.0034

Ghajari, M. (2011). *Influence of the body on the response of the helmeted head during impact.* [PhD Thesis, Imperial College London].

Ghajari, M., Caserta, D. G., & Galvanetto, U. (2010). Comparison of safety helmet testing standards. *Motorcylce and Motorcyclist Safety, Marie Curie Research Training Networks, European Commission, Brussels, Belgium.*

Ghajari, M., Galvanetto, U., Iannucci, L., & Willinger, R. (2011). Influence of the body on the response of the helmeted head during impact. *International Journal of Crashworthiness*, *16*(3), 285–295. https://doi.org/10.1080/13588265.2011.559798

Ghajari, M., Peldschus, S., Galvanetto, U., & Iannucci, L. (2011). Evaluation of the effective mass of the body for helmet impacts. *International Journal of Crashworthiness*, *16*(6), 621–631. https://doi.org/10.1080/13588265.2011.616078

Ghajari, M., Peldschus, S., Galvanetto, U., & Iannucci, L. (2013). Effects of the presence of the body in helmet oblique impacts. *Accident Analysis & Prevention*, *50*, 263–271. https://doi.org/10.1016/J.AAP.2012.04.016

Gilchrist, A., & Mills, N. J. (1994). Modelling of the impact response of motorcycle helmets. *International Journal of Impact Engineering*, *15*(3), 201–218. https://doi.org/10.1016/S0734-743X(05)80013-2

Guha, S. (2014). LSTC _ NCAC Hybrid III 50th Dummy Positioning & Post-Processing. *Livermore Software Technology Corporation, Troy, MI.*

Gurdjian, E. S., Hodgson, V. R., Thomas, L. M., & Patrick, L. M. (1968). Significance of relative movements of scalp, skull, and intracranial contents during impact injury of the head. *Journal of Neurosurgery*, *29*(1), 70–72. https://doi.org/10.3171/jns.1968.29.1.0070

Gurdjian, E. S., Roberts, V. L., & Thomas, L. M. (1966). Tolerance curves of acceleration and intracranial pressure and protective index in experimental head injury. *Journal of Trauma - Injury, Infection and Critical Care*, *6*(5), 600–604. https://doi.org/10.1097/00005373-196609000-00005

Halldin, P, Gilchrist, A., & Mills, N. J. (2001). A new oblique impacttest for motorcycle helmets. *International Journal of Crashworthiness*, *6*(1), 53–64. https://doi.org/10.1533/cras.2001.0162

Halldin, Peter, & Fahlstedt, M. (2018, 12–14 September). How sensitive are different headform design parameters in oblique helmeted impacts?. In *IRCOBI Conference Proceedings, Athens, Greece*, 424–425.

Herbst, B., Forrest, S., Chng, D., & Sances, A. (1998, 31 May - 4 June). Fidelity of anthropometric test dummy necks in rollover accidents. In *Proceedings of the 16th International Technical Conference on the Enhanced Safety of Vehicles, Windsor, Ontario, Canada,* 2093-2097.

Hering, A. M., & Derler, S. (2000, 20-22 September). Motorcycle Helmet Drop Tests Using a Hybrid III Dummy. In *IRCOBI Conference Proceedings, Montpellier, France,* 307–321.

Hodgson, V. R., Manson, M. W., & Thomas, L. M. (1972). Head Model for Impact. *SAE Technical Paper 720969.* https://doi.org/10.4271/720969

Hodgson, V. R., & Thomas, L. M. (1971). Breaking Strength of the Human Skull Vs. Impact Surface Curvature. *U.S. Department of Transport, National Highway Traffic Safety Administration, Washington D.C., United States.*

Hodgson, V. R., & Thomas, L. M. (1973). Breaking Strength of the Human Skull Vs. Impact Surface Curvature. *U.S. Department of Transport, National Highway Traffic Safety Administration, Washington D.C., United States.*

Holbourn, A. H. S. (1943). Mechanics of head injuries. *The Lancet*, *242*(6267), 438–441. https://doi.org/10.1016/S0140-6736(00)87453-X

Inder, T. E., Perlman, J. M., & Volpe, J. J. (2018). Intracranial Hemorrhage. In *Volpe's Neurology of the Newborn* (pp. 593-622.e7). StatPearls Publishing. https://doi.org/10.1016/B978-0-323-42876-7.00022-3

International Motorcycling Federation (2017). *FIM Racing Homologation Programme for Helmets* (Homologation Manual - FRHPhe-01)

International Motorcycling Federation (2022). *FIM Racing Homologation Programme for Helmets* (Homologation Manual - FRHPhe-02)

Jaśkiewicz, M., Jurecki, R., Witaszek, K., & Więckowski, D. (2013). Overview and analysis of dummies used for crash tests. *Scientific Journals of the Maritime University of Szczecin*, *35*(107), 22–31.

Japanese Industrial Standard. (2015). *Protective helmets for motor vehicle users* (JIS T 8133).

Juste-Lorente Ó, Maza M, Piccand M, López-Valdés FJ. (2021). The Influence of Headform/Helmet Friction on Head Impact Biomechanics in Oblique Impacts at Different Tangential Velocities. *Applied Sciences, 11(23)*:11318. https://doi.org/10.3390/app112311318

Juste-Lorente Ó, Maza M, Piqueras A, Lorente AI, López-Valdés FJ. (2022). Effects of Including a Penetration Test in Motorcyclist Helmet Standards: Influence on Helmet Stiffness and Impact Performance. *Applied Sciences, 12(5)*:2455. https://doi.org/10.3390/app12052455

Khosroshahi, S. F., Ghajari, M., & Galvanetto, U. (2015, 15-17 June). Assessment of Motorcycle Helmet Chin Bar Design Criteria with Respect to Basilar Skull Fracture using FEM. In *Proceedings of the 10th European LS-DYNA Conference, Wurzburg, Germany*, 1–7.

Kleiven, S. (2003). Influence of impact direction on the human head in prediction of subdural hematoma. *Journal of Neurotrauma*, *20*(4), 365–379. https://doi.org/10.1089/089771503765172327

Kleiven, S. (2013). Why Most Traumatic Brain Injuries are Not Caused by Linear Acceleration but Skull Fractures are. *Frontiers in Bioengineering and Biotechnology*, *1*, 15. https://doi.org/10.3389/fbioe.2013.00015

Kostopoulos, V., Markopoulos, Y. P., Giannopoulos, G., & Vlachos, D. E. (2002). Finite element analysis of impact damage response of composite motorcycle safety helmets. *Composites Part B:Engineering*, *33*(2), 99–107. https://doi.org/10.1016/S1359-8368(01)00066-X

Lissner, H. R., Lebow, M., & Evans, F. G. (1960). Experimental studies on the relation between acceleration and intracranial pressure changes in man. *Surgery, Gynecology & Obstetrics*, *111*, 329–338.

Liu, B. C., Ivers, R., Norton, R., Boufous, S., Blows, S., & Lo, S. K. (2004). Helmets for preventing injury in motorcycle riders. In *Cochrane Database of Systematic Reviews*, *4*, 1–42. https://doi.org/10.1002/14651858.CD004333.pub3

Liu, B. C., Ivers, R., Norton, R., Boufous, S., Blows, S., & Lo, S. K. (2008). Helmets for preventing injury in motorcycle riders. In *Cochrane Database of Systematic Reviews*, Issue 1, Art. No.: CD004333. https://doi.org/10.1002/14651858.CD004333.pub3

Lloyd, J. D. (2016). Biomechanics of Solo Motorcycle Accidents. *Journal of Forensic Biomechanics*, *07*(01). https://doi.org/10.4172/2090-2697.1000125

MacLeod, J. B. A., Digiacomo, J. C., & Tinkoff, G. (2010). An evidence-based review: Helmet efficacy to reduce head injury and mortality in motorcycle crashes: EAST practice management guidelines. *Journal of Trauma: Injury, Infection and Critical Care*, *69*(5), 1101–1111. https://doi.org/10.1097/TA.0b013e3181f8a9cc

Mahapatra, A., Kumar, R., & Kamal, R. (2012). *Textbook of Traumatic Brain Injury.* Jaypee Brothers Medical Publishers (P) Ltd.

Manfredi, E., Maza, M., & Juste-Lorente, O. (2018, 1-2 October). The International Motorcycling Federation sets a new standard for riders 'safety through the FIM Racing Homologation Programme for helmets. In *Proceedings of the 12th International Motorcycle Conference, Cologne, Germany.*Margulies, S. S., & Thibault, L. E. (1992). A proposed tolerance criterion for diffuse axonal injury in man. *Journal of Biomechanics*, *25*(8), 917–923. https://doi.org/10.1016/0021-9290(92)90231-O

McElhaney, J. H., Hopper, R. H., Nightingale, R. W., & Myers, B. S. (1995). Mechanisms of Basilar Skull Fracture. *Article in Journal of Neurotrauma*, *12*(4). https://doi.org/10.1089/neu.1995.12.669

Mcintosh, A., & Grzebieta, R. (2013, 27-30 May). Motorcycle Helmet Standards – Harmonisation and Specialisation? In *Proceedings of the 23rd International Technical Conference on the Enhanced Safety of Vehicles, Seoul, South Korea*, 1–10.

Mellor, A. N., StClair, V. J. M., & Chinn, B. P. (2007). Motorcyclists' helmets and visors: test methods and new technologies. *TRL Limited (UK)*.

Meng, S., Cernicchi, A., Kleiven, S., & Halldin, P. (2019). The biomechanical differences of shock absorption test methods in the US and European helmet standards. *International Journal of Crashworthiness 24(4)*, 399-412. https://doi.org/10.1080/13588265.2018.1464545

Meng, S., Cernicchi, A., Kleiven, S., & Halldin, P. (2020). High-speed helmeted head impacts in motorcycling: A computational study. *Accident Analysis and Prevention*, *134*, 105297. https://doi.org/10.1016/j.aap.2019.105297

Meng, S., Fahlstedt, M., & Halldin, P. (2018, 12-14 September). The effect of impact velocity angle on helmeted head impact severity: A rationale for motorcycle helmet impact test design. In *IRCOBI Conference Proceedings, Athens, Greece*, 454–469.

Mertz, H. J., Prasad, P., & Nusholtz, G. (1996). Head injury risk assessment for forehead impacts. *SAE Technical Paper 960099*. https://doi.org/10.4271/960099

Mesfin, F. B., Gupta, N., Shapshak, A. H., & Taylor, R. S. (2022). Diffuse Axonal Injury. *Encyclopedia of the Neurological Sciences*, 10–12. https://doi.org/10.1016/b0-12-226870-9/00726-7

Miller, J. D. (1993). Head injury. *Journal of Neurology, Neurosurgery, and Psychiatry*, 56:440-447.

Mills, N. J., & Gilchrist, A. (2008). Oblique impact testing of bicycle helmets. *International Journal of Impact Engineering*, *35*(9), 1075–1086. https://doi.org/10.1016/j.ijimpeng.2007.05.005

Mills, N. J., Wilkes, S., Derler, S., & Flisch, A. (2009). FEA of oblique impact tests on a motorcycle helmet. *International Journal of Impact Engineering*, *36*, 913–925.

Mohan, P., Park, C., Marzougui, D., Kan, C., Guha, S., Maurath, C., & Bhalsod, D. (2010, June). LSTC / NCAC Dummy Model Development. In *11th International LS-DYNA Users Conference, Detroit, Michigan, United States*, 53–64.

Mullally, W. J. (2017). Concussion. *The American Journal of Medicine*, *130*(8), 885–892. https://doi.org/10.1016/J.AMJMED.2017.04.016

Newman, J. A. (2005, 21-23 September). The biomechanics of head trauma and the development of the modern helmet. How far have we really come? *IRCOBI Conference Proceedings, Prague, Czech Republic*, 3–12.

National Highway Traffic Safety Administration. (2007). *Traffic Safety Facts (Laws): Motorcycle Helmet Use Laws* (DOT HS 810 726W). United States Department of Transport.

Ommaya, A. K., & Hirsch, A. E. (1971). Tolerances for cerebral concussion from head impact and whiplash in primates. *Journal of Biomechanics*, *4*(1), 13–21. https://doi.org/10.1016/0021-9290(71)90011-X

Ommaya, A. K., & Gennarelli, T. A. (1974). Cerebral Concussion and Traumatic Unconsciousness. *Brain*, *97*(1), 633–654. https://doi.org/10.1093/brain/97.1.633

Ono, K., Kikuchi, A., Nakamura, M., Kobayashi, H., & Nakamura, N. (1980). Human Head Tolerance to Sagittal Impact-Reliable Estimation Deduced from Experimental Head Injury Using Subhuman Primates and Human Cadaver Skulls. *SAE Technical Paper 801303.* https://doi.org/10.4271/2017-01-1433

Otte, D., Jessl, P., & Suren, E. G. (1984, 4-6 September). Impact points and resultant injuries to the head of motor-cyclists involved in accidents, with an without crash helmets. In *IRCOBI Conference Proceedings, Delft, The Netherlands.*

Otte, D, Chinn, B., Doyle, D., Sturrock, K., & Schuller, E. (1997). *Database COST 327:Accident Description and Analysis of Motorcycle Safety Helmets* (COST 327 Interim Report). Medical University Hanover.

Otte, Dietmar. (1991). Technical Demands on Safety in the Design of Crash Helmets for Biomechanical Analysis of Real Accident Situations. *SAE Technical Paper 912911*. https://doi.org/10.4271/912911.

Pang, T. Y., Thai, K. T., McIntosh, A. S., Grzebieta, R., Schilter, E., Dal Nevo, R., & Rechnitzer, G. (2011). Head and neck responses in oblique motorcycle helmet impacts: A novel laboratory test method. *International Journal of Crashworthiness*, *16*(3), 297–307. https://doi.org/10.1080/13588265.2011.559799

Peden, M., Scurfield, R., Sleet, D., Mohan, D., Hyder, A. A., Jarawan, E. & Mathers, C. (2004). *World report on road traffic injury prevention.* World Health Organization, Geneva, Switzerland.

Piantini, S., Pierini, M., Delogu, M., Baldanzini, N., Franci, A., Mangini, M., & Peris, A. (2016, 14-16 September). Injury Analysis of Powered Two-Wheeler versus Other-Vehicle Urban Accidents. In *IRCOBI Conference Proceedings, Malaga, Spain,* 840-853.

Plaga, J. A., Albery, C., Boehmer, M., Goodyear, C., & Thomas, G. (2005). *Design and Development of Anthropometrically Correct Head Forms for Joint Strike Fighter Ejection Seat Testing* (AFRL-HE-WP-TR-2005-0044). Air Force Research Laboratory.

Ramalho, A., Szekeres, P., & Fernandes, E. (2013). Friction and tactile perception of textile fabrics. *Tribology International*, *63*, 29–33. https://doi.org/10.1016/j.triboint.2012.08.018

Rigby, P., & Chan, P. (2009). Evaluation of the biofidelity of FMVSS No. 218 injury criteria. *Traffic Injury Prevention*, *10*(2), 170–177. https://doi.org/10.1080/15389580802607796

Rigby, P., Juhas, B., Wong, J., & Chan, P. (2011, 13-16 June). Evaluation of Biofidelity of ECE Regulation No. 22 Injury Criteria. In *Proceedings of the 22ⁿᵈ Enhanced Safety of Vehicles Conference, Washington D.C., United States*, 1–16.

Scanlon, V. C., Sanders, T. (2007). *Essentials of Anatomy and Physiology*. F. A. Davis Company.

Shuaeib, F. M., Hamouda, A. M. S., Hamdan, M. M., Radin Umar, R. S., & Hashmi, M. S. J. (2002). Motorcycle helmet: Part II. Materials and design issues. *Journal of Materials Processing Technology*, *123*(3), 422–431. https://doi.org/10.1016/S0924-0136(02)00047-X

Snell Foundation. (2020). Standard for Protective Headgear (M2020)

Takhounts, E. G., Craig, M. J., Moorhouse, K., & Mcfadden, J. (2013). Development of Brain Injury Criteria (BrIC). *SAE Technical Paper 2013-22-0010, https://doi.org/10.4271/2013-22-0010*.

Thai, K. T., McIntosh, A. S., & Pang, T. Y. (2015). Factors Affecting Motorcycle Helmet Use: Size Selection, Stability, and Position. *Traffic Injury Prevention*, *16*(3), 276–282. https://doi.org/10.1080/15389588.2014.934366

Thom, D. R., & Hurt, H. H. J. (1993, 4-6 November). Basilar skull fractures in fatal motorcycle crashes. In *Annual Proceedings/Association for the Advancement of Automotive Medicine, 37,* 61-76.

Thom, D. R., Hurt, H. H., & Smith, T. A. (1998, 31 May - 4 June). Motorcycle Helmet Test Headform and Test Apparatus Comparison. *Proceedings of the 16th International Technical Conference on the Enhanced Safety of Vehicles, Windsor, Ontario, Canada*, 2310–2322.

Trotta, A., Ní Annaidh, A., Burek, R. O., Pelgrims, B., & Ivens, J. (2018a). Evaluation of the head-helmet sliding properties in an impact test. *Journal of Biomechanics*, *75*, 28–34. https://doi.org/10.1016/j.jbiomech.2018.05.003

Trotta, A., Zouzias, D., De Bruyne, G., & Ní Annaidh, A. (2018b). The Importance of the Scalp in Head Impact Kinematics. *Annals of Biomedical Engineering*, *46*(6), 831–840. https://doi.org/10.1007/s10439-018-2003-0

United Nations Economic Commission for Europe. (2002). *Uniform provisions concerning the approval of protective helmets and their visors for drivers and passengers of motorcycles and mopeds* (05 series of amendments of Regulation No. 22)*.*

United Nations Economic Commission for Europe. (2021). *Uniform provisions concerning the approval of protective helmets and their visors for drivers and passengers of motorcycles and mopeds* (06 series of amendments of Regulation No. 22)*.*

United States Department of Transport. (2011). *Motorcycle Helmets* (FMVSS No. 218).

Unterharnscheidt, F. J. (1972). Translational versus rotational acceleration: animal experiments with mesured input. *Scandinavian Journal of Rehabilitation Medicine*, *14*(4), 24–26.

Vander Vorst, M., Chan, P., Zhang, J., Yogandan, N., & Pintar, F. (2004). A new biomechanically-based criterion for lateral skull fracture. In *Annual Proceedings/Association for the Advancement of Automotive Medicine, 48*, 181–195.

Vander Vorst, M., Stuhmiller, J., Ho, K., Yoganandan, N., & Pintar, F. (2003). Statistically and biomechanically based criterion for impact-induced skull fracture. In *Annual Proceedings/Association for the Advancement of Automotive Medicine, 47*, 363–381.

Versace, J. (1971). A review of the Severity Index. *SAE Technical Paper 710881*. https://doi.org/10.4271/710881

Walker, L. B., Harris, E. H., & Pontius, U. R. (1973). *Mass, Volume, Center of Mass, and Mass Moment of Inertia of Head and Head Neck of Human Body.* Tulane University, New Orleans, Louisiana, United States.

World Health Organization. (2006). *Helmets: A Road Safety Manual for Decision-makers and Practictioners.* World Health Organization, Geneva, Switzerland.

World Health Organization. (2018). *Global status report on road safety*. World Health Organization, Geneva, Switzerland.

Whyte, T., Stuart, C. A., Mallory, A., Ghajari, M., Plant, D. J., Siegmund, G. P., & Cripton, P. A. (2019). A review of impact testing methods for headgear in sports: Considerations for improved prevention of head injury through research and standards. In *Journal of Biomechanical Engineering, 141(7),* 070803. https://doi.org/10.1115/1.4043140

Whyte, T., Gibson, T., Anderson, R., Eager, D., & Milthorpe, B. (2016). Mechanisms of Head and Neck Injuries Sustained by Helmeted Motorcyclists in Fatal Real-World Crashes: Analysis of 47 In-Depth Cases. *Journal of Neurotrauma*, *33*(19), 1802–1807. https://doi.org/10.1089/neu.2015.4208

Whyte, Thomas, Gibson, T., Milthorpe, B., & Eager, D. (2015, 8-11 June). Mechanisms of head and neck injuries sustained by helmeted motorcyclists in NSW, Australia. In *Proceedings of the 24th International Technical Conference on Enhanced Safety of Vehicles, Gothenburg, Sweden.*

Williams, M. (1990). Evaluation of the penetration test for bicyclists' helmets: Comparative performance of hard shell and foam helmets. *Accident Analysis and Prevention*, *22*(4), 315–325. https://doi.org/10.1016/0001-4575(90)90047-O

Willinger, R., Deck, C., Halldin, P., & Otte, D. (2014, 18-19 November). Towards advanced bicycle helmet test methods. In *Proceedings of the 3rd International Cycling Safety Conference*, *Gothenburg, Sweden,* 1-11.

Wood, J. L. (1971). Dynamic response of human cranial bone. *Journal of Biomechanics*, *4*(1). https://doi.org/10.1016/0021-9290(71)90010-8

Yoganandan, N., & Pintar, F. A. (2004). Biomechanics of temporo-parietal skull fracture. *Clinical Biomechanics*, *19*(3), 225–239. https://doi.org/10.1016/j.clinbiomech.2003.12.014

Yoganandan, N., Pintar, F. A., Zhang, J., & Baisden, J. L. (2009). Physical properties of the human head: Mass, center of gravity and moment of inertia. *Journal of Biomechanics*, *42*(9), 1177–1192. https://doi.org/10.1016/j.jbiomech.2009.03.029

Zellmer, H. (1993). Investigation of the performance of motorcycle helmets under impact conditions. *SAE Technical Paper 933113*. https://doi.org/10.4271/933113

Zhang, J., Yoganandan, N., Pintar, F. A., & Gennarelli, T. A. (2006, 7-9 April). Role of translational and rotational accelerations on brain strain in lateral head impact. *Presented at Rocky Mountain Bioengineering Symposium & International ISA Biomedical Sciences Instrumentation Symposium*, *Terre Haute, Indiana, United States,* 501–506.

Zhang, L., Ramesh, D., Yang, K. H., & King, A. I. (2003, 25-26 September). Effectiveness of the Football Helmet Assessed By Finite Element Modeling and Impact Testing. In *IRCOBI Conference Proceedings, Lisbon, Portugal,* 27–38.

Zhang, L., Yang, K., & Gennarelli, T. A. (2008, 17-19 September). Mathematical modeling of cerebral concussion: Correlations of regional brain strain with clinical symptoms. In *IRCOBI Conference Proceedings, Bern, Switzerland,* 123–132.

Appendix: Mass and Inertia Properties of Human Heads from Published Cadaver Studies.

In this appendix, the physical properties of the human head obtained from published cadaver studies are presented. Table A1 shows length, breadth and circumference measurements of 83 human heads from Hodgson & Thomas (1971, 1973), Chandler et al. (1975) and Ching (2007). Table A2 shows mass and circumference measurements of 87 human heads from Hodgson & Thomas (1971, 1973), Chandler et al. (1975) and Ching (2007). Table A3 shows centre of gravity location in the X-axis (CG_X), centre of gravity location in the Z-axis (CG_Z) with respect to the head anatomical coordinate system and mass measurements of 58 human heads from Walker et al. (1973), Chandler et al. (1975), Beier et al. (1979) and Albery & Whitestone, (2003). Table A4 shows moment of inertia around X-axis (I_{XX}), moment of inertia around Y-axis (I_{YY}), moment of inertia around Z-axis (I_{ZZ}) and the non-zero product of inertia (I_{XZ}) with respect to the centre of gravity and the head anatomical coordinate system and mass measurements of 95 human heads from Hodgson & Thomas (1971), Walker et al. (1973), Chandler et al. (1975), Beier et al. (1979) and Albery & Whitestone (2003). At the end of this appendix, Table A5 includes the results from the linear regression analysis for each of the physical properties of the human head studied. Intercept and slope coefficients were statistically significant unless otherwise indicated.

Table A1. Human head cadaver length, breadth and circumference data taken from Hodgson & Thomas (1971, 1973), Chandler et al. (1975) and Ching (2007).

	Subject ID	Circumference (mm)	Length (mm)	Breadth (mm)
(Hodgson & Thomas, 1971)	1717	584	201	155
	1745	579	198	165
	1701	516	180	150
	1699	572	203	160
	1805	597	203	163
	1801	541	188	160
	1820	546	185	147
	1819	584	201	163
	1821	622	213	175
	1829	584	191	163
	1848	610	198	152
	1862	597	203	165
	1876	533	188	145
	1875	597	198	170
	1859	572	198	152
	1871	622	201	173
	1861	592	180	160
	1843	610	203	168
	1879	610	203	173
	188	554	185	160
	1849	620	203	173
	154	559	188	152
	1873	541	188	152
	1857	597	188	163
	1890	579	180	163
	1905	579	191	155
	1912	572	203	155
	1906	635	203	185
	1910	594	193	152
	1938	554	185	160

	1935	605	201	165
	1940	559	188	165
	1936	579	193	160
	1932	572	193	163
(Hodgson & Thomas, 1973)	2068	546	203	147
	2067	566	193	157
	2108	610	216	165
	2054	584	203	173
	2115	622	191	170
	2095	610	185	165
	2182	577	188	163
	2187	584	198	178
	2066	584	198	168
	1930	566	191	155
	2246	584	224	170
	2155	559	175	155
	2268	572	224	185
	2146	533	193	155
	2248	594	213	180
	2242	584	218	173
	2358	572	193	157
	2365	584	203	160
	2440	564	198	155
	2353	605	206	185
	2483	554	188	155
	2354	579	203	165
	2412	605	203	157
	2425	546	180	155
	2448	538	180	157
	2212	574	193	150
	2418	569	193	165
	2321	566	196	155
	2310	612	208	175
(Chandler et al., 1975)	1	569	200	153
	2	582	207	150
	3	591	209	154
	4	547	192	152
	5	578	201	154
	6	564	234	160
(Ching, 2007)	F02	537	184	143
	F05	533	181	143
	F06	543	150	112
	F07	540	180	150
	F15	540	185	140
	F17	527	174	143
	M09	530	180	142
	M10	603	250	155
	M11	564	187	151
	M12	585	200	157
	M14	557	189	159
	M18	553	186	146
	M19	552	187	153
	M20	608	197	164

N=83. Subject F13 from Ching study was not included because she had a metal plate in her head (Albery & Whitestone, 2003; Ching, 2007).

Table A2. Human head cadaver mass and circumference data taken from Hodgson & Thomas (1971, 1973), Chandler et al. (1975) and Ching (2007).

	Subject ID	Circumference (mm)	Mass (kg)
(Hodgson & Thomas, 1971)	1717	584	4.54
	1745	579	5.22
	1701	516	3.63
	1699	572	4.54
	1805	597	4.54
	1801	541	4.35
	1820	546	3.76
	1819	584	4.54
	1821	622	5.90
	1829	584	4.22
	44	579	4.08
	57	572	4.08
	1848	610	4.35
	1838	533	4.99
	1841	610	6.35
	1862	597	4.81
	1876	533	3.58
	1875	597	4.54
	1859	572	4.17
	1871	622	5.31
	1861	592	4.76
	1843	610	4.85
	1879	610	5.49
	188	554	4.17
	1849	620	5.90
	154	559	4.81
	1873	541	4.54
	1857	597	5.35
	1890	579	4.40
	1905	579	4.17
	1912	572	4.40
	1906	635	6.26
	1910	594	5.26
	1938	554	4.54
	1935	605	6.53
	1940	559	4.85
	1936	579	4.67
	1932	572	4.85
(Hodgson & Thomas, 1973)	2068	546	4.90
	2067	566	4.31
	2108	610	5.03
	2054	584	4.85
	2115	622	6.49
	2095	610	5.26
	2182	577	5.40
	2187	584	5.49
	2066	584	5.40
	1930	566	5.26
	2246	584	5.72
	2155	559	5.35
	2268	572	4.85
	2146	533	4.54
	2248	594	6.49
	2242	584	5.26

	2358	572	3.31
	2365	584	3.95
	2440	564	3.45
	2353	605	4.08
	2483	554	3.49
	2354	579	3.99
	2412	605	4.35
	2425	546	3.18
	2448	538	3.22
	2212	574	3.45
	2418	569	3.72
	2321	566	3.22
	2310	612	4.49
(Chandler et al., 1975)	1	569	4.03
	2	582	4.15
	3	591	4.82
	4	547	3.36
	5	578	4.11
	6	564	3.47
(Ching, 2007)	F02	537	2.98
	F05	533	2.78
	F06	543	3.00
	F07	540	2.75
	F15	540	3.09
	F17	527	2.87
	M09	530	3.04
	M10	603	4.38
	M11	564	3.53
	M12	585	3.96
	M14	557	3.75
	M18	553	3.21
	M19	552	2.92
	M20	608	4.45

N=87. Subject F13 from Ching study was not included because she had a metal plate in her head (Albery & Whitestone, 2003; Ching, 2007).

Table A3. Location of the centre of gravity in the X-axis (CG_X), location of the centre of gravity in the Z-axis (CG_Z) with respect to the head anatomical coordinate system and mass from Walker et al. (1973), Chandler et al. (1975), Beier et al. (1979) and Albery & Whitestone, (2003).

	Subject ID	Mass (kg)	CG_X (mm)	CG_Z (mm)
(Walker et al., 1973)	2986	4.70	13	15
	3121	4.10	17	18
	3079	4.18	3	20
	3072	4.28	6	25
	3055	3.93	0	20
	3107	5.76	10	17
	3106	5.13	15	16
	3061	5.07	6	11
	3129	4.38	11	25
	3111	4.29	7	28
	3114	4.27	9	29
	3117	4.14	8	23
	3026	4.19	1	26
	3152	4.46	9	23
	3125	4.15	14	17
	3356	4.53	-4	26

	3343	4.38	26	25
(Chandler et al., 1975)	1	4.03	-4	16
	2	4.15	4	24
	3	4.82	9	21
	4	3.36	0	28
	5	4.11	-4	27
	6	3.47	2	23
(Beier et al., 1979)	1023/75	4.21	7	33
	1059/75	4.12	14	22
	50/76	3.95	11	33
	60/76	4.03	9	34
	107/76	4.03	9	29
	233/76	4.19	10	31
	314/76	4.54	3	30
	455/76	4.65	7	42
	665/76	4.32	7	42
	712/76	3.71	7	29
	753/76	4.35	6	27
	833/76	4.34	4	27
	245/77	4.63	11	41
	392/77	4.63	9	33
	406/77	4.25	7	30
	448/77	5.26	11	29
	564/77	4.27	6	32
	662/77	3.68	10	27
	667/77	3.99	11	25
	791/77	4.14	8	27
	820/77	5.07	8	37
(Albery & Whitestone, 2003)	F02	2.98	-2	26
	F05	2.78	-3	29
	F06	3.00	4	22
	F07	2.75	-5	32
	F15	3.09	-1	32
	F17	2.87	8	28
	M09	3.04	-1	23
	M10	4.38	6	21
	M11	3.53	-1	28
	M12	3.96	1	37
	M14	3.75	-2	23
	M18	3.21	3	16
	M19	2.92	2	38
	M20	4.45	3	27

N=58. Subject F13 from Albery and Whitestone study was not included because she had a metal plate in her head (Albery & Whitestone, 2003).

Table A4. Moment of inertia around X-axis (IXX), moment of inertia around Y-axis (IYY), moment of inertia around Z-axis (IZZ) and the non-zero product of inertia (IXZ) with respect to the centre of gravity and the head anatomical coordinate system and mass measurements from Hodgson & Thomas (1971), Walker et al. (1973), Chandler et al. (1975), Beier et al. (1979) and Albery & Whitestone (2003).

	Subject ID	Mass (kg)	I_{XX} (kg·cm^2)	I_{YY} (kg·cm^2)	I_{ZZ} (kg·cm^2)	I_{XZ} (kg·cm^2)
(Hodgson & Thomas, 1971)	1717	4.54	-	226	-	-
	1745	5.22	-	260	-	-
	1701	3.63	-	136	-	-
	1699	4.54	-	226	-	-
	1805	4.54	-	237	-	-
	1801	4.35	215	-	-	-

	1820	3.76	192	-	-	-
	1819	4.54	226	-	-	-
	1821	5.90	395	-	-	-
	1829	4.22	249	-	-	-
	44	4.08	237	-	-	-
	57	4.08	226	-	-	-
	1848	4.35	-	237	-	-
	1838	4.99	-	215	-	-
	1841	6.35	-	350	-	-
	1862	4.81	-	260	-	-
	1876	3.58	-	158	-	-
	1875	4.54	-	237	-	-
	1859	4.17	-	203	-	-
	1871	5.31	-	305	-	-
	1861	4.76	-	249	-	-
	1843	4.85	-	271	-	-
	1879	5.49	-	305	-	-
	188	4.17	-	192	-	-
	1849	5.90	-	339	-	-
	154	4.81	-	226	-	-
	1873	4.54	-	203	-	-
	1857	5.35	-	282	-	-
	1890	4.40	-	226	-	-
	1905	4.17	-	215	-	-
	1912	4.40	-	215	-	-
	1906	6.26	-	373	-	-
	1910	5.26	-	271	-	-
	1938	4.54	-	203	-	-
	1935	6.53	-	362	-	-
	1940	4.85	-	226	-	-
	1936	4.67	-	237	-	-
	1932	4.85	-	237	-	-
(Walker et al., 1973)	2986	4.70	-	254	-	-
	3121	4.10	-	236	-	-
	3079	4.18	-	211	-	-
	3072	4.28	-	217	-	-
	3055	3.93	-	157	-	-
	3107	5.76	-	323	-	-
	3106	5.13	-	293	-	-
	3061	5.07	-	238	-	-
	3129	4.38	-	234	-	-
	3111	4.29	-	228	-	-
	3114	4.27	-	216	-	-
	3117	4.14	-	198	-	-
	3026	4.19	-	218	-	-
	3152	4.46	-	239	-	-
	3125	4.15	-	215	-	-
	3356	4.53	-	258	-	-
	3343	4.38	-	230	-	-
(Chandler et al., 1975)	1	4.03	160	197	175	22.2
	2	4.15	171	231	178	33.2
	3	4.82	207	272	231	34.7
	4	3.36	119	143	125	27.1
	5	4.11	178	226	176	24.3
	6	3.47	142	141	141	25.6
(Beier et al., 1979)	1023/75	4.21	195	234	152	21.1
	1059/75	4.12	182	211	158	34.1

	50/76	3.95	166	205	147	35.9
	60/76	4.03	175	200	144	24.8
	107/76	4.03	170	197	161	27.3
	233/76	4.19	183	213	168	27.9
	314/76	4.54	207	238	176	31.8
	455/76	4.65	223	260	188	18.9
	665/76	4.32	182	222	174	26.1
	712/76	3.71	143	159	131	19.7
	753/76	4.35	202	219	172	30.0
	833/76	4.34	189	221	168	33.4
	245/77	4.63	234	243	182	29.0
	392/77	4.63	213	257	180	36.6
	406/77	4.25	178	210	177	35.3
	448/77	5.26	250	295	222	38.9
	662/77	3.68	145	163	124	21.8
	667/77	3.99	166	192	130	20.0
	791/77	4.14	170	206	163	34.6
	820/77	5.07	251	284	208	33.9
(Albery & Whitestone, 2003)	F02	2.98	84	128	125	-
	F05	2.78	75	112	108	-
	F06	3.00	84	123	123	-
	F07	2.75	77	109	112	-
	F15	3.09	87	135	123	-
	F17	2.87	120	121	81	-
	M09	3.04	80	129	128	-
	M10	4.38	145	223	234	-
	M11	3.53	162	164	110	-
	M12	3.96	125	193	192	-
	M14	3.75	118	175	177	-
	M18	3.21	143	149	100	-
	M19	2.92	89	130	131	-
	M20	4.45	151	226	234	-

N=95. Subject F13 from Albery and Whitestone study was not included because she had a metal plate in her head (Albery & Whitestone, 2003). Subject 564/77 from Beier et al. study was not included because it was detected that the tensor of the principal axes of the moment of inertia has an error (Beier et al., 1979).

Table A5. Coefficients for the simple linear regression analysis between two physical head properties using different sets of cadaver human data.

Dependent variables	Independent variables	Intercept (Std. Error)	Slope (Std. Error)	R^2	*p-value*
Length	Circumference	**3.58E+01 (2.80E+01)**	**2.78E-01 (4.87E-02)**	**0.288**	**1.74E-07**
Breadth	Circumference	**-6.39E+00 (2.03E+01)***	**2.88E-01 (3.52E-02)**	**0.452**	**3.39E-12**
Mass	Circumference	**-9.17E+00 (1.60E+00)**	**2.36E-02 (2.79E-03)**	**0.458**	**6.12E-13**
CG_X	Mass	**-1.30E+01 (4.40E+00)**	**4.63E+00 (1.06E+00)**	**0.252**	**5.87E-05**
CG_Z	Mass	3.12E+01 (5.76E+00)	-1.13E+00 (1.39E+00)*	0.012	4.22E-01
I_{XX}	Mass	**-1.45E+02 (2.39E+01)**	**7.94E+01 (5.90E+00)**	**0.801**	**2.24E-17**
I_{YY}	Mass	**-8.29E+01 (9.40E+00)**	**6.97E+01 (2.13E+00)**	**0.926**	**2.39E-50**
I_{ZZ}	Mass	**-3.45E+01 (1.93E+01)***	**4.92E+01 (4.87E+00)**	**0.728**	**2.63E-12**
I_{XZ}	Mass	**5.48E-01 (1.01E+01)***	**6.67E+00 (2.39E+00)**	**0.246**	**1.00E-02**

Regression lines that are a good fit for the data are shown in bold font.
* Indicates non-significant result (p-value > 0.05).

Annex A: Paper A

Juste-Lorente, O.; Maza, M.; Piccand, M.; López-Valdés, F.J. (2021). The Influence of Headform/Helmet Friction on Head Impact Biomechanics in Oblique Impacts at Different Tangential Velocities. Applied Sciences, 11, 11318. https://doi.org/10.3390/app112311318

The Influence of Headform/Helmet Friction on Head Impact Biomechanics in Oblique Impacts at Different Tangential Velocities

Óscar Juste-Lorente [1],*, Mario Maza [1], Mathieu Piccand [2] and Francisco J. López-Valdés [3]

[1] Impact Laboratory—Aragon Institute for Engineering Research (I3A), University of Zaragoza, 44600 Alcañiz, Spain; mmaza@unizar.es

[2] FIM (Fédération Internationale de Motocyclisme), Route de Suisse 11, 1295 Mies, Switzerland; mathieu.piccand@fim.ch

[3] Instituto de Investigación Tecnológica (IIT), ICAI Engineering School, Comillas Pontifical University, Alberto Aguilera, 23, 28015 Madrid, Spain; fjlvaldes@comillas.edu

* Correspondence: ojuste@unizar.es

Abstract: Oblique impacts of the helmet against the ground are the most frequent scenarios in real-world motorcycle crashes. The combination of two factors that largely affect the results of oblique impact tests are discussed in this work. This study aims to quantify the effect of the friction at the interface between the headform and the interior of a motorcycle helmet at different magnitudes of tangential velocity. The helmeted headform, with low friction and high friction surface of the headform, was dropped against three oblique anvils at different impact velocities resulting in three different magnitudes of the tangential velocity (3.27 m/s, 5.66 m/s, 8.08 m/s) with the same normal component of the impact velocity (5.66 m/s). Three impact directions (front, left-side and right-side) and three repetitions per impact condition were tested resulting in 54 impacts. Tangential velocity variation showed little effect on the linear acceleration results. On the contrary, the rotational results showed that the effect of the headform's surface depends on the magnitude of the tangential velocity and on the impact direction. These results indicate that a combination of low friction with low tangential velocities may result into underprediction of the rotational headform variables that would not be representative of real-world conditions.

Keywords: motorcycle helmet; oblique impact; tangential velocity; friction

1. Introduction

According to the World Health Organization, three hundred and seventy eight thousand people died in 2016 as a direct result of a motorcycle collision, amounting to 28% of the world's road traffic related deaths [1]. Despite the proven effectiveness of helmets in the protection of the head [2,3], head injuries are the leading cause of death and long-term disability after a motorcycle crash [4].

Traditionally, motor-vehicle related head injuries have been grouped according to the injury mechanism [5]. Since Holbourn hypothesized that rotational motion of the brain could explain some head injuries unlikely to be caused by translational motion [6], a substantial amount of research has supported the relationship between head rotation and brain injuries [7–9]. The reaction force that the helmeted head experiences in the contact against a rigid surface can be decomposed into two components: a normal component perpendicular to the impact surface and a tangential component parallel to the impact surface. The magnitude of the reaction force normal component is related mainly to the height of the rider's fall on the ground while the reaction force tangential component is associated to the motorcyclist's travelling speed [10]. The magnitude of this tangential component is directly related to the rotation experienced by the rider's head.

Oblique impacts between the helmet and the ground are the most frequent collision scenarios in real world [11,12]. Consequently, different laboratory testing protocols measure the helmet energy absorption capabilities and the resulting kinematics of a headform that represents the human head in oblique impacts [13–16].

Mills et al. identified the impact velocity component normal to the road, the friction coefficient between the shell and road, and the impact direction as the factors that control the peak headform rotational acceleration in oblique impacts [17–19]. Meng et al. showed that the impact velocity component normal to the road needs to be of a certain magnitude to induce the headform angular motion [20]. A follow-up study revealed that, from lower to higher tangential impact velocities, the motion of the helmet transitions from rolling to sliding, which affected head kinematics and its injury outcome for different friction values between the helmet and the ground [21]. However, the effective friction coefficient of the helmet as a whole is a function of the friction coefficient at the road/shell and at the head/liner interfaces [22]. Therefore, the tangential component of the contact force causes not only the rolling/sliding motion of the helmet on the ground but, due to similar underlying mechanics, it can also cause a relative motion between the head and the interior surface of the helmet [23].

To our knowledge, neither experimental nor computational studies have quantified the interaction of friction and tangential velocity in the resulting kinematics of the headform. Thus, the objective of this study is to quantify the influence of the friction between the interior surface of the helmet and the headform in the resulting kinematics of the headform at different magnitudes of the tangential impact velocity.

2. Methods

2.1. Experimental Design and Test Matrix

The experimental method was designed to identify the influence of the two proposed factors (friction and tangential velocity) and their interaction in four kinematically-based head injury predictors (outcome): the Peak of the resultant Linear Acceleration (PLA), the Head Injury Criterion (HIC) [24], the Brain Injury Criterion (BrIC) [25] and the Peak of the resultant Angular Acceleration (PAA).

A factorial analysis with two factors was independently applied to three different impact directions of the helmet and the anvil (front, right side and left side) in order to induce a rotation in each axis of the helmeted headform as shown in Figure 1. Only two friction conditions (low friction: bare headform; high friction: coated headform) were used at the interface between the headform and the interior of the helmet because friction showed a linear response on head angular kinematics [17]. However, three impact speeds (6.5 m/s, 8 m/s and 9.9 m/s) were selected because previous studies showed that varying the tangential velocity had a non-linear effect on head rotational kinematics [21]. These impact speeds were used with three different anvil angles (65°, 45° and 35°, respectively) so that while the tangential component of the impact speed changed, its normal component remained constant (see Figure A2). The values chosen for the friction and the impact speeds were based on the parameters prescribed in existing testing standard procedures [26,27].
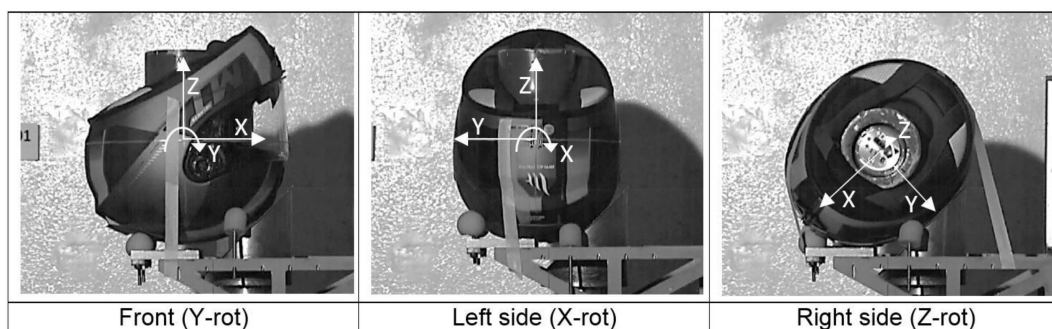

| Front (Y-rot) | Left side (X-rot) | Right side (Z-rot) |

Figure 1. Oblique impact point layouts and coordinate system.

Thus, a 2 × 3 factorial design was chosen for each impact direction in which three replicas were carried out per each combination of levels of the selected factors, resulting in a total of 54 drop tests, as shown in Table 1.

Table 1. Test matrix. For N from 1 to 3, indicating repeated tests for a particular condition.

Resultant Impact Velocity	Anvil	Headform	Impact Point	Test ID
6.5 m/s	60°	Bare headform	Front (Y-rot)	DT0322-0N-01
			Left side (X-rot)	DT0322-0N-02
			Right side (Z-rot)	DT0322-0N-04
		Covered headform	Front (Y-rot)	DT0321-0N-01
			Left side (X-rot)	DT0321-0N-02
			Right side (Z-rot)	DT0321-0N-04
8.0 m/s	45°	Bare headform	Front (Y-rot)	DT0320-0N-01
			Left side (X-rot)	DT0320-0N-02
			Right side (Z-rot)	DT0320-0N-04
		Covered headform	Front (Y-rot)	DT0319-0N-01
			Left side (X-rot)	DT0319-0N-02
			Right side (Z-rot)	DT0319-0N-04
9.9 m/s	35°	Bare headform	Front (Y-rot)	DT0318-0N-01
			Left side (X-rot)	DT0318-0N-02
			Right side (Z-rot)	DT0318-0N-04
		Covered headform	Front (Y-rot)	DT0317-0N-01
			Left side (X-rot)	DT0317-0N-02
			Right side (Z-rot)	DT0317-0N-04

2.2. Testing Procedure

The tests were performed at the Impact Laboratory of the University of Zaragoza. A free fall guided impact machine (Model: Quebrantahuesos 6.0, +D, Pozuelo de Alarcón, Spain) was used for the drop tests. In the drop tests, the helmeted headform is placed on a carriage and restrained by pre-cut paper tape to prevent helmet motion during the fall. After releasing the carriage assembly from a specific height, the helmeted headform impacts the top surface of an anvil and the carriage assembly continues to fall onto a cushioned bed plate without interfering with the helmeted headform kinematics.

The helmet used was a full-face motorcycle helmet (model: FF104 RAPIDE, MT, Cartagena, Spain) (Figure A1). In total, 18 full face helmets of the M (57–58) size were used (using three impact locations per helmet, although each impact location on each helmet was tested just one time). The outer shell of the tested helmet was made of Fibre Reinforce Composite (FRC). The liner of the helmet was made of expanded polystyrene (EPS). The retention system of the helmet was based on a double D-ring buckle. The helmet complied with the United Nations Economic Commission for Europe (UNECE) regulation and Department of Transportation (DOT) standard.

The baseline case was a drop test performed at an impact velocity of 8.0 m/s onto a 45° oblique anvil, which originated two impact velocity components (normal and tangential) with the same magnitude of 5.66 m/s. The tangential velocity component (V_T) of this test set-up was altered approximately ±40%, while keeping constant the normal velocity component (V_N). Therefore, six helmets were drop tested at 6.5 m/s onto a 60° oblique anvil, obtaining a V_N of 5.66 m/s and a V_T of 3.27 m/s. Finally, six more helmets were

drop tested at 9.9 m/s onto a 35° oblique anvil to obtain the same V_N and a V_T of 8.08 m/s. These two test conditions are referred as -40% V_T and $+40\%$ V_T respectively (Figure A2).

The oblique anvils were made from a solid steel cylinder with the diameter of 130 mm. The impact surface of the anvil was covered with a sheet of grade 80 close-coat aluminium oxide abrasive paper, that was replaced after significant damage or after three impacts. There was not variation of the friction between the anvil surface and the exterior helmet surface. All the helmets were tested with a 575-size magnesium alloy full headform (Model: 100_04_FMH, Cadex Inc., Saint-Jean-sur-Richelieu, QC, Canada).

To vary the value of the friction between the interior of the helmet and the surface of the headform, half of the helmets per test condition were tested with the original metallic surface of the headform (bare headform) and half of them were tested with the headform covered with a uniform thin layer of high-performance silicone rubber (Model: Dragon Skin 10, Smooth-On, Inc., Macungie, PA, USA). A total of 40 g of silicone rubber was uniformly spread in order to meet the thickness requirement of the FRHPhe-01 standard [27]. A spring balance method was used to provide an indication of the friction associated to the coating treatment. The average coefficient of friction (COF) measured between a woven cotton fabric and the bare headform and the covered headform were 0.20 and 0.78, respectively.

The headform was positioned inside the helmets using a helmet positioning index (HPI) of 40 mm. The retention system was adjusted under the chin of the headform and tightened to a tension of 75 N [27]. Before each impact, the helmet was re-positioned and the retention system re-tensioned.

Three new helmet samples were used per each tangential velocity and headform surface condition. Each helmet was tested on front (Y-rot), left side (X-rot) and right side (Z-rot) (see Figure 1 for the position and orientation of the helmet coordinate system). The first impact was a frontal impact, leading to rotation in the sagittal plane around the Y-axis. The second impact was a parietal impact on the left side, leading to rotation in the frontal plane around the X-axis. In these two impacts, the central vertical axis (Z-axis) of the headform was aligned to the vertical. The third impact was a temporal impact on the right side, leading to rotation in the transverse plane around the Z-axis. For this oblique impact, the sagittal plane of the headform was positioned parallel to the impact surface of the anvil and the transverse plane of the headform was coincident with the vertical plane of symmetry of the anvil. Figure 1 shows the three oblique impact directions.

A wireless system (Model: iCONO, +D, Pozuelo de Alarcón, Spain) was used to measure linear acceleration and angular velocity at the centre of gravity of the headform. The wireless system incorporates three linear accelerometers (Model: 64C-2000, MEAS, Nanshan District Shenzhen, China), three angular rate sensors (Model: ARS PRO-8k, DTS, Seal Beach, CA, USA) and an acquisition system (Model: SLICE NANO, DTS, Seal Beach, CA, USA). Data were recorded at 10 kHz. Head linear acceleration signals were filtered using a low-pass filter CFC-1000 and angular velocities signals were filtered using a CFC-180. High-speed video was captured at 1000 Hz (Model: Eosens mini, Mikrotron, Unterschleissheim, Germany). The end of the impact was estimated when the measured acceleration was lower than 5 g, which correlated well with the instant in which the helmeted headform separated from the anvil. Data post-processing was performed using an in-house developed and validated script of Matlab (Matlab R2013b, MathWorks, Natick, MA, USA).

2.3. Data Analysis

Data were sorted first by impact direction (front, left side & right side), and then by the two factors: tangential velocity (-40% V_T, base case & $+40\%$ V_T) and headform friction condition (bare headform & covered headform). Thus, for each impact direction, a two-way analysis of variance (ANOVA) was used to estimate how each injury predictor changed according to the levels of tangential velocity and headform friction surface. The two-way ANOVA also checks for interactions between the two factors—for example, if the effect of the covered headform depends on the levels of the tangential velocities. When there

were not significant differences in the interaction, the one-way ANOVA and the Tuckey's HSD post-hoc test were performed to study each factor individually. In case of a significant interaction, the two-way ANOVA is transformed into a one-way ANOVA and the Tuckey's HSD post-hoc test was performed to study each possible combination between the two factors. Significance level used for all statistical tests was $\alpha = 0.05$. To increase the statistical power of the post-hoc tests that resulted in significant differences, only those comparisons with the largest effect sizes (as measured by Cohen's d) were considered in this study. Statistical analysis was performed using an Excel add-in (Real Statistics Resource Pack).

3. Results

3.1. Front Impact Kinematics

Figure 2 shows high-speed video captures at t = 14 ms, ilustrating the change in the angle between a reference line on the helmet shell (initially parallel to the horizontal direction) and a reference line on the neck of the headform, due to the relative motion between the helmet and the bare headform for each V_T. However, in the case of the high friction of the coated headform, the angle remained almost constant regardless of the V_T value.

Figure 2. Comparison of the relative motion of the bare and covered headform inside the helmet at 14 ms of the front impact for each tangential velocity.

The comparison of the time history plots of the resultant linear acceleration is shown in Figure 3. The -40% V_T case (light grey traces) resulted in higher peak resultant linear acceleration and slightly shorter impact durations than the other two tangential velocities. This result might be influenced by the different location of the impact point between the helmet and the anvil, which was dependant on the tangential velocity component, as shown in Figure A3: reducing the magnitude of V_T shifted the impact point in the negative X direction. Within each value of V_T, the peak resultant acceleration of the high friction cases was consistently higher than the ones in the bare headform cases.

Figures 4 and 5 show the time history plot of the resultant angular velocity and the resultant angular acceleration. As expected, the influence of the magnitude of V_T in the angular velocity can be clearly identified in Figure 4. Regardless of the friction, the higher the magnitude of V_T, the higher the peak value of the angular velocity. Within each value of V_T, the coated headform (higher friction) resulted in higher magnitudes of angular velocity and a distinct maximum of the data trace, while the tests with the bare headform resulted in a monotonously growing curve.
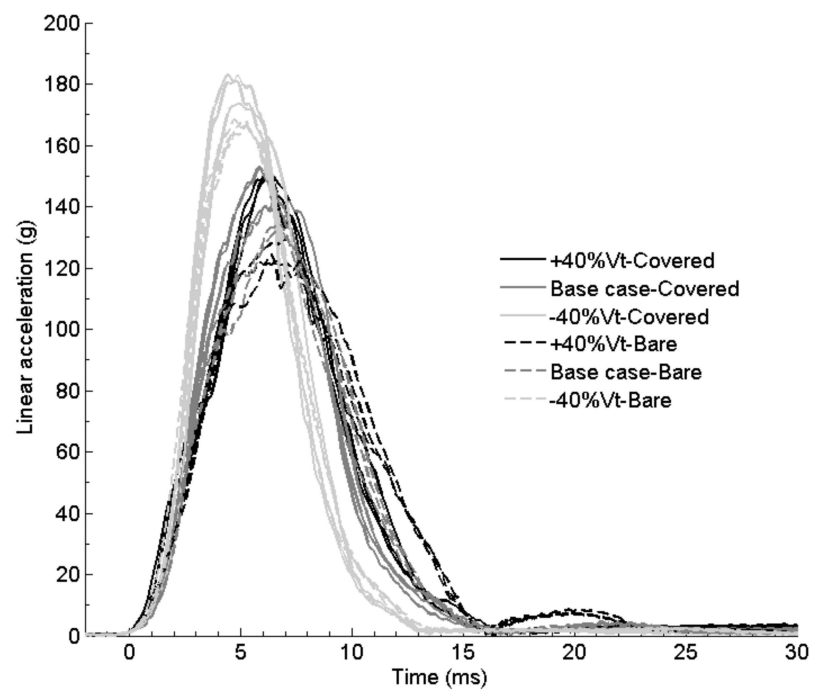
Figure 3. Time-history plot of the resultant linear acceleration for the front impacts. Solid lines correspond to covered headform and dashed lines correspond to bare headform test.
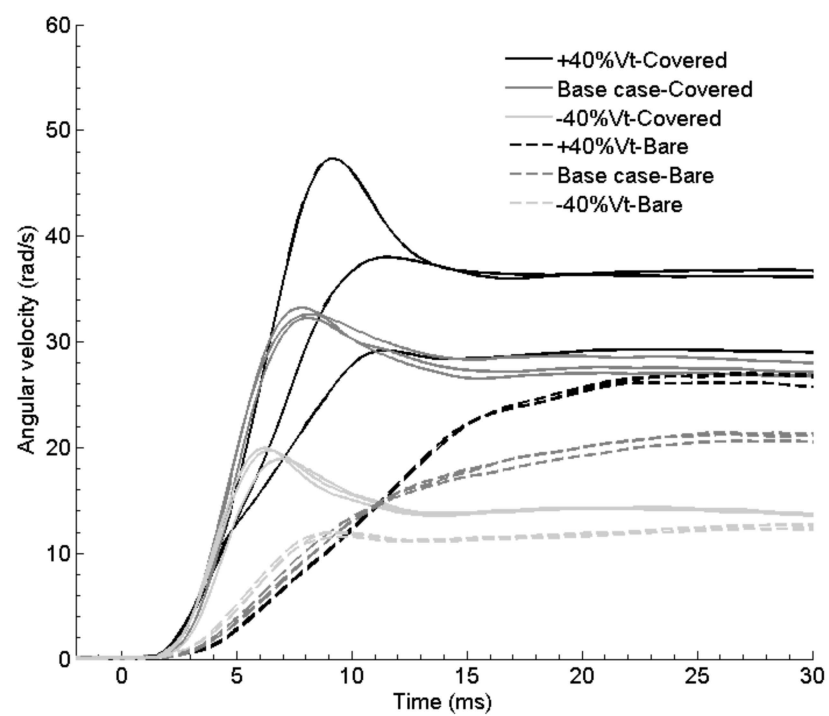
Figure 4. Resultant angular velocity for the front impacts. Solid lines correspond to covered headform and dashed lines correspond to bare headform test.

Figure 5. Resultant angular acceleration for the front impacts. Solid lines correspond to covered headform and dashed lines correspond to bare headform test.

The largest peak angular acceleration was obtained for one of the tests with the +40% V_T, while the other two repeats of the same condition resulted in two different responses and were comparable in peak magnitude to the -40% V_T cases (Figure 5). This lack of repeatability was attributed to the detachment of the helmet front vent in these two latter tests of the high friction tests. Note that these tests were not further included in the statistical analyses of the study. In the comparison between the baseline and the -40% V_T case, where there were not repeatability issues, the decrease in V_T is associated to a decrease in peak acceleration and shorter duration of the acceleration pulse. However, the peak angular acceleration did not show important differences between the different magnitudes of V_T while the duration of the acceleration pulse increased as the V_T increased in the low friction tests. Regardless the value of V_T, coating the headform with the silicone resulted in higher angular acceleration levels and shorter durations of the pulse, indicating a better coupling between the headform and the helmet.

3.2. Left Side Impact Kinematics

Figure 6 shows the high-speed video frames of the left-side impacts at t = 14 ms. Similarly to the previous configuration, the angle between a reference line on the helmet and the vertical central axis of the headform illustrated the relative motion between the helmet and the headform for each tangential velocity, that increased as the tangential velocity increased. In the +40% V_T case, when there was no additional room for the bare headform to move within the helmet, the shell of the helmet even deformed elastically. In the covered headform tests, the relative motion of the headform was reduced substantially.

No important differences were observed in the time history plots of the resultant linear acceleration (Figure 7) in left-side impacts: slightly lower peaks were observed in the lower friction tests, but the differences were not relevant.
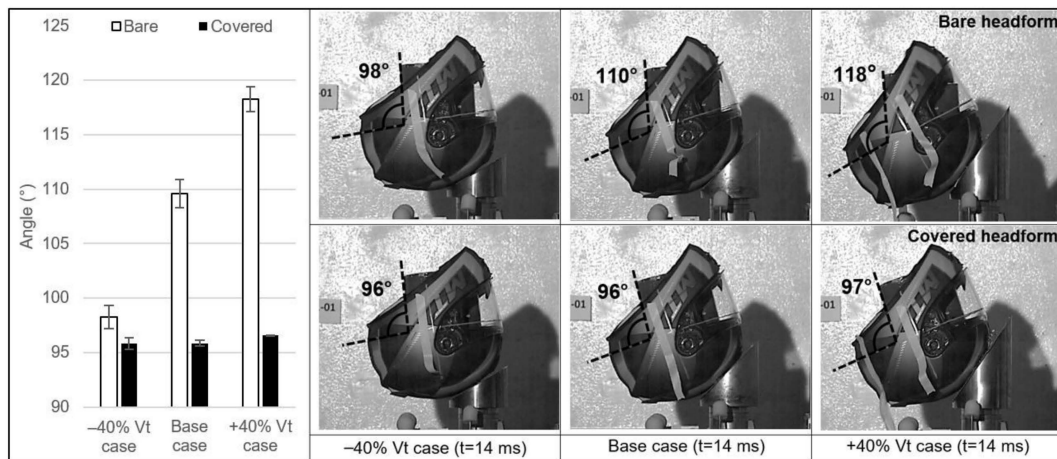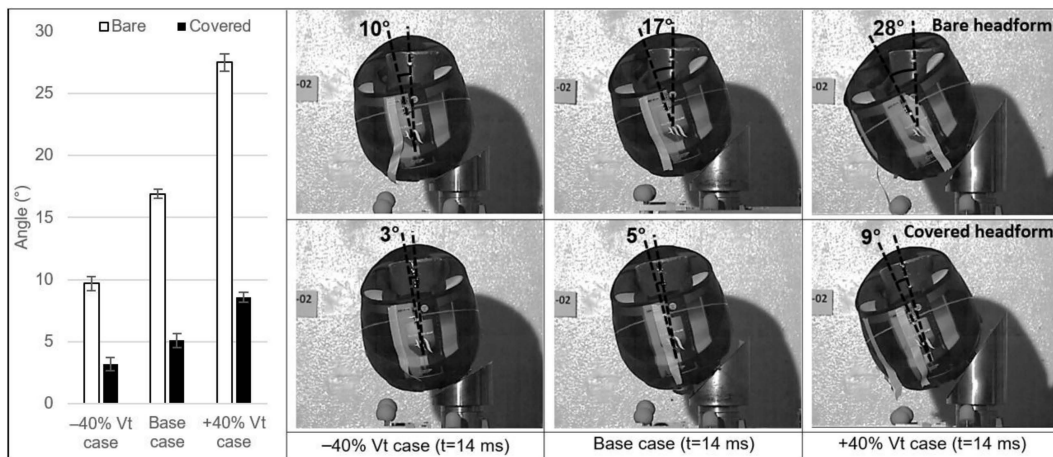
Figure 6. Comparison of the relative motion of the bare and covered headform inside the helmet at 14 ms of the left-side impact for each tangential velocity.
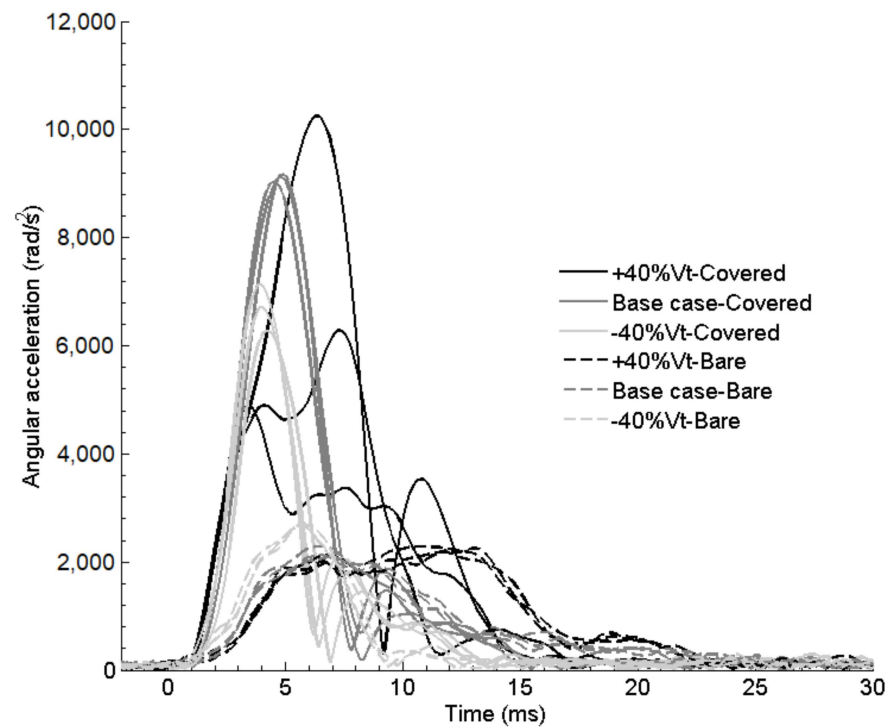

Figure 7. Resultant linear acceleration for the left side impacts. Solid lines correspond to covered headform and dashed lines correspond to bare headform test.

It is in the rotational behaviour of the headform where the differences began to arise. Figure 8 shows that the slopes of the traces corresponding to high friction are more similar than the slopes of the curves for the low friction at different magnitudes of V_T. As there was no relative motion between the headform and the helmet in the covered headform tests, the unique factor that influenced these slopes was the different magnitudes of V_T. On the contrary, in the bare headform tests, in which the relative motion increased as the V_T increased, there was a higher increase of the slopes of the curves as the magnitude of the tangential velocity increased resulting in that the +40% V_T slope was similar to the slopes of the high friction tests. This similitude at the highest V_T can be explained as the relative motion between the headform and the helmet is limited by the interaction of the geometry of the two solids. Higher values of V_T made this interaction to occur, and the headform and the helmet moved without relative motion increasing suddenly the slope and the magnitude of the angular velocity. Figure 9 shows completely different kinematics depending on the friction between the helmet and the headform: while the higher friction tests showed an initial global maximum and then a second local maximum, in the case of

the lower friction tests, the first maximum was local with the global maximum occurring about 8–10 ms later. The duration of the acceleration curve was longer also in the case of the lower friction tests. As for the influence of the magnitude of V_T, and independently of the value of the friction, higher values of V_T resulted in higher angular acceleration peaks.

Figure 8. Resultant angular velocity for the left side impacts. Solid lines correspond to covered headform and dashed lines correspond to bare headform test.

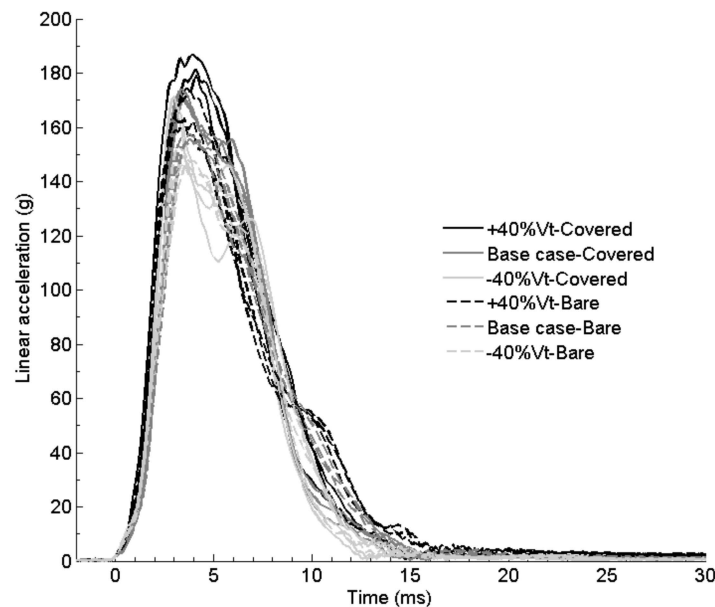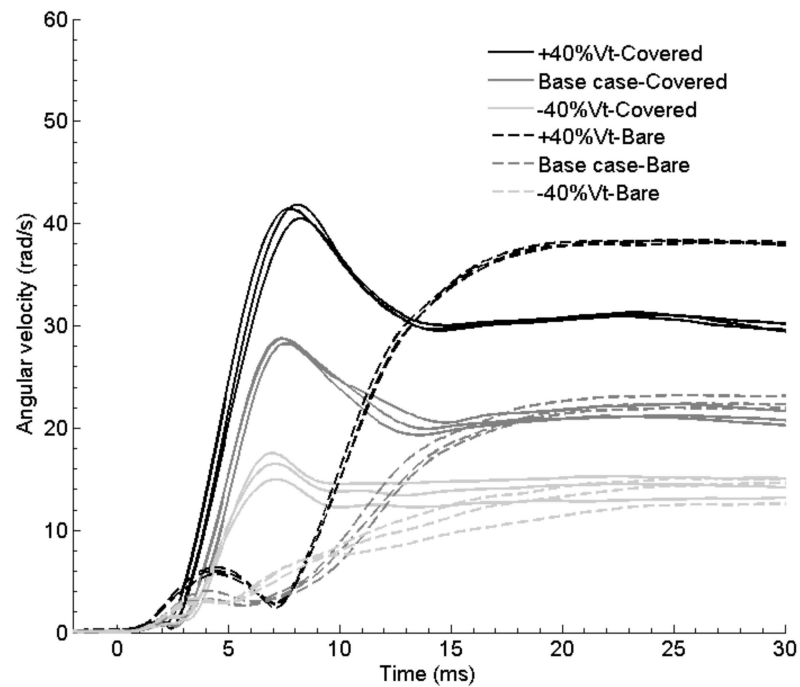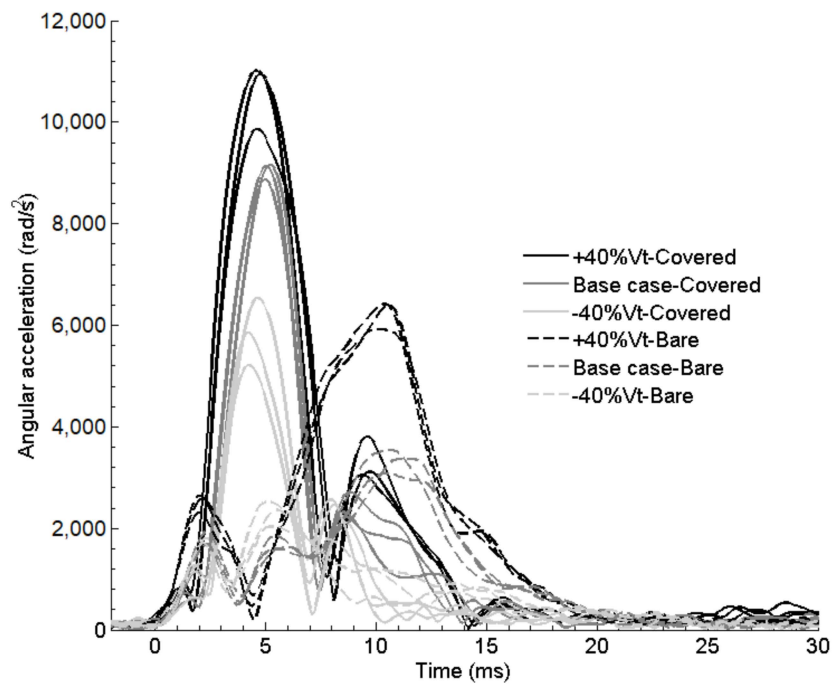**Figure 9.** Resultant angular acceleration for the left side impacts. Solid lines correspond to covered headform and dashed lines correspond to bare headform test.

3.3. Right Side Impact Kinematics

Attending to the images from the high-speed video (Figure 10), it can be seen two different relative motions (indicated by the two dotted white lines in the Figure). The first one is a relative rotation around the Z-axis because of the tangential input applied to the helmet, which was mainly observed with the bare headform and increased as the V_T increased (illustrated by the angular misalignment of the two dotted white lines). The second one is a relative rotation around the X-axis because of the torque created by the distance from the impact point and the centre of gravity of the helmeted headform. It is observed with both headform friction conditions and remained almost constant for the different magnitudes of the V_T (illustrated by the parallel misalignment between the two dotted white lines).
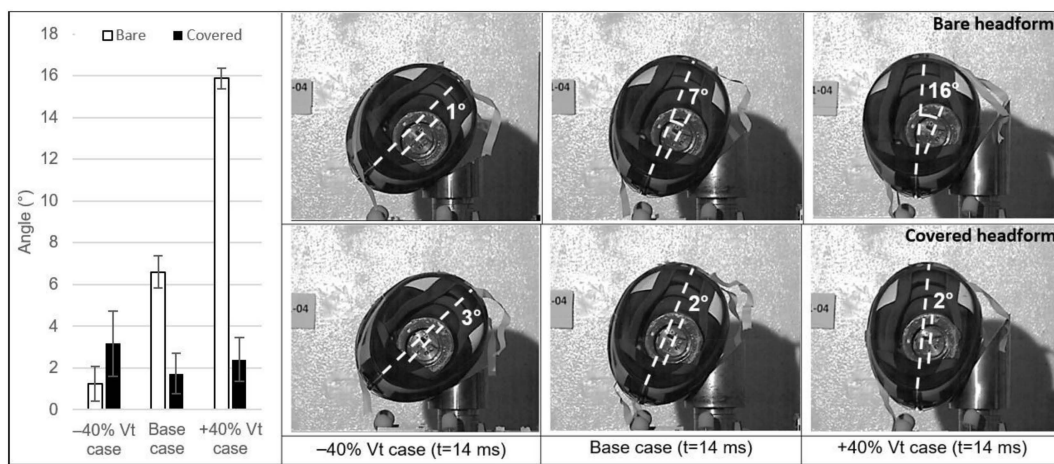
Figure 10. Comparison of the relative motion of the bare and covered headform inside the helmet at 14 ms of the right-side impact. Dashed lines indicate the headform position with respect to the helmet. The angle corresponds to the relative rotation around the Z-axis.

Similarly to the left-side impacts, the time history plot of the resultant linear acceleration did not show differences associated to either the magnitude of V_T or the friction condition (Figure 11).

Again, it is the rotational magnitudes the ones that were influenced by the change in these two parameters. The peak of the angular velocity was higher for higher values of V_T, independently of the friction condition (Figure 12). Increasing the friction between the helmet and headform resulted in a more identifiable angular velocity maximum, while the response of the bare headform produced slower increasing curve of the angular velocity, especially in the larger V_T cases. In the case of the angular acceleration, Figure 13 shows that higher values of V_T resulted in higher peaks of angular acceleration only when the headform was coated (high friction). When the friction was low (bare headform), no important differences were identified between the different values of V_T.

3.4. Data Statistical Analysis

The effect of the two factors and their interaction were analysed using a two-way ANOVA method for each injury predictor and each impact direction.

In addition, the post-hoc tests after the ANOVA allowed to quantify the effect of the headform surface treatment (bare vs. coated) for each level of the tangential velocity and the effect of the tangential velocity with respect to the base case level.

Regarding the peak of the resultant linear acceleration (PLA), there were significant differences in the effect of the coating factor for the front and left side impacts. The tangential velocity factor was significantly different for the three impact directions and the interaction term was not statistically significant at all (Table 2). Descriptive statistics of the test results and statistical results from the post-hoc tests for the PLA are presented in Table 3. Eight of the

eighteen PLA post-hoc comparisons resulted in significant differences (portrayed as shaded cells in Table 3). However, attending to the effect size only two comparisons (both in frontal impacts) were considered relevant: the increased PLA between the -40% V_T and baseline for the bare headform (167 ± 1 g vs. 135 ± 3 g) and the increased PLA between the -40% V_T and baseline for the covered headform (180 ± 5 g vs. 149 ± 6 g).
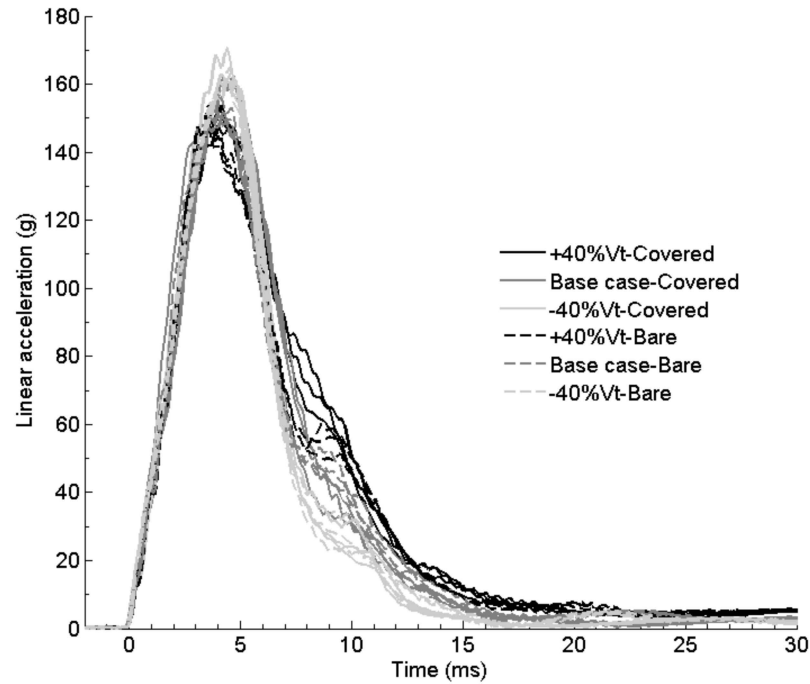
Figure 11. Resultant linear acceleration for the right side impacts. Solid lines correspond to covered headform and dashed lines correspond to bare headform test.
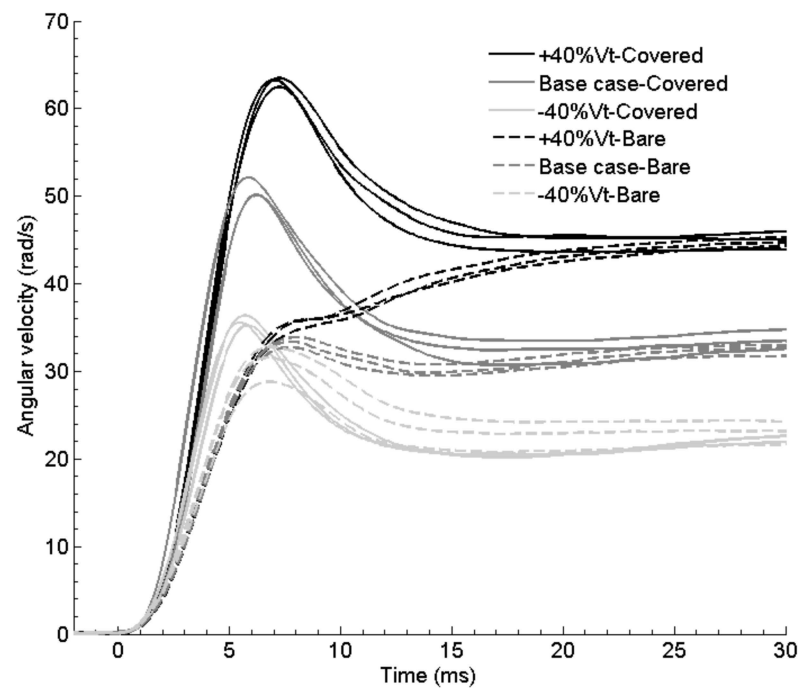
Figure 12. Resultant angular velocity for the right side impacts. Solid lines correspond to covered headform and dashed lines correspond to bare headform test.
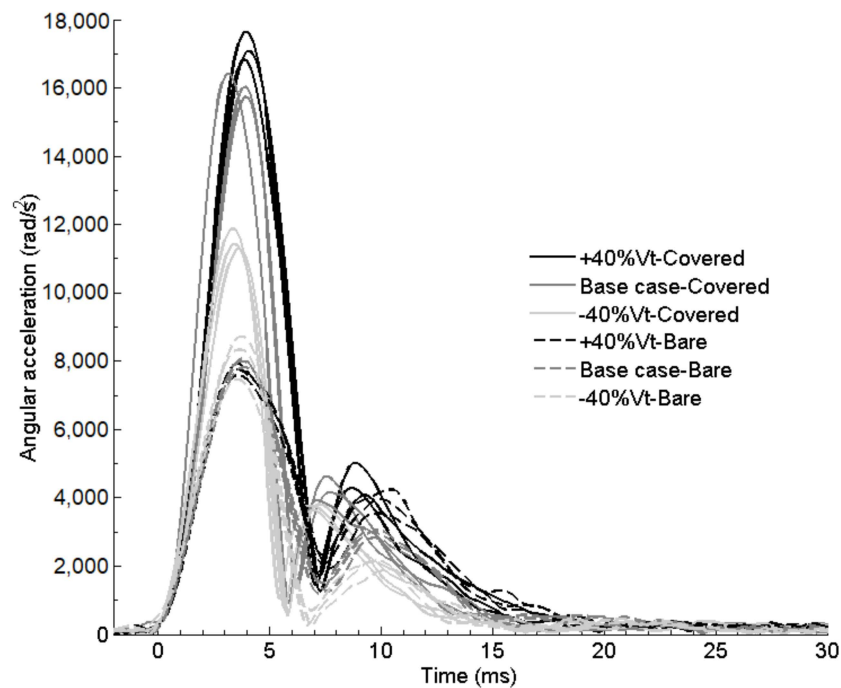
Figure 13. Resultant angular acceleration for the right side impacts. Solid lines correspond to covered headform and dashed lines correspond to bare headform test.

Table 2. Two-way ANOVA results (*p*-values) for the PLA. *p*-values < 0.05 portrayed as shaded cells.

	Front (Y-Rot)	**Left Side (X-Rot)**	**Right Side (Z-Rot)**
Coating	0.0005	0.00016	0.11161
Tangential velocity	1.37×10^{-6}	0.00095	0.00031
Interaction	0.72203	0.99408	0.73341

Table 3. Averages, standard deviation (SD), coefficient of variation (CV) and post-hoc results for PLA. *p*-values < 0.05 portrayed as shaded cells.

	PLA (g)		**Front (Y-Rot)**			**Left Side (X-Rot)**			**Right Side (Z-Rot)**		
			-40% V_T	**Base Case**	$+40\%$ V_T	-40% V_T	**Base Case**	$+40\%$ V_T	-40% V_T	**Base Case**	$+40\%$ V_T
Bare headform	Average		167	135	125	149	156	167	163	153	149
	SD		1	3	4	3	1	6	2	3	4
	CV(%)		0.64%	2.59%	2.90%	2.19%	0.73%	3.50%	1.28%	1.89%	2.40%
	V_T effect	Cohen's d	6.43		—	1.41	2.21		2.01	0.80	
		p-value	0.00011		—	0.12211	0.03969		0.01523	0.38922	
Covered	Average		180	149	150	164	172	182	165	158	151
	SD		5	6	0	13	2	4	5	6	3
	CV(%)		2.98%	3.70%	0.25%	7.78%	1.23%	2.16%	3.09%	3.67%	2.09%
	V_T effect	Cohen's d	6.23		—	1.61	2.01		1.41	1.41	
		p-value	0.00239		—	>0.05	>0.05		0.27546	0.27695	
Coating effect		Cohen's d	2.61	2.81	—	3.01	3.22	3.01	0.40	1.00	0.40
		p-value	0.01592	0.00186	—	0.11458	0.00032	0.01765	>0.05	>0.05	>0.05

Concerning the head injury criterion (HIC), there were significant differences for the coating and the tangential velocity factors for the three impact directions (see Table 4). The interaction between the factors was significant in the left and right-side impacts. Nine of

the eighteen HIC post-hoc comparisons resulted in significant differences but attending to the effect size (Cohen's d), only five were considered relevant (Table 5). The identified relevant differences were the following: the increased HIC between the -40% V_T and base case for the bare headform (1213 $\pm$ 30 vs. 870 $\pm$ 11) and covered headform (1382 $\pm$ 25 vs. 1058 $\pm$ 12) in the front impact; the decreased HIC between the -40% V_T and base case for the covered headform (1099 $\pm$ 116 vs. 1378 $\pm$ 11) in the left side impact; and the decreased HIC between the bare and covered headform for the base case (1056 $\pm$ 20 vs. 1378 $\pm$ 11) and for the $+40\%$ V_T case (1145 $\pm$ 68 vs. 1552 $\pm$ 102) in the left side impact.

Table 4. Two-way ANOVA results (*p*-values) for the HIC. *p*-values < 0.05 portrayed as shaded cells.

	Front (Y-Rot)	Left Side (X-Rot)	Right Side (Z-Rot)
Coating	5.23×10^{-7}	7.42×10^{-6}	2.45×10^{-7}
Tangential velocity	3.76×10^{-9}	0.00012	0.00692
Interaction	0.45659	0.00319	0.04017

Table 5. Averages, standard deviation (SD), coefficient of variation (CV) and post-hoc results for HIC. *p*-values < 0.05 portrayed as shaded cells.

	HIC		Front (Y-Rot)			Left Side (X-Rot)			Right Side (Z-Rot)		
			-40% V_T	Base Case	$+40\%$ V_T	-40% V_T	Base Case	$+40\%$ V_T	-40% V_T	Base Case	$+40\%$ V_T
Bare headform	Average		1213	870	857	1049	1056	1145	893	825	781
	SD		30	11	15	58	20	68	32	15	16
	CV(%)		2.51%	1.31%	1.73%	5.53%	1.86%	5.98%	3.64%	1.81%	2.10%
	V_T effect	Cohen's d	6.93		—	0.14	1.80		1.37	0.89	
		p-value	0.00005		—	0.99999	0.68434		0.10190	0.46244	
Covered	Average		1382	1058	947	1099	1378	1552	953	949	936
	SD		25	12	47	116	11	102	39	30	32
	CV(%)		1.82%	1.13%	4.96%	10.56%	0.83%	6.59%	4.04%	3.11%	3.47%
	V_T effect	Cohen's d	6.54		—	5.63	3.51		0.08	0.26	
		p-value	0.00004		—	0.00576	0.10668		0.99995	0.99216	
Coating effect		Cohen's d	3.41	3.80	—	1.01	6.50	8.22	1.21	2.50	3.13
		p-value	0.00179	0.00004	—	0.95603	0.00184	0.00022	0.18190	0.00204	0.00028

Regarding BrIC, the two-way ANOVA resulted in significant differences for the two factors and their interaction in the three impact configurations (Table 6). All BrIC post-hoc comparisons were statistically significant (Table 7). The effect size revealed significant differences for all comparisons. Due to the magnitude of the effect size, it is worth highlighting the differences between the baseline case and the $+40$ V_T case for the bare headform in the left side impact (0.280 $\pm$ 0.008 vs. 0.540 $\pm$ 0.002) and in the right-side impact (0.750 $\pm$ 0.007 vs. 1.060 $\pm$ 0.015).

Table 6. Two-way ANOVA results (*p*-values) for the BrIC. *p*-values < 0.05 portrayed as shaded cells.

	Front (Y-Rot)	Left Side (X-Rot)	Right Side (Z-Rot)
Coating	6.14×10^{-11}	2.86×10^{-10}	1.73×10^{-12}
Tangential velocity	2.78×10^{-10}	1.61×10^{-14}	6.35×10^{-14}
Interaction	4.60×10^{-7}	0.00131	9.13×10^{-7}

Table 7. Averages, standard deviation (SD), coefficient of variation (CV) and post-hoc results for BrIC. *p*-values < 0.05 portrayed as shaded cells.

BrIC		Front (Y-Rot)			Left Side (X-Rot)			Right Side (Z-Rot)		
		−40% V_T	Base Case	+40% V_T	−40% V_T	Base Case	+40% V_T	−40% V_T	Base Case	+40% V_T
Bare headform	Average	0.210	0.310	0.400	0.170	0.280	0.540	0.620	0.750	1.060
	SD	0.004	0.007	0.001	0.020	0.008	0.002	0.040	0.007	0.015
	CV(%)	1.88%	2.35%	0.27%	11.88%	2.78%	0.43%	6.54%	0.98%	1.44%
V_T effect — Cohen's d		6.15		—	6.76	15.99		7.99	19.06	
V_T effect — *p*-value		1.02×10^{-6}		—	2.46×10^{-6}	2.86×10^{-10}		9.23×10^{-5}	1.03×10^{-8}	
Covered	Average	0.350	0.580	0.680	0.260	0.440	0.630	0.770	1.140	1.430
	SD	0.011	0.008	0.158	0.022	0.002	0.010	0.013	0.029	0.004
	CV(%)	3.03%	1.33%	23.25%	8.47%	0.49%	1.63%	1.73%	2.51%	0.30%
V_T effect — Cohen's d		14.14		—	11.07	11.68		22.75	17.83	
V_T effect — *p*-value		2.03×10^{-9}		—	1.32×10^{-8}	6.84×10^{-9}		1.15×10^{-9}	1.95×10^{-8}	
Coating effect — Cohen's d		8.61	16.6	—	5.53	9.84	5.53	9.22	23.98	22.75
Coating effect — *p*-value		9.96×10^{-8}	9.29×10^{-10}	—	1.95×10^{-5}	5.14×10^{-8}	1.21×10^{-5}	3.24×10^{-5}	7.58×10^{-10}	1.21×10^{-9}

Finally, significant differences of the two-way ANOVA for the peak of the resultant angular acceleration (PAA) were found both for the coating factor, the magnitude of the tangential velocity and their interaction in all three impact directions (Table 8). In this case, all post-hoc comparisons for the covered headform resulted in significant differences and the effect size revealed strong differences in most cases. On the contrary, in the case of the bare headform, only one comparison for the tangential velocity with the bare headform resulted in significant differences (Table 9). This comparison was between the base case and the +40% V_T case in the left side impact (3330 ± 233 rad/s² vs. 6241 ± 277 rad/s²).

Table 8. Two-way ANOVA results (*p*-values) for the PAA. *p*-values < 0.05 portrayed as shaded cells.

	Front (Y-Rot)	Left Side (X-Rot)	Right Side (Z-Rot)
Coating	1.10×10^{-10}	3.02×10^{-11}	4.61×10^{-14}
Tangential velocity	0.00009	2.43×10^{-9}	9.12×10^{-8}
Interaction	3.56×10^{-6}	0.00280	2.04×10^{-8}

Table 9. Averages, standard deviation (SD), coefficient of variation (CV) and post-hoc results for PAA. *p*-values < 0.05 portrayed as shaded cells.

PAA (rad/s²)		Front (Y-Rot)			Left Side (X-Rot)			Right Side (Z-Rot)		
		−40% V_T	Base Case	+40% V_T	−40% V_T	Base Case	+40% V_T	−40% V_T	Base Case	+40% V_T
Bare headform	Average	2681	2168	2241	2305	3330	6241	8171	7955	7753
	SD	14	101	51	248	233	277	641	127	166
	CV(%)	0.51%	4.66%	2.26%	10.76%	7.01%	4.43%	7.84%	1.60%	2.15%
	V_T effect — Cohen's d	1.41		—	2.82		8.00	0.59		0.55
	V_T effect — *p*-value	0.08917		—	0.09604		2.56×10^{-5}	0.97741		0.98343
Covered	Average	6702	9106	7141	5864	9050	10607	11524	16055	17173
	SD	433	70	2778	663	161	646	308	339	421
	CV(%)	6.46%	0.77%	38.90%	11.30%	1.78%	6.09%	2.67%	2.11%	2.45%
	V_T effect — Cohen's d	6.60		—	8.75		4.28	12.45		3.07
	V_T effect — *p*-value	5.20×10^{-6}		—	1.00×10^{-5}		0.00729	5.39×10^{-8}		0.03035
Coating effect	Cohen's d	11.05	19.06	—	9.78	15.71	12.00	9.21	22.25	25.88
	p-value	9.34×10^{-8}	1.81×10^{-9}	—	3.08×10^{-6}	1.50×10^{-8}	3.26×10^{-7}	1.55×10^{-6}	6.99×10^{-11}	7.61×10^{-12}

4. Discussion

This study investigated the combined effect of the friction force between the interior surface of the helmet and the headform and different tangential velocities in helmet oblique impacts. The experimental data included in this manuscript are particularly relevant to design helmet oblique testing protocols capable of including real-world like characteristics. The data gathered here highlight the importance of the interaction between the friction between the head and the helmet and the tangential velocity in the resulting kinematics of the head.

4.1. The Variability of the Friction between the Human Skin and the Helmet Inner Liner

Human skin has been shown to exhibit a complex and highly variable friction behaviour. Ebrahimi et al. obtained an average friction coefficient between the interior of the helmet (nylon fabric) and the human skin of 0.683 [23]. However, other experiments using human cadaver heads estimated substantially lower values for the coefficient of friction between the interior of the helmet (polyester fabric, a common material used in the interior liner of helmets) and the scalp (0.29 ± 0.07) [28]. In a tactile perception study unrelated to helmets, Ramalho et al. reported a COF about 0.7 between polyester fabric and the volar forearm of in vivo volunteers [29]. This value could be even higher in the case of the head, as other experimental studies have revealed that friction coefficients at the volar forearm were lower (COF = 0.26) than those measured on the forehead (COF = 0.34) [30]. The variation of friction coefficients measured for the human skin has been suggested to depend on skin hydration [31], with moisture increasing the value of the COF between the skin and the fabric up to a maximum and then decreasing it, when there is excess of water in the interface [31,32]. As sweating is very common among helmeted riders specially in warmer weathers, this study is essential to understand how the performance of helmets can be affected by changes in the COF.

Although the influence of the COF had been addressed already in [23], to our knowledge, this is the first time that an experimental study combines the effect of varying the tangential component of the impact velocity and the COF at the same time. Our data shows

that the combination of different magnitudes of V_T and of COF influences differently the helmet performance.

4.2. Linear Acceleration-Based Injury Predictors

The experimental results included here regarding the V_T variation are consistent with two computational studies which concluded that the influence of increasing tangential velocity on the linear acceleration is insignificant [17,21]. In the right-side impacts, where the impact point was the same for the three tangential velocities, the PLA and HIC magnitudes decreased slightly as the tangential velocity increased (Figure 11). This slight decrease can be explained by an increased helmet rotation caused by higher values of V_T, which could bring new areas of uncrushed liner into the impact area, contributing to the decrease of PLA and HIC magnitudes [33].

It is true that in the front and left side impact directions the statistical analyses resulted in significant differences for the PLA and HIC magnitudes. However, for these impact directions, the central vertical axis (Z-axis) of the headform was aligned to the vertical and, consequently, the impact point location changed with the angle of the anvil (see Figure A3). PLA and HIC magnitudes decreased as the V_T increased in the front impacts while they increased as the tangential velocity increased in the left side impact direction. This opposite trend suggests that these differences are due to the variation of the impact point location and not due to the change in V_T.

Regarding the coating effect, the PLA and HIC magnitudes obtained were always higher for the tests with high friction. The relative motion of the headform in the helmet, which depends on the tangential velocity for the bare headform, modified the crushing liner area depending on the geometry of the headform close to the impact point. Therefore, depending on the liner density around the impact point and the crushing liner area variation, the PLA and HIC could decrease, remain constant or even increase. This is supported by Ebrahimi et al., that found that the average linear acceleration of the headform with the highest friction for the 15° anvil decreased by 26% while it increased by 10% for the 30° anvil [23].

4.3. Angular Motion-Based Injury Predictors

The significance of the interaction of the two analysed factors in the two-way ANOVA for the two angular injury predictors showed that the effect of the friction depends on the magnitude of the tangential velocity. This dependence of the friction effects with the V_T is mainly due to the combination of the rolling and sliding phenomena at the helmet/anvil interface, which was observed in the high friction tests and it was studied in detail by Meng et al. [21] and to the relative motion between the headform and the helmet, which was observed in the low friction tests.

In the case of the coated headform, brain injury criterion (BrIC) and peak of the resultant angular acceleration (PAA) increased as the tangential velocity increased for the three impact directions. Interestingly, our experiments showed that the relative increase of the angular injury predictors was higher from the −40% V_T case to the base case than from the base case to the +40% V_T case. As demonstrated in Meng et al., the effect of increasing V_T in the rotation of the helmet is negligible once the helmet is sliding [21]. This suggest that from −40% V_T case to the base case the helmets were in rolling phase while from base case to the +40% V_T case the helmets were in the transition phase from rolling to sliding.

In the bare headform tests, BrIC also increased as the V_T increased but PAA did not in the front and right-side directions, in which PAA were almost constant. In this case, in which the helmet was also rolling on the anvil for lower values of V_T as in the case of the coated headform, the lower friction between the headform and the helmet caused the bare headform to slide inside the helmet. This sliding motion limited the maximum angular acceleration (slope of the angular velocities curves) but not the maximum angular velocity, which also depends on the duration of the angular acceleration, which was higher for the higher V_T values (see Figure 5). In the left side impacts, the relative motion of the headform inside the helmet was prevented by the interaction of the geometry of the headform and

the geometry of the helmet, as the V_T increased. In the +40% V_T case, the relative motion came to an end and helmet and headform moved jointly increasing the headform rotational motion significantly.

4.4. Implications for Helmet Testing Programs

The existing interaction of the friction between the helmet and the headform and V_T needs to be recognized when a testing program is being planned. Existing helmet testing methods have been shown to use speeds which are lower than those found in real world situations, mainly due to limitation of the height of the helmet drop facilities of the testing laboratories [21]. This implies lower magnitude for the tangential component of the velocity than those found in real world situations. Therefore, on top of the underestimation caused by a lower tangential velocity, there may be an additional underestimation of the rotational motion of the head if the friction between the headform and the helmet is low and, consequently, the headform slides inside the helmet without being stopped by the interaction between the geometries of the headform and the helmet. As discussed above, there is evidence showing that the friction coefficient between the human head and the liner of the helmet can be around 0.7. This friction is expected to increase if there is sweating, which can be common especially in warm weathers [32]. Thus, as several existing testing programs are starting to investigate different injury metrics related to the rotation of the headform and these programs should be looking into testing the helmets so that they are effective in a worst-case (but possible) scenario, our study suggests that the friction at the interface helmet/headform in oblique helmet programs should be high enough to guarantee the joint motion of the unit without sliding of the headform.

In addition, most helmet standards call for helmets to be tested in linear impacts (without tangential component) at the highest levels of severity ignoring the helmet response to lower severity impacts. Recently, some helmet standards such as FRHPhe-01 [27] and ECE 22.06 [26] included a low severity linear impact test at 5 m/s and 6 m/s respectively in their test methods in order to avoid that helmets transmit unacceptably high levels of linear acceleration in low severity impact events. Beside of these low severity impact tests, these standards also include an oblique impact test at 8.0 m/s against a 45-degree anvil, which originate two impact velocity components (normal and tangential) with the same magnitude of 5.66 m/s. This study supports that the oblique impact test also included in these helmet standards could be sufficient to characterize the linear acceleration in low severity impacts without the need of a specific low severity test. Since the influence of the V_T on the linear acceleration is insignificant and the magnitude of the normal component of the impact velocity of the oblique test (5.66 m/s) is already within the range of the low-speed tests recently included in the aforementioned standards.

4.5. Limitations of the Study and Future Work

As aforementioned, the high-speed video analysis revealed that the front vent of the helmet was detached during the impact in two of the three replicas of the +40% V_T case with the headform covered. This fact was the cause of the low repeatability obtained for the angular velocity and angular acceleration in the mentioned condition. In consequence, these tests were not considered in the statistical analysis.

The rigid magnesium EN960 headforms do not have an outer layer to simulate the scalp tissue or hair because they are not designed to respond like a human head to impact. Therefore, slippage between the scalp and skull, the effect of the hair (which could reduce the head/helmet friction) and the tensioning effect of the skin were not covered in this work [33,34]. Even if a study identified that scalp tissue affects head biomechanics in a significant way [28], it also concluded that the friction coefficient of the outer layer of the headform and the interaction with the helmet reduced the relative effect of the scalp.

The influence of the neck and body in the kinematics of the headform was not included in this study. Several studies suggest that the neck and body play only a small role during helmeted head impacts [35,36] whereas other studies suggest that the presence of the neck

and body have a significant influence on head kinematics and that it is strongly dependent on the impact configuration [37,38]. Isolated head surrogate was used in this study due to its simplicity and because this is the condition used in the European helmet testing regulation [26].

Despite tissue-based metrics such as Maximum Principal Strain (MPS) are desirable for assessing brain injury risk since they are a measure of the primary injury mechanism, this study looked only into four kinematic-based metrics (PLA, HIC, BrIC and PAA). These were the parameters that could be obtained directly from test measurements. In addition, BrIC has been shown to have a good correlation with several tissue-based metrics in a bicycle helmet study [39].

Another limitation of this work is that only one full-face helmet model and three impact directions were tested. Therefore, the results of this study may vary for other helmet types and other impact directions. Future research should investigate the friction between different materials used as comfort padding and the human scalp, considering the physiological skin condition and the effect of sweat.

5. Conclusions

This study has evaluated the effect of the friction of the headform and the interior surface of the helmet in oblique impacts at different tangential velocities. As oblique testing helmet programs specify a friction in the contact between the headform and the interior surface of the helmet, the value of this friction needs to be chosen carefully. Since the influence of the friction depends on the magnitude of the tangential velocity, the magnitude of these two factors must be chosen jointly. The results of our experiments show that the combination of low friction with lower speeds that the ones occurring in real-world crashes may result into underprediction of the rotational headform variables that would not be representative of real-world conditions, in which a higher V_T or the sweat of the rider's head would increase the rotational motion experienced by the rider's head.

It has also been shown experimentally that the influence of increasing tangential velocity on the linear acceleration measured by the headform is negligible. Therefore, oblique testing programs including a normal component of the impact velocity that represents a low severity impact would assess if helmets may transmit unacceptably high levels of linear acceleration even in low severity impact events.

Appendix A. Helmet Model, Impact Velocities Diagram and Impact Point Locations
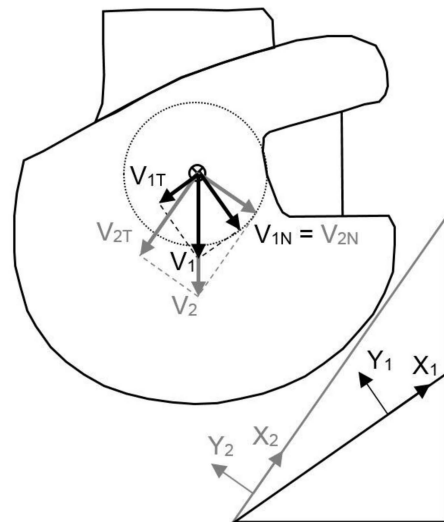

Figure A1. MT FF104 RAPIDE full-face helmet.

Figure A2. Impact velocities diagram. Modifying the angle of the anvil and the impact speed, the tangential component of the impact velocity can be modified keeping the magnitude of the normal component.
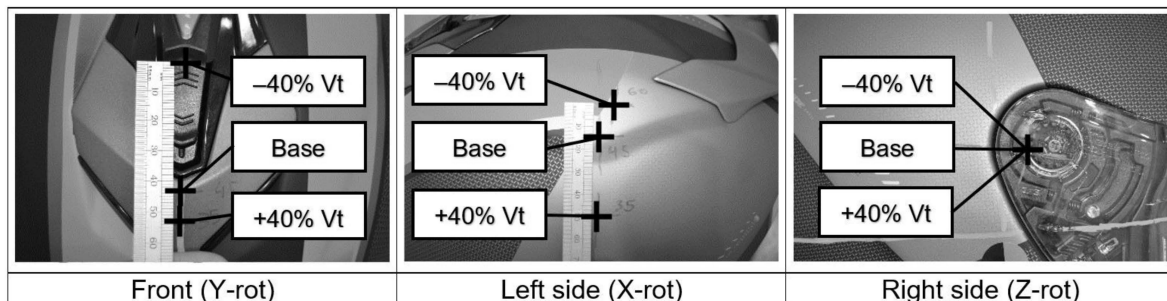
Figure A3. Impact point locations for each impact layout and tangential velocity.

References

1. World Health Organization. *Global Status Report on Road Safety 2018, Licence: C*; World Health Organization: Geneva, Switzerland, 2018.
2. MacLeod, J.B.A.; Digiacomo, J.C.; Tinkoff, G. An evidence-based review: Helmet efficacy to reduce head injury and mortality in motorcycle crashes: EAST practice management guidelines. *J. Trauma Acute Care Surg.* **2010**, *69*, 1101–1111. [CrossRef] [PubMed]

3. Liu, B.C.; Ivers, R.; Norton, R.; Boufous, S.; Blows, S.; Lo, S.K. Helmets for preventing injury in motorcycle riders. *Cochrane Database Syst. Rev.* **2008**. [CrossRef] [PubMed]

4. Lin, M.R.; Kraus, J.F. A review of risk factors and patterns of motorcycle injuries. *Accid. Anal. Prev.* **2009**, *41*, 710–722. [CrossRef] [PubMed]

5. Kleiven, S. Why Most Traumatic Brain Injuries are Not Caused by Linear Acceleration but Skull Fractures are. *Front. Bioeng. Biotechnol.* **2013**, *1*, 15. [CrossRef] [PubMed]

6. Holbourn, A.H.S. Mechanics of head injuries. *Lancet* **1943**, *242*, 438–441. [CrossRef]

7. Ommaya, A.K.; Gennarelli, T.A. Cerebral Concussion and Traumatic Unconsciousness. *Brain* **1974**, *97*, 633–654. [CrossRef]

8. Gennarelli, T.A.; Thibault, L.E. Biomechanics of Acute Subdural Hematoma. *J. Trauma Inj. Infect. Crit. Care* **1982**, *22*, 680–686. [CrossRef]

9. Gennarelli, T.A.; Thibault, L.E.; Adams, J.H.; Graham, D.I.; Thompson, C.J.; Marcincin, R.P. Diffuse axonal injury and traumatic coma in the primate. *Ann. Neurol.* **1982**, *12*, 564–574. [CrossRef]

10. Lloyd, J.D. Biomechanics of Solo Motorcycle Accidents. *J. Forensic Biomech.* **2016**, *7*, 125. [CrossRef]

11. Chinn, B.; Canaple, B.; Derler, S.; Doyle, D.; Otte, D.; Schuller, E.; Willinger, R. COST 327 Motorcycle Safety Helmets. European Commission. Directorate General for Energy and Transport. 2001. Available online: https://ec.europa.eu/transport/road_safety/sites/default/files/pdf/projects_sources/cost327_final_report.pdf (accessed on 11 November 2021).

12. Bourdet, N.; Mojumder, S.; Piantini, S.; Deck, C.; Pierini, M.; Willinger, R. Proposal of a new motorcycle helmet test method for tangencial impact. In Proceedings of the IRCOBI Conference, Málaga, Spain, 14–16 September 2016; pp. 479–489.

13. Aldman, B.; Lundell, B.; Thorngren, L. Non-perpendicular impacts—An experimental study on crash helmets. In Proceedings of the IRCOBI Conference, Birmingham, UK, 8–10 September 1976.

14. Halldin, P.; Gilchrist, A.; Mills, N.J. A new oblique impacttest for motorcycle helmets. *Int. J. Crashworthiness* **2001**, *6*, 53–64. [CrossRef]

15. Aare, M.; Halldin, P. A new laboratory rig for evaluating helmets subject to oblique impacts. *Traffic Inj. Prev.* **2003**, *4*, 240–248. [CrossRef] [PubMed]

16. Pang, T.Y.; Thai, K.T.; McIntosh, A.S.; Grzebieta, R.; Schilter, E.; Dal Nevo, R.; Rechnitzer, G. Head and neck responses in oblique motorcycle helmet impacts: A novel laboratory test method. *Int. J. Crashworthiness* **2011**, *16*, 297–307. [CrossRef]

17. Mills, N.J.; Wilkes, S.; Derler, S.; Flisch, A. FEA of oblique impact tests on a motorcycle helmet. *Int. J. Impact Eng.* **2009**, *36*, 913–925. [CrossRef]

18. Bonugli, E.; Cormier, J.; Reilly, M.; Reinhart, L. *Replicating Real-World Friction of Motorcycle Helmet Impacts and Its Effects on Head Injury Metrics*; SAE Technical Paper 2017-01-1433; SAE International: Warrendale, PA, USA, 2017. [CrossRef]

19. Finan, J.D.; Nightingale, R.W.; Myers, B.S. The influence of reduced friction on head injury metrics in helmeted head impacts. *Traffic Inj. Prev.* **2008**, *9*, 483–488. [CrossRef] [PubMed]

20. Meng, S.; Fahlstedt, M.; Halldin, P. The effect of impact velocity angle on helmeted head impact severity: A rationale for motorcycle helmet impact test design. In Proceedings of the IRCOBI Conference, Athens, Greece, 12–14 September 2018; pp. 454–469.

21. Meng, S.; Cernicchi, A.; Kleiven, S.; Halldin, P. High-speed helmeted head impacts in motorcycling: A computational study. *Accid. Anal. Prev.* **2020**, *134*, 105297. [CrossRef] [PubMed]

22. Mills, N.J.; Gilchrist, A. Finite-element analysis of bicycle helmet oblique impacts. *Int. J. Impact Eng.* **2008**, *35*, 1087–1101. [CrossRef]

23. Ebrahimi, I.; Golnaraghi, F.; Wang, G.G. Factors influencing the oblique impact test of motorcycle helmets. *Traffic Inj. Prev.* **2015**, *16*, 404–408. [CrossRef]

24. Versace, J. *A Review of the Severity Index*; SAE Technical Paper 710881; SAE International: Warrendale, PA, USA, 1971. [CrossRef]

25. Takhounts, E.G.; Craig, M.J.; Moorhouse, K.; Mcfadden, J. Development of Brain Injury. *Criteria* **2013**, *57*, 243–266.

26. *ECE 22.06. Uniform Provisions Concerning the Approval of Protective Helmets and of Their Visors for Drivers and Passengers of Motorcycles and Mopeds*; UNECE Regulation: Geneva, Switzerland, 2021.

27. *FRHPhe-01. FIM Racing Homologation Programme for Helmets*; FIM: Mies, Switzerland, 2017.

28. Trotta, A.; Annaidh, A.N.; Burek, R.O.; Pelgrims, B.; Ivens, J. Evaluation of the head-helmet sliding properties in an impact test. *J. Biomech.* **2018**, *75*, 28–34. [CrossRef]

29. Ramalho, A.; Szekeres, P.; Fernandes, E. Friction and tactile perception of textile fabrics. *Tribol. Int.* **2013**, *63*, 29–33. [CrossRef]

30. Cua, A.B.; Wilhelm, K.P.; Maibach, H.I. Elastic properties of human skin: Relation to age, sex, and anatomical region. *Arch. Dermatol. Res.* **1990**, *282*, 283–288. [CrossRef] [PubMed]

31. Derler, S.; Rossi, R.M.; Rotaru, G.M. Understanding the variation of friction coefficients of human skin as a function of skin hydration and interfacial water films. *Proc. Inst. Mech. Eng. Part J J. Eng. Tribol.* **2015**, *229*, 285–293. [CrossRef]

32. Gerhardt, L.-C.; Strässle, V.; Lenz, A.; Spencer, N.; Derler, S. Influence of epidermal hydration on the friction of human skin against textiles. *J. R. Soc. Interface* **2008**, *5*, 1317–1328. [CrossRef] [PubMed]

33. Mills, N.J.; Gilchrist, A. Oblique impact testing of bicycle helmets. *Int. J. Impact Eng.* **2008**, *35*, 1075–1086. [CrossRef]

34. Trotta, A.; Zouzias, D.; de Bruyne, G.; Annaidh, A.N. The importance of the scalp in head impact kinematics. *Ann. Biomed. Eng.* **2018**, *46*, 831–840. [CrossRef]

35.   Fahlstedt, M.; Halldin, P.; Alvarez, V.S.; Kleiven, S. Influence of the Body and Neck on Head Kinematics and Brain Injury Risk in Bicycle Accident Situations. In Proceedings of the IRCOBI Conference, Málaga, Spain, 14–16 September 2016; pp. 459–478.

36.   Willinger, R.; Deck, C.; Halldin, P.; Otte, D. Towards advanced bicycle helmet test methods. In Proceedings of the International Cycling Safety Conference, Göteborg, Sweden, 18–19 November 2014.

37.   Hering, A.M.; Derler, S. Motorcycle helmet drop tests using a hybrid iii dummy. In Proceedings of the IRCOBI Conference, Montpellier, France, 20–22 September 2000; pp. 307–321.

38.   Ghajari, M.; Galvanetto, U.; Iannucci, L.; Willinger, R. Influence of the body on the response of the helmeted head during impact. *Int. J. Crashworthiness* **2011**, *16*, 285–295. [CrossRef]

39.   Fahlstedt, M.; Abayazid, F.; Panzer, M.B.; Trotta, A.; Zhao, W.; Ghajari, M.; Gilchrist, M.D.; Ji, S.; Kleiven, S.; Li, X.; et al. Ranking and Rating Bicycle Helmet Safety Performance in Oblique Impacts Using Eight Different Brain Injury Models. *Ann. Biomed. Eng.* **2021**, *49*, 1097–1109. [CrossRef] [PubMed]

Annex B: Paper B

Juste-Lorente, O.; Maza, M.; Piqueras, A.; Lorente, A.I.; López-Valdés, F.J. (2022). Effects of Including a Penetration Test in Motorcyclist Helmet Standards: Influence on Helmet Stiffness and Impact Performance. *Applied Sciences*, *12*, 2455. https://doi.org/10.3390/app12052455

Article

Effects of Including a Penetration Test in Motorcyclist Helmet Standards: Influence on Helmet Stiffness and Impact Performance

Óscar Juste-Lorente [1],*, Mario Maza [1], Ana Piqueras [1], Ana I. Lorente [1] and Francisco J. López-Valdés [2]

1 Impact Laboratory, Aragon Institute for Engineering Research (I3A), University of Zaragoza, 44600 Alcañiz, Spain; mmaza@unizar.es (M.M.); apiquera@unizar.es (A.P.); analorente@unizar.es (A.I.L.)
2 Instituto de Investigación Tecnológica (IIT), ICAI Engineering School, Comillas Pontifical University, 28015 Madrid, Spain; fjlvaldes@comillas.edu
* Correspondence: ojuste@unizar.es

Abstract: Regulation ECE-22.05/06 does not require a helmet penetration test. Penetration testing is controversial since it has been shown that it may cause the helmet to behave in a non-desirable stiff way in real-world crashes. This study aimed to assess the effect of the penetration test in the impact performance of helmets. Twenty full-face motorcycle helmets were penetration tested at multiple locations of the helmet shell. Then, 10 helmets were selected and split into two groups (hard shell and soft shell) depending on the results of the penetration tests. These 10 helmets were then drop tested at front, lateral, and top areas at two different impact speeds (5 m/s and 8.2 m/s) to assess their impact performance against head injuries. The statistical analyses did not show any significant difference between the two groups (hard/soft shell) at 5 m/s. Similar results were observed at 8.2 m/s, except for the top area of the helmet in which the peak linear acceleration was significantly higher for the soft shell group than for the hard shell group (230 ± 12 g vs. 211 ± 11 g; *p*-value = 0.038). The results of this study suggest that a stiffer shell does not necessarily cause helmets to behave in a stiffer way when striking rigid flat surfaces. These experiments also showed that hard shell helmets can provide better protection at higher impact speeds without damaging helmet performance at lower impact speeds.

Keywords: motorcyclist helmet; penetration test; impact test; shell stiffness

1. Introduction

About 4000 people died in 2019 in the European Union as a direct result of moped and motorcycle crashes, accounting for 18% of the total motor vehicle fatalities [1]. Motorcyclists have an increased risk of injury in case of collision, which is particularly relevant in the case of head injuries [2]. The use of helmets is the most effective way of preventing motorcyclists' head injuries [3], and improving the impact performance of helmets leads to reduce the risk of head injury and fatalities. Most helmets are developed and designed according to the requirements prescribed in the relevant helmet standards. There are numerous motorcycle helmet safety standards around the world: ECE-22.05/06 in Europe [4,5], DOT and Snell in USA [6,7], and JIS-T in Japan [8] are among some of them. The objective of a motorcycle helmet standard is to ensure a minimum level of head protection under some specific test conditions. However, methods and requirements vary from one standard to another and, therefore, the performance against impact of motorcyclist helmets is influenced by the requirements included in each standard [9,10].

One of these requirements, which has been controversial over the last decades, is the need of a penetration test. The penetration test measures the resistance of the helmet shell to impacts against sharp objects. In these tests, the helmet is positioned on a headform or a spherical device support. Then, a conical striker is dropped to hit the outer surface of the

static helmet shell. The required performance criterion consists of ensuring that there is no contact between the striker tip and the headform or spherical support.

Over the years, some research has pointed out that the penetration test was either not necessary or that it could negatively influence helmet performance in more common real-life crash scenarios. In a statistical study, Otte et al. found that the frequency of motorcycle accidents involving penetrating objects was extremely small [11]. Shuaeib et al. stated that the penetration test is the main parameter that would determine the thickness of the helmet shell, leading to a thicker shell that would account for about 50% of the weight of the helmet [12]. Furthermore, some researchers stated that the penetration test causes helmets to be designed with a stiffer shell that could result in an increased risk of head injury in impacts against rigid flat surfaces [13,14]. These concerns resulted in the elimination of the penetration tests from some standards, while others continue demanding this requirement. In Europe, a penetration test is not required in the current regulation ECE-22.05/06 [4,5], while several other standards and regulations do require this procedure as part of the helmet assessment program [6–8,15].

However, the link between increased helmet shell stiffness and a higher acceleration headform response in case of impact has been addressed on the basis of simplified models of the helmet behavior that, for instance, do not take into account the effects on the helmet behavior of different impact velocities [16] and other contributing factors to impact energy management such as the role of the shell in producing a proper load distribution over a greater liner area [17] and the variation of protective padding density at different helmet locations [18,19]. The aim of this study was to empirically demonstrate if the inclusion of a penetration test in motorcyclist helmet testing standards results in an increased risk of head injury for the motorcyclists in a set of commercially available helmets. More specifically, the goal of this paper was to assess the influence of the shell resistance to the penetration test on the impact performance of helmets at two different impact velocities.

2. Materials and Methods

The experimental method was designed to study if the shell stiffness assessed by the penetration test influences the impact performance of motorcycle helmets. First, 20 full-face motorcycle helmet models were exposed to a penetration test. Then, on the basis of the observed results from the penetration tests, we classified four helmet models as hard shell helmets and six as soft shell helmets. The 10 remaining helmet models were unclassified and then not further considered in the study. Only the 10 classified helmet models were selected to be drop tested at two different velocities. A new helmet sample was used for each velocity, and therefore 20 helmets were drop tested. Thus, a total of 40 helmet samples were used in this study.

All the helmets were composed of composite shell and the protective padding was made of expanded polystyrene (EPS). The retention system of the helmets was based on the double D-ring buckle. All the helmets complied with the European regulation [4]. The tests were performed at the Impact Laboratory of the University of Zaragoza.

2.1. Penetration Test

A conventional penetration test was conducted on one sample of each helmet model (see Figure 1). The striker mass was 3 kg with a 60° conical head, and it was dropped from a height of 2 m above the surface of the helmet shell [15]. Between 2 and 4 points were randomly tested on each sample. Typical impacted areas were the front, top, lateral, and rear of the helmet shell on or above the test line, as defined by Snell [7]. Impacts on vent openings were not performed. The locations for the impact points as well as the order in which they were tested were randomly selected for each helmet as prescribed in the test procedure [6–8,15]. The intrusion of the conical tip of the striker into the helmet was measured after each impact. Then, the average and the standard deviation values of the intrusion measurements were calculated for each helmet and used as an indicator of the shell stiffness to classify the helmets. Only helmets with an average intrusion higher than

15 mm (soft shell helmets) and lower than 10 mm (hard shell helmets) were selected for the impact performance comparison and were exposed to the drop test. The rest of the helmets that resulted in intermediate values of intrusion were not further considered in the study.
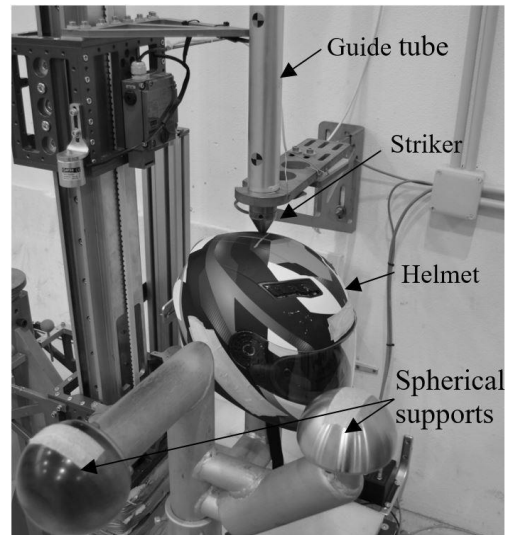

Figure 1. Penetration test set-up.

2.2. Impact Absorption Tests (Drop Tests)

The test matrix consisted of 60 impacts onto a flat anvil. After the selection process based on the penetration test results, a new sample of each selected helmet model was drop tested at 5 m/s and another sample at 8.2 m/s. Each helmet was tested on the front, lateral, and top areas (three impacts per helmet sample at each impact speed). The selected impact areas corresponded with the points B, X (right), and P, as described in the European regulation [5] and shown in Figure 2.
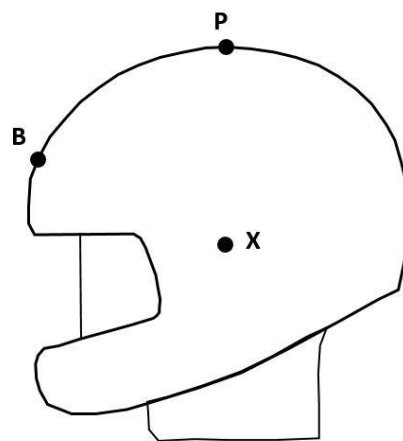
Figure 2. Impact points for the impact absorption tests.

A free fall guided impact machine (Model: Quebrantahuesos 6.0, +D, Pozuelo de Alarcón, Spain) was used for the impact absorption tests (see Figure 3). As the helmets tested were not of the same size, three metallic headform sizes were used (Model: 100_04_FMH, Cadex Inc., Saint-Jean-sur-Richelieu, QC, Canada) to ensure an appropriate fitting of the headform for each helmet size, as prescribed in the regulation [4,5]. Four helmet types were tested with the 535 mm headform circumference, three with the 575 mm headform, and three with the 605 mm headform [20]. The corresponding headform masses were 4.1 kg, 4.7 kg, and 5.6 kg respectively. The headforms were positioned inside the

helmets according to the requirements of Annex 5 of ECE-22.06 [5], and the retention system was adjusted under the chin of the headforms and tightened to a tension of 75 N [15]. Before each impact, the headform was re-positioned, and the retention system re-tensioned.

Figure 3. Impact absorption test set-up.

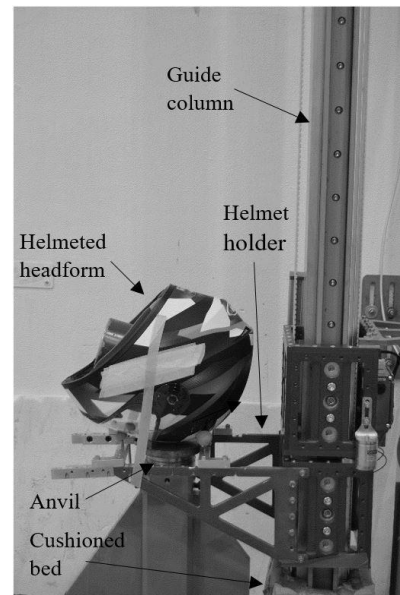A wireless system (Model: iCONO, +D, Pozuelo de Alarcón, Spain) was used to measure the linear acceleration at the center of gravity of the headforms. The wireless system incorporates three orthogonal uniaxial accelerometers (Model: 64C-2000, MEAS, Nanshan District Shenzhen, China) and an acquisition system (Model: SLICE NANO, DTS, Seal Beach, CA, USA). Data were recorded at 10 kHz, filtered using a low-pass filter CFC-1000, and post-processed using a validated and developed in-house script of Matlab (Matlab R2013b, MathWorks, Natick, MA, USA).

2.3. Statistical Hypothesis Testing

The objective of the main statistical hypothesis testing was to assess the influence of the shell stiffness on the impact performance of the helmets against head injuries. For that reason, the helmet models were classified into two groups (soft and hard shell groups) depending on the result of the penetration test. As aforementioned, 10 out of the 20 penetration tested helmets were selected for the impact performance comparison. Within the selected group, four helmet models were grouped into the hard shell group, while the remaining six helmet models were included in the soft shell group. Both groups had helmets of three different sizes. The hard shell group was composed of two helmets that were tested with the 535 headform, one with the 575 and one with the 605. The soft shell group was composed of two helmets tested with the 535 headform, two with the 575, and two with the 605.

The peak resultant linear acceleration (PLA) and the head injury criterion (HIC) measured at the center of gravity of the headform were the selected metrics to determine the impact performance of the helmets because they are the usual parameters included in helmet standards to assess head protection [5].

Since three different headform sizes were used in this study, a preliminary statistical hypothesis testing was carried out to rule out any possible influence of the headform size on the PLA or HIC variables. A non-parametric Kruskal–Wallis H test with a significance level of 0.05 was performed to analyze whether the size of the headform (three different sizes) was significantly related to the values of either PLA or HIC. The Kruskal–Wallis test is an extension of the two sample hypotheses testing to more than two independent

samples and it replaces the ANOVA test when sample sizes are small. The results of this analysis are included in the Appendix A.

After ensuring the independence of the PLA and HIC variables from the helmet size, we carried out the main statistical analysis for the comparison of the impact performance between the two shell groups. A non-parametric test, the Mann–Whitney *U* test for independent samples with a significance level of 0.05, was used for this analysis due to the limited sample size. Statistical analyses were performed using the Real Statistics Resource Pack add-in in Excel (Excel 2016, Microsoft, Redmond, WA, USA).

3. Results

The study results are presented into three subsections. First, the penetration test results of all tested helmets are reported. Second, the results of the impact absorption tests at two impact speeds are presented. Finally, the statistical analysis results of the influence of the shell stiffness on the impact performance of the helmets are shown.

3.1. Penetration Test Results

Out of a total of 20 penetration tested helmets, we selected 10 helmets and classified them into either the hard or soft shell group. The average of the intrusion values of each helmet model was used as an indicator of the shell stiffness to classify the helmets. The hard shell helmet group consisted of the four helmets in which the measured average intrusion in the penetration tests was under 10 mm. The six helmets that were included in the soft shell helmet group resulted in average intrusion higher than 15 mm. The helmets that exhibited results in between these two magnitudes were no longer considered in the study. Figure 4 includes the average and the standard deviation (SD) of the intrusion measured in the penetration test for each helmet. Details of the penetration test results for each helmet model are included in the Appendix A (Table A3). The mean average value of intrusion and SD for the hard shell group was 7 ± 3 mm, while the mean average of intrusion and SD for the soft shell group was 21 ± 6 mm.
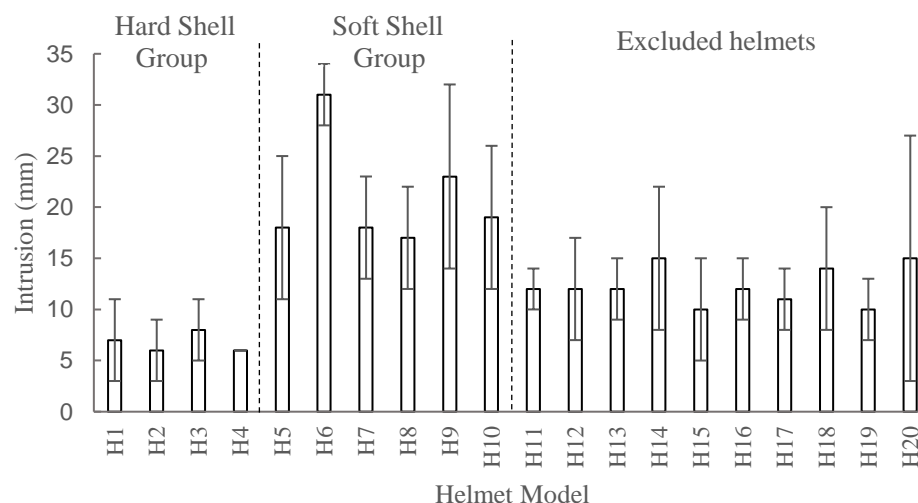
Figure 4. Mean and standard deviation (SD) of the intrusion measured in the penetration tests for each helmet model. The standard deviation of H4 was zero (3 sites were tested in this case).

3.2. Impact Absorption Test Results

At 5.0 m/s, PLA and HIC values were similar, regardless of impact point and shell type (Figure 5). The similarity between PLA and HIC values was even more noticeable when considering the standard deviations due to their similar range of values. While PLA values were between 120 and 140 g, regardless of the impact point and the shell stiffness, the HIC value was slightly higher for both shell groups when the helmet was dropped on the P point. Regardless of the slight magnitude differences observed between both shell

groups, different impact locations showed different trends between the two groups. While PLA and HIC values were higher for the hard shell group in the B and P impact points, they were lower in the X point.

Figure 5. Mean and standard deviation (SD) of the peak resultant linear acceleration (PLA) and head injury criterion (HIC) for each shell group and each impact point in the impact absorption tests at 5 m/s.

Figure 6 includes the mean and the SD of the PLA and HIC for each impact point at 8.2 m/s. One of the helmets (H7) of the soft shell group had a higher acceleration peak when testing B point (see Table A5 in Appendix A), causing the SD to be larger than in the other impact locations. Regardless of this helmet, the values measured for the hard shell helmets at 8.2 m/s resulted in more repeatable results and therefore reduced SD values. This effect was particularly true for HIC at the P location of the helmet. Again, different impact locations showed different trends. However, at this impact velocity, the results showed the opposite of what was observed at 5 m/s. In this case, while PLA and HIC values were lower for the hard shell group in the B and P impact points, they were higher in the X point.
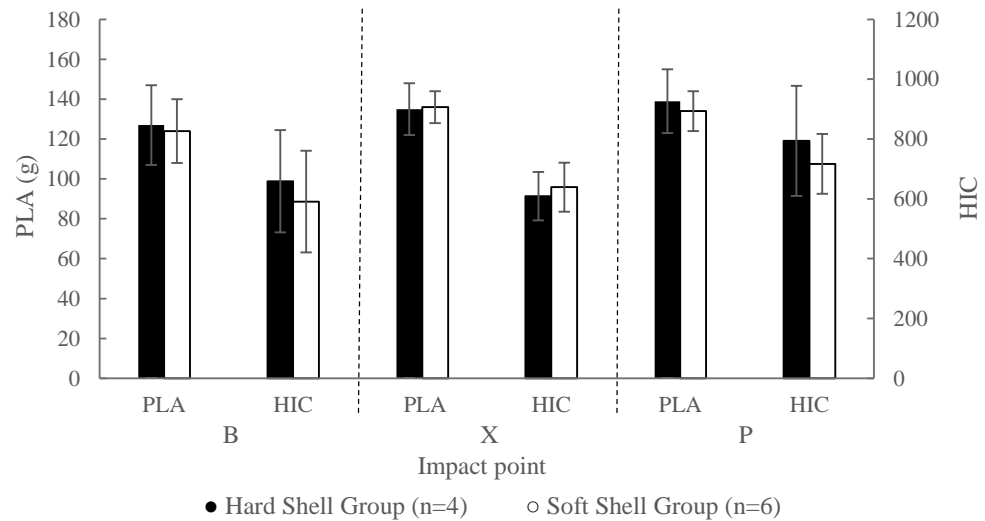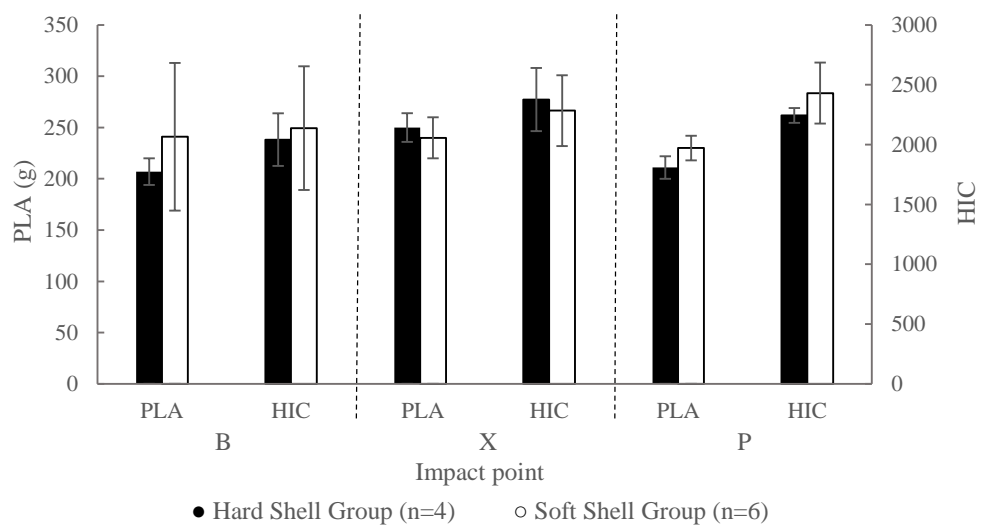

Figure 6. Mean and standard deviation (SD) of the peak resultant linear acceleration (PLA) and head injury criterion (HIC) for each shell group and each impact point in the impact absorption tests at 8.2 m/s.

In view of the observed results at the two impact velocities and for the different impact locations, we cannot conclude that helmets with stiffer shells result in higher acceleration or HIC (and therefore higher risk of injury) than those with less stiff shells.

3.3. Statistical Hypothesis Testing Results

Table 1 includes the results of the main statistical hypothesis testing (*p*-values) for each impact point tested at 5 m/s together with the mean and SD of the PLA and HIC for each shell stiffness group. Since all *p*-values are much higher than the significance level (0.05), the statistical analysis could not find any significant difference in PLA or HIC variables between the two shell groups at 5 m/s. Therefore, shell stiffness was not found to have an effect on the impact performance of the helmets tested at 5 m/s.

Table 1. Mean and SD of the PLA and HIC for each shell group with the Mann–Whitney *U* test results (*p*-value) for each impact point tested at 5 m/s. Significant values are shown in bold font.

Impact Point	Variable	Hard Shell Group (*n* = 4)	Soft Shell Group (*n* = 6)	*p*-Value
B	PLA (g)	127 ± 20	124 ± 16	0.9143
	HIC	659 ± 171	591 ± 170	0.6095
X	PLA (g)	135 ± 13	136 ± 8	0.6095
	HIC	609 ± 81	639 ± 82	0.4762
P	PLA (g)	139 ± 16	134 ± 10	0.9143
	HIC	794 ± 184	717 ± 100	0.6095

The same analysis was repeated for the data obtained in the drop tests at 8.2 m/s. As above, Table 2 includes the mean and SD of the PLA and HIC for each shell group together with the *p*-value for each impact point tested. In this case, PLA was significantly higher for the soft shell group (*p*-value = 0.0381) but only when the testing point was the P location. These results suggest that the effective PLA and HIC values provided by the helmet in drop tests are influenced by other parameters different from the shell stiffness alone.

Table 2. Mean and SD of the PLA and HIC for each shell group with the Mann–Whitney *U* test results (*p*-value) for each impact point tested at 8.2 m/s. Significant values are shown in bold font.

Impact Point	Variable	Hard Shell Group (*n* = 4)	Soft Shell Group (*n* = 6)	*p*-Value
B	PLA (g)	207 ± 13	241 ± 72	0.1714
	HIC	2042 ± 220	2138 ± 517	0.9143
X	PLA (g)	250 ± 14	240 ± 20	0.6095
	HIC	2377 ± 264	2284 ± 296	0.9143
P	PLA (g)	211 ± 11	230 ± 12	**0.0381**
	HIC	2244 ± 62	2431 ± 255	0.3524

4. Discussion

The objective of this study was to provide insight into the effects of including a penetration test, which is the main driver that determines helmet shell thickness and therefore of its stiffness, in order to improve the protective performance of helmets. To that end, the impact performance of 10 helmet models, which were sorted into either hard or soft shell groups, were compared at two impact speeds. PLA and HIC variables were selected to determine the protection capability of the helmets.

Since three headform sizes were used in the impact absorption tests, the influence of the headform size on the PLA or HIC variables was analyzed prior to carry out the main statistical analysis of this study. In Appendix A, Tables A1 and A2 include the PLA and HIC mean and the SD for each headform group, together with the *p*-value for each impact

point tested at 5 m/s and 8.2 m/s, respectively. The preliminary statistical hypothesis testing could not find any significant influence of the headform size on the PLA or HIC values at neither of the tested speeds. This result was expected because normally, the requirements of the helmet standards are the same for all headform sizes and therefore helmet manufacturers individually adjust the performance of each helmet size.

Regarding the impact performance comparison, the main statistical hypothesis testing showed no significant differences between the hard shell group and the soft shell group on the results of the impact absorption tests at 5 m/s. Similar results were observed in the tests at 8.2 m/s, except for the impacts on the helmet P point, which, showing contrary results to what had been suggested in previous research [13,14], resulted in significantly higher PLA for the soft shell group (*p*-value = 0.038), even if the HIC value was not significantly different (*p*-value = 0.352). These findings seem to be contradictory with the statement that including a penetration test in regulations causes helmets to be designed with a stiffer shell that behave very rigidly when striking flat surfaces [13,14]. While the above statement is correct for helmets in which only the shell thickness or helmet stiffness is increased [21], it does not hold for actual helmets in which both the shell and the protective padding can be varied jointly. Indeed, the impact performance of a motorcycle helmet depends both on the material and dimensions of the shell and on the characteristics of the protective padding or liner, and then there is a combination of the characteristics of the shell and liner that makes it possible to improve the helmet impact performance [22]. During an impact, a stiffer shell distributes the impact load over a greater area of the helmet, reducing the crushed volume of the liner and, therefore, decreasing the energy absorption, which may result in an increase of the linear acceleration. However, this effect can be compensated using a lower density of protective padding as long as its thickness is enough to prevent a bottom out effect. This practice is very common in current helmet design to compensate shell stiffness caused by shell geometry. For example, the higher shell stiffness due to the concavity form of the top part of full-face helmets is compensated with lower density or grooved shape liner at the top part [23]. This attempts to make the helmet impact response site-independent; however, other limitations such as liner thickness, especially at the side of the helmet, makes this point site-dependent because higher liner densities must be used at this location in order to prevent a bottom out effect of a liner. The site-dependent impact response could explain the contradictory results observed in the X point impacts (side impact) of this study. Therefore, a stiffer shell does not necessarily mean that the helmet will exhibit a global stiff mechanical behavior, but that the characteristics of the liner will be chosen to balance the effects of the stiffness of the shell, which depends on the material, thickness, and external geometry. Therefore, if a helmet stiffness increase caused by a stiffer shell can be compensated with the characteristics of the liner, the next question is: which type of stiff shell or soft shell improves the protection capabilities of the helmets?

Although no general trend was observed in the results of this study to provide a convincing answer to the above question, some particular results such as the significantly higher PLA for the soft shell group for the point P at 8.2 m/s and the extremely high acceleration peak in the impact on the B point of one helmet within the soft shell group also at 8.2 m/s suggest that hard shell helmets would provide better protection at higher impact speeds. These results are in line with a simulation study that stated that the impact speed is an important parameter in helmet design and concluded that for high impact speeds, the helmet should be designed with a stiffer shell and denser protective padding than for low speeds [16]. Furthermore, the importance of the impact speed in helmet impact performance can also be appreciated by comparing the impact absorption test results between both impact speeds for each impact location. If the PLA and HIC values within the hard shell group were lower at 5 m/s for the X point than the values of the soft shell group, then the results of the hard shell group were higher at 8.2 m/s for the X point and vice versa for the B and P points. These results also highlight that shell stiffness has an important influence in the overall dynamic performance of the helmets. While helmets with stiffer shells tend to absorb energy by liner deformation from the inside, where the

load distribution is determined by the compatibility of the liner dimensions and headform shape, helmets with softer shells tend to absorb energy predominantly from the outside, where the load distribution is determined by the geometry of the object hit. As a result of the higher load distribution capacity of helmets with stiffer shells, helmets with softer shells tend to bottom out sooner compared to helmets with stiffer shells [17]. In addition, hard shell helmets would provide better protection when striking objects with a greater variety of shapes, especially during concentrated impacts on small or sharp objects [24].

The results of our study suggest that hard shell helmets, even if they can be strongly influenced by the penetration test, would provide better protection at higher impact speeds without harming the helmet performance at lower impact speeds. In addition, another effect of the penetration test is the control of the size of the vent openings of the helmet, which could result in a decrease load distribution capacity on those areas if the size of the openings was large enough. However, the energy of the penetration test must be chosen carefully because high energy penetration tests could lead composite shells to do not delaminate for impacts into real-life crash scenarios [25], and delamination is an additional energy absorbing mechanism of composite shells that improves helmet impact performance [26]. On the negative side, hard shell helmets result in heavier helmets that may negatively impact rider's comfort. In this study, the hard shell helmets were around 200 g heaviest when compared with soft shell helmets of the same size.

A potential limitation of this study is the focus only on linear injury metrics (PLA and HIC) to assess the protection performance of the helmets. It is well known that these metrics do not consider the rotational kinematics of the head, which are proposed as the main mechanism of brain diffuse injuries [27]. In this regard, the project COST 327 carried out oblique tests at different impact speeds with two almost identical helmets that differed only in mass and shell stiffness, concluding that neither the helmet mass nor the shell stiffness seems to significantly affect the rotational accelerations and tangential forces in oblique impacts with composite shell helmets [28]. In addition, although rotational kinematics are being included in several recently proposed testing programs and only in oblique impacts [5,15], most existing mandatory helmet regulations only consider linear injury metrics to date [4,6–8].

Appendix A

Preliminary statistical hypothesis testing results about the influence of the headform size on the PLA or HIC variables.

Table A1. PLA and HIC mean and SD for each headform group with the Kruskal–Wallis H test results (*p*-value) for each impact point tested at 5 m/s.

Impact Point	Variable	Headform (E)	Headform (J)	Headform (M)	*p*-Value
B point	PLA (g)	125 ± 20	131 ± 8	120 ± 23	0.7967
	HIC	615 ± 174	691 ± 79	551 ± 235	0.7047
X point	PLA (g)	136 ± 14	135 ± 6	137 ± 9	0.9775
	HIC	610 ± 94	598 ± 68	679 ± 61	0.4372
P point	PLA (g)	136 ± 17	135 ± 11	135 ± 11	0.9426
	HIC	776 ± 168	707 ± 128	751 ± 141	0.7275

Table A2. PLA and HIC mean and SD for each headform group with the Kruskal–Wallis H test results (*p*-value) for each impact point tested at 8.2 m/s.

Impact Point	Variable	Headform (E)	Headform (J)	Headform (M)	*p*-Value
B point	PLA (g)	203 ± 16	213 ± 10	275 ± 96	0.2367
	HIC	1934 ± 287	2091 ± 251	2330 ± 657	0.6889
X point	PLA (g)	243 ± 16	238 ± 25	251 ± 16	0.5538
	HIC	2361 ± 274	2132 ± 330	2458 ± 165	0.3039
P point	PLA (g)	222 ± 12	221 ± 5	225 ± 26	0.7859
	HIC	2439 ± 212	2259 ± 127	2343 ± 314	0.3166

Table A3. Penetration test results: intrusion values by impacted area, mean, and standard deviation (SD) in millimeters for each helmet model. Intrusion values that failed the penetration test are shown in bold font.

Helmet	Front	Top	Lateral Right	Lateral Left	Rear	Mean	SD
H1	-	-	-	4	10	7	4
H2	-	4	5	-	10	6	3
H3	11	4	-	10	7	8	3
H4	-	6	6	-	6	6	0
H5	-	18	-	**25**	11	18	7
H6	-	33	29	-	-	31	3
H7	-	14	**23**	-	16	18	5
H8	13	14	**22**	-	-	17	5
H9	-	13	27	-	**30**	23	9
H10	12	18	-	26	-	19	7
H11	-	14	13	-	10	12	2
H12	-	15	15	-	7	12	5
H13	-	-	10	10	15	12	3
H14	-	22	-	10	13	15	7
H15	6	10	9	-	17	10	5

Table A3. *Cont.*

Helmet	Front	Top	Lateral Right	Lateral Left	Rear	Mean	SD
H16	14	14	11	7	-	12	3
H17	12	8	14	-	-	11	3
H18	-	7	18	-	17	14	6
H19	-	13	-	11	6	10	3
H20	-	29	8	-	7	15	12

Table A4. Impact absorption test results at 5 m/s: PLA and HIC results for each helmet model.

Helmet	B Point		X Point		P Point	
	PLA (g)	HIC	PLA (g)	HIC	PLA (g)	HIC
H1	146	818	129	626	142	905
H2	134	697	129	580	157	993
H3	99	416	154	711	117	609
H4	130	706	129	520	139	670
H5	139	761	138	638	144	849
H6	146	811	122	494	143	817
H7	105	376	146	746	122	628
H8	108	459	137	666	142	719
H9	123	605	139	636	123	602
H10	120	535	137	655	127	684

Table A5. Impact absorption test results at 8.2 m/s: PLA and HIC results for each helmet model.

Helmet	B Point		X Point		P Point	
	PLA (g)	HIC	PLA (g)	HIC	PLA (g)	HIC
H1	216	2257	241	2311	200	2211
H2	191	1917	235	2199	205	2317
H3	201	1799	265	2767	224	2272
H4	219	2196	257	2232	218	2178
H5	219	2272	210	1764	218	2405
H6	226	2339	230	2189	230	2742
H7	386	3020	269	2637	223	2117
H8	222	1713	243	2426	252	2702
H9	201	1805	247	2399	227	2195
H10	194	1681	241	2288	232	2427

References

1. European Commission. *Road Safety Thematic Report—Fatigue*; European Road Safety Observatory; European Commission, Directorate General for Transport: Brussels, Belgium, 2021.
2. Lin, M.R.; Kraus, J.F. A review of risk factors and patterns of motorcycle injuries. *Accid. Anal. Prev.* **2009**, *41*, 710–722. [CrossRef] [PubMed]
3. Liu, B.C.; Ivers, R.; Norton, R.; Boufous, S.; Blows, S.; Lo, S.K. Helmets for preventing injury in motorcycle riders. *Cochrane Database Syst. Rev.* **2008**. [CrossRef] [PubMed]
4. *ECE 22. 05*; Uniform Provisions Concerning the Approval of Protective Helmets and Their Visors for Drivers and Passengers of Motorcycles and Mopeds. UNECE Regulation: Geneva, Switzerland, 2002.

5.   *ECE 22. 06*; Uniform Provisions Concerning the Approval of Protective Helmets and of Their Visors for Drivers and Passengers of Motorcycles and Mopeds. UNECE Regulation: Geneva, Switzerland, 2021.

6.   Department of Transport (DOT). *FMVSS No. 218 Motorcycle Helmets*; National Highway Traffic Safety Administration (NHTSA): Washinton, DC, USA, 2011.

7.   *Snell M2020*; Standard for Protective Headgear. Snell Memorial Foundation: North Highlands, CA, USA, 2020.

8.   *Japanese Industrial Standard: JIS T 8133*; Protective Helmets for Motor Vehicle Users. Japanese Standards Association: Tokyo, Japan, 2015.

9.   Mcintosh, A.; Grzebieta, R. Motorcycle Helmet Standards—Harmonisation and Specialisation? In Proceedings of the 23rd International Technical Conference on the Enhanced Safety of Vehicles (ESV), Seoul, Korea, 27–30 May 2013; pp. 1–10.

10. Bourdet, N.; Deck, C.; Mojumder, S.; Willinger, R. Comparative Evaluation of DOT vs. ECE Motorcycle Helmet Test Method. In Proceedings of the IRCOBI Conference Proceedings, Athens, Greece, 12–14 September 2018; pp. 470–479.

11. Otte, D.; Chinn, B.; Doyle, D.; Sturrock, K.; Schuller, E. *Accident Description and Analysis of Motorcycle Safety Helmets*; Cost 327 Interim Reports; Accident Research Unit, Medical University: Hanover, Germany, 1997.

12. Shuaeib, F.M.; Hamouda, A.M.S.; Hamdan, M.M.; Umar, R.S.R.; Hashmi, M.S.J. Motorcycle helmet: Part II. Materials and design issues. *J. Mater. Process. Technol.* **2002**, *123*, 422–431. [CrossRef]

13. Ghajari, M.; Caserta, D.G.; Galvanetto, U. Comparison of safety helmet testing standards. In *Motorcycle and Motorcyclist Safety, Marie Curie Research Training Networks*; European Commission: Brussels, Belgium, 2010.

14. Fernandes, F.A.O.; Alves de Sousa, R.J. Motorcycle helmets—A state of the art review. *Accid. Anal. Prev.* **2013**, *56*, 1–21. [CrossRef] [PubMed]

15. *FRHPhe-01*; FIM Racing Homologation Programme for Helmets. FIM Mies: Mies, Switzerland, 2017.

16. Chang, L.-T.; Chang, C.-H.; Huang, J.-Z.; Chang, G.-L. A dynamic analysis of motorcycle helmet by finite element methods. In Proceedings of the IRCOBI Conference Proceedings, Sitges, Spain, 23–24 September 1999; pp. 371–382.

17. Beusenberg, M.; Happee, R. An experimental evaluation of crash helmet design and effectiveness in standard impact tests. In Proceedings of the IRCOBI Conference Proceedings, Eindhoven, The Netherlands, 8–10 September 1993; pp. 307–323.

18. di Landro, L.; Sala, G.; Olivieri, D. Deformation mechanisms and energy absorption of polystyrene foams for protective helmets. *Polym. Test.* **2002**, *21*, 217–228. [CrossRef]

19. Asiminei, A.G.; Van der Perre, G.; Verpoest, I.; Goffin, J. A transient finite element study reveals the importance of the bicycle material properties on head protection during impact. In Proceedings of the 2009 International Ircobi Conference on the Biomechanics of Injury, York, UK, 9–11 September 2009; pp. 357–360.

20. *CEN/TC 158*; EN 960:2006 Headforms for Use in the Testing of Protective Helmets. European Committee for Standardization: Brussels, Belgium, 2006.

21. Hopes, P.D.; Chinn, B.P. Helmets: A new look at design and possible protection. In Proceedings of the International Conference on the Biomechanics of Injury, Stockholm, Sweden, 13–15 September 1989; pp. 39–54.

22. Miyazaki, Y.; Ujihashi, S.; Jin, T.; Akiyama, S.; Cheolwoong, K. Effects of the mechanical properties of the shell and liner on the shock absorption of helmets. *Eng. Sport 6* **2006**, *3*, 145–150. [CrossRef]

23. Mills, N.J.; Wilkes, S.; Derler, S.; Flisch, A. FEA of oblique impact tests on a motorcycle helmet. *Int. J. Impact Eng.* **2009**, *36*, 913–925. [CrossRef]

24. Williams, M. Evaluation of the penetration test for bicyclists' helmets: Comparative performance of hard shell and foam helmets. *Accid. Anal. Prev.* **1990**, *22*, 315–325. [CrossRef]

25. Gilchrist, A.; Mills, N.J. Modelling of the impact response of motorcycle helmets. *Int. J. Impact Eng.* **1994**, *15*, 201–218. [CrossRef]

26. Kostopoulos, V.; Markopoulos, Y.P.; Giannopoulos, G.; Vlachos, D.E. Finite element analysis of impact damage response of composite motorcycle safety helmets. *Compos. Part B Eng.* **2001**, *33*, 99–107. [CrossRef]

27. Kleiven, S. Why Most Traumatic Brain Injuries are Not Caused by Linear Acceleration but Skull Fractures are. *Front. Bioeng. Biotechnol.* **2013**, *1*, 15. [CrossRef] [PubMed]

28. Chinn, B.; Canaple, B.; Derler, S.; Doyle, D.; Otte, D.; Schuller, E.; Willinger, R. *COST 327 Motorcycle Safety Helmets*; European Commission, Directorate General for Energy and Transport: Brussels, Belgium, 2001.